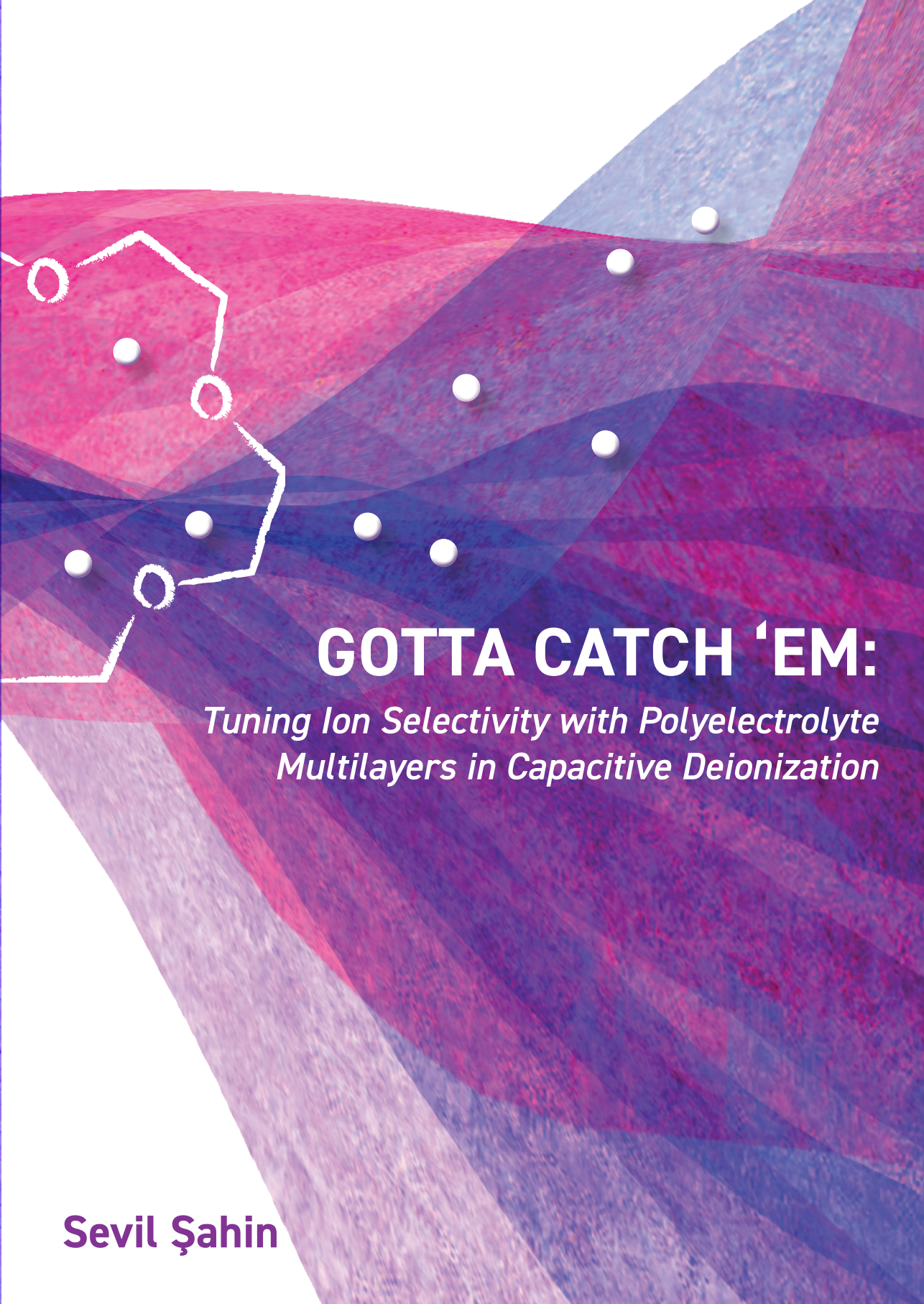

GOTTA CATCH 'EM:

Tuning Ion Selectivity with Polyelectrolyte Multilayers in Capacitive Deionization

Sevil Şahin

Propositions

1. Implementing polyelectrolyte multilayers in capacitive deionization processes is a promising way to tune ion selectivity.
   (this thesis)
2. The selectivity of ionophores highly depends on the solvent.
   (this thesis)
3. During the Covid pandemic, the standard of scientific publications was frequently lowered to inacceptable levels.
4. Surface-bound polyelectrolytes provide optimal opportunity to obtain romantic surfaces.
5. Self-organized fund allocation is more efficient and sustainable than the current research funding system.
6. Gender-specific awards and degrees are sexist.
7. Hunting as a sport is just murder.
8. Social media have become a court in countries where people do not trust the judicial system.

Propositions belonging to the thesis, entitled

Gotta Catch 'Em: Tuning Ion Selectivity with Polyelectrolyte Multilayers in Capacitive Deionization

Sevil Şahin,

Wageningen, 29 August 2022

Gotta Catch ‘Em:

Tuning Ion Selectivity with Polyelectrolyte Multilayers in Capacitive Deionization

Sevil Şahin

Thesis committee

Promotors
Dr L.C.P.M. de Smet
Associate professor, Laboratory of Organic Chemistry
Wageningen University & Research

Prof. Dr H. Zuilhof
Professor of Organic Chemistry
Wageningen University & Research

Other members
Prof. Dr E.J.R. Sudhölter, Delft University of Technology & University of Twente
Prof. Dr M.M.G. Kamperman, University of Groningen
Dr R.J. de Vries, Wageningen University & Research
Dr A.J. Michel, Voltea BV, Sassenheim

This research was conducted under the auspices of the Graduate School VLAG (Advanced studies in Food Technology, Agrobiotechnology, Nutrition and Health Sciences)

Gotta Catch 'Em:

Tuning Ion Selectivity with Polyelectrolyte Multilayers in Capacitive Deionization

Sevil Şahin

Thesis

submitted in fulfilment of the requirements for the degree of doctor
at Wageningen University
by the authority of the Rector Magnificus,
Prof. Dr A.P.J. Mol,
in the presence of the
Thesis Committee appointed by the Academic Board
to be defended in public
on Monday 29 August 2022
at 4 p.m. in the Omnia Auditorium.

Sevil Şahin
Gotta Catch 'Em: Tuning Ion Selectivity with Polyelectrolyte Multilayers in Capacitive Deionization
300 pages,

PhD thesis, Wageningen University, Wageningen, the Netherlands (2022)
With references, with summary in English

ISBN: 978-94-6447-235-6
DOI: https://doi.org/10.18174/570374

Table of Contents

Chapter 1

General Introduction

“So once you do know what the question actually is, you’ll know what the answer means.”

(The Hitchhiker's Guide to the Galaxy)

1.1 Ion-Selective Desalination and Capacitive Deionization

The availability of enough fresh water is a rapidly increasing challenge globally. By 2050, almost 6 billion peoples will experience clean water scarcity, according to 2018 edition of the United Nations World Water Development Report.[1] Besides the increase in demand for water due to the increasing world population, pollution of the current water sources contributes heavily to the existing fresh water scarcity.[1,2]

One solution to combat fresh water scarcity is developing innovative desalination technologies to treat waste water and saline water to obtain clean and fresh water. Desalination means the removal of salt from water and it has always been always important in human history.[3] One of the early descriptions of desalination belongs to Aristotle. He stated that:

> *"Salt water when it turns into vapor becomes sweet and the vapor does not form salt water again when it condenses"*
>
> *The Complete Works of Aristotle, Book II: Meteorology, Section 358 (Revised Oxford Translation by E. W. Webster. Princeton University Press, 1984, edited by J. Barnes).*

Aristotle's description is the basis of distillation, a widely used desalination process. Distillation is the oldest desalination method. During distillation, water vapor is produced by heating the saline water and then condensed into freshwater. Since Aristotle, desalination-based technologies have been commonly used and further developed. In the 20th century, desalination techniques became commercialized and over the years various conventional desalination methods have appeared.[4] For instance, more advanced distillation methods such as multi-effect, multi-stage-flash, vapor compression, and

membrane distillation techniques have been developed.[5] In 1956, the first studies started towards a new technology that is based on osmosis, reverse osmosis (RO).[6] Although the idea of osmosis has been known since 1748, there was no desalination technology that made use of this principle until 1956. In RO, water is pushed through a semi-permeable membrane and as a result the majority of the salt is separated from water.[6,7] The first RO desalination plant was built in 1977 for a municipality in the USA and since then it has become one of the most widely used desalination techniques.[6] However, both distillation- and RO-based technologies require a significant amount of energy input.[8–10] Also, these techniques are designed to desalinate "to completion" and they do not have any preference towards certain ions.[11]

Alternatively, one can remove salts from the water instead of removing the water from salts. For example, nanofiltration (NF) is used to remove majority of the divalent cations (*e.g.* Mg^{2+}, Ca^{2+}) from water *via* a membrane with a pore size of 1–10 nm to produce soft water.[6,12] Therefore, NF requires less energy than RO. Going one step further, electro-driven desalination methods have been suggested as even more energy efficient methods compared to the pressure-driven techniques such as NF. For instance, electrodialysis (ED) is an electro-driven technology and it separates ions from the water by passing the ions through ion-exchange membranes (IEMs) under an applied electrical potential.[5] IEMs are divided in two main categories: cation-exchange membrane (CEM) and anion-exchange membrane (AEM). CEMs are composed of negatively-charged polymers bearing functional groups, such carboxylate and sulfonate, to be able to reject anions while allowing cations to pass through. Similarly, AEMs are made of positively charged polymers with functional groups such as quaternary ammonium.[13] In other words, IEMs selectivity reject co-ions, and allow the passage of oppositely charged ions (counter-ions).[14] This permselective character is known as the Donnan exclusion.[14,15]

Ion-selective desalination is of relevance for multiple applications such as removing hazardous ions (*e.g.* heavy metals, arsenic, boron)[11,16–20] from wastewater, reducing the sodium concentration in greenhouse irrigation water, and removing hardness

ions from brackish water.[11,17,21–25] Furthermore, harvesting high-value metal ions (*e.g.* lithium, copper)[26–30] and nutrients (*e.g.* phosphate, potassium, nitrate)[17,31,32] from brackish water is also important from a sustainability viewpoint. For instance, phosphate is an essential nutrient for plant growth and its reserves are predicted to be depleted within the next 100 years.[33] In order to meet the global need for phosphate, harvesting phosphate from waste water is crucial. Similarly, re-using water after removing hazardous ions or the excess of certain (types of) ions is a promising solution to combat water scarcity and reduce contaminated waste water.

Capacitive deionization (CDI) is an electro-driven desalination technique that has the ability to remove ions selectively.[34] Although in the 1960s initially designed only for desalination of brackish water by Blair and Murphy,[35] within the last decade, CDI has also been explored for the selective separation of ions within the context of waste water treatment and resource recovery.[11] CDI is an environment-friendly method, at least for salt the concentrations below 10 g/L, as it can operate on low voltage values (≈ 1 V) and does not require high temperature, pressure, or chemicals for regeneration.[9,23,34]

In CDI, brackish water flows in between electrodes, and with an applied current or potential, ions migrate towards the porous electrode of opposite charge and are stored inside the electrodes. A standard CDI cell consists of two parallel electrodes (cathode and anode) that are separated by a non-conductive layer, called spacer.[9] The CDI electrodes are typically made of a conductive porous material such as activated carbon, carbon nanotubes, carbon aerogels, and graphene.[36,37] The principle of CDI is based on the electrical double layer (EDL) formation in the electrodes.[38] Ions transport through macropores and mesopores (interparticle pores) of the electrodes and reach micropores (intraparticle pores) where EDLs are formed and ions are stored (**Figure 1.1**).[9,39] As a result, desalinated water is produced. In order to harvest the ions that are stored in the electrodes in a second stream of water, the electrodes can be short-circuited (0 V) or the current/voltage can be reversed. The water recovery of the CDI-based approaches can increase up to 93.5%, which means that 100 L of brackish water yield 93.5 L of fresh water and 6.5 L of brine.[8]

CDI can also be operated with additional IEMs that are placed on the CDI electrodes. This mode of working is known as membrane capacitive deionization (MCDI) (**Figure 1.1**).[13,40,41] IEMs have fixed charges that allow the transport of counterions and prevent the transport of co-ions by acting as a filter. Therefore, IEMs increase the charge efficiency and energy consumption in an MCDI operation.

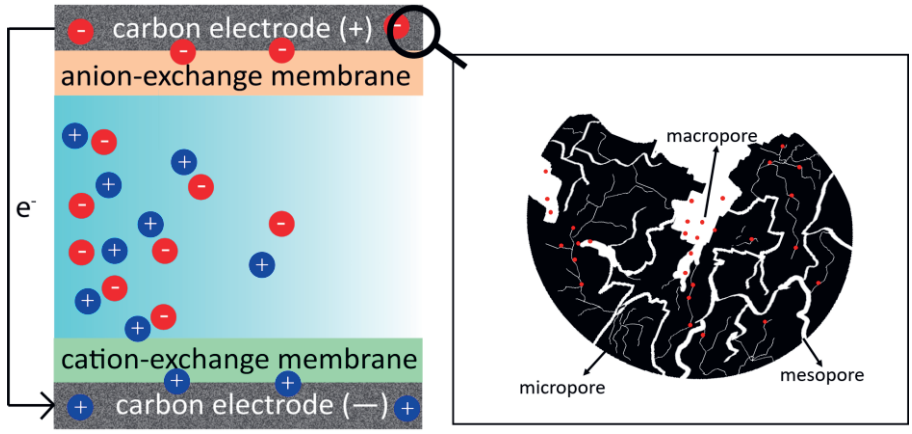

Figure 1.1. (Left) Schematic overview of ion adsorption in an MCDI process. Feed water flows in between the electrodes and with an applied voltage (or current) ions are adsorbed inside the electrodes. During the adsorption process, co-ions are rejected by the CEM and AEM. (Right) Ions are transported through the macropores and mesopores and eventually are stored inside micropores of the carbon electrodes.

Constant current (CC) and constant voltage (CV) are the most common charging modes in CDI.[42]. In a CC operation, during adsorption cycle, the potential increases and reaches a desired potential cut-off value. Similarly, during desorption cycle of a CC operation, potential decreases over time until a certain cut-off value. The main idea behind the cut-off potentials in adsorption and desorption cycles is to prevent side reactions such as oxidation of the electrodes or water splitting.[11] On the other hand, in a CV operation, the

current is at its maximum value at the beginning of adsorption cycle and gradually decreases as the electrodes become saturated over time and eventually reaches the value of zero. These two operation modes result in different CDI characteristics, including differences in the effluent concentration during the cycles, the ion transfer kinetic rate,[34,42,43] and the energy efficiency. [44–46] For instance, the ion transfer kinetic rate in a CC mode would be proportional to the charging current, while it will decrease in time in an operation with CV mode. In addition to CC (galvanostatic) and CV (potentiostatic) modes, the combination of these two can be used: galvanostatic charge/discharge cycling with potential limitation (GCPL).[47] In other words, a GCPL mode has consecutive CC and CV cycles. This approach is useful for holding the system at a certain potential for a desired amount time to make sure the electrodes are fully saturated until the cell reaches the cut-off potential.[11] Furthermore, CDI operations can be classified as single-pass and batch modes.[48,49] This classification is based on how the feed water circulates through the CDI cell. In a single-pass mode, the feed water passes the CDI cell only once, while in a batch mode there is a "fixed volume" of the water and it is recycled during the operation. **Figure 1.2** shows the change in effluent concentration for different operational modes in CDI. CC, CV, and GCPL operations are given in single-pass modes to facilitate a comparison in between them. The feed concentration remains unchanged in single-pass mode, typically the concentration variation is < 1 %, since it is an open system.[9] T In CC mode, the concentration decreases until a certain point and remains stable (below feed concentration) during adsorption cycle. The opposite trend is observed in desorption cycle of CC where the effluent concentration increases and remains stable during the cycle. On the other hand, in CV mode, the effluent concentration decreased in the beginning of the adsorption cycle and then gradually reaches the feed concentration, since the electrodes become saturated over time. During desorption in CV mode, the effluent concentration peaks at the beginning of the cycle and gradually decreases to the feed concentration. In case of the GCPL mode, we see the combination of the trends observed in CC and CV modes, as expected. As a comparison, the batch experiment with CV mode is added to **Figure 1.2**. Since in batch processes the system is closed and the solution circulates around , the effluent concentration does not go back to

the feed concentration and remains constant during the adsorption cycle. Then, during desorption cycle, the concentration increases until reaching the feed concentration.

The degree of ion selectivity and its dependence on time, as well as the desalination performance, energy consumption, and other CDI metrics can vary, based on the mode and operational parameters of CDI.[11,21,42,44,50–52] Therefore, to tune ion selectivity, multiple parameters, including the type of mode should be considered carefully. There are various approaches to introduce and/or tune the ion selectivity in CDI.[11] These include the modification of electrode materials (*e.g.* introducing certain functional groups and optimizing pore size), optimizing the operational parameters of the process, and using special-grade, ion-selective membranes. **Chapter 2** summarizes the literature on cation selectivity in (M)CDI and which parameters should be considered to target certain (types of) cations. One approach to tune ion selectivity involves the use of the polyelectrolytes, which will be discussed in the next section.

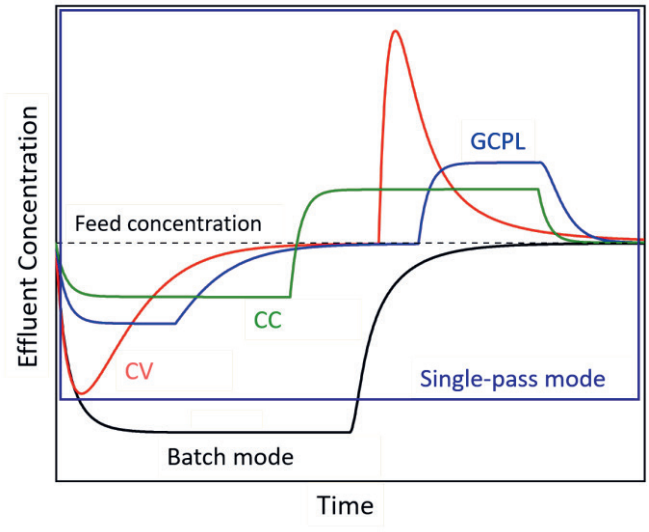

Figure 1.2. Typical desalination curves of CC, CV, and GCPL operations in single-pass modes and potentiostatic operation in batch mode (adapted from reference[11]).

1.2 Polyelectrolytes and Polyelectrolyte Multilayers

Polyelectrolytes (PEs) are polymers that contain charged or chargeable moieties that are present in a part of or all repeating units. In other words, these moieties are electrolyte groups, therefore PEs can dissociate in water.[53,54] Based on the type of charge involved, they are classified as either a polyanion (polyacid) or a polycation (polybase). Typically, the repeating units of a polyanion contain carboxylic and sulfonic acid groups.[54] Poly(styrene sulfonate) (PSS), poly(vinyl sulfonic acid) (PVS), poly(acrylic acid) (PAA), and poly(methacrylic acid) (PMAA) are amongst the common polyanions. On the other hand, polycations have positively charged functional groups, often nitrogen-based. Examples include, poly(allylamine hydrochloride) (PAH), poly(diallyldimethylammonium chloride) (PDADMAC), poly(ethyleneimine) (PEI) and poly(L-lysine) (PLL). Next to the fossil-based PEs, there are also natural (bio-based) PEs, such as alginic acid, pectin, chitin, chitosan, cellulose, and poly(lactic acid).[54–59]

Besides the type of charge and the source of the PEs, PEs can also be classified based on the amount of dissociation in aqueous solutions.[53,60–62] The pK_a value of a PE is the key factor to determine its degree of ionization at a given pH value. If a PE fully dissociates in water within a practical pH range of 2-12 , it is classified as a strong PE. In case of a polycation, pK_a value of ≥ 10 is a strong polycation. Next to that, for some polymers the ionization degree does not depend at all on the pH, like PDADMAC, which contain quaternary ammonium groups which are permanently charged, making is also a strong polycation. On the other hand, when the dissociation of a PE depends partially or strongly on the pH, then it is classified as a weak PE. For example, PEI and PAH are known as weak polycations with pK_a values of 9.7, and 8.8, respectively.[63,64] The pK_a of PAH (8.8), indicates that at this pH 50 % of the amino groups are protonated ($-NH_3^+$) , so PAH is nearly fully protonated at pH values lower than pH 6-6.5.[64,65] In case of a polyanion, when the pK_a value is ≤ 2, it is considered as a strong polyanion (PSS ≈1), while a pK_a value between 2 and 7 makes polyanion (PAA ≈5) a weak polyelectrolyte.[60] **Figure 1.3** gives an overview of the approximate pK_a values of strong and weak PEs.[66,67]

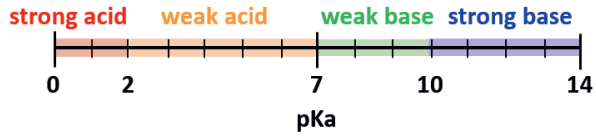

Figure 1.3. Overview of pK_a value ranges used to classify strong and weak polyelectrolytes.

Polycations and polyanions can be used to coat a surface *via* a layer-by-layer (LbL) process to yield a polyelectrolyte multilayer (PEM).[53,68,69] Although the history of LbL coatings dates back to 1960s, when Iler *et al.*[70] investigated the LbL coating of colloidal particles, LbL coatings of PEs were discovered by Decher in early the 1990s.[71,72] PEMs are easy to build.[73] Ultra-thin PEM films on solid supports can be prepared *via* versatile LbL methods such as spray- and spin-coating[68,73] as well as chemical and thermal depositions.[74] However, dip-coating method is one of the easiest and widely used PEM coating methods.[75] When a charged surface is alternatively dipped in an aqueous solution of a PE with opposite charge, a thin monomolecular PE coating is obtained, which changes the type of overall surface charge. After each dipping step (to deposit a polycation or polyanion), loosely attached (excess) polyelectrolytes are washed of by dipping the substrate in water or rinsing the substrate with water. The process of alternating adsorption of a polycation and a polyanion is repeated until the desired number of layers (thickness) is achieved.

The structure, morphology, and growth patterns (linear or exponential) of the PEMs highly depend on the coating conditions as well as the environment after the coating. For instance, the PEM structure is dependent on type of polyelectrolyte[76–79] (*e.g.* weak or strong, charge density, molecular weight), the ionic strength of the coating solution,[80–82] type of salt,[83–86] pH and temperature.[75,87–90] Depending on these conditions, the interactions between the PEs, and therefore the amount of dissociation, swelling, intrinsic and extrinsic charge compensations, and morphology of the PEM do not only differ, but can also be controled.[53,54] For example, a high ionic strength would reduce the repulsive interaction

within a PE chain and causes a more coiled PE structure. As a result, the PEM thickness and degree of swelling is affected by the salt concentration during the LbL process itself as well as under post-preparation conditions. Another example is that if pH of the aqueous environment of weak polyanions results in more dissociation of the acidic groups, the charge density would increase and hance also the degree of swelling of the PE. Therefore, multiple parameters need to be considered during and after coating PEMs.

PEMs can control the physical and chemical characteristics of various surfaces, making them suitable coatings for many areas such as drug delivery, tissue engineering, implants, antimicrobial coatings, sensors, optics, electronics, and also membranes.[54,73,91] One of the popular applications of PEM coatings is on membranes. So far, PEM-coated membranes are used in ion, gas and solvent separation, mainly in pressure-driven applications, as well as fouling control, micropollutant removal, and the dissociation of water.[53,56] **Chapter 3** summarizes a selection of recent literature on PEM-coated dense membranes and how PEMs introduce antifouling properties to membranes, increase membrane stability, and improve the separation processes by tuning selectivity towards certain solvents and ions. The ion-selective properties of PEMs are mainly based on rejecting certain (type of) ions due to their bigger hydrated size- and/or higher valence and allowing the ions with smaller valence and/or hydrated size.[89,92] In other words, PEM coatings can separate ions from each other based on size- and charge-exclusion principles. Since PEMs can change the surface properties (*e.g.* hydrophilicity, type and density of charge, and pore size) of membranes, they can tune ion selectivity of the membranes in different pressure- and electro-driven desalination processes.[93–98] **Figure 1.4** illustrates a schematic representation of an ion-selective separation process that involves a PEM and some examples of polycation and polyanions that can be used in such a PEM. For instance, Rijnaarts *et al.* used a $(PAH/PSS)_{5.5}$-coated CEM to achieve Na^+/Mg^{2+} selectivity under electrodialysis conditions.[98] Since the outermost charge of the PEM is positive (PAH-terminated), divalent and multivalent cations experienced a higher charge exclusion compared to the monovalent ones. A similar approach can also be used to tune monovalent

anion selectivity. Mulyati *et al.* used $(PDADMAC/PSS)_{7.5}$-coated AEM to tune Cl^-/SO_4^{2-} selectivity in an electrodialysis process.[97]

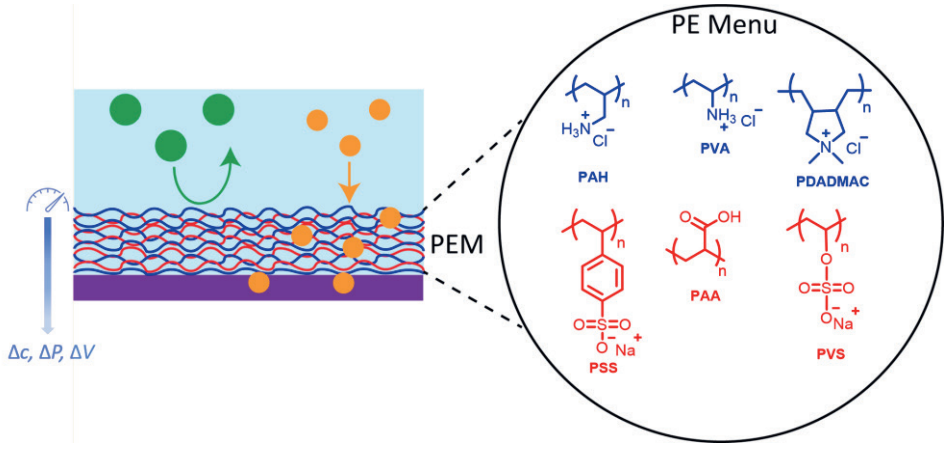

Figure 1.4. (Left) Schematic representation of a PEM-coated substrate and its selective separation process, where the driving force for the transport of ions can be difference in ion concentration (Δ*c*), pressure (Δ*P*) or electrical field (Δ*V*). Selectivity of a PEM can depend on various mechanisms, including size- and charge- rejection of certain (type of) ions. (Right) Examples of polycations (in blue) and polyanions (in red) that can be used in such a PEM. Abbreviations of the polyelectrolytes (PEs) follow as: **PAH:** poly(allylamine hydrochloride), **PVA:** poly(vinylamine hydrochloride), **PDADMAC:** poly(diallyldimethylammonium chloride), **PSS:** poly(4-styrenesulfonic acid sodium acid), **PAA:** poly(acrylic acid), **PVS:** poly(vinylsulfonic acid sodium acid).

To conclude this section, due to the tuneable properties of the PEMs in terms of ion selectivity, they have been implemented in multiple ion-selectivity studies. Going one step further, it is possible to improve ion-selectivity by combining PEMs with ion-selective receptors (ionophores). Therefore, besides their the charge- and size-based selectivity, affinity-based selectivity can be achieved *via* a thin coating that can be prepared *via* facile LbL approaches.

1.3 PEMs with Ion-Selective Receptors

Ion-selective receptors are a category of molecules that have affinity towards a certain (type of) ion(s).[99] Their ion selectivity is mostly based on host-guest chemistry. Host-guest chemistry relies on weak, reversible non-covalent interactions between the ionophores (host) and the species of interest (guest).[100] The relationship between host and guest has been described by Donald Cram (1986) as "*complexes that are composed of two or more molecules or ions held together in unique structural relationships by intermolecular forces*".[101] These intermolecular forces can be, for instance, Van der Waals forces, hydrogen bonds, electrostatic interactions, π–π interactions, and the combination of them. In most cases, the host, also known referred to as ionophore). Ionophore is a large macromolecule that exists in a variety of unique and novel structures. For example, uranyl salophenes,[102,103] cyclic polyamines,[103] or guanidinium groups[103–106] have been used as phosphate ionophores. Furthermore, podands, porphyrins, phthalocyanines, cyclodextrins, pillararenes, calixarenes, crown ethers, and many other macrocycles have been used due to their selectivity towards various metal ions.[99,101,107]

The selectivity of cyclic ionophores is highly dependent on the size of their cavity. When the ring is relatively smaller, it interacts with a relatively smaller ion. For instance, calix[4]arene derivatives make complexes with Li^+ and Na^+, whereas calix[6]arene derivatives interacts more with Mg^{2+} and Cu^{2+}.[108] Similarly, in crown ethers, their molecular recognition is based on their ring size and the size of the ion. Crown ethers are cyclic oligomers of ethylene oxides and due to the electron-rich character of the ring, they can electrostatically interact with metal ions.[109,110] In other words, the crown ether behaves as an electron donor and the metal ion behaves as an electron acceptor. **Figure 1.5** and **Table 1.1** illustrate some examples of crown ether derivatives and the size of different cations, respectively. The prefix shows the total number of atoms in the ring system (*e.g.*, 12, 15, and 18) and the suffix indicates the total number of oxygen atoms in the ring (*e.g.*, 4, 5, and 6). In the literature, 12-crown-4, 15-crown-5, and 18-crown-6 derivatives are known as Li^+,

Na^+, and K^+ ionophores, respectively, although this refers to cation selectivity rather than cation specificity.[94,109,111]

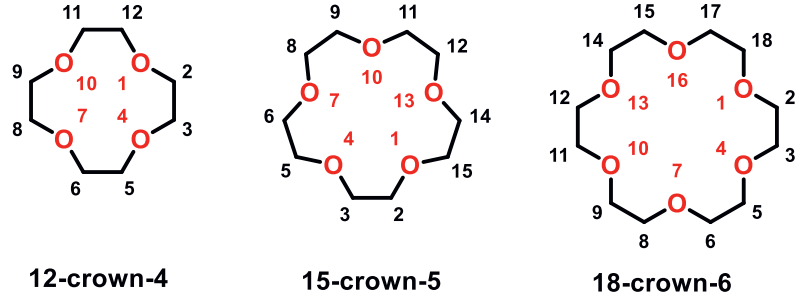

Figure 1.5. Examples of crown ether derivatives with different ring sizes. The prefix shows the total number of atoms in the ring system (*e.g.*, 12, 15, and 18) and the suffix indicated the total number of oxygen atoms in the ring (*e.g.*, 4, 5, and 6).

Table 1.1. Overview of the crystal and hydrated radii of some cations.

Ion	Crystal radius (Å)*	Hydrated radius (Å)*
Li^+	0.60	3.82
Na^+	0.95	3.58
K^+	1.33	3.31
Rb^+	1.48	3.29
Cs^+	1.69	3.29
Mg^{2+}	0.65	4.28
Ca^{2+}	0.99	4.12

*The given values are calculated for 25 °C.[112]

Crown ethers have a hydrophilic cavity as the oxygens are situated at the interior of the ring, while the exterior is hydrophobic. Also, compared to ions in water, the ion hydration shell within the complex is different or even removed. In other words, the ion hydration energy, the (hydrated size of) ions are relevant parameters and the ring size are important parameters in selectivity. For example, although 15-crown-5 derivatives are

known as Na^+ ionophores, they can also function as K^+ ionophores in aqueous solutions due to the smaller hydrated size/hydration energy of K^+ compared to Na^+ and Li^+.[94,112] This can imply that environmental conditions such as solvent polarity has an effect on the selectivity behavior of crown ethers.

Ionophores can be incorporated into PEMs *via* three main methods:

i) They can replace a PE in the PEM, but only when charged. For example, Toutianoush *et al.* built PEMs by combining sulfo-calixarene derivatives with poly(vinyl amine).[108]

ii) Ionophores can be added to the PEM during or after coating process and "trapped" within the layers *via* ionic interactions and/or hydrogen bonds.[111,113,114] However, without a covalent bond or strong electrostatic interactions, these two methods are not as stable as the typical PEMs since the ionophore units leach out after a certain period of time.[108]

iii) Ionophores can be covalently bound to one of the PE and the modified PE can be used in PEM formation. As a result, PEM has ionophore units that are stable. Numerous studies where macrocyclic ionophores were combined with a polyelectrolyte were reported.[55,94,105,106] For example, Cao *et al.* decorated poly(allylamine hydrochloride) (PAH) with guanidinium units to increase the affinity towards $H_2PO_4^-$.[106] A similar strategy was used by Kazemadab *et al.* to introduce a 15-crown-5 derivative to a PEM system by modifying the polycation with the crown ether prior the PEM coating.[94]

A schematic representation of an example of the third approach is given in **Figure 1.6**. First, a polycation (PAH) can be modified with ionophore units, 15-crown-5 (CE). Then, CE-containing PAH (PAHCE) can be used as a polycation together with a polyanion to build the PEM. Therefore, the resulting PEM will have ionophore units that have been introduced *via* stable covalent bonds. Besides the stability, another advantage of this method is the ability to tune the amount of ionophores. This can be done by adjusting the number of

ionophore units per polymer chain, or by increasing/decreasing the number of modified layers in the PEM during the coating process.

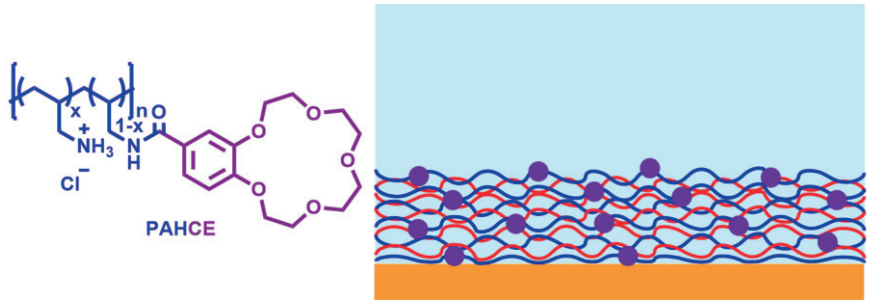

Figure 1.6. Schematic representation of (left) the polycation (PAH) that is functionalized with 15-crown-5 (CE) units *via* covalent attachment and (right) the PEM that is made with PAHCE and an unmodified polyanion. Blue, red, and purple colors represent the polycation, polyanion, and the crown ether units, respectively.

There are different ways to characterize PEMs (with or without ionophore units). For example, zeta potentials and water contact angles can be measured and typically yield zig-zag plot upon the layer build-up using two PEs. Alternatively, X-ray photoelectron spectroscopy (XPS) can be used to map the elemental composition of the PE layers. Similarly, UV (ultra-violet) and infrared (IR) spectroscopy can be used to identify certain functional groups of the PEM after the addition of each layer. Besides, techniques such as ellipsometry and atomic force microscopy (AFM) and can give information about the thickness of the PEMs.

Regarding determining the degree of ion selectivity of a PEM-system, one of the most common ways is implementing the PEM in a desalination system and measuring the concentration or conductivity of the effluent. For instance in a CDI operation, typically ion chromatography (IC) and/or inductively coupled plasma - optical emission spectrometry (ICP-OES) are used to determine the ion concentration. Therefore, the amount of

adsorption can be determined for ions of interest and then compared with each other to calculate the selectivity number. **Chapter 2** summarizes the common ion selectivity definitions for (M)CDI operations. Moreover, the adsorption efficiency of target ions can be measured *via* UV-vis spectroscopy by using UV-active agents[104] or detecting the amount of target ion within the PEM after exposure *via* XPS or Auger spectroscopy.

1.4 Quartz Crystal Microbalance with Dissipation Monitoring (QCM-D)

Next to the experimental techniques and approaches listed at the end of the Section 1.3, quartz crystal microbalance with dissipation monitoring (QCM-D) is also another useful technique to study the interaction of PEMs with different ions. QCM is a real-time gravimetric method that can give insight about the mass changes on surfaces *in-situ* at nanoscale resolution.[115,116] It functions as a highly sensitive balance for very small changes in mass. The core of the QCM technology is piezoelectricity. Piezoelectricity is a phenomenon was discovered by Paul-Jacques and Pierre Curie brothers in 1880.[117] The word piezoelectricity is derived from the Greek word "piezein" (πιέζω) which mean "press". Piezoelectricity is the ability to generate an electrical response with an applied mechanical change. Since this effect is reversible and the coupling between the electrical and mechanical states of a piezoelectric material (*e.g.* silk, sucrose, wood, bone, some ceramics, quartz), such materials will mechanically change (be deformed) when a voltage is applied.[116,118,119] Although there are various piezoelectric materials, quartz is the widely-used piezoelectric material for QCM technologies.

In a QCM sensor, quartz is sandwiched in between two electrodes (active and counter electrodes).[115] After an appropriate amount of voltage is applied on the sensor, it oscillates at a certain resonance frequency. When the voltage is turned off, oscillation decays exponentially. Then, the decay is recorded and the frequency data is extracted.[120] In 1959, Günter Sauerbrey formulated a relation that is known as Sauerbrey equation (**Equation 1.1**). In the Sauerbrey equation, Δm (ng $\cdot$ cm^{-2}) is the areal mass density of the

adsorbed film, C (1.77 ng · cm^{-2} · Hz^{-1}) is the mass-sensitivity constant, Δf_{n} (Hz) is the frequency shift and n is the harmonic number (3, 5, 7, 9, 11). QCM is an acoustic technology and has some similarities between acoustic musical instruments. The strings of a guitar resemble the overtones of frequency in a QCM operation. The smallest resonance frequency, f_1, is the fundamental frequency and when n> 1, the frequencies are called overtones. For AT-cut QCM sensors, only the odd harmonics (n= 1, 3, 5...) can excite the quartz crystal electrically so that the polarization occurs. For overtones that are even, the deformation of the crystal is symmetrical, which does not result in currents.

When the QCM sensor is coated with a thin film, this layer oscillates together with quartz, and therefore it is possible to calculate the mass of coated layer based on the change in frequency by using **Equation 1**.[120]

$$\Delta m = \frac{-C \cdot \Delta f_{\mathrm{n}}}{n} \qquad (\mathbf{1.1})$$

The areal mass data obtained *via* Sauerbrey equation can be used to model (estimate) the thickness of the layer of interest (Sauerbrey model). However, the thickness value obtained from Sauerbrey model is only valid for thin rigid films and the model does not give realistic results for soft and viscous layers as described by Kanazawa and Gordon in 1985,[121] since the Sauerbrey model underestimates the mass of the associated water for the viscoelastic layers. Therefore, information about the energy losses in the system (dissipation) is required to model the viscoelastic layers, which is possible with an extended version of QCM (QCM-D).[122,123] In addition to frequency data, QCM-D also measures the total energy loss in the system (dissipation) that can give information about structural and viscoelastic properties such as swelling, collapse, crosslinking, and morphology of a layer.[124–127] By using dissipation data of different overtones, it is possible to determine whether a layer is viscous, before using a suitable viscoelastic model (*e.g.* a Voigt-based model) calculate the wet thickness of the layer. When ΔD is virtually zero and/or harmonics of Δf overlap, the layer is considered to be rigid and therefore Sauerbrey model is used. In other words, this is the case when Δf/n is constant for different harmonics. On the other

hand, if there is a significant change in dissipation and/or harmonics of Δ*f* spread, Voigt-based viscoelastic models are suitable for such a layer.[124,127] For viscoelastic models, more than two harmonics of dissipation and frequency shifts should be studied for a realistic characterization. Therefore, we can get information about the wet thickness, density, viscosity, and elasticity of the layer.

Figure 1.7 shows schematically a typical adsorption process studied by QCM-D. A decrease in frequency followed by an increase in dissipation indicates a successfully-coated layer. By using dissipation (viscoelasticity-related) and frequency (mass-related) data, it is possible to study the layer build-up as well as interactions of various analytes (*e.g.* virus, bacteria, gas, surfactants, oils, proteins, and ions) with the different layers.[128–132] In other words, when a PEM-coated sensor is flushed with a solution of interest, molecules may interact with the surface, for example, the may bind to the surface. Based on the kinetics of the binding process, the total adsorbed mass, as well as the changes in the viscoelastic properties of the PEM, the affinity of the PEM towards the analyte can be determined.

QCM-D has been used to investigate the structural changes in PEMs and ionophore-containing coatings after exposed to various ions, as well as the affinities of these coating towards certain (type of) ions.[106,125,126,133] O'Neal *et al.* investigated the effect of different monovalent anions on the LbL-coated PEMs that are formed from PDADMAC and PSS.[125] They observed higher degrees of layer swelling when exposed to Br^- compared to Cl^- .This can be explained by the larger hydrated size of Br^- compared to Cl^- (3.30 Å *vs.* 3.32 Å)[112] and therefore larger amount of water in the PEM. Zhang *et al.* investigated the effect of an ionophore (*i.e.* 18-crown-6) on the K^+ selectivity of a hydrogel *via* QCM-D.[134] The ionophore-modified hydrogel exhibited a rapid K^+ ion selectivity compared to other cations including Na^+, NH_4^+, Mg^{2+}, and Ca^{2+}. Similarly, Cao *et al.* used a phosphate ionophore containing PEM and observed a higher frequency, and therefore higher adsorbed mass, for phosphate ions compared to the PEM without ionophore.[106]

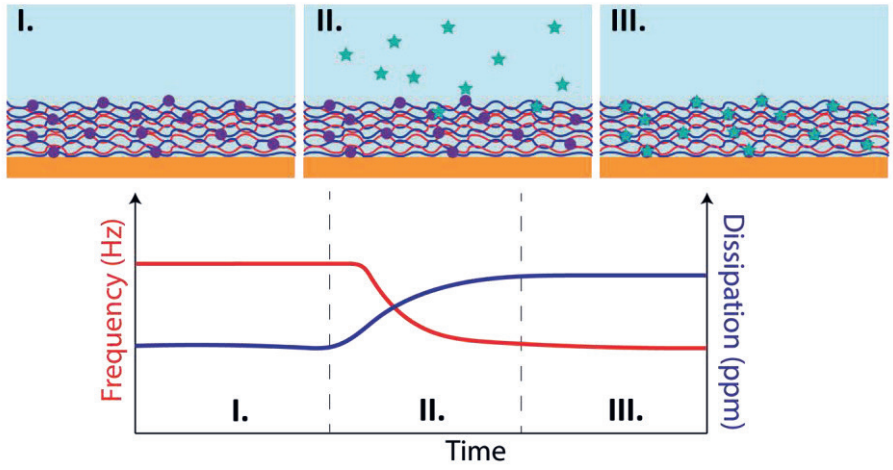

Figure 1.7. Schematic representation of the time-dependent changes in frequency and dissipation values of a PEM functionalized with affinity units (*e.g.* ionophores) coated on a QCM sensor in water *i)* before, *ii)* during, and *iii)* after the interaction with an analyte of interest (*e.g.* ion, protein, virus) during a QCM-D experiment. Based on the changes in frequency and dissipation, interactions between different analytes and coatings can be studied. Blue, red, and purple colors represent the polycation, polyanion, and the affinity units, respectively, while the green stars are the analyte of interest.

1.5 Aim and Outline of the Thesis

The aim of the work described in this thesis was to explore the use of layer-by-layer-coated polyelectrolyte multilayers (PEMs), with and without ionophore units, to tune the ion selectivity in capacitive deionization (CDI). Although CDI is a well-studied and established desalination method, its ability to differentiate the ions with the same type of charge was reported to be modest. Recent efforts to tune the ion-selective properties of CDI have mainly focused on optimizing operational parameters of the process as well as adjusting the pore size of the electrodes and decorating the electrodes with ion-selective layers. While those parameters allow some tuning of ion selectivity, we anticipated that the

use of PEM-coated ion-exchange membranes (IEMs) in CDI processes would further expand the window of control, mainly because of wide variety in possibilities to tune the physical and chemical characteristics of the PEMs, such as number of layers, type of polyelectrolyte, and additional ionophore units. In more detail, we studied *i)* the monovalent cation selectivity of the PEM-coated CEM in CDI, *ii)* tandem monovalent cation and anion selectivity with a PEM-coated AEM in CDI, *iii)* the effect of operational parameters of CDI (*e.g.* mode of operation, amount of voltage, concentration and composition of the feed solution) and number of layers in PEM on the overall monovalent cation selectivity, *iv)* the effect of 15-crown-5 derivatives on the Na^+ and K^+ selectivity of (bio-based) PEMs *via* a real-time gravimetric method, quartz crystal microbalance with dissipation monitoring. Overall, this thesis aims to develop PEM-based CDI operations to tune ion selectivity in an affordable, easy, and efficient way.

Chapter 2 –overviews the literature for cation selectivity in CDI operations. In this chapter, the common ion selectivity definitions, the main factors that affect the cation selectivity in CDI, and the recent methods to tune ion selectivity have been discussed. The use of electrode materials with different pore sizes and compositions, additional functional groups on electrode surface, introduction of standard or special-grade ion-selective membranes, optimizing the operational parameters in the CDI operation, or combinations of them are amongst the recent methods to tune the selectivity.

Chapter 3 – gives an overview of recent literature on PEM-coated dense membranes. The ability of the PEMs to introduce antifouling properties to the membranes and increase their stability, as well as improving the separation processes of solvents and ions are discussed. Moreover, the mechanisms behind the selective properties of PEMs (*e.g.* size- and charge- based rejection of ions) as well as the parameters that affect the ion selectivity of PEMs were addressed.

Chapter 4 – explores the selective separation of Na^+ and Mg^{2+} in CDI by using a PEM-coated standard grade cation-exchange membrane (PEM-CMX). The selectivity and

performance of the commercial standard-grade and monovalent cation-selective membranes were compared with the PEM-CMX. Furthermore, the performance and the selectivity of the PEM-CMX was tested for over 40 cycles of CDI.

Chapter 5 – focuses on tandem monovalent cation and anion selectivity in CDI by combining a PEM-coated anion-exchange membrane (PEM-AEM) with intercalation electrodes that are made of nickel hexacyanoferrate. The selectivity of the PEM-AEM towards NO_3^-, Cl^-, SO_4^{2-}, and $H_2PO_4^-$ in CDI was investigated. The factors that affect the selectivity number (*e.g.* type of the outermost layer and number of layers of the PEM, the composition of the feed solution, type of counter ion) were discussed.

Chapter 6 – covers an investigation on the effect of different operational modes, namely constant voltage (CV) and constant current (CC), in CDI and the effect of number of layers of PEM on the monovalent cation selectivity of a PEM-coated cation-exchange membrane (PEM-CMX). The selectivity and its dependency on time were explored. Then, the obtained selectivity numbers were rationalized by using an MCDI model based on the dynamic potential profile for the PEM-CMX. Next, the selectivity performance of the PEM-CMX was compared with commercial monovalent cation selective membranes by using feed solution with different compositions.

Chapter 7 – studies the interactions between polyelectrolyte multilayers (PEMs) containing 15-crown-5 (CE) groups and various cations by using quartz crystal microbalance with dissipation monitoring (QCM-D). First, the effect of CE units on the build-up and structure of the PEMs was analyzed. Then, the affinity of the PEMs (with or without CE units) towards Li^+, Na^+, K^+, Rb^+, and Mg^{2+} were compared. Finally, the effect of type of outermost layer and the type of polyelectrolyte on the cation affinity and PEM structure were described.

Chapter 8 – combines and explains the results obtained in **Chapters 3-7** in a broader context and lists suggestions for the future research.

References

(1) WWAP. *The United Nations World Water Development Report 2018: Nature-Based Solutions for Water*; **2018**.

(2) Boretti, A.; Rosa, L. Reassessing the Projections of the World Water Development Report. *npj Clean Water* **2019**, *2* (1). https://doi.org/10.1038/s41545-019-0039-9.

(3) Birkett, J. D. A Brief Illustrated History of Desalination. From the Bible to 1940. *Desalination* **1984**, *50*, 17–52. https://doi.org/10.1016/0011-9164(84)85014-6.

(4) Kumar, M.; Culp, T.; Shen, Y. Water Desalination - History, Advances, and Challenges. *Winter Bridg. Front. Eng.* **2016**, *46* (4), 21–29.

(5) He, T. xiang; Yan, L. jun. Application of Alternative Energy Integration Technology in Seawater Desalination. *Desalination.* **2009**, *249* (1), 104–108. https://doi.org/10.1016/j.desal.2008.07.026.

(6) Curto, D.; Franzitta, V.; Guercio, A. A Review of the Water Desalination Technologies. *Appl. Sci.* **2021**, *11* (2), 1–36. https://doi.org/10.3390/app11020670.

(7) Lee, K. P.; Arnot, T. C.; Mattia, D. A Review of Reverse Osmosis Membrane Materials for Desalination-Development to Date and Future Potential. *J. Memb. Sci.* **2011**, *370* (1–2), 1–22. https://doi.org/10.1016/j.memsci.2010.12.036.

(8) Porada, S.; Zhang, L.; Dykstra, J. E. Energy Consumption in Membrane Capacitive Deionization and Comparison with Reverse Osmosis. *Desalination* **2020**, *488*. https://doi.org/10.1016/j.desal.2020.114383.

(9) Porada, S.; Zhao, R.; Van Der Wal, A.; Presser, V.; Biesheuvel, P. M. Review on the Science and Technology of Water Desalination by Capacitive Deionization. *Prog. Mater. Sci.* **2013**, *58* (8), 1388–1442. https://doi.org/10.1016/j.pmatsci.2013.03.005.

(10) Wang, L.; Dykstra, J. E.; Lin, S. Energy Efficiency of Capacitive Deionization. *Environ. Sci. Technol.* **2019**, *53* (7), 3366–3378. https://doi.org/10.1021/acs.est.8b04858.

(11) Gamaethiralalage, J. G.; Singh, K.; Sahin, S.; Yoon, J.; Elimelech, M.; Suss, M. E.; Liang, P.; Biesheuvel, P. M.; Zornitta, R. L.; de Smet, L. C. P. M. Recent Advances in Ion Selectivity with Capacitive Deionization. *Energy Environ. Sci.* **2020**, *14*, 1095–1120. https://doi.org/10.1039/d0ee03145c.

(12) Wafi, M. K.; Hussain, N.; El-Sharief Abdalla, O.; Al-Far, M. D.; Al-Hajaj, N. A.; Alzonnikah, K. F. Nanofiltration as a Cost-Saving Desalination Process. *SN Applied Sciences*. 2019. https://doi.org/10.1007/s42452-019-0775-y.

(13) Hassanvand, A.; Wei, K.; Talebi, S.; Chen, G. Q.; Kentish, S. E. The Role of Ion Exchange Membranes in Membrane Capacitive Deionisation. *Membranes.* **2017**, *7*, 1–23. https://doi.org/10.3390/membranes7030054.

(14) Luo, T.; Abdu, S.; Wessling, M. Selectivity of Ion Exchange Membranes: A Review. *J. Memb. Sci.* **2018**, *555* (March), 429–454. https://doi.org/10.1016/j.memsci.2018.03.051.

(15) Strathmann, H. Electrodialysis, a Mature Technology with a Multitude of New Applications. *Desalination* **2010**, *264* (3), 268–288. https://doi.org/10.1016/j.desal.2010.04.069.

(16) Dong, Q.; Guo, X.; Huang, X.; Liu, L.; Tallon, R.; Taylor, B.; Chen, J. Selective Removal of Lead Ions through Capacitive Deionization: Role of Ion-Exchange Membrane. *Chem. Eng. J.* **2019**, *361*, 1535–1542. https://doi.org/10.1016/j.cej.2018.10.208.

(17) Choi, J.; Dorji, P.; Shon, H. K.; Hong, S. Applications of Capacitive Deionization: Desalination, Softening, Selective Removal, and Energy Efficiency. *Desalination* **2019**, *449*, 118–130. https://doi.org/10.1016/j.desal.2018.10.013.

(18) Huang, Z.; Lu, L.; Cai, Z.; Ren, Z. J. Individual and Competitive Removal of Heavy Metals Using Capacitive Deionization. *J. Hazard. Mater.* **2016**, *302*, 323–331. https://doi.org/10.1016/j.jhazmat.2015.09.064.

(19) Liu, P.; Yan, T.; Zhang, J.; Shi, L.; Zhang, D. Separation and Recovery of Heavy Metal Ions and Salt Ions from Wastewater by 3D Graphene-Based Asymmetric Electrodes: via Capacitive Deionization. *J. Mater. Chem. A* **2017**, *5*, 14748–14757. https://doi.org/10.1039/c7ta03515b.

(20) Chen, R.; Sheehan, T.; Ng, J. L.; Brucks, M.; Su, X. Capacitive Deionization and Electrosorption for Heavy Metal Removal. *Environ. Sci. Water Res. Technol.* **2020**, *6* (2), 258–282. https://doi.org/10.1039/c9ew00945k.

(21) Sahin, S.; Dykstra, J. E.; Zuilhof, H.; Zornitta, R. L.; De Smet, L. C. P. M. Modification of Cation-Exchange Membranes with Polyelectrolyte Multilayers to Tune Ion Selectivity in Capacitive Deionization. *ACS Appl. Mater. Interfaces* **2020**, *12* (31), 34746–34754. https://doi.org/10.1021/acsami.0c05664.

(22) Zhi Yi Leong, H. Y. Y. Capacitive Deionization of Divalent Cations for Water Softening Using Functionalized Carbon Electrodes. *ACS Omega* **2020**, *5*, 2097–2106. https://doi.org/10.1021/acsomega.9b02330.

(23) Gabrielli, C.; Maurin, G.; Francy-Chausson, H.; Thery, P.; Tran, T. T. M.; Tlili, M. Electrochemical Water Softening: Principle and Application. *Desalination* **2006**, *201*, 150–163. https://doi.org/10.1016/j.desal.2006.02.012.

(24) He, C.; Ma, J.; Zhang, C.; Song, J.; and Waite, T. D. Short-Circuited Closed-Cycle Operation of Flow-Electrode CDI for Brackish Water Softening. *Environ. Sci. Technol.* **2018**, *52*, 9350−9360. https://doi.org/10.1021/acs.est.8b02807.

(25) Singh, K.; Sahin, S.; Gamaethiralalage, J. G.; Zornitta, R. L.; de Smet, L. C. P. M. Simultaneous, Monovalent Ion Selectivity with Polyelectrolyte Multilayers and Intercalation Electrodes in Capacitive Deionization. *Chem. Eng. J.* **2021**, 128329. https://doi.org/10.1016/j.cej.2020.128329.

(26) Huang, S. Y.; Fan, C. S.; Hou, C. H. Electro-Enhanced Removal of Copper Ions from Aqueous Solutions by Capacitive Deionization. *J. Hazard. Mater.* **2014**, *278*, 8–15. https://doi.org/10.1016/j.jhazmat.2014.05.074.

(27) Bryjak, M.; Siekierka, A.; Kujawski, J.; Smolińska-Kempisty, K.; Kujawski, W. Capacitive Deionization for Selective Extraction of Lithium from Aqueous Solutions. *J. Membr. Sep. Technol.* **2015**, *4* (3), 110–115. https://doi.org/10.6000/1929-6037.2015.04.03.2.

(28) Lee, D. H.; Ryu, T.; Shin, J.; Ryu, J. C.; Chung, K. S.; Kim, Y. H. Selective Lithium Recovery from Aqueous Solution Using a Modified Membrane Capacitive Deionization System. *Hydrometallurgy* **2017**, *173*, 283–288. https://doi.org/10.1016/j.hydromet.2017.09.005.

(29) Siekierka, A.; Tomaszewska, B.; Bryjak, M. Lithium Capturing from Geothermal Water by Hybrid Capacitive Deionization. *Desalination* **2018**, *436*, 8–14. https://doi.org/10.1016/j.desal.2018.02.003.

(30) Shi, W.; Liu, X.; Ye, C.; Cao, X.; Gao, C.; Shen, J. Efficient Lithium Extraction by Membrane Capacitive Deionization Incorporated with Monovalent Selective Cation Exchange Membrane. *Sep. Purif. Technol.* **2019**, *210*, 885–890. https://doi.org/10.1016/j.seppur.2018.09.006.

(31) Ge, Z.; Chen, X.; Huang, X.; Ren, Z. J. Capacitive Deionization for Nutrient Recovery from Wastewater with Disinfection Capability. *Environ. Sci. Water Res. Technol.* **2018**, *4* (1), 33–39. https://doi.org/10.1039/c7ew00350a.

(32) Bian, Y.; Chen, X.; Lu, L.; Liang, P.; Ren, Z. J. Concurrent Nitrogen and Phosphorus Recovery Using Flow-Electrode Capacitive Deionization. *ACS Sustain. Chem. Eng.* **2019**, *7* (8), 7844–7850. https://doi.org/10.1021/acssuschemeng.9b00065.

(33) Cordell, D.; Drangert, J. O.; White, S. The Story of Phosphorus: Global Food Security and Food for Thought. *Glob. Environ. Chang.* **2009**, *19* (2), 292–305. https://doi.org/10.1016/j.gloenvcha.2008.10.009.

(34) Suss, M. E.; Porada, S.; Sun, X.; Biesheuvel, P. M.; Yoon, J.; Presser, V. Water Desalination via Capacitive Deionization: What Is It and What Can We Expect from It? *Energy Environ. Sci.* **2015**, *8*, 2296–2319. https://doi.org/10.1039/c5ee00519a.

(35) Blair, J. W.; Murphy, G. W. Electrochemical Demineralization of Water with Porous Electrodes of Large Surface Area. *Advances in Chemistry*, **1960**, 27, 206–223. https://doi.org/10.1021/ba-1960-0027.ch020.

(36) Huang, Z. H.; Yang, Z.; Kang, F.; Inagaki, M. Carbon Electrodes for Capacitive Deionization. *J. Mater. Chem. A* **2017**, *5* (2), 470–496. https://doi.org/10.1039/c6ta06733f.

(37) Cheng, Y.; Hao, Z.; Hao, C.; Deng, Y.; Li, X.; Li, K.; Zhao, Y. A Review of Modification of Carbon Electrode Material in Capacitive Deionization. *RSC Adv.* **2019**, *9* (42), 24401–24419. https://doi.org/10.1039/c9ra04426d.

(38) Lee, J. H.; Bae, W. S.; Choi, J. H. Electrode Reactions and Adsorption/Desorption Performance Related to the Applied Potential in a Capacitive Deionization Process. *Desalination* **2010**, *258* (1–3), 159–163. https://doi.org/10.1016/j.desal.2010.03.020.

(39) Biesheuvel, P. M.; Zhao, R.; Porada, S.; van der Wal, A. Theory of Membrane Capacitive Deionization Including the Effect of the Electrode Pore Space. *J. Colloid Interface Sci.* **2011**, *360* (1), 239–248. https://doi.org/10.1016/j.jcis.2011.04.049.

(40) Kim, J. S.; Kim, C. S.; Shin, H. S.; Rhim, J. W. Application of Synthesized Anion and Cation Exchange Polymers to Membrane Capacitive Deionization (MCDI). *Macromol. Res.* **2015**, *23*, 360–366. https://doi.org/10.1007/s13233-015-3049-6.

(41) Li, H.; Zou, L. Ion-Exchange Membrane Capacitive Deionization: A New Strategy for Brackish Water Desalination *Desalination.* **2011**, *275*, 62–66. https://doi.org/10.1016/j.desal.2011.02.027.

(42) Wang, L.; Lin, S. Membrane Capacitive Deionization with Constant Current vs Constant Voltage Charging: Which Is Better? *Environ. Sci. Technol.* **2018**, *52* (7). https://doi.org/10.1021/acs.est.7b06064.

(43) Zhao, R.; Biesheuvel, P. M.; Van Der Wal, A. Energy Consumption and Constant Current Operation in Membrane Capacitive Deionization. *Energy Environ. Sci.* **2012**, *5* (11), 9520–9527. https://doi.org/10.1039/c2ee21737f.

(44) Kang, J.; Kim, T.; Jo, K.; Yoon, J. Comparison of Salt Adsorption Capacity and Energy Consumption between Constant Current and Constant Voltage Operation in Capacitive Deionization. *Desalination* **2014**, *352*, 52–57. https://doi.org/10.1016/j.desal.2014.08.009.

(45) Han, L.; Karthikeyan, K. G.; Gregory, K. B. Energy Consumption and Recovery in Capacitive Deionization Using Nanoporous Activated Carbon Electrodes. *J. Electrochem. Soc.* **2015**, *162* (12), E282–E288. https://doi.org/10.1149/2.0431512jes.

(46) Qu, Y.; Campbell, P. G.; Gu, L.; Knipe, J. M.; Dzenitis, E.; Santiago, J. G.; Stadermann, M. Energy Consumption Analysis of Constant Voltage and Constant Current Operations in Capacitive Deionization. *Desalination* **2016**, *400*. https://doi.org/10.1016/j.desal.2016.09.014.

(47) Zornitta, R. L.; Srimuk, P.; Lee, J.; Krüner, B.; Aslan, M.; Ruotolo, L. A. M.; Presser, V. Charge and Potential Balancing for Optimized Capacitive Deionization Using Lignin-Derived, Low-Cost Activated Carbon Electrodes. *ChemSusChem* **2018**, *11*, 2101–2113. https://doi.org/10.1002/cssc.201800689.

(48) Jande, Y. A. C.; Kim, W. S. Modeling the Capacitive Deionization Batch Mode Operation for Desalination. *J. Ind. Eng. Chem.* **2014**, *20* (5), 3356–3360. https://doi.org/10.1016/j.jiec.2013.12.020.

(49) Porada, S.; Zhao, R.; Van Der Wal, A.; Presser, V.; Biesheuvel, P. M. Review on the Science and Technology of Water Desalination by Capacitive Deionization. *Progress in Materials Science*. Elsevier Ltd 2013, pp 1388–1442. https://doi.org/10.1016/j.pmatsci.2013.03.005.

(50) Biesheuvel, P. M.; Zhao, R.; Porada, S.; van der Wal, A. Theory of Membrane Capacitive Deionization Including the Effect of the Electrode Pore Space. *J. Colloid Interface Sci.* **2011**, *360* (1), 239–248. https://doi.org/10.1016/j.jcis.2011.04.049.

(51) Zhao, R.; van Soestbergen, M.; Rijnaarts, H. H. M.; van der Wal, A.; Bazant, M. Z.; Biesheuvel, P. M. Time-Dependent Ion Selectivity in Capacitive Charging of Porous Electrodes. *J. Colloid Interface Sci.* **2012**, *384*, 38–44. https://doi.org/10.1016/j.jcis.2012.06.022.

(52) Qu, Y.; Campbell, P. G.; Gu, L.; Knipe, J. M.; Dzenitis, E.; Santiago, J. G.; Stadermann, M. Energy Consumption Analysis of Constant Voltage and Constant Current Operations in Capacitive Deionization. *Desalination* **2016**, *400*, 18–24. https://doi.org/10.1016/j.desal.2016.09.014.

(53) Joseph, N.; Ahmadiannamini, P.; Hoogenboom, R.; Vankelecom, I. F. J. Layer-by-Layer Preparation of Polyelectrolyte Multilayer Membranes for Separation. *Polym. Chem.* **2014**, *5* (6), 1817–1831. https://doi.org/10.1039/c3py01262j.

(54) Visakh, P. M.; Bayraktar, O.; Pico, G. A. *Polyelectrolytes: Thermodynamics and Rheology*; **2014**. https://doi.org/10.1007/978-3-319-01680-1.

(55) Chopin, N.; Guillory, X.; Weiss, P.; Bideau, J.; Colliec-Jouault, S. Design Polysaccharides of Marine Origin: Chemical Modifications to Reach Advanced Versatile Compounds. *Curr. Org. Chem.* **2014**, *18* (7), 867–895. https://doi.org/10.2174/1385272818071405151523334.

(56) Zhao, Y.; Gao, C.; Van Der Bruggen, B. Technology-Driven Layer-by-Layer Assembly of a Membrane for Selective Separation of Monovalent Anions and Antifouling. *Nanoscale* **2019**, *11* (5), 2264–2274. https://doi.org/10.1039/c8nr09086f.

(57) Miller, M. D.; Bruening, M. L. Controlling the Nanofiltration Properties of Multilayer Polyelectrolyte Membranes through Variation of Film Composition. *Langmuir* **2004**, *20* (26), 11545–11551. https://doi.org/10.1021/la0479859.

(58) Lin, D.; Lopez-Sanchez, P.; Selway, N.; Gidley, M. J. Viscoelastic Properties of Pectin/Cellulose Composites Studied by QCM-D and Oscillatory Shear Rheology. *Food Hydrocoll.* **2018**, *79*, 13–19. https://doi.org/10.1016/j.foodhyd.2017.12.019.

(59) Gentile, P.; Frongia, M. E.; Cardellach, M.; Miller, C. A.; Stafford, G. P.; Leggett, G. J.; Hatton, P. V. Functionalised Nanoscale Coatings Using Layer-by-Layer Assembly for Imparting Antibacterial Properties to Polylactide-Co-Glycolide Surfaces. *Acta Biomater.* **2015**, *21*, 35–43. https://doi.org/10.1016/j.actbio.2015.04.009.

(60) Dickhaus, B. N.; Priefer, R. Determination of Polyelectrolyte pK_a Values Using Surface-to-Air Tension Measurements. *Colloids Surfaces A Physicochem. Eng. Asp.* **2016**, *488*, 15–19. https://doi.org/10.1016/j.colsurfa.2015.10.015.

(61) del Castillo, G. F. D. ; Hailes, R. L. N.; Dahlin, A. Large Changes in Protonation of Weak Polyelectrolyte Brushes with Salt Concentration-Implications for Protein Immobilization. *J. Phys. Chem. Lett.* **2020**, *11* (13), 5212–5218. https://doi.org/10.1021/acs.jpclett.0c01289.

(62) Nová, L.; Uhlík, F.; Košovan, P. Local pH and Effective pK_a of Weak Polyelectrolytes-Insights from Computer Simulations. *Phys. Chem. Chem. Phys.* **2017**, *19* (22), 14376–14387. https://doi.org/10.1039/c7cp00265c.

(63) Vleugels, L. F. W. (**2018**). Self-Organization of Polyelectrolytes: as Mediated by Surfactants, Dyes and Ions. Eindhoven University of Technology.

(64) Choi, J.; Rubner, M. F. Influence of the Degree of Ionization on Weak Polyelectrolyte Multilayer Assembly. *Macromolecules* **2005**, *38* (1), 116–124. https://doi.org/10.1021/ma048596o.

(65) Shiratori, S. S.; Rubner, M. F. Ph-Dependent Thickness Behavior of Sequentially Adsorbed Layers of Weak Polyelectrolytes. *Macromolecules* **2000**, *33* (11), 4213–4219. https://doi.org/10.1021/ma991645q.

(66) Burke, S. E.; Barrett, C. J. Acid-Base Equilibria of Weak Polyelectrolytes in Multilayer Thin Films. *Langmuir* **2003**, *19* (8), 3297–3303. https://doi.org/10.1021/la026500i.

(67) Landsgesell, J.; Holm, C.; Smiatek, J. Simulation of Weak Polyelectrolytes: A Comparison between the Constant PH and the Reaction Ensemble Method. *Eur. Phys. J. Spec. Top.* **2017**, *226* (4), 725–736. https://doi.org/10.1140/epjst/e2016-60324-3.

(68) Guzmán, E.; Rubio, R. G.; Ortega, F. A Closer Physico-Chemical Look to the Layer-by-Layer Electrostatic Self-Assembly of Polyelectrolyte Multilayers. *Adv. Colloid Interface Sci.* **2020**, *282*. https://doi.org/10.1016/j.cis.2020.102197.

(69) Richardson, J. J.; Björnmalm, M.; Caruso, F. Technology-Driven Layer-by-Layer Assembly of Nanofilms. *Science* **2015**, *348*, (6233). https://doi.org/10.1126/science.aaa2491.

(70) R. K. Iler. Multilayers of Colloidal Particles. *J. Colloid Interface Sci.* **1966**, *21* (6), 569–594. https://doi.org/10.1016/0095-8522(66)90018-3.

(71) Decher, G.; Hong, J. D.; Schmitt, J. Buildup of Ultrathin Multilayer Films by a Self-Assembly Process: III. Consecutively Alternating Adsorption of Anionic and Cationic Polyelectrolytes on Charged Surfaces. *Thin Solid Films* **1992**, *210–211*, 831–835. https://doi.org/10.1016/0040-6090(92)90417-A.

(72) Decher, G. Fuzzy Nanoassemblies: Toward Layered Polymeric Multicomposites. *Science* **1997**, *277*, 1232–1237. https://doi.org/10.1126/science.277.5330.1232.

(73) Richardson, J. J.; Cui, J.; Björnmalm, M.; Braunger, J. A.; Ejima, H.; Caruso, F. Innovation in Layer-by-Layer Assembly. *Chem. Rev.* **2016**, *116* (23), 14828–14867. https://doi.org/10.1021/acs.chemrev.6b00627.

(74) El-Hashani, A. M. (**2007**) Electrostatic Layer-by-Layer Assembly of Ultrathin Films and Membranes Containing Hexacyclen and p- Sulfonatocalix[n]Arene Macrocycles and Their Application for Highly Efficient Ion Separation. University of Cologne.

(75) Michel, M.; Toniazzo, V.; Ruch, D.; Ball, V. Deposition Mechanisms in Layer-by-Layer or Step-by-Step Deposition Methods: From Elastic and Impermeable Films to Soft Membranes with Ion Exchange Properties. *ISRN Mater. Sci.* **2012**, *2012*, 1–13. https://doi.org/10.5402/2012/701695.

(76) Bütergerds, D.; Kateloe, C.; Cramer, C.; Schönhoff, M. Influence of the Degree of Ionization on the Growth Mechanism of Poly(Diallyldimethylammonium)/Poly(Acrylic Acid) Multilayers. *J. Polym. Sci. Part B Polym. Phys.* **2017**, *55* (5), 425–434. https://doi.org/10.1002/polb.24283.

(77) Riegler, H.; Essler, F. Polyelectrolytes. 2: Intrinsic or Extrinsic Charge Compensation? Quantitative Charge Analysis of PAH/PSS Multilayers. *Langmuir* **2002**, *18* (17), 6694–6698. https://doi.org/10.1021/la020108n.

(78) Caruso, F.; Niikura, K.; Furlong, D. N.; Okahata, Y. 1. Ultrathin Multilayer Polyelectrolyte Films on Gold: Construction and Thickness Determination. *Langmuir* **1997**, *13* (13), 3422–3426. https://doi.org/10.1021/la960821a.

(79) Fares, H. M.; Schlenoff, J. B. Equilibrium Overcompensation in Polyelectrolyte Complexes. *Macromolecules* **2017**, *50* (10), 3968–3978. https://doi.org/10.1021/acs.macromol.7b00665.

(80) Tang, K.; Besseling, N. A. M. Formation of Polyelectrolyte Multilayers: Ionic Strengths and Growth Regimes. *Soft Matter* **2016**, *12* (4), 1032–1040. https://doi.org/10.1039/c5sm02118a.

(81) Dubas, S. T.; Schlenoff, J. B. Factors Controlling the Growth of Polyelectrolyte Multilayers. *Macromolecules* **1999**, *32* (24), 8153–8160. https://doi.org/10.1021/ma981927a.

(82) Lösche, M.; Schmitt, J.; Decher, G.; Bouwman, W. G.; Kjaer, K. Detailed Structure of Molecularly Thin Polyelectrolyte Multilayer Films on Solid Substrates as Revealed by Neutron Reflectometry. *Macromolecules* **1998**, *31* (25), 8893–8906. https://doi.org/10.1021/ma980910p.

(83) Salomäki, M.; Laiho, T.; Kankare, J. Counteranion-Controlled Properties of Polyelectrolyte Multilayers. *Macromolecules* **2004**, *37* (25), 9585–9590. https://doi.org/10.1021/ma048701u.

(84) Salomäki, M.; Kankare, J. Specific Anion Effect in Swelling of Polyelectrolyte Multilayers. *Macromolecules* **2008**, *41* (12), 4423–4428. https://doi.org/10.1021/ma800315j.

(85) El Haitami, A. E.; Martel, D.; Ball, V.; Nguyen, H. C.; Gonthier, E.; Labbe, P.; Voegel, J. C.; Schaaf, P.; Senger, B.; Boulmedais, F. Effect of the Supporting Electrolyte Anion on the Thickness of PSS/PAH Multilayer Films and on Their Permeability to an Electroactive Probe. *Langmuir* **2009**, *25* (4), 2282–2289. https://doi.org/10.1021/la803534y.

(86) Salomäki, M.; Tervasmäki, P.; Areva, S.; Kankare, J. The Hofmeister Anion Effect and the Growth of Polyelectrolyte Multilayers. *Langmuir* **2004**, *20* (9), 3679–3683. https://doi.org/10.1021/la036328y.

(87) Schönhoff, M.; Bieker, P. Linear and Exponential Growth Regimes of Multilayers of Weak Polyelectrolytes in Dependence on PH. *Macromolecules* **2010**, *43* (11), 5052–5059. https://doi.org/10.1021/ma1007489.

(88) Vidyasagar. A.; Sung, C.; Losensky, K, Lutkenshaus, J. L. PH-Dependent Thermal Transitions in Hydrated Layer-by-Layer Assemblies Containing Weak Polyelectrolytes. *Macromol. Res.* **2012**, *45*, 9169–9176.

(89) Ahmad, M.; Yaroshchuk, A.; Bruening, M. L. Moderate PH Changes Alter the Fluxes, Selectivities and Limiting Currents in Ion Transport through Polyelectrolyte Multilayers Deposited on Membranes. *J. Memb. Sci.* **2020**, *616*, 118570. https://doi.org/10.1016/j.memsci.2020.118570.

(90) Yoo, D.; Shiratori, S. S.; Rubner, M. F. Controlling Bilayer Composition and Surface Wettability of Sequentially Adsorbed Multilayers of Weak Polyelectrolytes. *Macromolecules* **1998**, *31* (13), 4309–4318. https://doi.org/10.1021/ma9800360.

(91) Campbell, J.; Vikulina, A. S. Layer-by-Layer Assemblies of Biopolymers: Build-up, Mechanical Stability and Molecular Dynamics. *Polymers* **2020**, *12* (9), 1–30. https://doi.org/10.3390/polym12091949.

(92) White, N.; Misovich, M.; Alemayehu, E.; Yaroshchuk, A.; Bruening, M. L. Highly Selective Separations of Multivalent and Monovalent Cations in Electrodialysis through Nafion Membranes Coated with Polyelectrolyte Multilayers. *Polymer* **2016**, *103*, 478–485. https://doi.org/10.1016/j.polymer.2015.12.019.

(93) Cheng, W.; Liu, C.; Tong, T.; Epsztein, R.; Sun, M.; Verduzco, R.; Ma, J.; Elimelech, M. Selective Removal of Divalent Cations by Polyelectrolyte Multilayer Nanofiltration Membrane: Role of Polyelectrolyte Charge, Ion Size, and Ionic Strength. *J. Memb. Sci.* **2018**, *559*, 98–106. https://doi.org/10.1016/j.memsci.2018.04.052.

(94) Kazemabad, M.; Verliefde, A.; Cornelissen, E. R.; D'Haese, A. Crown Ether Containing Polyelectrolyte Multilayer Membranes for Lithium Recovery. *J. Memb. Sci.* **2020**, *595*, 117432. https://doi.org/10.1016/j.memsci.2019.117432.

(95) Cheng, C,; Yaroshchuk, A.; Bruening, M. L. Fundamentals of Selective Ion Transport through Multilayer Polyelectrolyte Membranes. *Langmuir* **2013**, *29*, 1885–1892. https://doi.org/10.1021/la304574e.

(96) Armstrong, J. A.; Eduardo, E.; Bernal, L.; Yaroshchuk, A.; Bruening, M. L. Separation of Ions Using Polyelectrolyte-Modified Nanoporous Track-Etched Membranes. *Langmuir* **2013**, *29*, 10287–10296. https://doi.org/10.1021/la401934v.

(97) Mulyati, S.; Takagi, R.; Fujii, A.; Ohmukai, Y.; Matsuyama, H. Simultaneous Improvement of the Monovalent Anion Selectivity and Antifouling Properties of an Anion Exchange Membrane in an Electrodialysis Process, Using Polyelectrolyte Multilayer Deposition. *J. Memb. Sci.* **2013**, *431*, 113–120. https://doi.org/10.1016/j.memsci.2012.12.022.

(98) Rijnaarts, T.; Reurink, D. M.; Radmanesh, F.; de Vos, W. M.; Nijmeijer, K. Layer-by-Layer Coatings on Ion Exchange Membranes: Effect of Multilayer Charge and Hydration on Monovalent Ion Selectivities. *J. Memb. Sci.* **2019**, *570–571*, 513–521. https://doi.org/10.1016/j.memsci.2018.10.074.

(99) Ganjali, M. R.; Norouzi, P.; Rezapour, M.; Faridbod, F.; Pourjavid, M. R. Supramolecular Based Membrane Sensors. *Sensors* **2006**, *6* (8), 1018–1086. https://doi.org/10.3390/s6081018.

(100) Lehn, J. M. *Supramolecular Chemistry Concepts and Prospectives*. **1995**. Wiley-VCH, Weinheim.

(101) Haj-Zaroubi. M. (**2002**) The Anatomy of the Host-Guest Binding Energetics of Bicyclic Guanidinium-Oxoanion Ion-Pairs. Technical University of Munich.

(102) Wróblewski, W.; Wojciechowski, K.; Dybko, A.; Brzózka, Z.; Egberink, R. J. M.; Snellink-Ruël, B. H. M.; Reinhoudt, D. N. Uranyl Salophenes as Ionophores for Phosphate-Selective Electrodes. *Sensors Actuators, B Chem.* **2000**, *68* (1), 313–318. https://doi.org/10.1016/S0925-4005(00)00450-0.

(103) Berchmans, S.; Issa, T. B.; Singh, P. Determination of Inorganic Phosphate by Electroanalytical Methods: A Review. *Anal. Chim. Acta* **2012**, *729*, 7–20. https://doi.org/10.1016/j.aca.2012.03.060.

(104) Paltrinieri, L.; Wang, M.; Sachdeva, S.; Besseling, N. A. M.; Sudhölter, E. J. R.; de Smet, L. C. P. M. Fe_3O_4 Nanoparticles Coated with a Guanidinium-Functionalized Polyelectrolyte Extend the pH Range for Phosphate Binding. *J. Mater. Chem. A* **2017**, *5*, 18476–18485. https://doi.org/10.1039/c7ta04054g.

(105) Paltrinieri, L.; Remmen, K.; Müller, B.; Chu, L.; Köser, J.; Wintgens, T.; Wessling, M.; de Smet, L. C. P. M.; Sudhölter, E. J. R. Improved Phosphoric Acid Recovery from Sewage Sludge Ash Using Layer-by-Layer Modified Membranes. *J. Memb. Sci.* **2019**, *587*, 117162. https://doi.org/10.1016/j.memsci.2019.06.002.

(106) Cao, Z.; Gordiichuk, P. I.; Loos, K.; Sudhölter, E. J. R.; De Smet, L. C. P. M. The Effect of Guanidinium Functionalization on the Structural Properties and Anion Affinity of Polyelectrolyte Multilayers. *Soft Matter* **2016**, *12* (5), 1496–1505. https://doi.org/10.1039/c5sm01655j.

(107) Barbera, L. (**2017**) The Supramolecular Chemistry of Water Soluble Calixarenes , Cyclodextrins and Pillararenes. University of Messina.

(108) Toutianoush, A.; Schnepf, J.; Hashani, A. El; Tieke, B. Selective Ion Transport and Complexation in Layer-by-Layer Assemblies of p-Sulfonato-Calix[n] Arenes and Cationic Polyelectrolytes. *Adv. Funct. Mater.* **2005**, *15* (4), 700–708. https://doi.org/10.1002/adfm.200400223.

(109) Pedersen, C. J. Salts, Cyclic Polyethers and Their Complexes with Metal. *J. Am. Chem. Soc.* **1967**, No. 157, 7017–7036.

(110) Liu, Z.; Nalluri, S. K. M.; Fraser Stoddart, J. Surveying Macrocyclic Chemistry: From Flexible Crown Ethers to Rigid Cyclophanes. *Chem. Soc. Rev.* **2017**, *46* (9), 2459–2478. https://doi.org/10.1039/c7cs00185a.

(111) Zhai, H.; Qu, R.; Li, X.; Liu, Y.; Wei, Y.; Feng, L. Crown Ether Modified Membranes for Na^+-Responsive Controllable Emulsion Separation Suitable for Hypersaline Environments. *J. Mater. Chem. A* **2020**, *8* (5), 2684–2690. https://doi.org/10.1039/c9ta12418g.

(112) Nightingale, E. R. Phenomenological Theory of Ion Solvation. Effective Radii of Hydrated Ions. *J. Phys. Chem.* **1959**, *63* (9), 1381–1387. https://doi.org/10.1021/j150579a011.

(113) Gu, H.; Dai, R.; Wei, Y.; Ji, H. F. Functional Layer-by-Layer Multilayer Films for Ion Recognition. *Anal. Methods* **2013**, *5* (14), 3454–3457. https://doi.org/10.1039/c3ay40372f.

(114) Stekolshchikova, A. A.; Radaev, A. V.; Orlova, O. Y.; Nikolaev, K. G.; Skorb, E. V. Thin and Flexible Ion Sensors Based on Polyelectrolyte Multilayers Assembled onto the Carbon Adhesive Tape. *ACS Omega* **2019**, *4*, 15421–15427.

(115) Qiao, X.; Zhang, X.; Tian, Y.; Meng, Y. Progresses on the Theory and Application of Quartz Crystal Microbalance. *Appl. Phys. Rev.* **2016**, *3* (3). https://doi.org/10.1063/1.4963312.

(116) Dixon, M. C. Quartz Crystal Microbalance with Dissipation Monitoring: Enabling Real-Time Characterization of Biological Materials and Their Interactions. *J. Biomol. Tech.* **2008**, *19* (3), 151–158.

(117) Brashaw, L. Understanding Piezoelectric Quartz Crystals. *J. Chem. Educ.* **2000**, *8*, 50–58. https://doi.org/10.1021/ed036p288.

(118) Wang, Z.; Pan, X.; He, Y.; Hu, Y.; Gu, H.; Wang, Y. Piezoelectric Nanowires in Energy Harvesting Applications. *Adv. Mater. Sci. Eng.* **2015**, *2015*. https://doi.org/10.1155/2015/165631.

(119) Yucel, T.; Cebe, P.; Kaplan, D. L. Structural Origins of Silk Piezoelectricity. *Adv. Funct. Mater.* **2011**, *21* (4), 779–785. https://doi.org/10.1002/adfm.201002077.

(120) Sauerbrey, G. Verwendung von Schwingquarzen Zur Wägung Dünner Schichten Und Zur Mikrowägung. *Zeitschrift für Phys.* **1959**, *155* (2), 206–222. https://doi.org/10.1007/BF01337937.

(121) Kanazawa, K., K.; Gordon, J. G. Frequency of a Quartz Microbalance in Contact with Liquid. *Anal. Chem.* **1985**, *57*, 1770–1771.

(122) Janshoff, A.; Galla, H. J.; Steinem, C. Piezoelectric Mass-Sensing Devices as Biosensors - An Alternative to Optical Biosensors? *Angew. Chemie - Int. Ed.* **2000**, *39* (22), 4004–4032. https://doi.org/10.1002/1521-3773(20001117)39:22<4004::AID-ANIE4004>3.0.CO;2-2.

(123) Tonda-Turo, C.; Carmagnola, I.; Ciardelli, G. Quartz Crystal Microbalance with Dissipation Monitoring: A Powerful Method to Predict the in Vivo Behavior of Bioengineered Surfaces. *Front. Bioeng. Biotechnol.* **2018**, *6*, 1–7. https://doi.org/10.3389/fbioe.2018.00158.

(124) Parveen, N.; Jana, P. K.; Schönhoff, M. Viscoelastic Properties of Polyelectrolyte Multilayers Swollen with Ionic Liquid Solutions. *Polymers* **2019**, *11* (8). https://doi.org/10.3390/polym11081285.

(125) O'Neal, J. T., Dai, E. Y.; Zhang, Y., Clark, K. B.; Wilcox, K. G.; George, I. M.; Ramasamy, N. E.; Enriquez, D.; Batys, P.; Sammalkorpi, M. QCM-D Investigation of Swelling Behavior of Layer-by-Layer Thin Films upon Exposure to Monovalent Ions. *Langmuir* **2018**, *34*, 999–1009. https://doi.org/10.1021/acs.langmuir.7b02836.

(126) Feldötö, Z.; Varga, I.; Blomberg, E. Influence of Salt and Rinsing Protocol on the Structure of PAH/PSS Polyelectrolyte Multilayers. *Langmuir* **2010**, *26* (22), 17048–17057. https://doi.org/10.1021/la102351f.

(127) Dunér, G.; Thormann, E.; Dedinaite, A. Quartz Crystal Microbalance with Dissipation (QCM-D) Studies of the Viscoelastic Response from a Continuously Growing Grafted Polyelectrolyte Layer. *J. Colloid Interface Sci.* **2013**, *408* (1), 229–234. https://doi.org/10.1016/j.jcis.2013.07.008.

(128) Reviakine, I.; Johannsmann, D.; Richter, R. P. Hearing What You Cannot See and Visualizing What You Hear: Interpreting Quartz Crystal Microbalance Data from Solvated Interfaces. *Anal. Chem.* **2011**, *83* (23), 8838–8848. https://doi.org/10.1021/ac201778h.

(129) Cao, Z.; Guo, J.; Fan, X.; Xu, J.; Fan, Z.; Du, B. Detection of Heavy Metal Ions in Aqueous Solution by P(MBTVBC-Co-VIM)- Coated QCM Sensor. *Sensors Actuators, B Chem.* **2011**, *157* (1), 34–41. https://doi.org/10.1016/j.snb.2011.03.023.

(130) Liu, Z.; Hedayati, P.; Ghatkesar, M. K.; Sun, W.; Onay, H.; Groenendijk, D.; van Wunnik, J.; Sudhölter, E. J. R. Reducing Anionic Surfactant Adsorption Using Polyacrylate as Sacrificial Agent Investigated by QCM-D. *J. Colloid Interface Sci.* **2021**, *585*, 1–11. https://doi.org/10.1016/j.jcis.2020.11.090.

(131) Escuderos, M. E.; Sánchez, S.; Jiménez, A. Quartz Crystal Microbalance (QCM) Sensor Arrays Selection for Olive Oil Sensory Evaluation. *Food Chem.* **2011**, *124* (3), 857–862. https://doi.org/10.1016/j.foodchem.2010.07.007.

(132) Selyanchyn, R.; Wakamatsu, S.; Hayashi, K.; Lee, S. A Nano-Thin Film-Based Prototype QCM Sensor Array for Monitoring Human Breath and Respiratory Patterns. *Sensors* **2015**, *15*, 18834–18850. https://doi.org/10.3390/s150818834.

(133) Wei, J.; Hoagland, D. A.; Zhang, G.; Su, Z. Effect of Divalent Counterions on Polyelectrolyte Multilayer Properties. *Macromolecules* **2016**, *49* (5), 1790–1797. https://doi.org/10.1021/acs.macromol.5b02151.

(134) Zhang, Z.; Dou, Q.; Gao, H.; Bai, B.; Zhang, Y.; Hu, D.; Yetisen, A. K.; Butt, H.; Yang, X.; Li, C.; et al. 30 s Response Time of K^+ Ion-Selective Hydrogels Functionalized with 18-Crown-6 Ether Based on QCM Sensor. *Adv. Healthc. Mater.* **2018**, *7* (5), 1–7. https://doi.org/10.1002/adhm.201700873.

Chapter 2

Recent Advances in Cation Selectivity with Capacitive Deionization

An adapted version of this chapter is part of the following review:

Gamaethiralalage, J.G.; Singh, K.; Sahin, S.; Yoon, J.; Elimelech, M.; Suss, M.E.; Liang, P.; Biesheuvel, P.M.; Zornitta, R.L.; de Smet, L.C.P.M. Recent Advances in Ion Selectivity with Capacitive Deionization, *Energy Environ. Sci.* **2021**, 14, 1095-1120.

“There is a difference between knowing the path and walking the path.”

(Matrix)

2.1 General Introduction

Within the last decade, in addition to water desalination, capacitive deionization (CDI) has been used in the selective separation of ions in multicomponent solutions as well as for resource recovery as outlined in Chapter 1. Given the scope of this thesis, Chapter 2 is focused on the selectivity of cations in CDI. For CDI-related anion selectivity – both at the level of electrodes and membranes – intercalation materials, as well as a review on modelling and theory of CDI processes with a focus on ion selectivity, we refer to our study covering a more complete review on recent advances in pursuing ion selectivity with CDI.[1] Numerous methods have been suggested to improve or introduce cation selectivity in CDI. For instance, the use of electrode materials with different pore sizes and compositions, the presence of additional functional groups on electrode surface, the introduction of standard or special-grade ion-selective membranes, and the optimization of the operational parameters in CDI operation, or combinations of them. The cation-selective CDI literature can be categorized in two sections: selectivity achieved with electrodes (**Chapter 2.2** or with implementation of membranes (**Chapter 2.3**).

Furthermore, some of the widely used selectivity definitions are provided in **Table 2.1** to enable a comparison between different studies in literature. One of the challenging aspects in reviewing literature on ion selectivity in CDI stems from the many different approaches utilized by different research groups. Although a direct comparison between these studies may not be fully possible, at least the table can ease the comparison of different selectivity definitions. These definitions are based on taking solutions with two competing ions (of the same polarity), *i* and *j*, into account. In some literature, the two components are referred to as target (*t*) and competing (*c*) ions. It is evident that ρ and $S_{i/j}$ are similar in nature as both parameters calculate the selectivity based on the amount of ions removed by the electrodes. However, *R* reflects the amount of ions left in the effluent. Therefore, taking *i* to be the ion of interest, a ρ or $S_{i/j}$ value *above one* indicates that the system is selective towards the ion of interest, while in the R-definition this is the case for a value *less than one*.

Table 2.1. Commonly used ion-selectivity definitions in literature. Here, *i* and *j* are two competing ions.

Symbol	Equation	Description
ρ	$\frac{\frac{c_{\mathrm{i,in}} - c_{\mathrm{i,f}}}{c_{\mathrm{i,in}}}}{\frac{c_{\mathrm{j,in}} - c_{\mathrm{j,f}}}{c_{\mathrm{j,in}}}}$	$c_{\mathrm{i,in}}$ and $c_{\mathrm{i,f}}$ are initial and final concentrations of the target ion. $c_{\mathrm{j,in}}$ and $c_{\mathrm{j,f}}$ are initial and final concentrations of the competing ion.
$S_{i/j}$	$\frac{\int_0^t \left(c_{\mathrm{i,inf}} - c_{\mathrm{i,eff}}\right)dt / c_{\mathrm{i,inf}}}{\int_0^t \left(c_{\mathrm{j,inf}} - c_{\mathrm{j,eff}}\right)dt / c_{\mathrm{j,inf}}}$	$c_{\mathrm{i,inf}}$, $c_{\mathrm{i,eff}}$, $c_{\mathrm{j,inf}}$, $c_{\mathrm{j,eff}}$ are concentrations (c) of influent (inf) and effluent (eff) of two competing ions, *i* and *j*, respectively.
R	$\frac{R_{\mathrm{i}}}{R_{\mathrm{j}}}$	R_{i} and R_{j} are calculated by dividing the effluent concentration by feed concentration of each ion.

2.2 Electrodes for Cation Selectivity

In this section covers an overview of the types of electrodes and electrode materials that have been explored within the context of cation selectivity in CDI. In CDI, porous carbon is the most commonly used electrode material for desalination and selective ion separation. One of the most-studied parameters for ion selectivity is the pore characteristics of the electrode material. In 2001, Eliad *et al.* demonstrated the relationship between ion selectivity and the size of the hydrated ion, concluding that the monovalent ions were preferred over divalent ions. It was attributed to the smaller hydrated size of the studied monovalent ions compared to the average pore size of the electrode, *i.e.* carbon.[2] Similarly, Gabelich *et al.* also studied the effect of the micropore size of carbon aerogel electrodes and reported selectivity towards monovalent over divalent cations.[3] This claim was later confirmed by Avraham *et al*.[4] They studied the same effect by using carbon fiber as the electrode material. Moreover, Han *et al.* studied the dependence of selectivity on pore size distribution using three different types of activated carbon cloth.[5] Depending on the mesoporosity/microporosity ratio, the electrodes revealed distinct trends for ions with different hydrated radii. A larger hydrated radius caused a reduction in electrosorption of the ion with increased microporosity of the electrode whereas smaller ions were better accommodated on the surface of the electrode. These results indicate that micropores

adsorb more ions with smaller hydrated radius when the hydrated size of ion is comparable to pore size.[5] This ion-sieving effect is illustrated in **Figure 2.1B** Hou and Huang studied this phenomenon for multicomponent mixtures concluding that the affinity among the monovalent cations is affected by their hydrated radii. This trend was also confirmed by other studies.[6–8] Furthermore, they also observed divalent over monovalent cation selectivity from a mixture containing two competing ions.[9] Mossad *et al.* also observed that Ca^{2+} and Mg^{2+} were preferentially electrosorbed compared to Na^{+} in line with Hou and Huang.[10] Between Ca^{2+} and Mg^{2+}, a higher Ca^{2+} removal efficiency was observed, which again was attributed to the smaller hydrated radii of calcium ions. Furthermore, Hassanvand *et al.* reported that normalized electrosorption capacities of Ca^{2+}, Na^{+}, and K^{+} are comparable when the ions have equivalent ratios in the feed solution. However, Ca^{2+} adsorbed and then desorbed slower than Na^{+} and K^{+} due to its larger size (**Figure 2.1B**) and therefore slower diffusion rate.[11] Seo *et al.* investigated the effect of morphological characteristics of carbon aerogel electrodes on the electrosorption rates of different cations and – contrary to previous series of observations on size-based selectivity – observed a higher selectivity for Ca^{2+} and Mg^{2+} over the monovalent ions. The authors rationalized their results in terms of the pore structure (branched micropores and highly accessible mesopores) and wettability of the electrodes.[12]

In addition to the pore size and morphological characteristics of the electrodes, the valence of the adsorbing ion has an influence on its selectivity. Studies have reported that ions with a higher valence are more effectively adsorbed in the EDL due to their stronger interactions with the electrodes.[10,12–14] In a mixture of mono- and divalent ions, at equilibrium the divalent ions were preferably electrosorbed as a result of the higher electrostatic attraction (**Figure 2.1A**).[15] Gao *et al.* obtained a higher divalent ion selectivity using carbon nanotube and carbon nanofiber electrodes due to charge-exclusion effect as depicted in (**Figure 2.1B**).[8] They also stated that ions with smaller hydrated radii were preferred if they have the same valence. Ions with identical valence are electrosorbed according to their hydration energy (**Figure 2.1D**). Thus, ions with lower hydration energy are preferred as their hydration shell can be readily rearranged inside the pores.[16]

In addition to the properties of the electrode and the adsorbing ion, the operational parameters in CDI can affect the ion selectivity. Zhao *et al.* proposed and validated a theory of selectivity for a solution with 5:1 Na^+ and Ca^{2+} feed ratio.[17] The authors reported a time-dependent selectivity as Na^+ was electrosorbed 5 times more than Ca^{2+} at the early stage of desalination cycle. The higher electrosorption of sodium ions is explained by the higher concentration, causing higher diffusion to the pores of the electrode (**Figure 2.1C**). However, with time, the preference switches to Ca^{2+} due to the stronger interaction between the divalent ion and the electrode surface, causing a ion-swapping effect, shown in **Figure 2.1A**. Hou and Huang also studied the effect of feed concentration on ion selectivity.[9] By varying the concentrations of K^+, Na^+, Ca^{2+}, and Mg^{2+}, the authors observed that an increase in Na^+ concentration over other cations yielded preferential electrosorption of Na^+, which was attributed to the higher availability of sodium ions. Apart from varying the feed concentration, they also studied the effect of applied potential on the electrosorption capacities of different ions, and concluded that increasing the voltage increased the preferential removal of K^+ over Na^+ and Na^+ over Ca^{2+}.

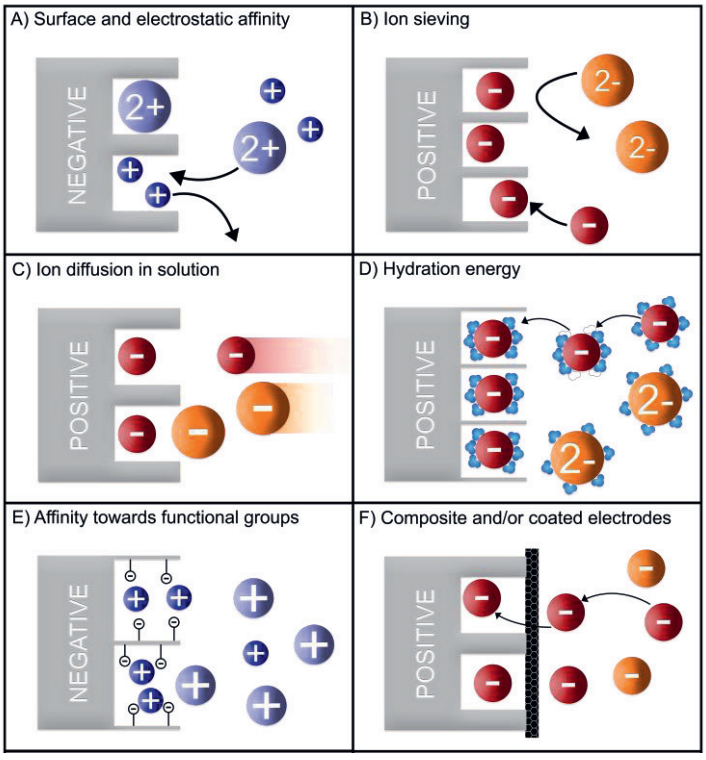

Figure 2.1. Generalized selectivity mechanisms for porous carbon electrodes based on (A) surface and electrostatic effect, (B) ion sieving, (C) ion diffusion in solution, (D) hydration energy, (E) affinity towards functional groups, and (F) composite and/or coated electrodes. The displayed mechanisms were based on the main selectivity feature of the electrode/electrolyte reported in literature and some works may be categorized into more than one panel. For matters of simplicity, the hydration shells are only depicted in the mechanisms where they play an important role in obtaining selectivity. Also, the mechanisms demonstrated above apply for both cations and anions.

The use of modified electrodes and/or composite electrodes is also a common method of enhancing ion selectivity (**Figure 2.1F**). In one study that employed carbon nanotube (CNT)/zeolite composite electrodes, Ca^{2+} and Mg^{2+} adsorption increased in single-

salt batch experiments, with increasing zeolite to CNT ratio.[18] However, the performance of the zeolite-CNT electrodes deteriorated within a few cycles, suggesting that it was either degraded or not fully regenerated. Yoon *et al*. used a calcium-alginate coated carbon electrode in CDI.[19] The coated cathode adsorbed more Ca^{2+} over Na^{+}. While no selectivity coefficients were presented, we estimated a selectivity (ρ) of 2.5 for calcium ions over sodium ions using the provided graphs. The selectivity was attributed to the strong affinity of Ca^{2+} towards alginate. Similarly, Kim *et al.* reached Ca^{2+} over Na^{+} selectivity of 3.5 - 5.5 ($S_{i/j}$) with a calcium-selective nanocomposite layer (**Figure 2.1F**).[20]

Moreover, selective adsorption of divalent (calcium and magnesium) over monovalent (sodium) ions has recently been achieved via activated carbon (AC) electrodes, that were modified with mordenite (MOR), a zeolite mineral.[21] The resulting MOR-AC electrodes displayed a preference for hardness ions in multi-ionic solutions with selectivity values of 8.0 and 7.5 for Ca^{2+}/Na^{+} and Mg^{2+}/ Na^{+} selectivity, respectively. The electrode was found to be highly regenerable and stable over 50 cycles. Another common way of separating monovalent cations from the divalent ones is the chemically charging of porous carbon electrodes (via oxidation processes) to introduce carboxylic or sulfonic acid functional groups to the electrode surface. For instance, in 2021 Guyes *et al.* obtained a Na^{+}/Ca^{2+} selectivity of 1.6 with sulfonated cathodes.[22] The selectivity is attributed to the preferential storage of Na^{+} at sulfonic acid-functionalized cathode nanopores in combination with using short charging times. However, at longer charging times, the monovalent cation selectivity was found to be lost. In a follow-up study it was shown that the selectivity of sulfonated carbon electrodes can be tuned towards divalent cations via the optimization of the operational conditions, which also resulted in an experimental energy consumption of less than 0.1 kWh/m^3.[23] Furthermore, oxidized electrodes have also demonstrated size-based ion selectivity among monovalent cations, where smaller size ions have been preferentially electrosorbed over larger ions.[24] The origin of this selectivity was attributed to the more dense counterion packing of the smaller ions at the chemically charged micropores.

Apart from more commonly targeted alkali and alkaline-earth metals, selective removal of heavy metals has also been of interest in CDI. In 2010, Li *et al.* utilized electrodes made of graphene nanoflakes to remove Fe^{3+} and compared the electrosorption capacity with Mg^{2+}, Ca^{2+}, and Na^{+} in single-salt experiments.[25] The Fe^{3+} were preferred over the others, which was attributed to its higher valence (**Figure 2.1A**). Between Ca^{2+} and Mg^{2+}, Ca^{2+} were preferred due to their smaller hydrated radii (**Figure 2.1B**), as described before, whereas Na^{+} exhibited the lowest electrosorption among all. In another study, Huang *et al.* employed activated carbon electrodes to remove Cu^{2+} from aqueous solutions.[26] They also compared the Cu^{2+} electrosorption in the presence of NaCl, natural organic matter (NOM), and dissolved reactive silica in binary salt solutions, and reported that Cu^{2+} removal decreases with an increasing amount of the competitive species. However, no significant decrease in Cu^{2+} electrosorption was observed in the presence of dissolved reactive silica.

A heavy metal (Pb^{2+}) and salt (Na^{+}) recovery method from wastewater using 3D graphene-based electrodes was proposed by Liu *et al.*[27] They used 3D graphene electrodes modified with ethylenediamine triacetic acid (EDTA) and 3-aminopropyltriethoxysilane (APTES) as the cathode and the anode, respectively. Two different mechanisms were presented for Pb^{2+} and Na^{+} removal. Pb^{2+} is adsorbed *via* a chelation reaction with EDTA (**Figure 2.1E**), whereas Na^{+} is adsorbed *via* electrosorption in the pores. Based on these mechanisms, the separation of ions was achieved during the desorption stage. First, Na^{+} was desorbed by applying an inverse potential, followed by a short circuit potential. Afterwards Pb^{2+} was desorbed in a separate step using nitric acid as an eluent.

Selective removal of Pb^{2+} over Ca^{2+} and Mg^{2+} was studied by Dong *et al.* by using activated carbon electrodes in an asymmetric CDI setup. This setup only contained an AEM (hence asymmetric), as the Pb^{2+} desorption was reported inefficient when a CEM was used as well, thus hindering its selectivity.[28] The asymmetric system was selective towards Pb^{2+} over Ca^{2+} and Mg^{2+}. The selectivity mechanism was hypothesized to be a swapping process where Ca^{2+} and Mg^{2+} are initially adsorbed due to their higher mobilities, but later replaced

by Pb^{2+} owing to its higher affinity towards the native functional groups (*e.g.*, carboxyl groups) present on the electrode.

Recently, Zhang *et al.* used activated carbon in flow CDI to selectively remove Cu^{2+} from a solution which also contained Na^{+}.[29] A higher affinity towards Cu^{2+} was obtained in the system. This was attributed to the preferential adsorption of Cu^{2+} on the carbon particles and was also reduced to Cu. The preference of carbon towards divalent over monovalent cations, as shown in **Figure 2.1A** was also reported here. The Na^{+} removed from the feed remained in the electrolyte of the flow electrode. In 2021, Gao *et al.* prepared FeS_2@N, S co-doped carbon (FeS_2@NSC) composite electrodes, which were explored for the selective electrosorption of Cu^{2+}.[30] In this study, FeS_2@NSC electrodes resulted in Cu^2/Na^{+} selectivity over 70, which was explained by the Faradic redox reactions of the Cu^{2+}/Cu^{+} and Fe^{2+}/Fe^{3+} couples. During the electrosorption cycle, Fe^{2+} is oxidized to Fe^{3+} and simultaneously the target Cu^{2+} ions are reduced to Cu^{+} ions and stored inside the electrodes. In 2021, Tian *et al*. prepared a composite electrodes from activated carbon and an amino phosphoric acid chelating cation-exchange resin (D86O), which were employed in the separation of vanadium(IV) oxide (VO^{2+}) from multi-ionic solutions containing metal ions.[31] The selectivity of the resulting D860/AC electrodes followed the order of $VO^{2+} > Fe^{2+} > Al^{3+}$. The hydration radius of the ion was found to have a significant effect on adsorption selectivity. Moreover, while the electrosorption of Fe^{2+} and Al^{3+} was explained by the formation EDLs, the dominant adsorption of VO^{2+} was attributed to the formation of chemical bonds of the VO^{2+} with the electrode.

The removal of an unconventional ion, uranium (VI), using phosphate-functionalized graphene hydrogel electrodes was studied by Liao *et al.*[32] The electrodes were tested in equimolar solutions (0.3 mM) containing uranium (VI) and a series of interfering metals ions (Cs^{+}, Co^{2+}, Ni^{2+}, Sr^{2+}, and Eu^{3+}). The authors reported that the electrodes preferred uranium (VI) over all the other metals that were tested. Furthermore, they observed that the uranium (VI) is more selective against monovalent metal ions compared to that of divalent or trivalent ions. This phenomenon was attributed to the

stronger electrostatic interaction between trivalent ions and the electrode surface, thus adsorbing more trivalent ions resulting in reduced selectivity of uranium (VI). Apart from ion valence, the selectivity of the electrode is also attributed to the formation of strong acid-base complexes with the phosphate groups attached to the electrode (**Figure 2.1E**).

To conclude this section, the use of various electrode materials and/or modification of electrodes and electrode surfaces, as well as tuning operational conditions have evidently proven to be successful strategies to tune cation selectivity in CDI processes.

2.3 Membranes for Cation Selectivity

In the previous section, CDI cation selectivity was discussed in terms of electrodes, also the use of membranes plays a vital role in CDI. This section is dedicated for exploring the studies which rely on membranes for achieving ion selectivity. Several different studies have demonstrated the advantages of using ion-exchange membranes (IEMs) to prevent co-ion repulsion, reduce anode oxidation, and to boost the salt removal by employing gradient of solutions in multi-chamber cells.[33,34] An IEM can also be used as a barrier for specific ions, and therefore, improve the ion selectivity.

Commercially available cation-exchange membranes (CEMs) like Neosepta CMX typically have negatively charged functional groups (*e.g.*, carboxylate, sulfonate, and phenolate) in the membrane backbone, which only allow cations to migrate through the membrane.[35] On the other hand there are CEMs that exhibit affinities towards certain monovalent ions, such as monovalent cation-selective membranes CSO (*e.g.*, Selemion) and CMS, (*e.g.*, Neosepta). CMS membrane has a highly cross-linked (bulk) structure which allows monovalent cations with smaller hydrated size to diffuse through the membrane, while rejecting the cations with bigger hydrated size. On the other hand, CSO membrane is coated with a thin positively charged layer which rejects divalent over monovalent cations due to the charge exclusion effect.[36–38] In general, the selectivity of such resins and membranes is based on the difference in charge (**Figure 2.2B**) and/or size (**Figure 2.2.C**) of

the ions, as well as the affinity of the membranes towards certain type of ions (**Figure 2.2A**).[39]

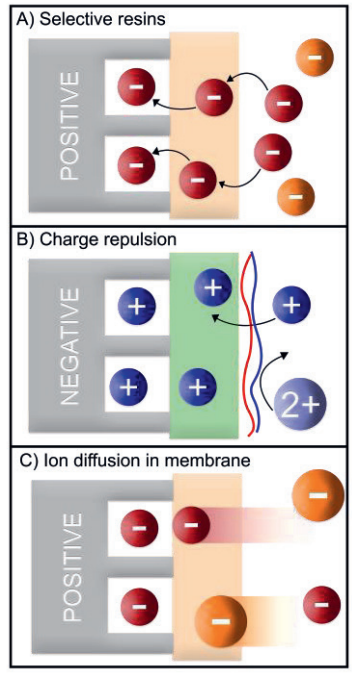

Figure 2.2. Generalized selectivity mechanisms in MCDI based on (A) selective resins (or membranes), (B) charge repulsion, and (C) ion diffusion in membranes. The mechanisms demonstrated above apply for both cations and anions.

In CDI experiments using a CMX membrane, selectivity towards divalent over monovalent cations was reported.[40,41] Although the CMX membrane was not designed to differentiate between different cations, its negatively charged outermost layer attracts divalent more than the monovalent cations.[42] Hassanvand *et al.* stated that the implementation of CMX in CDI leads to sharper desorption peaks of divalent cations since larger amounts of di- over monovalent cations are temporarily stored within the CMX membrane.[11] On the other hand, the CMS membrane resulted in preferential transport of

monovalent over divalent cations.[43] Similarly, Choi *et al.* used a CMS membrane and obtained monovalent cation selectivity (*R*) of 1.8 for sodium over calcium ions.[42] By selectively removing Na^+, a Ca^{2+}-rich solution was obtained. In addition, the selectivity attained its maximum value at higher cell voltages, pH, and lower TDS (total dissolved solids) concentration.

Similar to Choi *et al*., Shi *et al.* also used an MCDI system equipped with a CMS membrane to recover Li^+ in the presence of Mg^{2+}, and obtained a selectivity (ρ) of 3.[43] They observed a decrease in the selectivity from ≈ 3 to 2 upon increasing voltage. We assume that the increase in driving force reduced the blocking effect of the membrane as there are more charge interactions between divalent cations and the electrodes compared to monovalent cations. An increase in flow rate also increased the selectivity until a certain flow rate after which, the selectivity decreased. Furthermore, they studied the effect of operation time, and found that the adsorption was found to be slower for Mg^{2+} compared to Li^+. Sahin *et al.* implemented a layer-by-layer (LbL) polyelectrolyte multilayer (PEM) on a CMX membrane in order to tune the monovalent cation selectivity in MCDI (**Figure 2.2B**).[44] While the bare CMX membrane had a ρ of ≈ 0.5 for Na^+ over Mg^{2+}, the selectivity of the PEM-coated membrane was found to be ≈ 3. This switch in selectivity was attributed to the charge rejection experienced by ions with higher valence (**Figure 2.1B**) due to the presence of the PEM. In 2022, after switching from constant voltage to constant current operation mode and optimization of series operational parameters, the same PEM-coated CMX membrane was reported to be practically fully mono- over divalent cation selective.[45] Recently, another example of LbL-coated CMX membrane was fabricated by using tannic acid and polyethyleneimine and the dense structure and abundant positive charge of the PEM coating resulted in a Na^+/Mg^{2+} selectivity of ≈42 in a constant current operation.[46]

He *et al.* performed FCDI experiments with a CMX and AEM (both Fujifilm Type-1). They varied the current density and the hydraulic retention time (HRT) in a single pass, galvanostatic mode and reached a maximum selectivity (ρ) of ≈ 6 for Ca^{2+} over Na^+, for the lowest current density and HRT.[47] They hypothesized that Ca^{2+} transport is favored due to

the passive adsorption of Ca^{2+} on the membrane surface. Similarly, Wang *et al*. focused on the effect of current density, HRT, and ratio of different ions in the feed solution [40]. They observed a selectivity (ρ) of ≈ 3 for calcium ions over sodium ions. Higher current density and HRT produced higher the selectivity, which agrees well with He *et al*. Moreover, increase in Ca^{2+} over Na^{+} in the feed caused an increase in Ca^{2+} selectivity.

2.4 Concluding Remarks

Upon reviewing literature it becomes evident that the interest in ion-selective CDI is growing swiftly. When compared to the use of membranes in CDI, this recently has led to significant advances, especially in the use of different electrode materials for cation as well as anion selectivity. However, a direct comparison of these studies is challenging due to diversity in methods, techniques, and materials employed in achieving ion selectivity,. Furthermore, ion-selectivity studies carried out in single-salt solutions to compare individual electrosorption rates to obtain selectivity numbers, provide little information on the electrosorption behavior in competitive environments that resemble real-life cases. While it is challenging to introduce a standardized procedure to report ion selectivity, due to numerous different ion combinations, it may be sensible to provide a selectivity coefficient for one ion in a mixture over the others, an approach commonly used in sensor studies.[48,49] Also, the dependence of ion selectivity on operation parameters such as applied current, cell voltage, ion concentration, and pH, among others, will have to be systematically studied to find optimum conditions that enhance selectivity for the CDI cell. A standard set of operational parameters, similar to those proposed to objectively assess CDI systems,[50] would further enable a better comparison between upcoming ion-selective literature. For example, it would be beneficial to provide at least one set of experiments using single-pass mode under constant current, with the values of feed and outlet concentration of each ion clearly defined.

References

(1) Gamaethiralalage, J. G.; Singh, K.; Sahin, S.; Yoon, J.; Elimelech, M.; Suss, M. E.; Liang, P.; Biesheuvel, P. M.; Zornitta, R. L.; de Smet, L. C. P. M. Recent Advances in Ion Selectivity with Capacitive Deionization. *Energy Environ. Sci.* **2020**, *14*, 1095–1120. https://doi.org/10.1039/d0ee03145c.

(2) Eliad, L.; Salitra, G.; Soffer, A.; Aurbach, D. Ion Sieving Effects in the Electrical Double Layer of Porous Carbon Electrodes: Estimating Effective Ion Size in Electrolytic Solutions. *J. Phys. Chem. B* **2001**, *105* (29), 6880–6887. https://doi.org/10.1021/jp010086y.

(3) Gabelich, C. J.; Tran, T. D.; Suffet, I. H. Electrosorption of Inorganic Salts from Aqueous Solution Using Carbon Aerogels. *Environ. Sci. Technol.* **2002**, *36*, 3010–3019. https://doi.org/10.1021/es0112745.

(4) Avraham, E.; Yaniv, B.; Soffer, A.; Aurbach, D. Developing Ion Electroadsorption Stereoselectivity, by Pore Size Adjustment with Chemical Vapor Deposition onto Active Carbon Fiber Electrodes. Case of Ca^{2+} /Na^{+} Separation in Water Capacitive Desalination. *J. Phys. Chem. C.* **2008**, *112*, 7385–7389. https://doi.org/10.1021/jp711706z.

(5) Han, L.; Karthikeyan, K. G.; Anderson, M. A.; Gregory, K. B. Exploring the Impact of Pore Size Distribution on the Performance of Carbon Electrodes for Capacitive Deionization. *J. Colloid Interface Sci.* **2014**, *430*, 93–99. https://doi.org/10.1016/j.jcis.2014.05.015.

(6) Dykstra, J. E.; Dijkstra, J.; Van der Wal, A.; Hamelers, H. V. M.; Porada, S. On-Line Method to Study Dynamics of Ion Adsorption from Mixtures of Salts in Capacitive Deionization. *Desalination* **2016**, *390*, 47–52. https://doi.org/10.1016/j.desal.2016.04.001.

(7) Suss, M. E. Size-Based Ion Selectivity of Micropore Electric Double Layers in Capacitive Deionization Electrodes. *J. Electrochem. Soc.* **2017**, *164* (9), E270–E275. https://doi.org/10.1149/2.1201709jes.

(8) Gao, Y.; Pan, L.; Li, H. B.; Zhang, Y.; Zhang, Z.; Chen, Y.; Sun, Z. Electrosorption Behavior of Cations with Carbon Nanotubes and Carbon Nanofibres Composite Film Electrodes. *Thin Solid Films* **2009**, *517* (5), 1616–1619. https://doi.org/10.1016/j.tsf.2008.09.065.

(9) Hou, C. H.; Huang, C. Y. A Comparative Study of Electrosorption Selectivity of Ions by Activated Carbon Electrodes in Capacitive Deionization. *Desalination* **2013**, *314*, 124–129. https://doi.org/10.1016/j.desal.2012.12.029.

(10) Mossad, M.; Zhang, W.; Zou, L. Using Capacitive Deionisation for Inland Brackish Groundwater Desalination in a Remote Location. *Desalination* **2013**, *308*, 154–160. https://doi.org/10.1016/j.desal.2012.05.021.

(11) Hassanvand, A.; Chen, G. Q.; Webley, P. A.; Kentish, S. E. A Comparison of Multicomponent Electrosorption in Capacitive Deionization and Membrane Capacitive Deionization. *Water Res.* **2018**, *131*, 100–109. https://doi.org/10.1016/j.watres.2017.12.015.

(12) Seo, S. J.; Jeon, H.; Lee, J. K.; Kim, G. Y.; Park, D.; Nojima, H.; Lee, J.; Moon, S. H. Investigation on Removal of Hardness Ions by Capacitive Deionization (CDI) for Water Softening Applications. *Water Res.* **2010**, *44*, 2267–2275. https://doi.org/10.1016/j.watres.2009.10.020.

(13) Xu, P.; Drewes, J. E.; Heil, D.; Wang, G. Treatment of Brackish Produced Water Using Carbon Aerogel-Based Capacitive Deionization Technology. *Water Res.* **2008**, *42*, 2605–2617. https://doi.org/10.1016/j.watres.2008.01.011.

(14) Mossad, M.; Zou, L. A Study of the Capacitive Deionisation Performance under Various Operational Conditions. *J. Hazard. Mater.* **2012**, *213–214*, 491–497. https://doi.org/10.1016/j.jhazmat.2012.02.036.

(15) Li, Y.; Zhang, C.; Jiang, Y.; Wang, T. J.; Wang, H. Effects of the Hydration Ratio on the Electrosorption Selectivity of Ions during Capacitive Deionization. *Desalination* **2016**, *399*, 171–177. https://doi.org/10.1016/j.desal.2016.09.011.

(16) Kalluri, R. K.; Biener, M. M.; Suss, M. E.; Merrill, M. D.; Stadermann, M.; Santiago, J. G.; Baumann, T. F.; Biener, J.; Striolo, A. Unraveling the Potential and Pore-Size Dependent Capacitance of Slit-Shaped Graphitic Carbon Pores in Aqueous Electrolytes. *Phys. Chem. Chem. Phys.* **2013**, *15* (7), 2309–2320. https://doi.org/10.1039/c2cp43361c.

(17) Zhao, R.; van Soestbergen, M.; Rijnaarts, H. H. M.; van der Wal, A.; Bazant, M. Z.; Biesheuvel, P. M. Time-Dependent Ion Selectivity in Capacitive Charging of Porous Electrodes. *J. Colloid Interface Sci.* **2012**, *384*, 38–44. https://doi.org/10.1016/j.jcis.2012.06.022.

(18) Liu, Y.; Ma, W.; Cheng, Z.; Xu, J.; Wang, R.; Gang, X. Preparing CNTs/Ca-Selective Zeolite Composite Electrode to Remove Calcium Ions by Capacitive Deionization. *Desalination* **2013**, *326*, 109–114. https://doi.org/10.1016/j.desal.2013.07.022.

(19) Yoon, H.; Lee, J.; Kim, S. R.; Kang, J.; Kim, S.; Kim, C.; Yoon, J. Capacitive Deionization with Ca-Alginate Coated-Carbon Electrode for Hardness Control. *Desalination* **2016**, *392*, 46–53. https://doi.org/10.1016/j.desal.2016.03.019.

(20) Kim, J.; Jain, A.; Zuo, K.; Verduzco, R.; Walker, S.; Elimelech, M.; Zhang, Z.; Zhang, X.; Li, Q. Removal of Calcium Ions from Water by Selective Electrosorption Using Target-Ion Specific Nanocomposite Electrode. *Water Res.* **2019**, *160*, 445–453. https://doi.org/10.1016/j.watres.2019.05.016.

(21) Nie, P.; Hu, B.; Shang, X.; Xie, Z.; Huang, M.; Liu, J. Highly Efficient Water Softening by Mordenite Modified Cathode in Asymmetric Capacitive Deionization. *Sep. Purif. Technol.* **2020**, *250*. https://doi.org/10.1016/j.seppur.2020.117240.

(22) Guyes, E. N.; Shocron, A. N.; Chen, Y.; Diesendruck, C. E.; Suss, M. E. Long-Lasting, Monovalent-Selective Capacitive Deionization Electrodes. *npj Clean Water* **2021**, *4* (1). https://doi.org/10.1038/s41545-021-00109-2.

(23) Uwayid, R.; Guyes, E. N.; Shocron, A. N.; Gilron, J.; Elimelech, M.; Suss, M. E. Perfect Divalent Cation Selectivity with Capacitive Deionization. *Water Res.* **2022**, *210*, 117959. https://doi.org/10.1016/j.watres.2021.117959.

(24) Guyes, E. N.; Malka, T.; Suss, M. E. Enhancing the Ion-Size-Based Selectivity of Capacitive Deionization Electrodes. *Environ. Sci. Technol.* **2019**, *53* (14). https://doi.org/10.1021/acs.est.8b06954.

(25) Li, H.; Zou, L.; Pan, L.; Sun, Z. Using Graphene Nano-Flakes as Electrodes to Remove Ferric Ions by Capacitive Deionization. *Sep. Purif. Technol.* **2010**, *75* (1), 8–14. https://doi.org/10.1016/j.seppur.2010.07.003.

(26) Huang, S.-Y.; Fan, C.-S.; Hou, C.-H. Electro-Enhanced Removal of Copper Ions from Aqueous Solutions by Capacitive Deionization. *J. Hazard. Mater.* **2014**, *278*, 8–15. https://doi.org/10.1016/J.JHAZMAT.2014.05.074.

(27) Liu, P.; Yan, T.; Zhang, J.; Shi, L.; Zhang, D. Separation and Recovery of Heavy Metal Ions and Salt Ions from Wastewater by 3D Graphene-Based Asymmetric Electrodes: via Capacitive Deionization. *J. Mater. Chem. A* **2017**, *5*, 14748–14757. https://doi.org/10.1039/c7ta03515b.

(28) Dong, Q.; Guo, X.; Huang, X.; Liu, L.; Tallon, R.; Taylor, B.; Chen, J. Selective Removal of Lead Ions through Capacitive Deionization: Role of Ion-Exchange Membrane. *Chem. Eng. J.* **2019**, *361*, 1535–1542. https://doi.org/10.1016/j.cej.2018.10.208.

(29) Zhang, X.; Yang, F.; Ma, J.; Liang, P. Effective Removal and Selective Capture of Copper from Salty Solution in Flow Electrode Capacitive Deionization. *Environ. Sci. Water Res. Technol.* **2020**, *6* (2), 341–350. https://doi.org/10.1039/c9ew00467j.

(30) Gao, Y.; Li, Z.; Fu, Z.; Zhang, H.; Wang, G.; Zhou, H. Highly Selective Capacitive Deionization of Copper Ions in FeS2@N, S Co-Doped Carbon Electrode from Wastewater. *Sep. Purif. Technol.* **2021**, *262*, 118336. https://doi.org/10.1016/j.seppur.2021.118336.

(31) Tian, X.; Bao, S.; Zhang, Y. Selective Adsorption Mechanism of Resin-Activated Carbon Composite Electrode for Capacitive Deionization. *Colloids Surfaces A Physicochem. Eng. Asp.* **2021**, *610*, 125935. https://doi.org/10.1016/j.colsurfa.2020.125935.

(32) Liao, Y.; Wang, M.; Chen, D. Electrosorption of Uranium(VI) by Highly Porous Phosphate-Functionalized Graphene Hydrogel. *Appl. Surf. Sci.* **2019**, *484*, 83–96. https://doi.org/10.1016/j.apsusc.2019.04.103.

(33) Biesheuvel, P. M.; Zhao, R.; Porada, S.; van der Wal, A. Theory of Membrane Capacitive Deionization Including the Effect of the Electrode Pore Space. *J. Colloid Interface Sci.* **2011**, *360* (1), 239–248. https://doi.org/10.1016/j.jcis.2011.04.049.

(34) Zornitta, R. L.; Ruotolo, L. A. M. Simultaneous Analysis of Electrosorption Capacity and Kinetics for CDI Desalination Using Different Electrode Configurations. *Chem. Eng. J.* **2018**, *332* (September 2017), 33–41. https://doi.org/10.1016/j.cej.2017.09.067.

(35) Hassanvand, A.; Wei, K.; Talebi, S.; Chen, G. Q.; Kentish, S. E. The Role of Ion Exchange Membranes in Membrane Capacitive Deionisation. *Membranes* **2017**, *7*, 1–23. https://doi.org/10.3390/membranes7030054.

(36) Moreno, J.; Díez, V.; Saakes, M.; Nijmeijer, K. Mitigation of the Effects of Multivalent Ion Transport in Reverse Electrodialysis. *J. Memb. Sci.* **2018**, *550*, 155–162. https://doi.org/10.1016/j.memsci.2017.12.069.

(37) Rijnaarts, T.; Reurink, D. M.; Radmanesh, F.; de Vos, W. M.; Nijmeijer, K. Layer-by-Layer Coatings on Ion Exchange Membranes: Effect of Multilayer Charge and Hydration on Monovalent Ion Selectivities. *J. Memb. Sci.* **2019**, *570–571*, 513–521. https://doi.org/10.1016/j.memsci.2018.10.074.

(38) Luo, T.; Abdu, S.; Wessling, M. Selectivity of Ion Exchange Membranes: A Review. *J. Memb. Sci.* **2018**, *555*, 429–454. https://doi.org/10.1016/j.memsci.2018.03.051.

(39) McNair, R.; Szekely, G.; Dryfe, R. A. W. Ion-Exchange Materials for Membrane Capacitive Deionization. *ACS ES&T Water* **2021**, *1* (2), 217–239. https://doi.org/10.1021/acsestwater.0c00123.

(40) Wang, L.; Lin, S. Mechanism of Selective Ion Removal in Membrane Capacitive Deionization for Water Softening. *Environ. Sci. Technol.* **2019**, *53*, 5797−5804. https://doi.org/10.1021/acs.est.9b00655.

(41) Sata, T.; Sata, T.; Yang, W. Studies on Cation-Exchange Membranes Having Permselectivity between Cations in Electrodialysis. *J. Memb. Sci.* **2002**, *206*, 31–60. https://doi.org/10.1016/S0376-7388(01)00491-4.

(42) Choi, J.; Lee, H.; Hong, S. Capacitive Deionization (CDI) Integrated with Monovalent Cation Selective Membrane for Producing Divalent Cation-Rich Solution. *Desalination* **2016**, *400*, 38–46. https://doi.org/10.1016/j.desal.2016.09.016.

(43) Shi, W.; Liu, X.; Ye, C.; Cao, X.; Gao, C.; Shen, J. Efficient Lithium Extraction by Membrane Capacitive Deionization Incorporated with Monovalent Selective Cation Exchange Membrane. *Sep. Purif. Technol.* **2019**, *210*, 885–890. https://doi.org/10.1016/j.seppur.2018.09.006.

(44) Sahin, S.; Dykstra, J. E.; Zuilhof, H.; Zornitta, R. L.; De Smet, L. C. P. M. Modification of Cation-Exchange Membranes with Polyelectrolyte Multilayers to Tune Ion Selectivity in Capacitive Deionization. *ACS Appl. Mater. Interfaces* **2020**, *12* (31), 34746–34754. https://doi.org/10.1021/acsami.0c05664.

(45) Sahin, S.; Zuilhof, H.; Zornitta, R. L.; de Smet, L. C. P. M. Enhanced Monovalent over Divalent Cation Selectivity with Polyelectrolyte Multilayers in Membrane Capacitive Deionization via Optimization of Operational Conditions. *Desalination* **2022**, *522*, 115391. https://doi.org/10.1016/j.desal.2021.115391.

(46) Wang, W.; Sun, J.; Zhang, Y.; Zhang, Y.; Hong, G.; Moutloali, R. M.; Mamba, B. B.; Li, F.; Ma, J.; Shao, L. Mussel-Inspired Tannic Acid/Polyethyleneimine Assembling Positively Charged Membranes with Excellent Cation Permselectivity. *Sci. Total Environ.* **2022**, *817*, 153051. https://doi.org/10.1016/j.scitotenv.2022.153051.

(47) He, C.; Ma, J.; Zhang, C.; Song, J.; Waite, T. D. Short-Circuited Closed-Cycle Operation of Flow-Electrode CDI for Brackish Water Softening. *Environ. Sci. Technol.* **2018**, *52* (16), 9350–9360. https://doi.org/10.1021/acs.est.8b02807.

(48) Bakker, E.; Pretsch, E.; Bühlmann, P. Selectivity of Potentiometric Ion Sensors. *Analytical Chemistry* **2000**, 1127–1133. https://doi.org/10.1021/ac991146n.

(49) Peveler, W. J.; Yazdani, M.; Rotello, V. M. Selectivity and Specificity: Pros and Cons in Sensing. *ACS Sensors* **2016**, *1* (11), 1282–1285. https://doi.org/10.1021/acssensors.6b00564.

(50) Hawks, S. A.; Ramachandran, A.; Porada, S.; Campbell, P. G.; Suss, M. E.; Biesheuvel, P. M.; Santiago, J. G.; Stadermann, M. Performance Metrics for the Objective Assessment of Capacitive Deionization Systems. *Water Res.* **2019**, *152*, 126–137. https://doi.org/10.1016/j.watres.2018.10.074.

Chapter 3

Polyelectrolyte Multilayer Coatings on Dense Membranes and Their Advanced Functionalities

An adapted version of this chapter is part of the following review:
Durmaz, E. N.*; Sahin, S.*; Virga, E.*; de Beer, S.; de Smet, L. C. P. M.; de Vos W. M. Polyelectrolytes as Building Blocks for Next-Generation Membranes with Advanced Functionalities, , *ACS Appl. Polym. Mater.,* **2021**, 3 (9), 4347-4374.

*contributed equally.

“Only those who risk going too far find out how far they can go.”

(Walter Bishop, Fringe)

3.1 General Introduction

In the shadow of global warming and water scarcity, advanced separation technologies are needed to provide access to clean water more than ever. Nowadays, achieving environmentally-friendly, selective, and low-cost separations of chemical species is one of the major challenges in this regard. One of the promising technologies addressing this challenge is membrane technology. Membranes are being applied in various separation processes, including ion separation, nutrient recovery, pollutant removal, and also gas and molecular/solvent separations.[1–6]

A membrane is basically a barrier that separates two different phases (components) from each other by letting one phase passing through while restricting passage of the second phase. Based on the applications that they are designed for membranes have certain properties. One common way of categorizing membranes relates to their density, which can vary from low/porous to high/dense (*i.e.* non-porous).[1,7] A porous membrane typically consists of a ceramic or a polymeric matrix with pores with an average diameter between 2 nm to 20 µm and its selectivity is based on the pore size dimensions of the membrane. On the other hand, a dense membrane has an average pore diameter ≤2 nm[8] and its selectivity is achieved by the dense and uniform film where components pass through due to a certain driving force such as a concentration, electrical potential, or pressure gradient.[1,9,10] Due to the smaller pore size of this film, the permeability of the components is smaller in dense membranes, resulting in higher flux values compared to the those of porous membranes. Therefore, porous membranes are mainly suitable for micro- and ultrafiltration processes, while dense membranes are typically used in nanofiltration, reverse osmosis, and various electro-driven desalination technologies, including electrodialysis and capacitive deionization.

Going one step further, combining polyelectrolyte multilayers (PEMs) with membranes can result in advanced functionalities that go beyond the standard separation properties of the membranes.[6] PEM-coated membranes can have properties such as

stimuli-responsiveness, fouling control, stability, specific selectivity, sustainability, and antimicrobial activity. Since Decher demonstrated the layer-by-layer (LbL) deposition of PEMs on flat surfaces,[11] PEMs have been proven to be highly versatile coatings on porous as well as dense membranes. In the current chapter the recent studies where advanced membrane properties of the PEM-coated dense membranes, such as reverse osmosis membranes (ROMs) and various ion-exchange membranes (IEMs), including cation-exchange (CEM), anion-exchange (AEM), Nafion, and bipolar membranes (BPMs) have been reviewed. Although such membranes are already designed to be selective for a certain type of ions (IEMs) and/or show size-based exclusion properties,[5] incorporation of PEMs can further tune their selectivity or impart other desired functionalities.[12]

3.2 Specific Selectivity

Following the successes of PEM coatings on porous supports, one of the most common applications of PEM-coated dense membranes is tuning the ion selectivity of IEMs in desalination processes. **Figure 3.1A** demonstrates the main mechanism to achieve monovalent/divalent cation selectivity via PEM-coated dense membranes. The alternating adsorption of PAH and PSS on a standard cation-exchange membrane can tune the monovalent cation selectivity in desalination. In 2014, Abdu *et al.* modified a standard-grade CEM (CMX) with an LbL assembly of PEI and PSS and implemented the PEM-coated membrane in an electrodialysis (ED) system (**Figure 3.1B**).[13] The $(PEI/PSS)_n$ coating resulted in a higher Ca^{2+} rejection compared to the pristine CMX and moderate increase in ohmic resistance (PEM-CMX = 60.06 $\Omega \cdot cm^2$, CMX = 45.25 $\Omega \cdot cm^2$). Furthermore, the terminating layer makes a small but distinct difference in selectivity: PEI-terminated layers demonstrated higher Na^+/Ca^{2+} selectivity values compared to the PSS-terminated layers (≈18% increase). The selectivity was rationalized by the charge exclusion of divalent cations and the higher hydrophobicity of the PEI-terminated CMX. 6.5 bilayers of PEI/PSS were enough to reach a permselectivity value ($P_{\mathrm{Ca}}^{\mathrm{Na}}$) of 1.24, which is comparable with the commercial monovalent cation-selective membrane (CMS) ($P_{\mathrm{Ca}}^{\mathrm{Na}}$= 1.23). Also, PEM-CMX

required ≈50 Wh/mol Na^+ while CMS required ≈80 Wh/mol Na^+, meaning that similar selectivity values can be achieved with a lower energy consumption value by using PEM-coated CMX. In another ED study, White *et al.* implemented $(PSS/PAH)_n$ layers on a Nafion 115 membrane and obtained K^+/Mg^{2+} selectivity as high as >1000.[14] In 2016, White *et al.* coated $(PAH/PSS)_{5.5}$ on Nafion 117 to achieve Li^+/Co^{2+} and K^+/La^{3+} selectivities in ED.[15] Compared to the mono-/divalent cation selectivity of bare Nafion (<2), they reported Li^+/Co^{2+} and K^+/La^{3+} selectivities exceeding 1000. Yang *et al.* used the same approach in Donnan dialysis with $(PAH/PSS)_{5.5}$-coated Nafion 115 membrane to differentiate within the monovalent cations and reached K^+/Li^+ selectivity values between 8 and 60,[16] although later the authors reported lower selectivities due to variations in different batches of the Nafion membranes.[17] The selectivity was attributed to the larger hydrated radius of Li^+ that resulted in a lower diffusion coefficient through the dense PEM layer. Besides, a pH-induced swelling resulted in a further increase of the K^+/Li^+ selectivity, which was believed to be related to an increased accessibility of cation-exchange sites within the PEM at lower pH. In 2019, Rijnaarts *et al.* further investigated the mechanism of monovalent cation selectivity in ED and explained that after 8 layers of PAH/PSS the multilayer starts to have excess of PAH in the multilayer.[18] The overall positive charge, due to excess PAH, increased with higher number of layers, resulting in increased charge-exclusion towards divalent cations. Sahin *et al.* reported a similar observation where bare CMX demonstrated selectivity to Mg^{2+}, while the addition of a PEM resulted in a Na^+/Mg^{2+} selectivity of ≈3 in a capacitive deionization (CDI) system due to the charge-exclusion effect of the PEM towards Mg^{2+} ions.[19] The positively charged PEM rejected the Mg^{2+} more than Na^+, resulting in monovalent cation selectivity.

PEMs were also coated on AEMs to achieve mono-/divalent anion selectivity in multiple studies including ED,[20,21] reverse ED,[22] dialysis,[23] and CDI.[24] For instance, Mulyati *et al.* used $(PAH/PSS)_{7.5}$ on a standard- grade AEM (Neosepta, AMX) and achieved Cl^-/SO_4^{2-} selectivity in ED.[20] **Figures 3.1C** and **3.1D** depict the change in the chloride concentration in the diluted compartments for the bare and PEM-coated anion-exchange membranes. In

case of PEM-coated AMX, the chloride concentration is lower than the one with bare AMX, meaning an increase in chloride over sulfate selectivity. Therefore, the addition of a PEM is a feasible way of introducing selectivity in ED. Recently, Cl^-/SO_4^{2-} selectivity between 7 and 14 was reported by using PDADMAC/PSS-coated (PDADMAC: poly(diallyldimethylammonium chloride)) AEM in CDI.[24] The authors reported that Cl^- selectivity was preserved even at low concentrations of Cl^- in the solution. Additionally, recent studies reported on the use of biodegradable polyelectrolytes (*e.g.,* 2-hydroxypropyltrimethyl ammonium chloride chitosan, HACC,[21,25,26] and N-O-sulfonic acid benzyl chitosan, NSBC[26]) as alternatives for synthetic polyelectrolytes. Upon the addition of the resulting PEMs, the Cl^-/SO_4^{2-} selectivity increased.

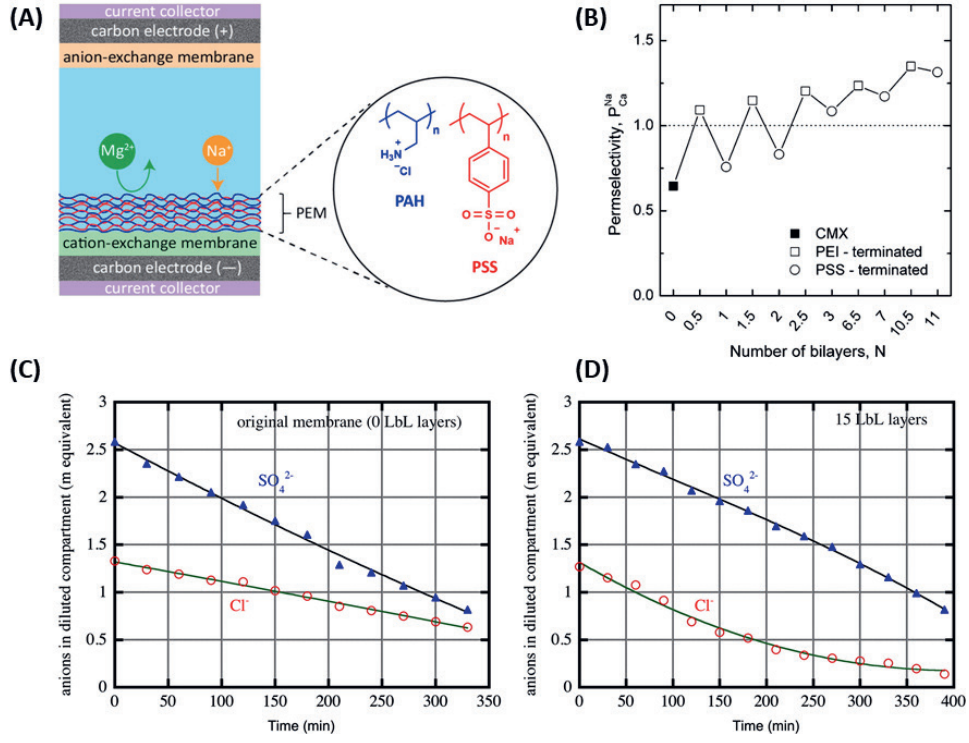

Figure 3.1. (A) Illustration of a PEM application on a standard cation-exchange membrane to achieve Na^+/Mg^{2+} selectivity in capacitive deionization. PAH and PSS stand for

poly(allylamine hydrochloride) and poly(styrenesulfonate), respectively. Adapted with permission from reference.[19] Copyright 2020, American Chemical Society. (B) The trend in permselectivity (*P*) as a function of the type of the terminating layer. CMX and PEI stand for standard cation-exchange membrane and poly(ethylenimine), respectively. The empty squares represent the PEI-terminated and the empty circles represent the PSS-terminated multilayers. Adapted with permission from reference.[13] Copyright 2014, American Chemical Society. (C) The change in the anion concentration in time in the diluted compartments of the experiments with the bare membrane and (D) the membrane with 15 layers. (C) and (D) are adapted with permission from reference.[20] Copyright 2013, Elsevier.

So far, multiple ion selectivity definitions have been used by various research groups, which often limits the possibility to directly compare reported selectivity values. The most common selectivity definitions are listed in **Table 3.1.**

Table 3.1. Commonly used ion selectivity definitions in the literature.

Symbol	Equation	Description
P_j^i [13] or S_j^i [18]	$\frac{J_i \cdot c_j}{J_j \cdot c_i}$	J_i and J_j are the flux (in mol·m^{-2}·s^{-1}) of the target and competing ions, respectively. c_i and c_j (in mol/L) are the concentrations of the target and the competing ion on the diluate side, respectively.
F_j^i [15]*	$\frac{J_i}{J_j}$	J_i and J_j are the flux (in mol·m^{-2}·s^{-1}) of the target and competing ions, respectively, when the source phase contains equal concentrations of the target and the competing ions.
ρ_j^i [19] or β_j^i [10]	$\frac{\frac{(c_{i,0} - c_{i,f})}{c_{i,0}}}{\frac{(c_{j,0} - c_{j,f})}{c_{j,0}}}$	$c_{i,0}$ and $c_{i,f}$ are initial and final concentrations of the target ion. $c_{j,0}$ and $c_{j,f}$ are initial and final concentrations of the competing ion.
R_j^i [18]	$\frac{R_j}{R_i}$	R_i and R_j are the resistance (in Ω·cm^2) of the target and the competing ion, respectively.

* In literature, there is no symbol used for this type of selectivity; here we introduce *F* for matters of clarity.

There are several factors that may affect the ion selectivity of a PEM-modified membrane during desalination operations. Therefore, we summarized cation and anion selectivity studies in **Table 3.2** and **Table 3.3**, respectively, to understand the effects of these factors on selectivity. For each selectivity value of a modified and/or bare membrane, the number of layers in the PEM, the desalination method and the operational conditions as well as the flux values (if applicable) are listed. Standard-grade AEMs and CEMs (*i.e.,* Fujifilm type 1 AEM and CEM, Neosepta CSE and ASE, and CJMA-2 standard CEM from Hefei Chemjoy Polymer Material) were abbreviated as CMX and AMX in **Table 3.2** and **Table 3.3**, respectively. Special-grade cation-exchange membranes (CSO (Selemion) and CMS (Neosepta)), as well as anion-exchange membranes (ASV (Selemion) and ACS (Neosepta)) were added in the tables for comparison, as they are commercially available monovalent-ion selective membranes.

As stated above, building PEMs on dense membranes improves their mono-/divalent ion selectivities. The terminating layer has a major effect on monovalent ion selectivity since the main mechanism of selectivity is the charge exclusion of divalent ions. As can be seen in multiple entries of **Table 3.2** (*i.e.,* **1**, **5-9**, **11-13**), the terminating layer needs to be the polycation in order to achieve monovalent cation selectivity. Similarly, the terminating layer should be the polyanion to achieve monovalent anion selectivity as shown in multiple entries (*i.e.,* **1**, **3**, **5-7**, **9-12**, **14**) in **Table 3.3**. In entry **10** of **Table 3.2**, bare Nafion 115 shows $F_{\mathrm{Mg}}^{\mathrm{K}}\approx$ 2 selectivity and by using the same conditions, $F_{\mathrm{Mg}}^{\mathrm{K}}$>1000 was achieved with PEM-coated Nafion 115. In an anion selectivity study (entries **1** and **2** of **Table 3.3**), a similar switch can be observed. Since the bare CMX and AMX have fixed negative and positive charges, respectively, divalent cations interact more with CMX while AMX shows affinity towards divalent anions. Another important parameter for tuning ion selectivity is the number of layers in the PEM, as the increased charge density and thickness of the PEM can further increase the rejection of divalent ions. For instance, by increasing the number of PE layers from 3 to 11, $F_{\mathrm{Co}}^{\mathrm{Li}}$ increased from >23 to >6500 (in entries **13-15** of **Table 3.2**). The effect of the number of layers on anion selectivity can be seen, *e.g.*, in entries **39-42** of

Table 3.3, where the rejection of SO_4^{2-} with 5 layers was reduced by factor of ≈2 with 15 layers of PEs. However, increasing the number of layers to 23 did not improve the Cl^- selectivity further. As explained in detail[12,27] and demonstrated in numerous studies,[18–20,24] the overcompensation of charge by the polycation can result in an excess of positive charges in the PEM. While in case of monovalent cation selectivity this is a desired effect, an overall positive charge can reduce the rejection of divalent anions and therefore result in a lower mono-/divalent anion selectivity. The examples show that the type and the amount of charge of the PEM and the valence of ions can determine the affinity of the PEM towards ions. Next to the effect of charge (type and valency), also the hydration energy of ions is a key factor in selectivity. For instance, K^+/Li^+ (entry **21**, **Table 3.2**), NO_3^-/ Cl^- and $H_2PO_4^-$ (entries **46** and **47**, **Table 3.3**) selectivities can be explained by the differences in the hydration energy values. To be specific, ions with a smaller hydration energy will pass through the PEM-coated membranes more easily.

Moreover, the coating procedure of the PEMs can have a significant effect on the selectivity value. For instance, in entries **28** and **30** of **Table 3.2**, the only difference in between the experiments was the recipe for preparing the coating. In recipe 1 (entry **28**) has a 15 min rinsing step with 0.5 M NaCl, while in recipe 2 (entry **30**), the rinsing step (1 min) is with demineralized water. Faster rinsing steps with demineralized water causes a higher intrinsic charge compensation between the PEs, resulting in a denser and less hydrated PEM. Therefore, with recipe 2, a less hydrated PEM can be established and a higher selectivity value ($R_{\mathrm{Mg}}^{\mathrm{Na}}$=7.8) was achieved compared to the PEM prepared with recipe 1 ($R_{\mathrm{Mg}}^{\mathrm{Na}}$=5.7). The degree of hydration in PEMs can also be tuned by crosslinking as shown in an anion separation study, which can be explained by two factors. First, crosslinking causes more compact PEMs that increases the rejection larger ions. Secondly, the sulfonate groups of the crosslinking agent increase the amount of negative charge within the PEM, resulting in a higher rejection of divalent anions. In **Table 3.3**, the crosslinked PEM (entry **10**, **Table 3.3**) shows a ≈2 times higher $P_{\mathrm{SO_4}}^{\mathrm{Cl}}$ value compared to the PEM without crosslinking (entry **12**, **Table 3.3**).

Not only the characteristics of the PEM and ions, but also the experimental conditions of desalination process are crucial while optimizing the ion selectivity. We first highlight an example that includes an ED process performed at different salt concentrations. With a source phase concentration of 0.01 M for both KNO_3 and $Mg(NO_3)_2$, F_{Mg}^{K} was found to be 22.1 ± 3.5 (**Table 3.2**, entry **6**). For the same system, when the concentration of both salts was increased to 0.02 M, F_{Mg}^{K} increased to 96 ± 26 (entry **8**, **Table 3.2**). Similarly, when the salt concentrations were 0.1 M, F_{Mg}^{K} was reported to >20000, further indicating the importance of the salt concentration for the system. It was hypothesized that the relatively lower source-phase concentrations caused more water splitting and therefore a higher Mg^{2+} flux. In entries **11** and **12** of **Table 3.2**, the same effect can be observed, where the higher concentration resulted in increased F_{Co}^{Li} (>360 *vs.* >1600). Also, in another ED study, a 10 times higher source-phase concentration resulted in ≈10 times higher $F_{SO_4}^{Cl}$ (entries **31** and **32**, **Table 3.3**). Although the higher $F_{SO_4}^{Cl}$ could be sourced from the charge screening or ion adsorption in the PEM, a ≈10 times increase in $F_{SO_4}^{Cl}$ even with the bare AMX (entries **35** and **36**, **Table 3.3**) showed that this increase is not due to the PEM. Instead, the increase in Cl^- flux in a higher source concentration is the main reason for the improved selectivity. Moreover, in both ED and diffusion dialysis (DD) studies, $F_{SO_4}^{Cl}$ are higher when the source-phase contains an excess of Cl^- compared to SO_4^{2-} (entries **26** and **34**, **Table 3.3**). Therefore, both total salt concentration and the ion ratio affect the ion selectivity.

Another experimental condition is that the amount of driving force during the desalination process. In a constant current (CC) operation, when the current density increases, less rejections of divalent ions are observed. For instance, increasing the current density from 1.27 to 2.54 mA/cm^2, F_{Mg}^{K} decreased from >1000 to 22.1 (entry **5** and **6**, respectively, in **Table 3.2**). Therefore, while comparing two F_{Mg}^{K} values from two different studies, the amount of current/voltage as well as the type of method should be considered to achieve a fair comparison. One indication is the flux values of the ions to compare the selectivity values. For instance, in an ED study, F_{Mg}^{Na} is 1.7 when the flux of Na^+ is ≈ 3.5×10^4

nmol·cm^{-2}·s^{-1} (entry **33**, **Table 3.2**). However, in another ED study, F_{Mg}^{K}>1000 can be achieved since the driving force, and therefore the flux of the monovalent cation (K^+, in this case) is much (≈10^4) smaller (entry **5**, **Table 3.2**).

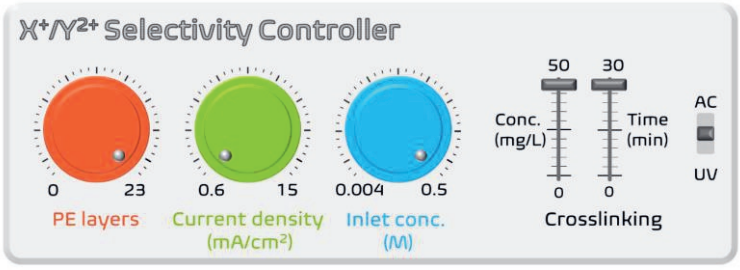

Figure 3.2. Schematic representation of the main parameters that affect the mono-/divalent cation selectivity in PEM-coated dense membranes. The values are taken from the citations that are listed in **Table 3.2** and **Table 3.3** and as such do not represent optimized values. AC and UV stand for alternating current electrical field and ultraviolet approaches to establish crosslinking between PEs with agents like 1,4-bis(2',3'-epoxypropyl) perfluoro-1-butane and (4,4-diazos-tilbene-2,2-disulfonic acid disodium salt, respectively.

In conclusion, for an optimized system, the coating conditions of the PEM build-up (*i.e.,* rinsing step, number of layers, degree of crosslinking), operational parameters (*i.e.,* the composition of the salt solution) as well as the current density/voltage values should be considered carefully. To sum up, the combination of higher number of layers, therefore the charge density of the PEM, higher inlet concentration, and the smaller driving force (current/voltage) lead to higher X^+/Y^{2+} selectivity values (**Figure 3.2**). Also, the stability of the PEM depends on the duration of the process as well as the operating conditions. For instance, overlimiting current values (depending on the operation) can cause water splitting and even electromigration of the PEs.[15] As a result, reduction in current efficiency, fouling

of membrane with insoluble metal hydroxides, and even lack of stability in long-term operations can occur. Also, film stability in ED can be affected by the chlorine generation during the operation.[28]

Table 3.2. Overview of selectivity values and experimental details of the reported studies towards mono/divalent cations. Here, ED: electrodialysis, DD: diffusion dialysis, RM: resistance measurement, MCDI: membrane capacitive deionization, and RP: receiving phase. CC and CV represent a desalination process with constant current or constant voltage, respectively.

Entry	PEM/ Membrane	No. layers	Method	Conditions	Flux	Select. No.	Ref
1	PEI/PSS on CMX	21	ED	CC, 15 mA/cm^2, 0.05 M NaCl and 0.05 M $CaCl_2$	Ca^{2+}: 44.0, Na^+: 60.1	P_{Ca}^{Na}=1.35	13
2	CMX	bare	ED	CC, 15 mA/cm^2, 0.05 M NaCl and 0.05 M $CaCl_2$	Ca^{2+}: 64.5, Na^+: 40.3	P_{Ca}^{Na}=0.64	13
3	CSO	bare	ED	CC, 15 mA/cm^2, 0.05 M NaCl and 0.05 M $CaCl_2$	Ca^{2+}: 35.2, Na^+: 60.8	P_{Ca}^{Na}=1.72	13
4	CMS	bare	ED	CC, 15 mA/cm^2, 0.05 M NaCl and 0.05 M $CaCl_2$	Ca^{2+}: 41.8, Na^+: 53.1	P_{Ca}^{Na}=1.23	13
5	PSS/PAH on Nafion 115	11	ED	CC, 1.27 mA/cm^2, 0.01 M KNO_3 and 0.01 M $Mg(NO_3)_2$	K^+: 6.9 ± 0.2, Mg^{2+}: <0.005	F_{Mg}^{K}>1000	14
6	PSS/PAH on Nafion 115	11	ED	CC, 2.54 mA/cm^2, 0.01 M KNO_3 and 0.01 M $Mg(NO_3)_2$	K^+: 6.28 ± 0.58, Mg^{2+}: 0.318	F_{Mg}^{K}=22.1 ±3.5	14

7	PSS/PAH on Nafion 115 *(1-side)*	11	ED	CC, 2.54 mA/cm^2, 0.01 M KNO_3 and 0.01 M $Mg(NO_3)_2$	ND	F^{K}_{Mg}=10.0 ±3.8	[14]
8	PSS/PAH on Nafion 115	11	ED	CC, 2.54 mA/cm^2, 0.02 M KNO_3 and 0.02 M $Mg(NO_3)_2$	K^+: 13.5 ± 0.6, Mg^{2+}: 0.149	F^{K}_{Mg}=96±26	[14]
9	PSS/PAH on Nafion 115	11	ED	CC, 2.54 mA/cm^2, 0.1 M KNO_3 and 0.1 M $Mg(NO_3)_2$	K^+: 25.2 ± 1.6, Mg^{2+}: < 0.001	F^{K}_{Mg}>20000	[14]
10	Nafion 115	bare	ED	CC, 1.27 mA/cm^2, 0.01 M KNO_3 and 0.01 M $Mg(NO_3)_2$	K^+: 6.4 ± 0.3, Mg^{2+}: 3.6 ± 0.1	F^{K}_{Mg}=1.8 ±0.1	[14]
11	PSS/PAH on Nafion 117	11	ED	CC, 0.63 mA/cm^2, 0.01 M $LiNO_3$ and 0.01 M $Co(NO_3)_2$	Li^+: 2.95 ± 0.2, Co^{2+}: 1.29 ± 0.51 (pmol cm^{-2} s^{-1})	F^{Li}_{Co}>1600	[15]
12	PSS/PAH on Nafion 117	11	ED	CC, 0.63 mA/cm^2, 0.02 M $LiNO_3$ and 0.02 M $Co(NO_3)_2$	Li^+: 3.18 ± 0.3, Co^{2+}: 2.55 ± 1.71 (pmol·cm^{-2}·s^{-1})	F^{Li}_{Co}>360	[15]
13	PSS/PAH on Nafion 117	11	ED	CC, 0.63 mA/cm^2, 0.1 M $LiNO_3$ and 0.1 M $Co(NO_3)_2$	Li^+: 6.79± 0.18, Co^{2+} < 1 (pmol·cm^{-2}·s^{-1})	F^{Li}_{Co}>6500	[15]
14	PSS/PAH on Nafion 117	4	ED	CC, 0.63 mA/cm^2, 0.01 M $LiNO_3$ and 0.01 M $Co(NO_3)_2$	Li^+: 2.39 ± 0.10, Co^{2+}: 3.85± 2.49 (pmol·cm^{-2}·s^{-1})	F^{Li}_{Co}>430	[15]
15	PSS/PAH on Nafion 117	3	ED	CC, 0.63 mA/cm^2, 0.01 M$LiNO_3$ and 0.01 M $Co(NO_3)_2$	Li^+: 1.62 ± 0.10, Co^{2+}: 37.3 ± 25.5 (pmol·cm^{-2}·s^{-1})	F^{Li}_{Co}>23	[15]

16	PSS/PAH on Nafion 117	11	ED	CC, 0.63 mA/cm^2, 0.01 M K(OAc) and 0.01 M $La(OAc)_3$	K^+: 0.46 ± 0.27, La^{3+}: 1.58 ± 1.00 (pmol·cm^{-2}·s^{-1})	F^K_{La}>93	[15]
17	PSS/PAH on Nafion 117	11	ED	CC, 0.63 mA/cm^2, 0.02 M K(OAc) and 0.02 M $La(OAc)_3$	K^+: 4.40 ± 0.02, La^{3+}: 1.27 ± 0.46 (pmol·cm^{-2}·s^{-1})	F^K_{La}>2400	[15]
18	PSS/PAH on Nafion 117	11	ED	CC, 0.63 mA/cm^2, 0.1 M K(OAc) and 0.1 M $La(OAc)_3$	K^+: 7.85 ± 0.69, La^{3+}: <1 (pmol·cm^{-2}·s^{-1})	F^K_{La}>7000	[15]
19	Nafion 117	bare	ED	CC, 0.63 mA/cm^2, 0.01 M $LiNO_3$ and 0.01 M $Co(NO_3)_2$	Li^+: 1.9 ± 0.4, Co^{2+}: 3.0 ± 0.7	F^{Li}_{Co}=0.66±0.08	[15]
20	Nafion 117	bare	ED	CC, 0.63 mA/cm^2, 0.01 M K(OAc) and 0.01 M $La(OAc)_3$	ND	F^K_{La}= 1.61 ± 0.26	[15]
21	PSS/PAH on Nafion 115	11	DD	0.01 M KNO_3 and 0.01 M $LiNO_3$ + 0.01 HNO_3 in RP	K^+:2.01 ± 0.21, Li^+: 0.039 ± 0.013	up to F^K_{Li}=57±22	[16,17]
22	PSS/PAH on Nafion 115	11	DD	0.02 M KNO_3 and 0.02 M $LiNO_3$ + 0.01 HNO_3 in RP	K^+:2.83 ± 0.31, Li^+: 0.035 ± 0.003	F^K_{Li}=80±9	[16]
23	PSS/PAH on Nafion 115	11	DD	0.1 M KNO_3 and 0.1 M $LiNO_3$ + 0.01 HNO_3 in RP	K^+:5.28 ± 0.69, Li^+: 0.25 ± 0.05	F^K_{Li}=38±13	[16]
24	PSS/PAH on Nafion 115	11	DD	0.01 M KNO_3 and 0.01 M $LiNO_3$ + 0.02 HNO_3 in RP	K^+: 0.35 ± 0.06, Li^+:0.047 ± 0.010	F^K_{Li}=8.3±1.8	[16]

25	Nafion 115	bare	DD	0.01 M KNO_3 and 0.01 M $LiNO_3$ + 0.02 HNO_3 in RP	K^+: 4.97 ± 0.44, Li^+: 3.03 ± 0.36	F_{Li}^{K}=1.7±0.3	[16]
26	PSS/PAH on Nafion 115	11	ED	CC, 0.64 mA/cm^{2,} 0.01 M KNO_3 and 0.01 M $LiNO_3$ + 0.01 HNO_3 in RP	K^+: 2.99± 0.13, Li^+: 1.33 ± 0.03	F_{Li}^{K}=2.3±0.1	[16]
27	Nafion 115	bare	ED	CC, 0.64 mA/cm^{2,} 0.01 M KNO_3 and 0.01 M $LiNO_3$ + 0.01 HNO_3 in RP	K^+: 5.56 ± 0.81, Li^+: 4.19 ± 0.38	F_{Li}^{K}=1.3±0.1	[16]
28	PAH/PSS on CMX (recipe 1)	11	RM	0.5 M NaCl, 0.5 M $MgCl_2$	ND	R_{Mg}^{Na}=5.7	[18]
29	PAH/PSS on CMX (recipe 1)	21	RM	0.5 M NaCl, 0.5 M $MgCl_2$	ND	R_{Mg}^{Na}= 5.8	[18]
30	PAH/PSS on CMX (recipe 2)	11	RM	0.5 M NaCl, 0.5 M $MgCl_2$	ND	R_{Mg}^{Na}=7.8	[18]
31	CSO	bare	RM	0.5 M NaCl, 0.5 M $MgCl_2$	ND	R_{Mg}^{Na}=6.9	[18]
32	CMX	bare	RM	0.5 M NaCl, 0.5 M $MgCl_2$	ND	R_{Mg}^{Na}=3.5	[18]
33	PAH/PSS on CMX (recipe 2)	11	ED	CV, 3.5 V, 25mM NaCl and 10mM $MgCl_2$	Na^+≈ 3.5×10^4 Mg^{2+}≈ $0.5\times10^{4*}$	P_{Mg}^{Na} = 1.7	[18]

34	CMX	bare	ED	CV, 3.5 V, 25mM NaCl and 10mM $MgCl_2$	$Na^+ \approx 2\times10^4$ $Mg^{2+} \approx 1.5\times10^4$*	P_{Mg}^{Na} = 0.5	18
35	PAH/PSS on CMX	11	MCDI	CV, 0-1 V, 4 mM NaCl, 4 mM $MgCl_2$	ND	β_{Mg}^{Na} = 2.8 ± 0.2	19
36	CMX	bare	MCDI	CV, 0-1 V, 4 mM NaCl, 4 mM $MgCl_2$	ND	β_{Mg}^{Na}=0.5 ±0.04	19
37	CMS	bare	MCDI	CV, 0-1 V, 4 mM NaCl, 4 mM $MgCl_2$	ND	β_{Mg}^{Na}=0.4 ±0.1	19

**Estimated from the graphs reported in the cited references.*

Table 3.3. Overview of selectivity values and experimental details of the reported studies towards mono/divalent anions. Here, ED: electrodialysis, RED: reverse electrodialysis, DD: diffusion dialysis, CDI: capacitive deionization. CC and CV represent a desalination process with constant current or constant voltage, respectively. PSS-MA stands for poly(styrenesulfonic acid-co-maleic acid) sodium salt.

Entry	PEM/ Membrane	No. layers	Method	Conditions	Flux	Select. No.	Ref
1	PSS/PAH on AMX	15	ED	CC, 2 mA/cm^2, 0.01 M NaCl, 0.01 M Na_2SO_4	ND	$P_{SO_4}^{Cl}$≈2.5*	20
2	AMX	bare	ED	CC, 2 mA/cm^2, 0.01 M NaCl, 0.01M Na_2SO_4	ND	$P_{SO_4}^{Cl}$≈0.8*	20

3	PSS-MA and HACC *(crosslinked)*	15	ED	CC 15 mA/cm^2, 50 mM NaCl and 50 mM Na_2SO_4	ND	$P_{SO_4}^{Cl}$=4.81	21
4	AMX	bare	ED	CC 15 mA/cm^2, 50 mM NaCl and 50 mM Na_2SO_4	ND	$P_{SO_4}^{Cl}$=0.81	21
5	PSS/HACC on AMX	18	ED	CC, 5 mA/cm^2, 0.02 M NaCl and 0.02 M Na_2SO_4	ND	$P_{SO_4}^{Cl}$=2.9	29
6	PSS/HACC on AMX	14	ED	CC, 5 mA/cm^2, 0.02 M NaCl and 0.02 M Na_2SO_4	ND	$P_{SO_4}^{Cl}$≈2*	29
7	PSS/HACC on AMX	6	ED	CC, 5 mA/cm^2, 0.02 M NaCl and 0.02 M Na_2SO_4	ND	$P_{SO_4}^{Cl}$≈1.5*	29
8	AMX	bare	ED	CC, 5 mA/cm^2, 0.02 M NaCl and 0.02 M Na_2SO_4	ND	$P_{SO_4}^{Cl}$=0.66	29
9	PSS/HACC on AMX + crosslinked	17	ED	CC, 5 mA/cm^2, 0.05 M NaCl and 0.05M Na_2SO_4	ND	$P_{SO_4}^{Cl}$≈3.8*	30
10	PSS/HACC on AMX + crosslinked	11	ED	CC, 5 mA/cm^2, 0.05 M NaCl and 0.05 M Na_2SO_4	ND	$P_{SO_4}^{Cl}$=4.36 ±0.13	30
11	PSS/HACC on AMX + crosslinked	5	ED	CC, 5 mA/cm^2, 0.05 M NaCl and 0.05 M Na_2SO_4	ND	$P_{SO_4}^{Cl}$≈1.5*	30
12	PSS/HACC on AMX	11	ED	CC, 5 mA/cm^2, 0.05 M NaCl and 0.05 M Na_2SO_4	ND	$P_{SO_4}^{Cl}$≈2.1*	30

13	AMX	bare	ED	CC, 5 mA/cm^2, 0.05 M NaCl and 0.05 M Na_2SO_4	ND	$P_{SO_4}^{Cl}$=0.39 ±0.06	30
14	NSBC/HACC on AMX	15	ED	CC,10 mA/cm^2, 0.05 M NaCl and 0.05 M Na_2SO_4	ND	$P_{SO_4}^{Cl}$=47.04	26
15	AMX	bare	ED	CC,10 mA/cm^2, 0.05 M NaCl and 0.05 M Na_2SO_4	ND	$P_{SO_4}^{Cl}$=0.81	26
16	ACS	bare	ED	CC,10 mA/cm^2, 0.05 M NaCl and 0.05 M Na_2SO_4	ND	$P_{SO_4}^{Cl}$=13.6	26
17	ASV	bare	ED	CC,10 mA/cm^2, 0.05 M NaCl and 0.05 M Na_2SO_4	ND	$P_{SO_4}^{Cl}$=22.3	26
18	PSS/PEI on CMX	11	RED	CC, 4.0 mA/cm^2, 0.05M NaCl and 0.05 Na_2SO_4	Cl^-: 106.5, SO_4^{2-}: 50.1	$P_{SO_4}^{Cl}$=1.67	22
19	PSS/PEI on CMX	15	RED	CC, 4.0 mA/cm^2, 0.05M NaCl and 0.05 Na_2SO_4	Cl^-: 106.0, SO_4^{2-}: 43.3	$P_{SO_4}^{Cl}$=2.44	22
20	PSS/PEI on CMX	21	RED	CC, 4.0 mA/cm^2, 0.05M NaCl and 0.05 Na_2SO_4	Cl^-: 85.5, SO_4^{2-}: 42.1	$P_{SO_4}^{Cl}$=1.89	22
21	CMX	bare	RED	CC, 4.0 mA/cm^2, 0.05M NaCl and 0.05 Na_2SO_4	Cl^-: 103.2, SO_4^{2-}: 95.3	$P_{SO_4}^{Cl}$=1.1	22

22	ACS	bare	RED	CC, 4.0 mA/cm^2, 0.05M NaCl and 0.05 Na_2SO_4	Cl^-: 105.3, SO_4^{2-}: 35.1	$P_{SO_4}^{Cl}$=2.7	22
23	PSS/PAH on AMX	11	DD	0.01 M NaCl and 0.01 M Na_2SO_4	Cl^-: 1.47 ± 0.20, SO_4^{2-}: 0.31 ± 0.16	$F_{SO_4}^{Cl}$=5.3 ±1.7	23
24	PSS/PAH on AMX	11	DD	0.1 M NaCl and 0.1 M Na_2SO_4	Cl^-: 8.14 ± 0.39, SO_4^{2-}: 0.06 ± 0.01	$F_{SO_4}^{Cl}$=137 ±31	23
25	PSS/PAH on AMX	11	DD	0.01 M NaCl and 0.1 M Na_2SO_4	Cl^-:1.55 ± 0.06, SO_4^{2-}: 0.57 ± 0.09	$F_{SO_4}^{Cl}$=27.9 ±5.0	23
26	PSS/PAH on AMX	11	DD	0.1 M NaCl and 0.01 M Na_2SO_4	Cl^-:7.40 ± 0.53, SO_4^{2-}:Not Detected	$F_{SO_4}^{Cl}$>200	23
27	AMX	bare	DD	0.01 M NaCl and 0.01 M Na_2SO_4	Cl^-: 6.12 ± 0.12, SO_4^{2-}: 3.70 ± 0.22	$F_{SO_4}^{Cl}$=1.66 ±0.08	23
28	AMX	bare	DD	0.1 M NaCl and 0.1 M Na_2SO_4	Cl^-:30.0 ± 1.9, SO_4^{2-}: 2.30 ± 0.19	$F_{SO_4}^{Cl}$=13.0 ±0.4	23
29	AMX	bare	DD	0.01 M NaCl and 0.1 M Na_2SO_4	Cl^-:2.85 ± 0.07, SO_4^{2-}: 6.61 ± 0.12	$F_{SO_4}^{Cl}$=4.3 ±0.1	23

30	AMX	bare	DD	0.1 M NaCl and 0.01 M Na_2SO_4	Cl^-:35.16 ± 3.17, SO_4^{2-}:0.36 1 ± 0.064	$F_{SO_4}^{Cl}$=9.9 ±1.0	23
31	PSS/PAH on AMX	11	ED	CC, 1.13 mA/cm², 0.01 M NaCl and 0.01 M Na_2SO_4	Cl^-:6.72 ± 0.13, SO_4^{2-}:0.91 ± 0.09	$F_{SO_4}^{Cl}$=7.4 ±0.6	23
32	PSS/PAH on AMX	11	ED	CC, 1.13 mA/cm², 0.1 M NaCl and 0.1 M Na_2SO_4	Cl^-:19.37 ± 0.37 , SO_4^{2-}:0.28 ± 0.02	$F_{SO_4}^{Cl}$=69.3 ±5.2	23
33	PSS/PAH on AMX	11	ED	CC, 1.13 mA/cm², 0.01 M NaCl and 0.1 M Na_2SO_4	Cl^-:4.54 ± 0.21, SO_4^{2-}:2.65 ± 0.28	$F_{SO_4}^{Cl}$=17.3 ±2.4	23
34	PSS/PAH on AMX	11	ED	CC, 1.13 mA/cm², 0.1 M NaCl and 0.01 M Na_2SO_4	Cl^-: 18.38 ± 0.77, SO_4^{2-}:0.01 8 ± 0.008	$F_{SO_4}^{Cl}$>81	23
35	AMX	bare	ED	CC, 1.13 mA/cm², 0.01 M NaCl and 0.01 M Na_2SO_4	Cl^-:7.38 ± 0.31, SO_4^{2-}:5.57 ± 0.26	$F_{SO_4}^{Cl}$=1.32 ±0.01	23
36	AMX	bare	ED	CC, 1.13 mA/cm², 0.1 M NaCl and 0.1 M Na_2SO_4	Cl^-:34.11 ± 1.63 SO_4^{2-}: 3.13 ± 0.12	$F_{SO_4}^{Cl}$=10.9 ±0.2	23
37	AMX	bare	ED	CC, 1.13 mA/cm², 0.01 M NaCl and 0.1 M Na_2SO_4	Cl^-: 3.62 ± 0.29, SO_4^{2-}:11.3 4 ± 0.57	$F_{SO_4}^{Cl}$=3.2 ±0.1	23

38	AMX	bare	ED	CC, 1.13 mA/cm^2, 0.1 M NaCl and 0.01 M Na_2SO_4	Cl^-:57.76 ± 5.04, SO_4^{2-}:0.69 5 ± 0.11	$F_{SO_4}^{Cl}$=8.4 ±1.1	23
39	PSS/PDADMAC	15	CDI	CV, (±)1 V, 10 mM NaCl, 10 mM Na_2SO_4	ND	7 <$\beta_{SO_4}^{Cl}$<14	24
40	PSS/PDADMAC	14	CDI	CV, (±)1 V, 10 mM NaCl, 10 mM Na_2SO_4	ND	$\beta_{SO_4}^{Cl}$≈2	24
41	PSS/PDADMAC	5	CDI	CV, (±)1 V, 10 mM NaCl, 10 mM Na_2SO_4	ND	3<$\beta_{SO_4}^{Cl}$<6	24
42	PSS/PDADMAC	23	CDI	CV, (±)1 V, 10 mM NaCl, 10 mM Na_2SO_4	ND	$\beta_{SO_4}^{Cl}$≈1*	24
43	PSS/PDADMAC	14	CDI	CV, (±)1 V, 10 mM NaCl, 10 mM Na_2SO_4	ND	$\beta_{SO_4}^{Cl}$≈1.5*	24
44	AMX	bare	CDI	CV, (±)1 V, 10 mM NaCl, 10 mM Na_2SO_4	ND	$\beta_{SO_4}^{Cl}$≈2	24
45	ACS	bare	CDI	CV, (±)1 V, 10 mM NaCl, 10 mM Na_2SO_4	ND	$\beta_{SO_4}^{Cl}$≈7	24
46	PSS/PDADMAC	15	CDI	CV, (±)1 V, 10 mM NaCl, 10 mM NaH_2PO_4	ND	1.5<$\beta_{H_2PO_4}^{Cl}$ <5.5*	24
47	PSS/PDADMAC	15	CDI	CV, (±)1 V, 10 mM NaCl, 10 mM $NaNO_3$	ND	$\beta_{Cl}^{NO_3}$≈1.5*	24

3.3 Fouling Control

PEM-coated AEMs were also used in antifouling studies in ED[20,31] and reverse ED.[22] When the terminating layer is PSS, the negatively charged hydrophilic outermost layer improved the antifouling properties of the AEM against various foulants including sodium dodecylbenzene sulfonate,[20] sodium dodecyl sulfate (SDS),[31] and humic acid.[22] For example, Zhao *et al.* demonstrated that deposition of $(PSS/PDADMAC)_{5.5}$ on AEM prevented the SDS formation on the membrane, and therefore, the electrical resistance reduced and ion transport through the membrane was unaffected in presence of SDS (**Figure 3.3**).[31] Moreover, a PEM coating can simultaneously enhance the energy conversion efficiency by three-fold compared to the pristine AEM, while still perform as an antifouling layer.[22] Likewise, ROMs have been combined with PEMs to reduce membrane fouling.[32–34] For instance, Ishigami *et al.* coated ROMs with $(PAH/PSS)_3$ and $(PAH/PSS)_6$ and concluded that the surface roughness decreased, and hydrophilicity increased with higher number of layers.[32] In filtration experiments, the modified membranes were tested against hydrophobic foulants, humic acid and dodecyl trimethyl ammonium bromide (DTAB). The polyanion-terminated PEM coating reduced the amount of fouling in all cases, even for a cationic surfactant (DTAB). Moreover, a real-time surface technique called quartz crystal microbalance with dissipation (QCM-D) was used to determine bovine serum albumin (BSA) fouling. The QCM-D fouling study showed that the PEM coating resulted in ≈2 times less protein fouling. The surface mass densities of adsorbed BSA were calculated as 3.0 $mg \cdot m^{-2}$ and 1.5 $mg \cdot m^{-2}$ for pristine gold sensors and gold sensors coated with $(PAH/PSS)_3$, respectively, further proving the antifouling character of the PEM. More recently, PEMs were used as sacrificial coatings for fouling control for ROMs.[35,36] When the membrane was fouled with organic foulants, both the biofilm and the PEM were flushed with concentrated brine solution and a fresh PEM was coated *in-situ*.[36]

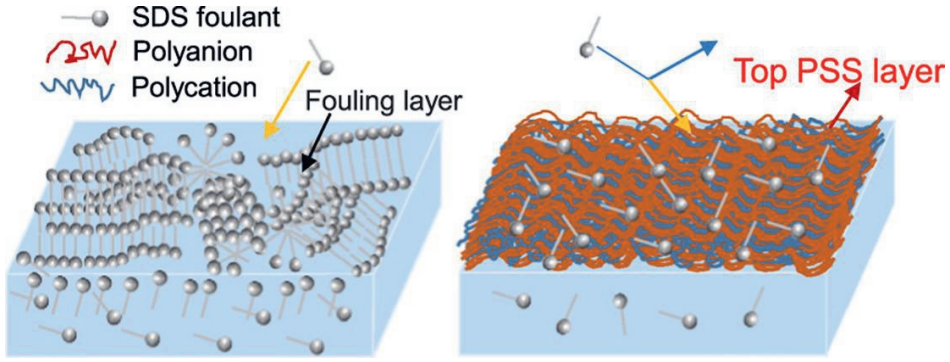

Figure 3.3. The comparison of the bare (left) and the PEM-coated (right) membranes for SDS (sodium dodecyl sulfate) fouling. Adapted with permission from reference.[31] Copyright 2018, Elsevier.

3.4 Catalytic Effect in Dissociation of Water

Another application of PEM-coated IEMs is to improve the water splitting capability of the membrane.[13,37] In 2013, Abdu *et al.* deposited a PEM in between the anion-exchange and cation-exchange layers of a BPM.[37] The PEM enhanced the rate of water dissociation due to the fixed charge groups of the PEM that behave as catalysts. In 2014, the same research group reported this also for a PEM-coated CEM.[13] In that work, water dissociation occurred with PEI-terminated multilayers, while PSS-terminated multilayers showed no significant catalytic effect, allowing switchable water splitting at the membrane-PEM interface.

3.5 Solvent Transport and Separation

Furthermore, PEMs can improve the performance of direct methanol fuel cells when applied on Nafion membranes.[38,39] Jiang and Tang showed that $(PDADMAC/PAA)_n$ (PAA: poly(acrylic acid) multilayers reduced the methanol transport of Nafion membranes significantly as well as lowered the proton conductivity of the membrane.[38] LbL assembly of different polyelectrolyte combinations have also been employed in RO for the separation of isopropanol-water mixtures yielding promising separation factors up to 1075.[39]

3.6 Stability

Besides their various applications, PEMs also have been proven to be highly stable coatings on dense membranes. They can be built at different pH values ranging from 2.3 to 9.3,[16] remain intact in salt solutions up to 0.5 M,[18] and under electric fields.[19,24] In order to improve the chemical and physical stability of PEMs further, covalent bonds within the loose multilayers can be formed via UV irradiation.[25,40]

3.7 Concluding Remarks

Overall, it can be concluded that PEMs are highly promising coatings that contribute to the formation of next-generation membranes with advanced functionalities. In many ways the field is still developing, and much more exciting work on these versatile materials are expected in the near future. For example, by focusing not on just one single functionality, but rather use polyelectrolytes in smart ways to achieve multifunctional membranes, where for example, low fouling, easy to clean and specific selectivities are combined.[41] Moreover, based on the successes of the early examples of PEMs including ion-selective receptors,[42–45] the recovery and harvest of specific ions from aqueous solutions via PEM-coated dense membranes can be further tuned in the future. We thus foresee a very

bright future for PEM-coated membranes, for applications in water treatment, but also in industrial processes that require the separation of organic solvents and gasses.

References

(1) Ezugbe, E. O.; Rathilal, S. Membrane Technologies in Wastewater Treatment: A Review. *Membranes.* **2020**, *10* (5). https://doi.org/10.3390/membranes10050089.

(2) Yan, T.; Ye, Y.; Ma, H.; Zhang, Y.; Guo, W.; Du, B.; Wei, Q.; Wei, D.; Ngo, H. H. A Critical Review on Membrane Hybrid System for Nutrient Recovery from Wastewater. *Chem. Eng. J.* **2018**, *348*, 143–156. https://doi.org/10.1016/j.cej.2018.04.166.

(3) Rathore, A. S.; Shirke, A. Recent Developments in Membrane-Based Separations in Biotechnology Processes: Review. *Prep. Biochem. Biotechnol.* **2011**, *41* (4), 398–421. https://doi.org/10.1080/10826068.2011.613976.

(4) Rajendran, S. R. C. K.; Mason, B.; Doucette, A. A. Review of Membrane Separation Models and Technologies: Processing Complex Food-Based Biomolecular Fractions. *Food Bioprocess Technol.* **2021**, *14* (3), 415–428. https://doi.org/10.1007/s11947-020-02559-x.

(5) Luo, T.; Abdu, S.; Wessling, M. Selectivity of Ion Exchange Membranes: A Review. *J. Memb. Sci.* **2018**, *555* (December 2017), 429–454. https://doi.org/10.1016/j.memsci.2018.03.051.

(6) Li, X.; Liu, C.; Van Der Bruggen, B. Polyelectrolytes Self-Assembly: Versatile Membrane Fabrication Strategy. *J. Mater. Chem. A* **2020**, *8* (40), 20870–20896. https://doi.org/10.1039/d0ta07154d.

(7) Bazzarelli, F.; Giorno, L. Encyclopedia of Membranes. *Encycl. Membr.* **2020**. https://doi.org/10.1007/978-3-642-40872-4.

(8) Tan, X. M.; Rodrigue, D. A Review on Porous Polymeric Membrane Preparation. Part II: Production Techniques with Polyethylene, Polydimethylsiloxane, Polypropylene, Polyimide, and Polytetrafluoroethylene. *Polymers (Basel).* **2019**, *11* (8). https://doi.org/10.3390/polym11081310.

(9) Luo, T.; Abdu, S.; Wessling, M. Selectivity of Ion Exchange Membranes: A Review. *J. Memb. Sci.* **2018**, *555* (March), 429–454. https://doi.org/10.1016/j.memsci.2018.03.051.

(10) Gamaethiralalage, J. G.; Singh, K.; Sahin, S.; Yoon, J.; Elimelech, M.; Suss, M. E.; Liang, P.; Biesheuvel, P. M.; Zornitta, R. L.; de Smet, L. C. P. M. Recent Advances in Ion Selectivity with Capacitive Deionization. *Energy Environ. Sci.* **2020**, *14*, 1095–1120. https://doi.org/10.1039/d0ee03145c.

(11) Decher, G. Fuzzy Nanoassemblies: Toward Layered Polymeric Multicomposites. *Science* **1997**, *277*, 1232–1237. https://doi.org/10.1126/science.277.5330.1232.

(12) Joseph, N.; Ahmadiannamini, P.; Hoogenboom, R.; Vankelecom, I. F. J. Layer-by-Layer Preparation of Polyelectrolyte Multilayer Membranes for Separation. *Polym. Chem.* **2014**, *5* (6), 1817–1831. https://doi.org/10.1039/c3py01262j.

(13) Said, Abdu, M.-C.; Manuel-César, Wong, J. E.; García-Gabaldón, M.; Wessling, M. Layer-by-Layer Modification of Cation Exchange Membranes Controls Ion Selectivity and Water Splitting. *ACS Appl. Mater. Interfaces* **2014**, *6*, 1843−1854.

(14) White, N.; Misovich, M.; Yaroshchuk, A.; Bruening, M. L. Coating of Nafion Membranes with Polyelectrolyte Multilayers to Achieve High Monovalent/Divalent Cation Electrodialysis Selectivities. *ACS Appl. Mater. Interfaces* **2015**, *7*, 6620−6628.

(15) White, N.; Misovich, M.; Alemayehu, E.; Yaroshchuk, A.; Bruening, M. L. Highly Selective Separations of Multivalent and Monovalent Cations in Electrodialysis through Nafion Membranes Coated with Polyelectrolyte Multilayers. *Polymer,* **2016**, *103*, 478–485. https://doi.org/10.1016/j.polymer.2015.12.019.

(16) Yang, Liu, Tang, Chao, Ahmad, Muhammad, Yaroshcuk, Andriy, Bruening, M. L. High Selectivities among Monovalent Cations in Dialysis through Cation-Exchange Membranes Coated with Polyelectrolyte Multilayers. *ACS Appl. Mater. Interfaces* **2018**, *10*, 44134–44143.

(17) Yang, L.; Tang, C.; Ahmad, M.; Yaroshchuk, A.; Bruening, M. Erratum: High Selectivities among Monovalent Cations in Dialysis through Cation-Exchange Membranes Coated with Polyelectrolyte Multilayers (ACS Applied Materials and Interfaces (2018) 10: 50 (44134−44143) DOI: 10.1021/Acsami.8b16434). *ACS Appl. Mater. Interfaces* **2021**, *13* (18), 22073. https://doi.org/10.1021/acsami.1c06321.

(18) Rijnaarts, T.; Reurink, D. M.; Radmanesh, F.; de Vos, W. M.; Nijmeijer, K. Layer-by-Layer Coatings on Ion Exchange Membranes: Effect of Multilayer Charge and Hydration on Monovalent Ion Selectivities. *J. Memb. Sci.* **2019**, *570–571*, 513–521. https://doi.org/10.1016/j.memsci.2018.10.074.

(19) Sahin, S.; Dykstra, J. E.; Zuilhof, H.; Zornitta, R. L.; de Smet, L. C. P. M. Modification of Cation-Exchange Membranes with Polyelectrolyte Multilayers to Tune Ion Selectivity in Capacitive Deionization. *ACS Appl. Mater. Interfaces* **2020**, *12* (31), 34746–34754. https://doi.org/10.1021/acsami.0c05664.

(20) Mulyati, S.; Takagi, R.; Fujii, A.; Ohmukai, Y.; Matsuyama, H. Simultaneous Improvement of the Monovalent Anion Selectivity and Antifouling Properties of an Anion Exchange Membrane in an Electrodialysis Process, Using Polyelectrolyte Multilayer Deposition. *J. Memb. Sci.* **2013**, *431*, 113–120. https://doi.org/10.1016/j.memsci.2012.12.022.

(21) Zhao, Y.; Gao, C.; Van Der Bruggen, B. Technology-Driven Layer-by-Layer Assembly of a Membrane for Selective Separation of Monovalent Anions and Antifouling. *Nanoscale* **2019**, *11* (5), 2264–2274. https://doi.org/10.1039/c8nr09086f.

(22) Gao, H.; Zhang, B.; Tong, X.; Chen, Y. Monovalent-Anion Selective and Antifouling Polyelectrolytes Multilayer Anion Exchange Membrane for Reverse Electrodialysis. *J. Memb. Sci.* **2018**, *567*, 68–75. https://doi.org/10.1016/j.memsci.2018.09.035.

(23) Ahmad, M.; Tang, C.; Yang, L.; Yaroshchuk, A.; Bruening, M. L. Layer-by-Layer Modification of Aliphatic Polyamide Anion-Exchange Membranes to Increase Cl−/SO42− Selectivity. *J. Memb. Sci.* **2019**, *578*, 209–219. https://doi.org/10.1016/j.memsci.2019.02.018.

(24) Singh, K.; Sahin, S.; Gamaethiralalage, J. G.; Zornitta, R. L.; de Smet, L. C. P. M. Simultaneous, Monovalent Ion Selectivity with Polyelectrolyte Multilayers and Intercalation Electrodes in Capacitive Deionization. *Chem. Eng. J.* **2021**, 128329. https://doi.org/10.1016/j.cej.2020.128329.

(25) Liu, H.; Ruan, H.; Zhao, Y.; Pan, J.; Sotto, A.; Gao, C.; van der Bruggen, B.; Shen, J. A Facile Avenue to Modify Polyelectrolyte Multilayers on Anion Exchange Membranes to Enhance Monovalent Selectivity and Durability Simultaneously. *J. Memb. Sci.* **2017**, *543*, 310–318. https://doi.org/10.1016/j.memsci.2017.08.072.

(26) Zhao, Y.; Zhu, J.; Ding, J.; Van der Brugge, B.; Shen, J.; Gao, C. Electric-Pulse Layer-by-Layer Assembled of Anion Exchange Membrane with Enhanced Monovalent Selectivity. *J. Memb. Sci.* **2018**, *548*, 81–90. https://doi.org/10.1016/j.memsci.2017.11.007.

(27) Riegler, H.; Essler, F. Polyelectrolytes. 2: Intrinsic or Extrinsic Charge Compensation? Quantitative Charge Analysis of PAH/PSS Multilayers. *Langmuir* **2002**, *18* (17), 6694–6698. https://doi.org/10.1021/la020108n.

(28) Cheng, C.; White, N.; Shi, H.; Robson, M.; Bruening, M. L. Cation Separations in Electrodialysis through Membranes Coated with Polyelectrolyte Multilayers. *Polymer* **2014**, *55* (6), 1397–1403. https://doi.org/10.1016/j.polymer.2013.12.002.

(29) Zhao, Y.; Tang, K.; Liu, H.; Van der Bruggen, B.; Sotto Díaz, A.; Shen, J.; Gao, C. An Anion Exchange Membrane Modified by Alternate Electro-Deposition Layers with Enhanced Monovalent Selectivity. *J. Memb. Sci.* **2016**, *520*, 262–271. https://doi.org/10.1016/j.memsci.2016.07.026.

(30) Liu, H.; Ruan, H.; Zhao, Y.; Pan, J.; Sotto, A.; Gao, C.; van der Bruggen, B.; Shen, J. A Facile Avenue to Modify Polyelectrolyte Multilayers on Anion Exchange Membranes to Enhance Monovalent Selectivity and Durability Simultaneously. *J. Memb. Sci.* **2017**, *543*, 310–318. https://doi.org/10.1016/j.memsci.2017.08.072.

(31) Zhao, Z.; Shi, S.; Cao, H.; Li, Y.; Van der Bruggen, B. Layer-by-Layer Assembly of Anion Exchange Membrane by Electrodeposition of Polyelectrolytes for Improved Antifouling Performance. *J. Memb. Sci.* **2018**, *558* (1), 1–8. https://doi.org/10.1016/j.memsci.2018.04.035.

(32) Ishigami, T.; Amano, K.; Fujii, A.; Ohmukai, Y.; Kamio, E.; Maruyama, T.; Matsuyama, H. Fouling Reduction of Reverse Osmosis Membrane by Surface Modification via Layer-by-Layer Assembly. *Sep. Purif. Technol.* **2012**, *99*, 1–7. https://doi.org/10.1016/j.seppur.2012.08.002.

(33) Karkhanechi, H.; Razi, F.; Sawada, I.; Takagi, R.; Ohmukai, Y.; Matsuyama, H. Improvement of Antibiofouling Performance of a Reverse Osmosis Membrane through Biocide Release and Adhesion Resistance. *Sep. Purif. Technol.* **2013**, *105*, 106–113. https://doi.org/10.1016/j.seppur.2012.12.016.

(34) Ma, W.; Soroush, A.; Van Anh Luong, T.; Brennan, G.; Rahaman, M. S.; Asadishad, B.; Tufenkji, N. Spray- and Spin-Assisted Layer-by-Layer Assembly of Copper Nanoparticles on Thin-Film Composite Reverse Osmosis Membrane for Biofouling Mitigation. *Water Res.* **2016**, *99*, 188–199. https://doi.org/10.1016/j.watres.2016.04.042.

(35) Nava-Ocampo, M. F.; Bucs, S. S.; Farinha, A. S. F.; Son, M.; Logan, B. E.; Vrouwenvelder, J. S. Sacrificial Coating Development for Biofouling Control in Membrane Systems. *Desalination* **2020**, *496*. https://doi.org/10.1016/j.desal.2020.114650.

(36) Son, M.; Yang, W.; Bucs, S. S.; Nava-Ocampo, M. F.; Vrouwenvelder, J. S.; Logan, B. E. Polyelectrolyte-Based Sacrificial Protective Layer for Fouling Control in Reverse Osmosis Desalination. *Envrionmental Sci. Technol. Lett.* **2018**, *5* (9), 584–90. https://doi.org/10.1021/acs.estlett.8b00400.

(37) Abdu, S.; Kittikun, S.; Wong, John, E.; Muljadi, E. S.; Meling, T.; Wessling, M. Catalytic Polyelectrolyte Multilayers at the Bipolar Membrane Interface. *ACS Appl. Mater. Interfaces* **2013**, *5*, 10445–10455. https://doi.org/10.1021/am403019y.

(38) Jiang, S. P.; Tang, H. Methanol Crossover Reduction by Nafion Modification via Layer-by-Layer Self-Assembly Techniques. *Colloids Surfaces A Physicochem. Eng. Asp.* **2012**, *407*, 49–57. https://doi.org/10.1016/j.colsurfa.2012.05.006.

(39) Xiang, Y.; Lu, S.; Jiang, S. P. Layer-by-Layer Self-Assembly in the Development of Electrochemical Energy Conversion and Storage Devices from Fuel Cells to Supercapacitors. *Chem. Soc. Rev.* **2012**, *41* (21), 7291–7321. https://doi.org/10.1039/c2cs35048c.

(40) Nguyen, T. T. T.; Belbekhouche, S.; Dubot, P.; Carbonnier, B.; Grande, D. From the Functionalization of Polyelectrolytes to the Development of a Versatile Approach to the Synthesis of Polyelectrolyte Multilayer Films with Enhanced Stability. *J. Mater. Chem. A* **2017**, *5* (46), 24472–24483. https://doi.org/10.1039/c7ta06855g.

(41) Ilyas, S.; de Grooth, J.; Nijmeijer, K.; De Vos, W. M. Multifunctional Polyelectrolyte Multilayers as Nanofiltration Membranes and as Sacrificial Layers for Easy Membrane Cleaning. *J. Colloid Interface Sci.* **2015**, *446*, 365–372. https://doi.org/10.1016/j.jcis.2014.12.019.

(42) Paltrinieri, L.; Remmen, K.; Müller, B.; Chu, L.; Köser, J.; Wintgens, T.; Wessling, M.; de Smet, L. C. P. M.; Sudhölter, E. J. R. Improved Phosphoric Acid Recovery from Sewage Sludge Ash Using Layer-by-Layer Modified Membranes. *J. Memb. Sci.* **2019**, *587* (December 2018), 117162. https://doi.org/10.1016/j.memsci.2019.06.002.

(43) Kazemabad, M.; Verliefde, A.; Cornelissen, E. R.; D'Haese, A. Crown Ether Containing Polyelectrolyte Multilayer Membranes for Lithium Recovery. *J. Memb. Sci.* **2020**, *595*. https://doi.org/10.1016/j.memsci.2019.117432.

(44) Liang, Y.; Lin, S. Mechanism of Permselectivity Enhancement in Polyelectrolyte-Dense Nanofiltration Membranes via Surfactant-Assembly Intercalation. *Environ. Sci. Technol.* **2021**, *55* (1), 738–748. https://doi.org/10.1021/acs.est.0c06866.

(45) Paltrinieri, L.; Poltorak, L.; Chu, L.; Puts, T.; van Baak, W.; Sudhölter, E. J. R.; de Smet, L. C. P. M. Hybrid Polyelectrolyte-Anion Exchange Membrane and Its Interaction with Phosphate. *React. Funct. Polym.* **2018**, *133*, 126–135. https://doi.org/10.1016/j.reactfunctpolym.2018.10.005.

Chapter 4

Modification of Cation-Exchange Membranes with Polyelectrolyte Multilayers to Tune Ion Selectivity in Capacitive Deionization

This chapter was adapted from:

Sahin, S.; Dykstra, J. E.; Zuilhof, H.; Zornitta, R. L.; de Smet, L. C. P. M. Modification of Cation-Exchange Membranes with Polyelectrolyte Multilayers to Tune Ion Selectivity in Capacitive Deionization. *ACS Appl. Mater. Interfaces* **2020**, 12 (31), 34746−34754.

Abstract

Capacitive deionization (CDI) is a desalination technique that can be applied for the separation of target ions from water streams. For instance, mono- and divalent cation selectivity was studied by other research groups in the context of water softening. Another focus is on removing Na^+ from recirculated irrigation water (IW) in greenhouses, aiming to maintain nutrients. This is important as an excess of Na^+ has toxic effects for plant growth by decreasing the uptake of other nutrients. In this study, we investigated selective separation of sodium (Na^+) and magnesium (Mg^{2+}) in MCDI using a polyelectrolyte multilayer (PEM) on a standard grade cation-exchange membrane (Neosepta, CMX). Alternating layers of poly(allylamine hydrochloride) (PAH) and poly(styrene sulfonate) (PSS) were coated on a CMX membrane (CMX-PEM) using the layer-by-layer (LbL) technique. The layer formation was examined with X-ray photoelectron spectroscopy (XPS) and static water contact angle measurements (SWA) for each layer. For each membrane, i.e. the CMX-PEM membrane, CMX membrane, and for a special-grade cation-exchange membrane (Neosepta, CIMS), the Na^+/Mg^{2+} selectivity was investigated by performing MCDI experiments, and selectivity values of 2.8 ± 0.2, 0.5 ± 0.04 and 0.4 ± 0.1 were found, respectively, over up to 40 cycles. These selectivity values indicate flexible switching from a Mg^{2+}-selective membrane to a Na^+-selective membrane by straightforward modification with a PEM. We anticipate that our modular functionalization method may facilitate the further development of ion-selective membranes and electrodes.

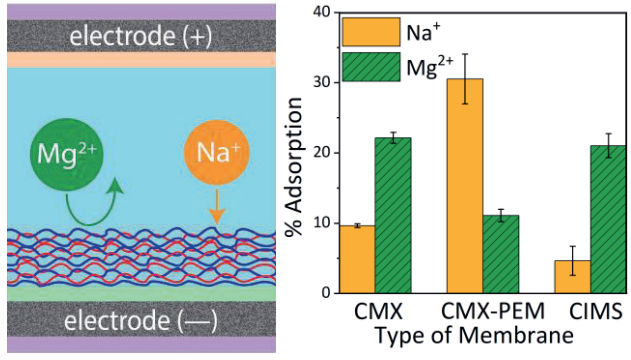

4.1 Introduction

Over the last decade, capacitive deionization (CDI) has been used for ion-selective desalination[1–3], especially for the recovery of nutrients (phosphate[4–6] and nitrate[7–10]) and valuable ions (lithium[11], potassium[12], ammonia[13], fluoride[14]), removal of heavy metals,[15–18], and water softening.[19–21] The selective capture of target ions from a multi-ionic solution or the enrichment of the target ion by removing the competing ions are the main ideas behind these applications.[1] For instance, the separation of monovalent from divalent cations using CDI has been vastly studied in the context of water softening.[19–21] Efforts were made on selective materials or optimizations of experimental parameters to selectively remove hardness ions (Mg^{2+} and Ca^{2+}) from alkali metal cations. Another focus is on removing Na^{+} from recirculated irrigation water (IW) in greenhouses, aiming to maintain nutrients.[22–25] This is important as an excess of Na^{+} has toxic effects for plant growth by decreasing the uptake of other nutrients.[26]

CDI is a desalination technique in which ions are removed from brackish water by an electric potential applied to a pair of electrodes.[27,28] As a result, the outlet water contains a lower salt concentration. The combination of ion-exchange membranes (IEMs) and CDI is called membrane capacitive deionization (MCDI), which improves charge efficiency of the electrodes and provides higher separation capacity compared to CDI.[27] While there is an ongoing debate on the energy efficiency and operational costs of MCDI compared to other well-established desalination technologies,[29–32] it has also been shown that MCDI can be competitive, at least for salt concentrations up to 40 mM.[33] IEMs have fixed charges that allow the transport of counterions (anions in an anion-exchange membrane, cations in a cation-exchange membrane), and prevent the unwanted transport of co-ions, resulting in an increased charge efficiency.[28,34–36]

Numerous studies have been published on separation of monovalent cations from divalent cations by using multi-ionic solutions in CDI.[20,21,37–41] For instance, Seo *et al.* showed higher removal rates for di- over monovalent cations by optimizing the pore structure and wettability of carbon electrodes,[38] the mostly used type of CDI electrodes. Zhao *et al.*

achieved time-dependent selectivity using a solution with a concentration ratio of Na^+/Ca^{2+} = 5, where in the early stage of the desalination process, the dominantly present Na^+ ions were preferentially electrosorbed, while later on they were gradually replaced by the minority Ca^{2+} cations.[39] Another study from Hou and Huang also demonstrated a higher affinity towards divalent cations using carbon electrodes.[41] Recently, He *et al*.[20] and Wang and Lin[21] studied the dependence of selectivity on operating conditions such as current density and hydraulic retention time in MCDI operated in constant current mode. They implemented standard-grade IEMs in a CDI cell and reported a higher Ca^{2+} over Na^+ selectivity. Besides optimization of operational conditions, introducing a selective layer can also tune the selectivity. Yoon *et al*. [40] and Kim *et al.*[37] prepared composite coatings onto carbon electrodes to obtain Ca^{2+} over Na^+ selectivities in MCDI.

One interesting and alternative way of introducing selectivity to CDI-based separations is using layer-by-layer (LbL)-coated polyelectrolyte multilayers (PEMs). PEMs, which were first demonstrated by Decher in early 1990s,[42,43] are composed of alternating layers of oppositely charged polymers. They are attractive because of their high stability and easy and cheap preparation,[44] which provides versatile control over the physicochemical properties of surfaces. Surface characteristics such as chemical charge, morphology, and swelling properties can be tuned by sequentially constructed PEMs. Therefore, PEMs can regulate the interactions with surrounding environments.[45–49] PEMs have been employed in ion separations, mainly pressure driven,[50,51] and more recently also electro driven.[52–54] These studies showed that monovalent ion permeation and divalent ion rejection can be controlled by tuning the PEM properties. The mechanism of selectivity is based on Donnan charge exclusion effect. [54,55] When the outermost charge of the surface has the same charge as the divalent ion, divalent ions are rejected more compared to monovalent ions due to their higher charge density.[56]

Based on these advancements we now study, for the first time, the combination of PEMs and CDI. So far, several research groups have investigated the use of PEMs for the selective ion separation by using different combinations of mono- and divalent cations (*i.e.* Na^+/Ca^{2+},[52] K^+/Mg^{2+},[48] Li^+/Co^{2+},[49] Na^+/Mg^{2+} [54]) and they all reported a monovalent cation

selectivity. Out of these combinations, we chose to study Na^+/Mg^{2+} selectivity of PEM where molar ion ratio is 1:1.

In this study, we aimed to develop a simple method to separate Na^+ from Mg^{2+} in a binary solution by switching the selectivity of a commercial cation-exchange membrane. The feasibility of a PEM on a standard grade cation-exchange membrane (Neosepta, CMX) was investigated in MCDI operation for the selective separation of Na^+ and Mg^{2+}. Alternating layers of poly(allylamine hydrochloride) (PAH) and poly(styrene sulfonate) (PSS) were prepared onto a CMX membrane (CMX-PEM) using the LbL technique. The layer formation was examined with X-ray photoelectron spectroscopy (XPS) and static water contact angle measurements (SWA) for each layer. Then, the CMX-PEM membrane was implemented in an MCDI cell, which was operated in a constant voltage operation mode. During the operation, samples were collected from the effluent solution. The collected samples were analyzed with inductively coupled plasma - optical emission spectrometry (ICP-OES) afterwards. The selectivity value was calculated based on the adsorption ratio of Na^+ over Mg^{2+}. The selectivity, reproducibility and performance of the operation were compared with an unmodified CMX membrane and a special-grade cation-exchange membrane (Neosepta, CIMS) under the same conditions. The CIMS membrane was chosen as an additional reference membrane due its crosslinked outermost layer, which showed a higher monovalent cation selectivity in electrodialysis.[54] Finally, the stability and selectivity of the PEM-CMX membrane was tested in a MCDI operation for 40 cycles, and an outlook on the potential of this novel approach was provided.

4.2 Materials and Methods

Materials. Poly(allylamine hydrochloride) (PAH, Mw = 17,500 Da), poly(sodium 4-styrenesulfonate) (PSS, Mw = 70,000 Da), sodium chloride (NaCl, ≥ 99%), anhydrous magnesium chloride ($MgCl_2$, ≥ 98%), sodium 2-mercaptoethanesulfonate (MESNA, analytical standard, ≥ 98.0) were purchased from Sigma Aldrich. Hydrochloric acid (36.5 - 28.0% NF grade) was purchased from VWR International. Nitric acid (65%, for analysis) and ethanol (absolute) were purchased from Merck Millipore. Acetone (HPLC grade, 99.9%) and dichloromethane (stabilized with amylene) were purchased from BIOSELVE BV. All chemicals were used as received without further purification. The inorganic salts were kept in a vacuum oven overnight prior to use.

Neosepta cation-exchange (CMX), anion-exchange (AMX), and monovalent cation-selective (CIMS) membranes (Astom Corp., Japan) were soaked in a solution of 4 mM NaCl and 4 mM $MgCl_2$ for at least 48 h before use. The porous carbon electrodes, which were deposited on a graphite foil substrate, were supplied by Voltea BV, Netherlands. Glass fiber pre-filters (25 mm in diameter) with a pore size of 2.0 µm (Merck Millipore) were used as spacer for MCDI experiments. Flat substrates of gold sputtered on glass (1 × 1 cm) were purchased from ECsens. Milli-Q water (18.2 MΩ.cm, Milli-Q Integral 3 system, Millipore) was used to prepare salt and polyelectrolyte solutions.

Layer-by-layer (LbL) Coating onto Membrane. The use of PEMs in pressure- and electro-driven ion-selective separations have been reported in previous studies.[49,51,54,57–59] Out of the several PEM systems and preparation conditions that have been used, we adopted a procedure of Bruening and co-workers[58] and built $(PAH/PSS)_5PAH$ layers. The pre-treated CMX membrane was modified by alternating dipping in PAH (polycation) (0.02 M PAH in 1 M NaCl, pH = 2.3) and PSS (polyanion) (0.02 M PSS in 0.5 M NaCl, pH = 2.3) solutions for 10 min each to form the multilayers. After each layer coating, the CMX was soaked in Milli-Q water (3 × 3 min) to remove any weakly attached polyelectrolytes. The CMX membrane

was coated with 11 polyelectrolyte layers in total, and the membrane was referred to as CMX-PEM. The CMX-PEM was stored in a solution of 4 mM NaCl and 4 mM $MgCl_2$.

Layer-by-layer (LbL) Coating on Gold Substrates. The growth and properties of the multilayers were characterized on gold model substrates. Although gold is chemically different from IEMs, the bulk and surface properties of PEMs are not dependent on the type of surface characteristics of the substrate after a sufficient number of layers,[50,54] making gold a suitable model surface. Prior to LbL coating, gold substrates were sonicated for 5 min in Milli-Q water, and dried in a stream of argon. Sonication was repeated with acetone, ethanol, and dichloromethane and the gold substrates were subsequently cleaned from organic material by 5 min of air-based plasma by a plasma cleaner (Diener electronic GmbH, Germany).[60] Afterwards, the surfaces were immersed in 10 mM of MESNA solution overnight. Thiol groups of MESNA form strong dative bonds (40-50 kcal mol^{-1}) with gold surfaces while the sulfonate groups ($R\text{-}SO_3^-$) of MESNA supply a negative surface charge.[61] Then, the gold substrates were coated with the PEM using the same LbL procedure as the one employed for the CMX, before drying the substrates in a vacuum oven at 30 °C.

Characterizations. The properties of the multilayers were first characterized using X-ray photoelectron spectroscopy (XPS),static water contact angle measurements (SWA), spectroscopic ellipsometry, and atomic force microscopy (AFM).

SWA values were measured using a Krüss drop shape analyzer (DSA 30) by depositing Milli-Q water drops of 3 µL onto the PEM-coated gold surface. Contact angles were measured with a charge-couple device (CCD) camera using a sessile drop method. For each surface, the contact angle value was the average value of three measurements on different locations of the samples to study the homogeneity of the coating.

The XPS spectra of PEM-coated gold substrates were obtained (20 scans each experiment) by a JPS-9200 photoelectron spectrometer (JEOL, Japan) under ultra-high vacuum conditions. The spectra were obtained using a monochromatic Al Kα source at 12 kV and 20 mA. All spectra were corrected with Shirley background fitting and processed

with CASA XPS software (version 2.3.16). The PEM-coated gold substrates were analyzed by spectroscopic ellipsometry. The dry (optical) thickness of the PEM coating was measured using an Accurion Nanofilm_ep4 imaging ellipsometer. The ellipsometric data were acquired in air at room temperature using light in the wavelength range of λ = 400.6−761.3 nm at an angle of incidence of 50º. The data were fitted with EP4 software using a multilayer model (used refractive index of gold: 1.397).

The AFM images of air-dried samples of CMX and PEM-CMX were acquired by an Asylum Research MFP-3D SA AFM (Oxford Instruments, United Kingdom) in amplitude and height modes with a scanning size of 5 µm × 5 µm.

Electrosorption Experiments. The experiments were performed using a lab-scale MCDI cell with dimensions of 6 cm × 10.5 cm × 18.5 cm (total volume of 70 mL). The cell with two carbon electrodes (5.6 cm × 6.0 cm), each with a square opening inside (1.5 cm × 1.5 cm), a CMX, an AMX, and a spacer was firmly assembled. The water enters the MCDI cell and flows radially to the outlet in the bottom center (schematic representation of the MCDI system can be found in the Supporting Information, **Figure S4.1**. At the exit of the cell, a conductivity probe and a pH electrode record the conductivity and pH online. A port in between conductivity and pH probes was used for sampling during the experiments. The deaerated feed solution (5 L of 4 mM NaCl and 4 mM $MgCl_2$) was pumped through the system at constant flow rate (7.5 mL/min) using a peristaltic pump (Masterflex). We note that given the large volume of the feed solution, the operation mode behaves like a single-pass mode.[62] A potentiostat (Autolab PGSTAT302N, Metrohm) provided a charging voltage of 1.0 V and a discharge voltage of 0 V (short circuit) during the electrosorption and regeneration, respectively. The conductivity (conductivity module 856, Metrohm) and pH (flat membrane, combined pH electrode, Metrohm) were monitored online. The electrosorption/desorption experiments were carried out for 10 cycles of 40 min each, except for the stability test of the CMX-PEM membrane which included 40 cycles.

Depending on the experiment, a CMX, CMX-PEM or CIMS membrane was used as a cation-exchange membrane (**Figure 4.1**). All CDI experiments were performed at least

three times for each membrane. During 3 cycles, *i.e.* adsorption and desorption of each experiment, 8 samples (for each adsorption or desorption steps) were collected for further analysis. The samples (each 1.5 mL) were taken at 20, 120, 220, 320, 420, 600, 900, and 1100 s of each adsorption step. After switching sample port a sample was taken after 15 s to account for the dead volume between the cell and the point of sampling.

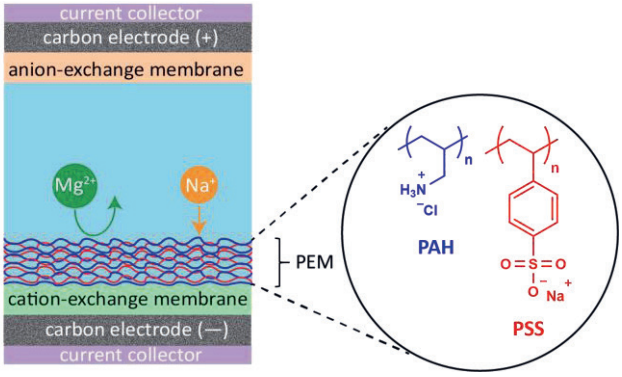

Figure 4.1. Schematic representation of the cell configuration. CMX-PEM represents the membrane that was modified with polyelectrolytes (PAH and PSS). For each type of experiment, either CMX, CMX-PEM or CIMS membranes were used as a cation-exchange membrane.

Inductively coupled plasma atomic emission spectroscopy (PerkinElmer Avio 500 ICP-OES) was used to measure the Na^+ and Mg^{2+} concentrations of the samples. The argon flow to produce plasma was set to 10 L/min. The high energy based Avio 500 ICP-OES polychromator with two sulfur chemiluminescence detectors (SCD) covered a spectral range of 163-782 nm, with a measuring resolution of 0.006 nm at 200 nm. The samples were diluted 20 times with 1% nitric acid solution before measurement. Selectivity of Na^+ over Mg^{2+} (ρ, sometimes also defined as β in literature[24,63]) was calculated according to

Equation 4.1,[20,21] where c_0 and c_f represent the initial and final ion concentrations in the solution, respectively:

$$\rho \, {}^{\mathrm{Na}}_{\mathrm{Mg}} = \frac{(c_{0,\mathrm{Na}^+} - c_{\mathrm{f,Na}^+})}{c_{0,\mathrm{Na}^+}} / \frac{(c_{0,\mathrm{Mg}^{2+}} - c_{\mathrm{f,Mg}^{2+}})}{c_{0,\mathrm{Mg}^{2+}}} \quad \textbf{(4.1)}$$

The charge efficiency (Λ) and the specific energy consumption (η, kJ/mg) for the charging step were calculated using **Equations 4.2** and 4.**3**, respectively: in which, F is the Faraday constant (96485.3 C/mol), z is the ion valence (+2 for Mg^{2+}, and +1 for Na^+), Δn is the total amount of salt adsorbed (mol), I is the current measured during the electrosorption step, which runs from t_1 (start of adsorption) to t_2 (end of adsorption), V_{cell} is the cell voltage applied during the experiment, and m_{sr} is the total mass of salt removed (g) during the desalination process. Salt adsorption capacity (SAC) is calculated by dividing the amount of adsorbed salt (in mg) by mass of carbon electrode ($m_{electrode}$ = 1.79 g). M_w is the molecular weight of the salt.

$$\Lambda = \frac{F.(z_{\mathrm{Mg}^{2+}}.\Delta n_{\mathrm{Mg}^{2+}} + z_{\mathrm{Na}^+}.\Delta n_{\mathrm{Na}^+})}{\int_{t_1}^{t_2} I \mathrm{d}t} \quad \textbf{(4.2)}$$

$$\eta = V_{\mathrm{cell}} \cdot \frac{\int_{t_1}^{t_2} I \, \mathrm{d}t}{m_{\mathrm{sr}}} \quad \textbf{(4.3)}$$

$$\mathrm{SAC} = \frac{(M_{w\,\mathrm{MgCl_2}}.\Delta n_{\mathrm{Mg}^{2+}} + M_{w\,\mathrm{NaCl}}.\Delta n_{\mathrm{Na}^+})}{m_{\mathrm{electrode}}} \quad \textbf{(4.4)}$$

4.3 Results and Discussion

Characterization of Multilayers. In order to study whether the layer build-up was successful, gold substrates were characterized after each layer addition via SWA and XPS analyses (**Figure 4.2**).

The wettability of the gold substrates coated with a PEM was studied with SWA measurements (**Figure 4.2A**). The first data point belongs to the pre-treated gold substrate (MESNA-Au). Upon the addition of PE layers, the SWA data shows an odd-even effect. When the PSS was the top layer, the contact angle was lower than the layer with PAH on top, indicating that the PSS-terminated multilayers were more hydrophilic than the PAH-terminated ones. This is in agreement with similar studies reported in literature regarding the hydrophilicity of the layers and their odd-even effect[64–66] and it shows the successful build-up of 11 layers.

The chemical composition of the surface of the substrates was measured with XPS after the addition of each layer (**Figure 4.2B**). The % abundances of nitrogen (N) (only present in PAH) and sulfur (S) (only present in PSS) were obtained from XPS wide scan spectra. This was followed by the calculation of N/S ratio data that – just like the SWA studies – showed an alternating trend, indicating the successful deposition of PAH and PSS layers.[65,67] Wide-scan XPS spectra of the layers (**Figure S4.2**) and elemental composition as a function of the number of layers (**Figure S4.3**) can be found in the Supporting Information. Next to the SWA and XPS data, also AFM and ellipsometry confirm the presence of the PEMs (**Figure S4.4** and related text).

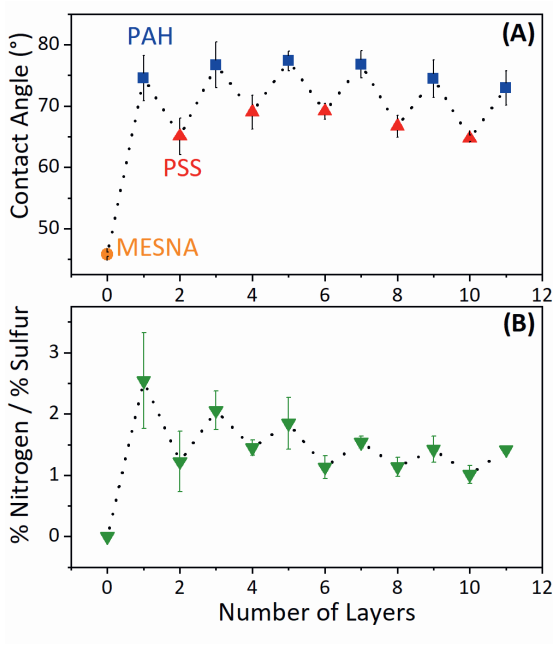

Figure 4.2. Surface characterization of gold substrates. Odd number layers have PAH and even number layers have PSS as the outermost layer. The initial data point is MESNA-coated gold substrate. (A) Static water contact angle data shows wettability of the outermost layer with increased number of layer. (B) Nitrogen/sulfur atomic ratios were obtained from wide scan X-ray photoelectron spectra for each number of layer. (Reported data is based on 3 samples per data point and 3 measurements for each sample. Dotted lines are guide to eye).

MCDI Performance. The performance of the CMX-PEM membrane was evaluated based on conductivity and current data obtained for a 40-cycle constant voltage experiment. **Figure 4.3** shows the data obtained for the adsorption steps 4-6, 24-26, and 37-39 with a salt mixture of 4 mM NaCl and 4 mM $MgCl_2$. The current reached its maximum and minimum values during adsorption and desorption, respectively (**Figure 4.3A**). The coulombic efficiency and the amount of charge were found to be stable throughout the adsorption steps (Supporting Information, **Table 4.S1**). **Figure 4.3B** indicates the change in

effluent conductivity as function of time at given adsorption steps. The decrease and increase in conductivity indicates electrosorption and desorption of ions, respectively. At the end of each step, the effluent conductivity returned to the feed conductivity value demonstrating the saturation of electrodes (all cycles are provided in the Supporting Information, **Figure S4.5**).

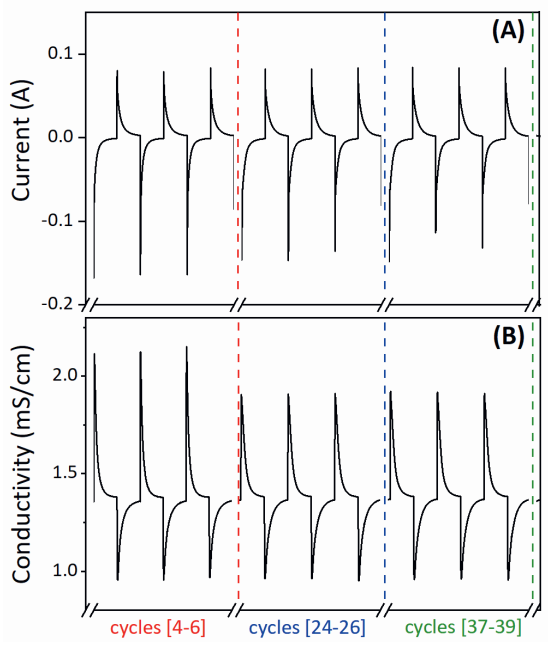

Figure 4.3. The MCDI operation of the CMX-PEM membrane for the cycles 4-6, 24-26, and 37-39. Time-course variation of (A) current and (B) effluent conductivity data at a constant voltage process (dashed lines are guide to eye).

Comparison of Ion Selectivities. Figure 4.4 shows the effluent concentration of Na^+ and Mg^{2+} as function of time, both for the adsorption and desorption step of an electrosorption cycle in constant voltage operation. The ions are adsorbed faster in the early stage of each electrosorption step. Therefore, the adsorption rate of ions reached a maximum value, here around ~ 120 s. After this point, the adsorption rate started to decrease and eventually ion

concentrations returned to their initial values, suggesting that electrodes became saturated at the end of each adsorption step. In a constant voltage operation, the current changes during the adsorption steps. As a result, the relative adsorption rate of each type of cation changes as well, indicating that the selectivity can be time-dependent, which refers to the variation in ion selectivity during electrosorption, as already described in literature.[10,39,68,69] The time where the maximum selectivity value was observed (~ 220 s) will be abbreviated as t_s from now on. At t_s, while CMX-PEM adsorbed more Na^+ compared to Mg^{2+}, CMX and CIMS showed the opposite trend during adsorption steps (**Figures 4.4A**, **4.4B**, **4.4C**). The affinities of the membranes towards either Na^+ or Mg^{2+} were also confirmed with the effluent concentration data during desorption (**Figures 4.4D**, **4.4E**, **4.4F**). To conclude this section, **Figure 4.4** shows that it is possible to switch CMX's selectivity from Mg^{2+} to Na^+ by simply coating it with a PEM.

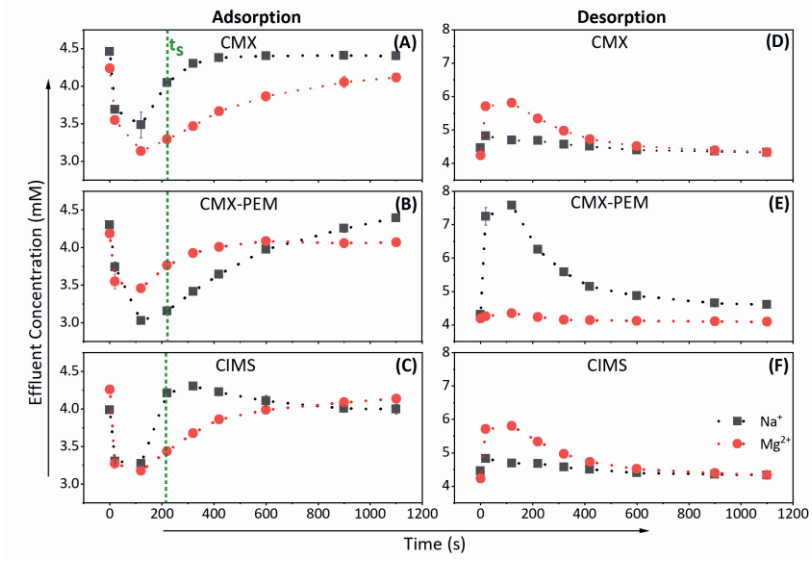

Figure 4.4. The change in effluent concentrations in time for (**4.4A, 4.4B, 4.4C**) adsorption and **(4.4D, 4.4E, 4.4F)** desorption steps for CMX, CMX-PEM, and CIMS, respectively. t_s indicates the points where the maximum selectivity values were observed during adsorption steps.

Before starting the electrosorption cycles, the ion solution of 4 mM (for each cation) was recirculated through the MCDI cell. Upon this recirculation the ion concentration was found to slightly increase. However, this deviation has no influence on the final selectivity as we used these increased concentrations to calculate the selectivities.

Next, to facilitate a quantitative comparison, the $\rho_{\mathrm{Mg}}^{\mathrm{Na}}$ values for each type of membrane were calculated based on **Equation 4.1**. CMX-PEM showed $\rho_{\mathrm{Mg}}^{\mathrm{Na}} = 2.8 \pm 0.2$, whereas CMX ($0.5 \pm 0.0$) and CIMS ($0.2 \pm 0.1$) showed more affinity towards Mg^{2+} (**Figure 4.5**).

Now we report that PEMs can increase the monovalent ion selectivity in MCDI as well. The affinity of bare CMX membrane towards divalent cations was also reported by other studies.[21,70,71] The CMX membrane has a preference for divalent cations which can be understood by the coulombic interactions between the negative outermost layer of the membrane and the cations. Since the charge density of Mg^{2+} is around six times higher than the one of Na^{+},[56] there is a stronger ionic interaction between the bare CMX membrane and Mg^{2+}. On the other hand, the deposition of the PEM on top of the CMX membrane resulted in a rejection of divalent cations, which can also be rationalized by charge effects. First, the outer layer of the PEM, which is positive in charge, rejects divalent cations more than monovalent cations due to Donnan exclusion.[57]

Second, also the overall high charge density of PEM coatings may contribute to this effect. It is known that the PAH/PSS system shows an over-charge compensation effect.[72,73] In a recent reflectometry study of Rijnaarts *et al*.[54] this effect was found for the PAH/PSS system after four bilayers onwards and the excess of positive charge further increased for thicker multilayers. In our study we used similar coating conditions and hence it is reasonable to assume that our $(PAH/PSS)_{5.5}$ system has an overall positive charge.

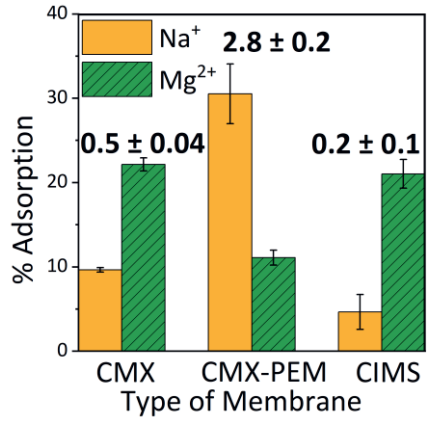

Figure 4.5. The adsorption percentage and selectivity values of the membranes. Each ρ_{Mg}^{Na} was calculated at t_s using the data from 3 separate experiments including 3 adsorption steps per each experiment.

In order to test PEM stability during the 40-cycle MCDI operation of CMX-PEM membrane, ICP-OES samples were taken from the 5th, 25th, and 40th cycle. The average $\rho_{\mathrm{Mg}}^{\mathrm{Na}}$ value was found to be 2.5 ± 0.1, meaning that the PEM was stable during the 40-cycle experiment. The selectivity values per each cycle are provided in the Supporting Information, **Table 4.S2**.

To facilitate a comparison, an overview of different approaches that achieved mono- or divalent cation selectivity in CDI was made (**Table 4.1**). From this table it becomes clear that different experimental conditions and/or modification of electrodes or membranes can change selectivity values. In more detail, it shows that the selectivity does not only depend on the chemical structure or the surface modification of the membrane, but also on many other factors, such as pore size and surface area of the carbon electrode[74,75], ionic charge and hydrated size of cations[41], as well as the composition and initial concentration of feed solution[21,41] and operational parameters (applied voltage[41], current density[21], operating time[38], and flow rate[38,76]).

In order to understand the effect of the addition of a PEM on monovalent cation selectivity, all the operational conditions (*i.e.* flow rate, current, time) were kept constant for each type of membrane. While it is difficult to compare selectivities obtained from different desalination techniques, and higher selectivities have been reported for the combination of LbL and electrodialysis,[49,67] our results are in line with the findings of other electrodialysis studies that also employed LbL-coated Neosepta ion-exchange membranes.[52,54,66] For example, Abdu *et al.* deposited polyethylenimine/PSS films on a Neosepta CMX ion-exchange membrane and obtained a Na^+/Ca^{2+} selectivity of 1.4.[52] Similarly, Mulyati *et al.* found that Neosepta anion-exchange membranes modified with PAH/PSS layers exhibit Cl^-/SO_4^{2-} selectivities of ~2.5.[66] CMX-PEM has a promising Na^+ selectivity compared to the other CDI systems listed in **Table 4.1**, although it has to be acknowledged that the selectivity is time-dependent during electrosorption. In order to optimize the process and improve the separation, at t_s a potential of 0 V can be applied to the system, followed by a washing step of the electrode to obtain a Na^+-rich solution after each cycle. Once the desired amount of Na^+ has been removed, the Mg^{2+} that is still present in the treated solution can be removed with a post-treatment step.

Table 4.1. Overview of selectivity values for various reported CDI systems/conditions towards either mono- or divalent cations in CDI. Cited work with values for ρ made use of **Equation 4.1**.

Selective Layer / Optimization	Selectivity definition	Feed ratio (Na/X^{2+})	Selectivity number	Reference
operational conditions	*	5	$Na^+ > Ca^{2+} = 5$ $Ca^{2+} > Na^+ = 3$	[39]
operational conditions	ρ_{Na}^{Ca}	1	1.5	[41]
operational conditions	ρ_{Na}^{Ca}	25	6	[20]
operational conditions	ρ_{Na}^{Ca}	1.3	2.8-3.3	[21]
Ca-alginate layer	ρ_{Na}^{Ca} **	1	2.5	[40]
nanocomposite layer	$S_{t/c}$***	10-1	$Ca^{2+} > Na^+ = 3.5\text{-}5.4$	[37]
CMX membrane	ρ_{Mg}^{Na}	1	0.5	this work
CMX-PEM	ρ_{Mg}^{Na}	1	2.8	this work
CIMS	ρ_{Mg}^{Na}	1	0.2	this work

*based on Gouy-Chapman theoretical approach,** see reference for the selectivity definition, ***calculated based on **Equation 4.1**.

Calculations of Energy Consumption. Capacitive deionization is a well-known technology used for water desalination with low-energy consumption. Therefore, the paramount parameters that should be taken into account when evaluating the CDI performance for ion selectivity using modified membranes are salt adsorption capacity (SAC, in mg/g), the

charge efficiency *(Λ)* and specific energy consumption (*η)*. SAC is the amount of salt removed during electrosorption and it was calculated by integrating salt concentration over time by using **Equation 4.4**. *Λ* indicates how much of the charge provided to the electrode is effectively used for electrosorption. In this sense, the closer the value of *Λ* to 100%, the better. In practice, 100% charge efficiency is seldom achieved due to electrode degradation, co-ion repulsion, cell resistivity, and faradaic reactions which usually take place together with the electrode polarization.

Table 4.2 summarizes the obtained SAC, *Λ* and *η* values of CDI experiments carried out with CMX-PEM, CMX, and CIMS membranes.

It is noted that water splitting near the polyelectrolyte/membrane interface may reduce current efficiency and form insoluble metal hydroxides to foul the membrane.[49] However, we did not observe this issue in our system. The SAC value for CMX and PEM-CMX did not differ from each other, indicating that there is no significant effect of PEM on the SAC (**Table 4.2**). Also, the constant SAC value of PEM-CMX during the long-term desalination process (SI, **Table 4.S1**) is a strong indication of the stability of the PEM. The *Λ* values for CMX and CMX-PEM membranes were around 69%, showing that the addition of PEM has no significant effect on *Λ*. These values are slightly lower than those for CMX reported in the literature (88 ± 5%),[77] which can be associated with the type of carbon electrode and the cell design. Furthermore, since we did not have a single-salt solution, ICP-OES data were used to calculate the amounts of salt removed. However, due to the limited availability of concentration data points, this approach may have resulted in an underestimation of the integrated values of salt removal, lowering Δn and hence the *Λ* values. Furthermore, any leakage current would reduce the effective applied current and hence decrease the *Λ* values. The *Λ* value of the CIMS membrane was even lower (54%). The results show that the modified and bare CMX membranes have a better performance than the CIMS membrane, which can be rationalized by a higher resistance due to the crosslinking nature of the CIMS membrane.[54]

Following the same trend, *η* of the CIMS membrane was higher than *η* of the CMX membrane. This was expected since *η* is linked to the *Λ* according to **Equations 4.2** and **4.3**.

The η values observed during the electrosorption process were comparable with the literature values.[77,78]

Table 4.2: Comparison of salt adsorption capacity, charge efficiency, and specific energy consumption of the membranes.

Type of membrane	*SAC (mg/g)*	*Λ* (%)	*η* (kJ/g)
CMX-PEM	3.5 ± 0.6	68 ± 14 %	2.7 ± 0.6
CMX	3.5 ± 0.3	69 ± 9 %	2.8 ± 0.4
CIMS	2.5 ± 0.3	54 ± 7%	3.8 ± 0.5

4.4 Conclusions

This study distinctively describes the control of monovalent/divalent ion selectivity in the process of membrane capacitive deionization (MCDI) simply by adding a thin polyelectrolyte multilayer (PEM) onto the membrane surface. PEMs have already been used as ion-selective coatings, mainly in pressure-driven, and more recently also in electro-driven processes, in particular electrodialysis. Based on the promising results of PEMs in other desalination processes, we combined, for the first time, PEMs and MCDI to obtain monovalent cation selectivity. A thorough interface analysis, investigation of the layer stability and a detailed comparison with selectivity performance of various reported CDI systems/conditions are included in our study. For the resulting CMX-PEM membrane, we obtained a Na^+/Mg^{2+} selectivity of almost three, while the bare CMX showed a preference for Mg^{2+}. These results provide a proof-of-concept for a smooth switching from a Mg^{2+}-selective membrane to a Na^+-selective membrane by straightforward modification with a PEM. Furthermore, it is shown that the layers have high stability even after long-term desalination operation. Our work demonstrates a new way of achieving ion selectivity in CDI using PEMs. Given the large toolbox of available polyelectrolytes and variety of polyelectrolyte functionalization schemes, we anticipate that our modular approach may facilitate the further development of the separation and recovery of other ions by controlling interfacial properties at the nanoscale.

References

(1) Zhang, X.; Zuo, K.; Zhang, X.; Zhang, C.; Liang, P. Selective Ion Separation by Capacitive Deionization (CDI) Based Technologies: A State-of-the-Art Review. *Environ. Sci. Water Res. Technol.* **2020**, *6* (2), 243–257. https://doi.org/10.1039/c9ew00835g.

(2) Volfkovich, Y. M. Capacitive Deionization of Water (A Review). *Russ. J. Electrochem.* **2020**, *56* (1), 18–51. https://doi.org/10.1134/S1023193520010097.

(3) Choi, J.; Dorji, P.; Shon, H. K.; Hong, S. Applications of Capacitive Deionization: Desalination, Softening, Selective Removal, and Energy Efficiency. *Desalination* **2019**, *449*, 118–130. https://doi.org/10.1016/j.desal.2018.10.013.

(4) Zhu, E.; Hong, X.; Ye, Z.; Hui, K. S.; Hui, K. N. Influence of Various Experimental Parameters on the Capacitive Removal of Phosphate from Aqueous Solutions Using LDHs/AC Composite Electrodes. *Sep. Purif. Technol.* **2019**, *215*, 454–462. https://doi.org/10.1016/j.seppur.2019.01.004.

(5) Bian, Y.; Chen, X.; Lu, L.; Liang, P.; Ren, Z. J. Concurrent Nitrogen and Phosphorus Recovery Using Flow-Electrode Capacitive Deionization. *ACS Sustain. Chem. Eng.* **2019**, *7* (8), 7844–7850. https://doi.org/10.1021/acssuschemeng.9b00065.

(6) Jiang, J.; Kim, D. I.; Dorji, P.; Phuntsho, S.; Hong, S.; Shon, H. K. Phosphorus Removal Mechanisms from Domestic Wastewater by Membrane Capacitive Deionization and System Optimization for Enhanced Phosphate Removal. *Process Saf. Environ. Prot.* **2019**, *126*, 44–52. https://doi.org/10.1016/j.psep.2019.04.005.

(7) Kim, Y. J.; Choi, J. H. Selective Removal of Nitrate Ion Using a Novel Composite Carbon Electrode in Capacitive Deionization. *Water Res.* **2012**, *46* (18), 6033–6039. https://doi.org/10.1016/j.watres.2012.08.031.

(8) Gan, L.; Wu, Y.; Song, H.; Zhang, S.; Lu, C.; Yang, S.; Wang, Z.; Jiang, B.; Wang, C.; Li, A. Selective Removal of Nitrate Ion Using a Novel Activated Carbon Composite Carbon Electrode in Capacitive Deionization. *Sep. Purif. Technol.* **2019**, *212*, 728–736. https://doi.org/10.1016/j.seppur.2018.11.081.

(9) Hawks, S. A.; Cerón, M. R.; Oyarzun, D. I.; Pham, T. A.; Zhan, C.; Loeb, C. K.; Mew, D.; Deinhart, A.; Wood, B. C.; Santiago, J. G.; et al. Using Ultramicroporous Carbon for the Selective Removal of Nitrate with Capacitive Deionization. *Environ. Sci. Technol.* **2019**, *53* (18), 10863–10870. https://doi.org/10.1021/acs.est.9b01374.

(10) Mubita, T. M.; Dykstra, J. E.; Biesheuvel, P. M.; van der Wal, A.; Porada, S. Selective Adsorption of Nitrate over Chloride in Microporous Carbons. *Water Res.* **2019**, *164*, 114885. https://doi.org/10.1016/j.watres.2019.114885.

(11) Shi, W.; Liu, X.; Ye, C.; Cao, X.; Gao, C.; Shen, J. Efficient Lithium Extraction by Membrane Capacitive Deionization Incorporated with Monovalent Selective Cation Exchange Membrane. *Sep. Purif. Technol.* **2019**, *210*, 885–890. https://doi.org/10.1016/j.seppur.2018.09.006.

(12) Kim, S.; Yoon, H.; Shin, D.; Lee, J.; Yoon, J. Electrochemical Selective Ion Separation in Capacitive Deionization with Sodium Manganese Oxide. *J. Colloid Interface Sci.* **2017**, *506*, 644–648. https://doi.org/10.1016/j.jcis.2017.07.054.

(13) Zhang, C.; Ma, J.; Waite, T. D. Ammonia-Rich Solution Production from Wastewaters Using Chemical-Free Flow-Electrode Capacitive Deionization. *ACS Sustain. Chem. Eng.* **2019**, *7* (7), 6480–6485. https://doi.org/10.1021/acssuschemeng.9b00314.

(14) Pan, J.; Zheng, Y.; Ding, J.; Gao, C.; Van Der Bruggen, B.; Shen, J. Fluoride Removal from Water by Membrane Capacitive Deionization with a Monovalent Anion Selective Membrane. *Ind. Eng. Chem. Res.* **2018**, *57* (20), 7048–7053. https://doi.org/10.1021/acs.iecr.8b00929.

(15) Liu, P.; Yan, T.; Zhang, J.; Shi, L.; Zhang, D. Separation and Recovery of Heavy Metal Ions and Salt Ions from Wastewater by 3D Graphene-Based Asymmetric Electrodes: Via Capacitive Deionization. *J. Mater. Chem. A* **2017**, *5* (28), 14748–14757. https://doi.org/10.1039/c7ta03515b.

(16) Ji, Q.; An, X.; Liu, H.; Guo, L.; Qu, J. Electric Double-Layer Effects Induce Separation of Aqueous Metal Ions. *ACS Nano* **2015**, *9* (11), 10922–10930. https://doi.org/10.1021/acsnano.5b04027.

(17) Huang, Z.; Lu, L.; Cai, Z.; Ren, Z. J. Individual and Competitive Removal of Heavy Metals Using Capacitive Deionization. *J. Hazard. Mater.* **2016**, *302*, 323–331. https://doi.org/10.1016/j.jhazmat.2015.09.064.

(18) Chen, R.; Sheehan, T.; Ng, J. L.; Brucks, M.; Su, X. Capacitive Deionization and Electrosorption for Heavy Metal Removal. *Environ. Sci. Water Res. Technol.* **2020**, *6* (2), 258–282. https://doi.org/10.1039/c9ew00945k.

(19) Choi, J.; Lee, H.; Hong, S. Capacitive Deionization (CDI) Integrated with Monovalent Cation Selective Membrane for Producing Divalent Cation-Rich Solution. *Desalination* **2016**, *400*, 38–46. https://doi.org/10.1016/j.desal.2016.09.016.

(20) He, C.; Ma, J.; Zhang, C.; Song, J.; Waite, T. D. Short-Circuited Closed-Cycle Operation of Flow-Electrode CDI for Brackish Water Softening. *Environ. Sci. Technol.* **2018**, 52, 9350−9360. https://doi.org/10.1021/acs.est.8b02807.

(21) Wang, L.; Lin, S. Mechanism of Selective Ion Removal in Membrane Capacitive Deionization for Water Softening. *Environ. Sci. Technol.* **2019**, *53*, 5797−5804. https://doi.org/10.1021/acs.est.9b00655.

(22) Savvas, D.; Mantzos, N.; Barouchas, P. E.; Tsirogiannis, I. L.; Olympios, C.; Passam, H. C. Modelling Salt Accumulation by a Bean Crop Grown in a Closed Hydroponic System in Relation to Water Uptake. *Sci. Hortic.* **2007**, *111* (4), 311–318. https://doi.org/10.1016/j.scienta.2006.10.033.

(23) Savvas, D.; Chatzieustratiou, E.; Pervolaraki, G.; Gizas, G.; Sigrimis, N. Modelling Na and Cl Concentrations in the Recycling Nutrient Solution of a Closed-Cycle Pepper Cultivation. *Biosyst. Eng.* **2008**, *99* (2), 282–291. https://doi.org/10.1016/j.biosystemseng.2007.10.008.

(24) Singh, K.; Qian, Z.; Biesheuvel, P. M.; Zuilhof, H.; Porada, S.; de Smet, L. C. P. M. Nickel Hexacyanoferrate Electrodes for High Mono/Divalent Ion-Selectivity in Capacitive Deionization. *Desalination* **2020**, *481*, 114346. https://doi.org/10.1016/j.desal.2020.114346.

(25) Qian, Z.; Miedema, H.; de Smet, L. C. P. M.; Sudhölter, E. J. R. Modelling the Selective Removal of Sodium Ions from Greenhouse Irrigation Water Using Membrane Technology. *Chem. Eng. Res. Des.* **2018**, *134*, 154–161. https://doi.org/10.1016/j.cherd.2018.03.040.

(26) Zhang, J. L.; Flowers, T. J.; Wang, S. M. Mechanisms of Sodium Uptake by Roots of Higher Plants. *Plant Soil* **2010**, *326* (1), 45–60. https://doi.org/10.1007/s11104-009-0076-0.

(27) Suss, M. E.; Porada, S.; Sun, X.; Biesheuvel, P. M.; Yoon, J.; Presser, V. Water Desalination via Capacitive Deionization: What Is It and What Can We Expect from It? *Energy Environ. Sci.* **2015**, *8*, 2296–2319. https://doi.org/10.1039/c5ee00519a.

(28) Kim, J. S.; Kim, C. S.; Shin, H. S.; Rhim, J. W. Application of Synthesized Anion and Cation Exchange Polymers to Membrane Capacitive Deionization (MCDI). *Macromol. Res.* **2015**, *23*, 360–366. https://doi.org/10.1007/s13233-015-3049-6.

(29) Qin, M.; Deshmukh, A.; Epsztein, R.; Patel, S. K.; Owoseni, O. M.; Walker, W. S.; Elimelech, M. Comparison of Energy Consumption in Desalination by Capacitive Deionization and Reverse Osmosis. *Desalination* **2019**, *455*, 100–114. https://doi.org/10.1016/j.desal.2019.01.003.

(30) Ramachandran, A.; Oyarzun, D. I.; Hawks, S. A.; Campbell, P. G.; Stadermann, M.; Santiago, J. G. Comments on "Comparison of Energy Consumption in Desalination by Capacitive Deionization and Reverse Osmosis." *Desalination* **2019**, *461*, 30–36. https://doi.org/10.1016/j.desal.2019.03.010.

(31) Qin, M.; Deshmukh, A.; Epsztein, R.; Patel, S. K.; Owoseni, O. M.; Walker, W. S.; Elimelech, M. Response to Comments on "Comparison of Energy Consumption in Desalination by Capacitive Deionization and Reverse Osmosis." *Desalination* **2019**, *462*, 48–55. https://doi.org/10.1016/j.desal.2019.04.004.

(32) Lin, S. Energy Efficiency of Desalination: Fundamental Insights from Intuitive Interpretation. *Environ. Sci. Technol.* **2020**, *54*, 76–84. https://doi.org/10.1021/acs.est.9b04788.

(33) Porada, S.; Zhang, L.; Dykstra, J. E. Energy Consumption in Membrane Capacitive Deionization and Comparison with Reverse Osmosis. *Desalination* **2020**, 455, 100–114. https://doi.org/10.1016/j.desal.2020.114383.

(34) Hassanvand, A.; Wei, K.; Talebi, S.; Chen, G. Q.; Kentish, S. E. The Role of Ion Exchange Membranes in Membrane Capacitive Deionisation. *Membranes* **2017**, *7*, 1–23. https://doi.org/10.3390/membranes7030054.

(35) Li, H.; Zou, L. Ion-Exchange Membrane Capacitive Deionization: A New Strategy for Brackish Water Desalination. *Desalination* **2011**, *275*, 62–66. https://doi.org/10.1016/j.desal.2011.02.027.

(36) Porada, S.; Zhao, R.; Van Der Wal, A.; Presser, V.; Biesheuvel, P. M. Review on the Science and Technology of Water Desalination by Capacitive Deionization. *Prog. Mater. Sci.* **2013**, *58* (8), 1388–1442. https://doi.org/10.1016/j.pmatsci.2013.03.005.

(37) Kim, J.; Jain, A.; Zuo, K.; Verduzco, R.; Walker, S.; Elimelech, M.; Zhang, Z.; Zhang, X.; Li, Q. Removal of Calcium Ions from Water by Selective Electrosorption Using Target-Ion Specific Nanocomposite Electrode. *Water Res.* **2019**, *160*, 445–453. https://doi.org/10.1016/j.watres.2019.05.016.

(38) Seo, S. J.; Jeon, H.; Lee, J. K.; Kim, G. Y.; Park, D.; Nojima, H.; Lee, J.; Moon, S. H. Investigation on Removal of Hardness Ions by Capacitive Deionization (CDI) for Water Softening Applications. *Water Res.* **2010**, *44*, 2267–2275. https://doi.org/10.1016/j.watres.2009.10.020.

(39) Zhao, R.; van Soestbergen, M.; Rijnaarts, H. H. M.; van der Wal, A.; Bazant, M. Z.; Biesheuvel, P. M. Time-Dependent Ion Selectivity in Capacitive Charging of Porous Electrodes. *J. Colloid Interface Sci.* **2012**, *384*, 38–44. https://doi.org/10.1016/j.jcis.2012.06.022.

(40) Yoon, H.; Lee, J.; Kim, S. R.; Kang, J.; Kim, S.; Kim, C.; Yoon, J. Capacitive Deionization with Ca-Alginate Coated-Carbon Electrode for Hardness Control. *Desalination* **2016**, *392*, 46–53. https://doi.org/10.1016/j.desal.2016.03.019.

(41) Hou, C. H.; Huang, C. Y. A Comparative Study of Electrosorption Selectivity of Ions by Activated Carbon Electrodes in Capacitive Deionization. *Desalination* **2013**, *314*, 124–129. https://doi.org/10.1016/j.desal.2012.12.029.

(42) Decher, G.; Hong, J. -D. Buildup of Ultrathin Multilayer Films by a Self-assembly Process, 1 Consecutive Adsorption of Anionic and Cationic Bipolar Amphiphiles on Charged Surfaces. *Makromol. Chemie. Macromol. Symp.* **1991**, *46*, 321–327. https://doi.org/10.1002/masy.19910460145.

(43) Decher, G. Fuzzy Nanoassemblies: Toward Layered Polymeric Multicomposites. *Science* **1997**, *277*, 1232–1237. https://doi.org/10.1126/science.277.5330.1232.

(44) Richardson, J. J.; Cui, J.; Björnmalm, M.; Braunger, J. A.; Ejima, H.; Caruso, F. Innovation in Layer-by-Layer Assembly. *Chem. Rev.* **2016**, *116* (23), 14828–14867. https://doi.org/10.1021/acs.chemrev.6b00627.

(45) Cao, Z.; Gordiichuk, P. I.; Loos, K.; Sudhölter, E. J. R.; de Smet, L. C. P. M. The Effect of Guanidinium Functionalization on the Structural Properties and Anion Affinity of Polyelectrolyte Multilayers. *Soft Matter* **2016**, *12*, 1496–1505. https://doi.org/10.1039/c5sm01655j.

(46) Paltrinieri, L.; Wang, M.; Sachdeva, S.; Besseling, N. A. M.; Sudhölter, E. J. R.; de Smet, L. C. P. M. Fe_3O_4 Nanoparticles Coated with a Guanidinium-Functionalized Polyelectrolyte Extend the pH Range for Phosphate Binding. *J. Mater. Chem. A* **2017**, *5*, 18476–18485. https://doi.org/10.1039/c7ta04054g.

(47) Paltrinieri, L.; Remmen, K.; Müller, B.; Chu, L.; Köser, J.; Wintgens, T.; Wessling, M.; de Smet, L. C. P. M.; Sudhölter, E. J. R. Improved Phosphoric Acid Recovery from Sewage Sludge Ash Using Layer-by-Layer Modified Membranes. *J. Memb. Sci.* **2019**, *587*, 117162. https://doi.org/10.1016/j.memsci.2019.06.002.

(48) Cheng, C.; Yaroshchuk, A.; Bruening, M. L. Fundamentals of Selective Ion Transport through Multilayer Polyelectrolyte Membranes. *Langmuir* **2013**, *29* (6), 1885–1892. https://doi.org/10.1021/la304574e.

(49) White, N.; Misovich, M.; Alemayehu, E.; Yaroshchuk, A.; Bruening, M. L. Highly Selective Separations of Multivalent and Monovalent Cations in Electrodialysis through Nafion Membranes Coated with Polyelectrolyte Multilayers. *Polymer* **2016**, *103*, 478–485. https://doi.org/10.1016/j.polymer.2015.12.019.

(50) Krasemann, L.; Tieke, B. Selective Ion Transport across Self-Assembled Alternating Multilayers of Cationic and Anionic Polyelectrolytes. *Langmuir* **2000**, *16*, 287–290. https://doi.org/10.1021/la991240z.

(51) Cheng, W.; Liu, C.; Tong, T.; Epsztein, R.; Sun, M.; Verduzco, R.; Ma, J.; Elimelech, M. Selective Removal of Divalent Cations by Polyelectrolyte Multilayer Nanofiltration Membrane: Role of Polyelectrolyte Charge, Ion Size, and Ionic Strength. *J. Memb. Sci.* **2018**, *559*, 98–106. https://doi.org/10.1016/j.memsci.2018.04.052.

(52) Said, Abdu, M.-C.; Manuel-César, Wong, J. E.; García-Gabaldón, M.; Wessling, M. Layer-by-Layer Modification of Cation Exchange Membranes Controls Ion Selectivity and Water Splitting. *ACS Appl. Mater. Interfaces* **2014**, *6*, 1843−1854.

(53) Cheng, C.; White, N.; Shi, H.; Robson, M.; Bruening, M. L. Cation Separations in Electrodialysis through Membranes Coated with Polyelectrolyte Multilayers. *Polymer* **2014**, *55*, 1397–1403. https://doi.org/10.1016/j.polymer.2013.12.002.

(54) Rijnaarts, T.; Reurink, D. M.; Radmanesh, F.; de Vos, W. M.; Nijmeijer, K. Layer-by-Layer Coatings on Ion Exchange Membranes: Effect of Multilayer Charge and Hydration on Monovalent Ion Selectivities. *J. Memb. Sci.* **2019**, *570–571*, 513–521. https://doi.org/10.1016/j.memsci.2018.10.074.

(55) Stanton, B. W.; Harris, J. J.; Miller, M. D.; Bruening, M. L. Ultrathin, Multilayered Polyelectrolyte Films as Nanofiltration Membranes. *Langmuir* **2003**, *19* (17), 7038–7042. https://doi.org/10.1021/la034603a.

(56) Tansel, B. Significance of Thermodynamic and Physical Characteristics on Permeation of Ions during Membrane Separation: Hydrated Radius, Hydration Free Energy and Viscous Effects. *Sep. Purif. Technol.* **2012**, *86*, 119–126. https://doi.org/10.1016/j.seppur.2011.10.033.

(57) Ouyang, L.; Malaisamy, R.; Bruening, M. L. Multilayer Polyelectrolyte Films as Nanofiltration Membranes for Separating Monovalent and Divalent Cations. *J. Memb. Sci.* **2008**, *310*, 76–84. https://doi.org/10.1016/j.memsci.2007.10.031.

(58) Zhu, Y.; Ahmad, M.; Yang, L.; Misovich, M.; Yaroshchuk, A.; Bruening, M. L. Adsorption of Polyelectrolyte Multilayers Imparts High Monovalent/Divalent Cation Selectivity to Aliphatic Polyamide Cation-Exchange Membranes. *J. Memb. Sci.* **2017**, *537*, 177–185. https://doi.org/10.1016/j.memsci.2017.05.043.

(59) de Grooth, J.; Oborný, R.; Potreck, J.; Nijmeijer, K.; de Vos, W. M. The Role of Ionic Strength and Odd-Even Effects on the Properties of Polyelectrolyte Multilayer Nanofiltration Membranes. *J. Memb. Sci.* **2015**, *475*, 311–319. https://doi.org/10.1016/j.memsci.2014.10.044.

(60) Kuzmyn, A. R.; De Los Santos Pereira, A.; Pop-Georgievski, O.; Bruns, M.; Brynda, E.; Rodriguez-Emmenegger, C. Exploiting End Group Functionalization for the Design of Antifouling Bioactive Brushes. *Polym. Chem.* **2014**, *5*, 4124–4131. https://doi.org/10.1039/c4py00281d.

(61) Hinterwirth, H.; Kappel, S.; Waitz, T.; Prohaska, T.; Lindner, W.; Lämmerhofer, M. Quantifying Thiol Ligand Density of Self-Assembled Monolayers on Gold Nanoparticles by Inductively Coupled Plasma-Mass Spectrometry. *ACS Nano* **2013**, *7*, 1129–1136. https://doi.org/10.1021/nn306024a.

(62) Lee, J.; Srimuk, P.; Zwingelstein, R.; Zornitta, R. L.; Choi, J.; Kim, C.; Presser, V. Sodium Ion Removal by Hydrated Vanadyl Phosphate for Electrochemical Water Desalination. *J. Mater. Chem. A* **2019**, *7* (8), 4175–4184. https://doi.org/10.1039/c8ta10087j.

(63) Suss, M. E. Size-Based Ion Selectivity of Micropore Electric Double Layers in Capacitive Deionization Electrodes. *J. Electrochem. Soc.* **2017**, *164* (9), E270--E275. https://doi.org/10.1149/2.1201709jes.

(64) Kolasińska, M.; Warszyński, P. The Effect of Support Material and Conditioning on Wettability of PAH/PSS Multilayer Films. *Bioelectrochemistry* **2005**, *66*, 65–70. https://doi.org/10.1016/j.bioelechem.2004.03.009.

(65) Gentile, P.; Frongia, M. E.; Cardellach, M.; Miller, C. A.; Stafford, G. P.; Leggett, G. J.; Hatton, P. V. Functionalised Nanoscale Coatings Using Layer-by-Layer Assembly for Imparting Antibacterial Properties to Polylactide-Co-Glycolide Surfaces. *Acta Biomater.* **2015**, *21*, 35–43. https://doi.org/10.1016/j.actbio.2015.04.009.

(66) Mulyati, S.; Takagi, R.; Fujii, A.; Ohmukai, Y.; Matsuyama, H. Simultaneous Improvement of the Monovalent Anion Selectivity and Antifouling Properties of an Anion Exchange Membrane in an Electrodialysis Process, Using Polyelectrolyte Multilayer Deposition. *J. Memb. Sci.* **2013**, *431*, 113–120. https://doi.org/10.1016/j.memsci.2012.12.022.

(67) White, N.; Misovich, M.; Yaroshchuk, A.; Bruening, M. L. Coating of Nafion Membranes with Polyelectrolyte Multilayers to Achieve High Monovalent/Divalent Cation Electrodialysis Selectivities. *ACS Appl. Mater. Interfaces* **2015**, *7*, 6620−6628.

(68) Li, L.; Wu, L.; Wu, F.; Song, S.; Zhang, X.; Fu, C.; Yuan, D.; Xiang, Y. Review - Recent Research Progress in Surface Modification of LiFePO4 Cathode Materials. *J. Electrochem. Soc.* **2017**, *164*, A2138–A2150. https://doi.org/10.1149/2.1571709jes.

(69) Dykstra, J. E.; Dijkstra, J.; Van der Wal, A.; Hamelers, H. V. M.; Porada, S. On-Line Method to Study Dynamics of Ion Adsorption from Mixtures of Salts in Capacitive Deionization. *Desalination* **2016**, *390*, 47–52. https://doi.org/10.1016/j.desal.2016.04.001.

(70) Sata, T.; Sata, T.; Yang, W. Studies on Cation-Exchange Membranes Having Permselectivity between Cations in Electrodialysis. *J. Memb. Sci.* **2002**, *206*, 31–60. https://doi.org/10.1016/S0376-7388(01)00491-4.

(71) Luo, T.; Abdu, S.; Wessling, M. Selectivity of Ion Exchange Membranes: A Review. *J. Memb. Sci.* **2018**, *555*, 429–454. https://doi.org/10.1016/j.memsci.2018.03.051.

(72) Riegler, H.; Essler, F. Polyelectrolytes. 2: Intrinsic or Extrinsic Charge Compensation? Quantitative Charge Analysis of PAH/PSS Multilayers. *Langmuir* **2002**, *18* (17), 6694–6698. https://doi.org/10.1021/la020108n.

(73) Joseph, N.; Ahmadiannamini, P.; Hoogenboom, R.; Vankelecom, I. F. J. Layer-by-Layer Preparation of Polyelectrolyte Multilayer Membranes for Separation. *Polym. Chem.* **2014**, *5* (6), 1817–1831. https://doi.org/10.1039/c3py01262j.

(74) Gabelich, C. J.; Tran, T. D.; Suffet, I. H. Electrosorption of Inorganic Salts from Aqueous Solution Using Carbon Aerogels. *Environ. Sci. Technol.* **2002**, *36*, 3010–3019. https://doi.org/10.1021/es0112745.

(75) Avraham, E.; Yaniv, B.; Soffer, A.; Aurbach, D. Developing Ion Electroadsorption Stereoselectivity, by Pore Size Adjustment with Chemical Vapor Deposition onto Active Carbon Fiber Electrodes. Case of Ca^{2+} /Na^{+} Separation in Water Capacitive Desalination. *J. Phys. Chem. C* **2008**, *112*, 7385–7389. https://doi.org/10.1021/jp711706z.

(76) Mossad, M.; Zhang, W.; Zou, L. Using Capacitive Deionisation for Inland Brackish Groundwater Desalination in a Remote Location. *Desalination* **2013**, *308*, 154–160. https://doi.org/10.1016/j.desal.2012.05.021.

(77) Yoon, H.; Jo, K.; Kim, K. J.; Yoon, J. Effects of Characteristics of Cation-Exchange Membrane on Desalination Performance of Membrane Capacitive Deionization. *Desalination* **2019**, *458*, 116–121. https://doi.org/10.1016/j.desal.2019.02.009.

(78) Zornitta, R. L.; Srimuk, P.; Lee, J.; Krüner, B.; Aslan, M.; Ruotolo, L. A. M.; Presser, V. Charge and Potential Balancing for Optimized Capacitive Deionization Using Lignin-Derived, Low-Cost Activated Carbon Electrodes. *ChemSusChem* **2018**, *11* (13), 2101–2113. https://doi.org/10.1002/cssc.201800689.

Supplementary Information to:

Modification of Cation-Exchange Membranes with Polyelectrolyte Multilayers to Tune Ion Selectivity in Capacitive Deionization

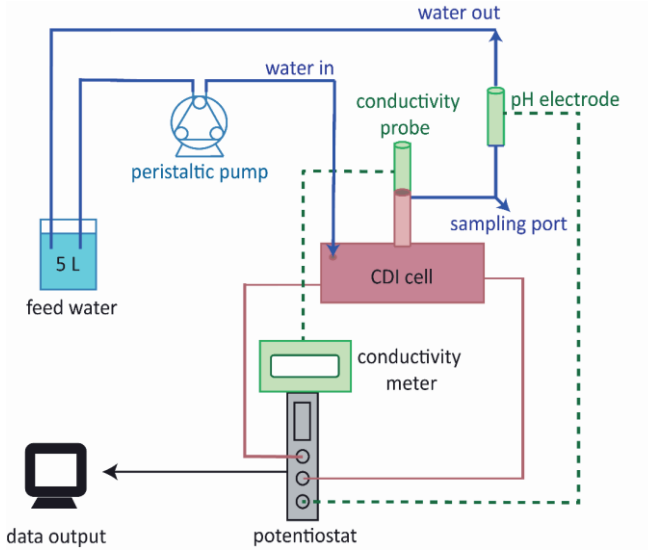

Figure S4.1: Schematic representation of the MCDI system.

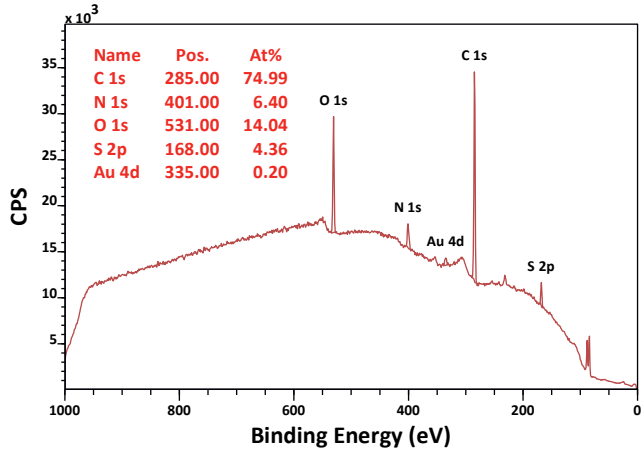

Figure S4.2: Wide-scan XPS spectrum of a MESNA-(PAH/PSS)$_5$PAH coating on gold substrates.

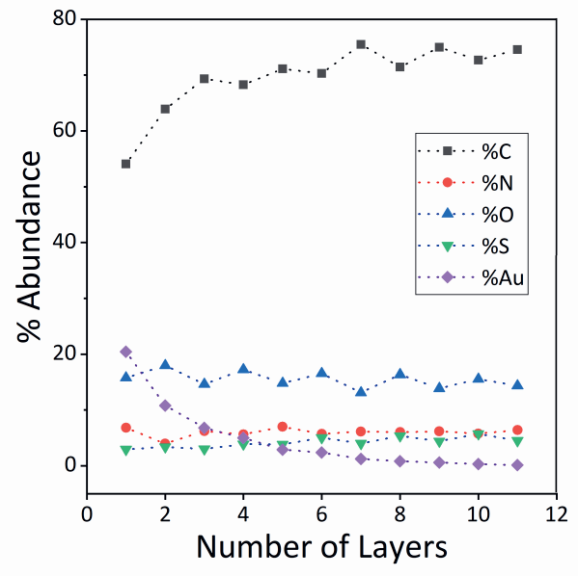

Figure S4.3: % Abundance of carbon (C), nitrogen (N), oxygen (O), sulfur (S), and gold (Au) as a function of the layer number. Data was obtained with X-ray photoelectron spectroscopy.

The AFM height profile images of an air-dried bare CMX sample (**Figure S4.4A**) show (sub)micron-sized features, which is slightly smaller than those reported by Sarapulova *et al.*[1] The AFM image of the PEM-CMX sample (**Figure S4.4B**) give a slightly higher root-mean-square (RMS) value (58 vs. 37 nm), while no clear difference in the feature sizes were observed in the height (**Figures S4.4A** and **S4.4B**) and the amplitude (**Figures S4.4C** and **S4.4D**). We conclude that the AFM data do confirm the presence of the PEM and that, apart from the overall surface roughness, the main surface characteristics are not affected by the addition of the PEM.

The dry, optical thickness of the PEM of PEM-coated gold substrates was found to be 16.4 ± 0.9 nm, which is comparable with literature.[2,3]

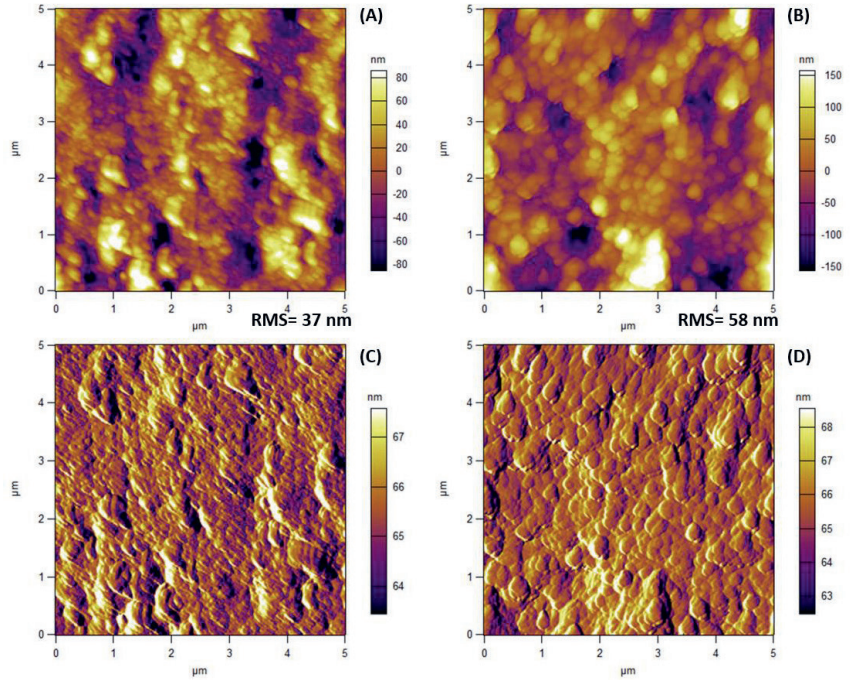

Figure S4.4. AFM images of air-dried membranes (scanning size 5 µm × 5 µm), obtained in height mode (A) CMX (B) PEM-CMX and amplitude mode (C) CMX and (D) PEM-CMX.

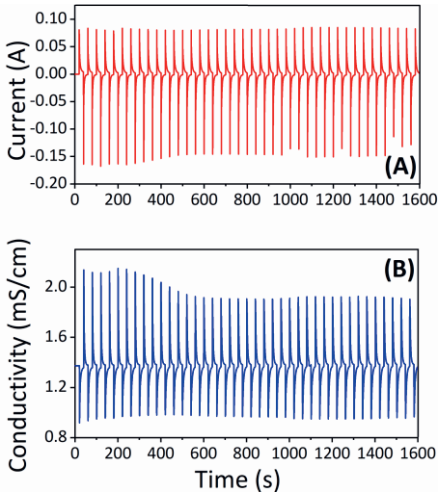

Figure S4.5: (A) Current and (B) conductivity data recorded online during a 40-cycle experiment using a CMX-PEM membrane.

Table S4.1: Coulombic efficiency, desalination capacity, and salt adsorption capacity values of different adsorption steps using a CMX-PEM membrane during a 40-cycle MCDI experiment.

Step	Coulombic efficiency (%)	Desalination capacity (mS.mL/cm)	Salt adsorption capacity (mg/g)
5	94.1	191.9	3.6
25	97.1	191.6	3.9
40	95.4	191.9	4.0

The Coulombic efficiency was calculated as stated in the literature.[4] The desalination capacity was calculated by multiplying the integration of the conductivity graphs of adsorption cycles with the flow rate of 7.5 mL/min. Salt adsorption capacity was calculated by using **Equation 4.4**.

Table S4.2: The selectivity values $\rho_{\mathrm{Mg}}^{\mathrm{Na}}$ for different adsorption steps of experiments using CMX, CMX-PEM, and CIMS. The average was calculated using the data from 9 steps (*i.e.*, 3 steps per experiment) per membrane.

Step	CMX	CMX-PEM	CIMS
1	0.4	2.8	0.4
2	0.5	3.0	0.2
3	0.5	3.1	0.1
4	0.4	2.4	0.2
5	0.4	2.8	0.2
6	0.4	2.9	0.1
7	0.4	2.5	0.3
8	0.5	2.6	0.3
9	0.4	2.5	0.3
AVE	0.4	2.7	0.2
STDEVA	0.1	0.3	0.1

References

(1) Sarapulova, V.; Shkorkina, I.; Mareev, S.; Pismenskaya, N. *et al.* Transport Characteristics of Fujifilm Ion-Exchange Membranes as Compared to Homogeneous Membranes AMX and CMX and to Heterogeneous. *Membranes* **2019**, 9(84), 1–23. https://doi:10.3390/membranes9070084.

(2) Rijnaarts, T.; Reurink, D. M.; Radmanesh, F.; de Vos, W. M.; Nijmeijer, K. Layer-by-Layer Coatings on Ion Exchange Membranes: Effect of Multilayer Charge and Hydration on Monovalent Ion Selectivities. *J. Memb. Sci.* **2019**, *570–571*, 513–521. https://doi.org/10.1016/j.memsci.2018.10.074.

(3) Cao, Z.; Gordiichuk, P. I.; Loos, K.; Sudhölter, E. J. R.; De Smet, L. C. P. M. The Effect of Guanidinium Functionalization on the Structural Properties and Anion Affinity of Polyelectrolyte Multilayers. *Soft Matter* **2016**, *12*, 1496–1505. https://doi.org/10.1039/c5sm01655j.

(4) Hawks, S. A.; Ramachandran, A.; Porada, S.; Campbell, P. G.; Suss, M. E.; Biesheuvel, P. M.; Santiago, J. G.; Stadermann, M. Performance Metrics for the Objective Assessment of Capacitive Deionization Systems. *Water Res.* **2019**, *152*, 126–137. https://doi.org/10.1016/j.watres.2018.10.074.

Chapter 5

Simultaneous, Monovalent Ion Selectivity with Polyelectrolyte Multilayers and Intercalation Electrodes in Capacitive Deionization

This chapter was adapted from:

Singh, K.*, Sahin, S.*, Gamaethiralalage, J. G., Zornitta, R. L., & de Smet, L. C. P. M. Simultaneous, Monovalent Ion Selectivity with Polyelectrolyte Multilayers and Intercalation Electrodes in Capacitive Deionization. *Chem. Eng. J.*, **2021**, 128329.

*contributed equally

Abstract

Selective ion separation via capacitive deionization (CDI) is of relevance because of its environmental and industrial applications in water purification and softening, heavy metal removal, and resource recovery. Conventionally, carbon electrodes and ion-selective membranes have been used for selective removal of anions and cations. In this study, we engineered a CDI cell with two identical NiHCF electrodes, separated by an anion exchange membrane coated with a polyelectrolyte multilayer (PEM), for simultaneous and selective separation of monovalent over divalent anions and cations. The modified membrane rejects divalent over monovalent anions while the NiHCF electrodes selectively adsorb monovalent over divalent ions. A separation factor (β) of 7 < β < 14 was obtained for Cl− over SO42−, while an average β of ≈ 17 was obtained for Na+ over Mg2+, reflecting the preference of the modified membrane and the electrodes, respectively. Moreover, this preference was preserved at low concentrations of monovalent ions as well. This tandem use of intercalation electrodes and a PEM membrane provides a new and facile method for simultaneous cation and anion selectivity in CDI, opening new avenues for enhanced and tunable separations from complex ion mixtures.

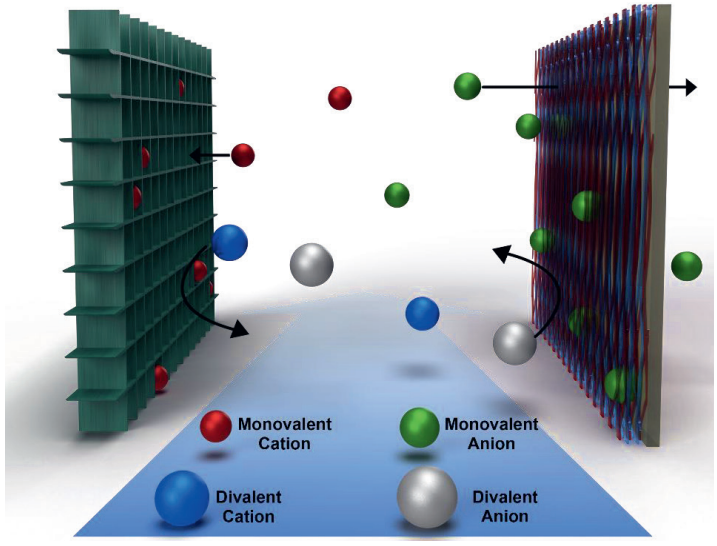

5.1 Introduction

Capacitive deionization, CDI, is a water desalination technique in which ions are removed from water under the influence of an applied current or a potential difference,[1–3] and stored in capacitive electrodes. CDI has been proven to be also applicable in selective ion removal and has been successfully used for cationic as well as anionic separations from aqueous ion mixtures.[4–8] Selective ion removal is necessary for various applications, including water softening,[9] recovery of resources such as lithium[10] or phosphate,[11] and treatment of irrigation water in greenhouses.[12]

Conventionally, due to the limited ion selectivity of the bare porous carbon[13], it has been typically used with either surface modifications[14–16] or coupled with ion-exchange membranes in (M)CDI,[17,18] to selectively separate both cations and anions. Alternative pathways to induce ion selectivity in CDI have recently been explored in literature.[4,8,19] On membrane level, special-grade commercial membranes, surface-modified ion-exchange membranes (IEMs), and selective resin coated carbon electrodes have been used for cation and anion selectivity.[20–22] Recently, a polyelectrolyte multilayer (PEM) modified cation-exchange membrane was used to obtain selectivity towards monovalent cation in MCDI.[19] This approach of coating PEMs[23–25] onto a membrane by a layer-by-layer (LbL) technique[26,27] is a facile and efficient method, and is based on alternating immersions of the membrane into oppositely charged polyelectrolyte solutions. The repeated action results in a thin multilayer whose thickness and composition can be controlled.[28] The final selectivity of a PEM-coated IEM depends on the type of the polyelectrolytes (PEs) used, the terminating layer, and the total number of layers deposited on the membrane surface.[29–31] A PEM can function as a selective layer via different mechanisms including electrostatic repulsion, also referred as charge exclusion,[31–33] and preferential transport of ions, based on their dehydration energy.[34] Thin films deposited via the LbL technique find use as functional materials and interfaces in various fields, including tissue engineering and capillary electrophoresis,[28] selective ion separation such as heavy metal removal, and anti-fouling applications.[35,36] PEMs have already been used in electro-driven systems, such as

electrodialysis, to introduce and tune ion selectivity.[30,31,37] Thus, a PEM-modified membrane is promising for selective ion removal in CDI.

On the electrode level, intercalation materials have been successfully used for selective cation separations in CDI.[4,8,38] Prussian blue analogues (PBAs) are a subclass of intercalation materials[4,39,40] that store only cations in their interstitial lattice sites, unlike graphite, layered oxides, and carbides that can intercalate both cations and anions.[41] The intercalation of ions in PBAs is accompanied by the reduction of a redox-active element in the lattice. [42] These materials have found use in a variety of applications including energy storage,[40] brackish water desalination,[43] and selective ion removal.[4,6] Among all PBAs, nickel hexacyanoferrate, NiHCF, is among the most used intercalation electrode material in CDI[4,39,44] due to its ease of fabrication, non-toxic nature, high charge storage capacity, energy efficiency,[44] and fast ion-adsorption kinetics.[45] Most importantly, NiHCF shows an inherent size-based selectivity towards monovalent cations[4,39,46] as it has demonstrated ≈ 20 times higher affinity towards Na^+ over Mg^{2+} and Ca^{2+}.[4] However, unlike carbon, NiHCF particles do not store anions in their lattice sites and therefore, their size-based selectivity excludes anions.

In this study, we introduce simultaneous cation and anion selectivity to a symmetric CDI system, assembled according to the rocking chair configuration,[47,48] by implementing measures at both the electrode and the membrane level. This was accomplished by integrating a PE**M**-**c**oated AE**M** (MCM) with two identical NiHCF electrodes in an electrode – membrane – electrode sandwich. Poly(diallyl dimethylammonium chloride) (PDADMAC) and poly(sodium 4-styrenesulfonate) (PSS) were chosen as polycation and polyanion, respectively, to prepare PEMs on an AEM surface via the LbL deposition because they are strong PEs in a wide range of the pH and the concentration of the salt solution. Also, they remain physically (under pressure)[49] and chemically (against oxidants)[50] stable and have been successfully used in ED for anion selectivity.[36]

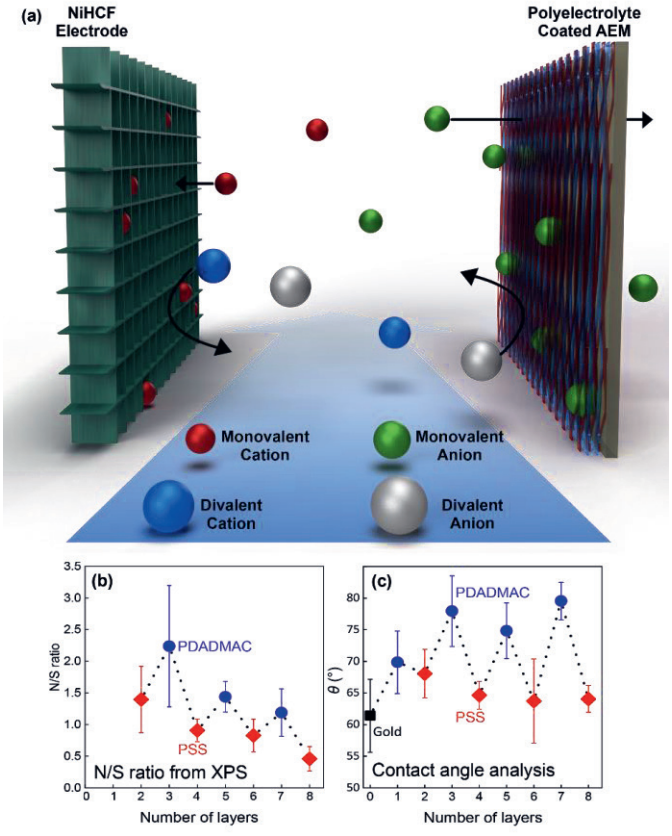

Figure 5.1: (a) Illustration of the cathodic chamber producing the diluate in the symmetric CDI cell, fully illustrated elsewhere,[48] with an NiHCF electrode and a PEM-coated AEM, separated by a flow channel containing a feed with multiple types of ions. Upon applying an electric current or a potential difference to the cell, the cations are driven towards the NiHCF electrode to the left and selectively stored in the lattices.[4] Simultaneously, the anions are selectively allowed to pass through the modified membrane on the right, resulting in a diluted feed in the middle. Surface characterization of the PEM with **(b)** XPS survey scans providing the N/S ratio and **(c)** static water contact angle (θ) analyses as a function of the number of layers on the membrane surface.

The schematic in **Figure 5.1a** depicts one half of the cell, representing the diluate chamber. The other half of this symmetric cell, depicted elsewhere,[48] undergoes a mirrored operation and produces a concentrated stream. The NiHCF electrodes selectively adsorb cations, based on their size, by storing them in interstitial lattice sites, as demonstrated elsewhere.[4] Simultaneously, the MCM selectively separates anions migrating from the diluate, providing an elegant, one-step configuration for both cation and anion selectivity. Furthermore, we also elucidate the effect of the number of layers coated onto the membrane, and the ionic content of the feed on selective anion separation.

5.2 Methods

Poly(diallyl dimethylammonium chloride) (PDADMAC, 20 % wt. H_2O), poly(sodium 4-styrenesulfonate) (PSS) sodium chloride (both from Sigma Aldrich) and hydrochloric acid (36.5 - 28.0 %, VWR) were used as received. Standard-grade (Neosepta ASE, Astom) and special-grade monovalent-selective (Neosepta ACS, Astom) AEMs were soaked in Milli-Q water (Milli-Q Integral 3 system, Millipore) for 48 h before use. The multilayer fabrication procedure was adopted from literature with some modifications.[19] Briefly, the standard-grade AEM was dipped in PSS and PDADMAC solutions, by a robotic arm (Dobot), prepared in Milli-Q water, alternately from solutions of 0.05 M polymer in 0.5 M NaCl at pH = 2.3 each for 20 min. After each layer deposition, the membrane was dipped in MQ water for 3 min to remove weakly attached polymers. The process was repeated until the desired amount of layers, namely 5, 9, 10, 14, 15, 23, and 31 were reached. When the total number of layers coated onto the membrane surface was odd, a negatively charged PSS was the terminating PE, while the positively charged PDADMAC was the terminating PE when the total number of layers was even. The LbL coating workflow is illustrated in **Figure S5.1**. Furthermore, the PEMs were coated onto model gold surfaces[19] (1 cm × 1 cm purchased from ECsens) and characterized with X-ray photoelectron spectroscopy (XPS) and static water contact angle analysis (SWA), an approach similar to those of previous reports.[36,51] The experimental

details are described in the **Section 6S.1** and **S.2** of the Supporting information, provided after the conclusion of this chapter.

The NiHCF active particles were synthesized via co-precipitation method.[4] Briefly, 24 mM and 12 mM solutions of $NiCl_2 \cdot 6H_2O$ (Alfa Aesar) and $Na_4[Fe(CN)_6] \cdot 10H_2O$ (Sigma-Aldrich), respectively, were added drop-wise to the reaction solution (1 % v/v solution of HCl in water) and stirred at 600 rpm for ≈ 12 h. The product was washed three times with Milli-Q water during vacuum filtration and dried at 60 °C under vacuum. The dried powder was milled with conductive carbon black (Cabot) and mixed with polytetrafluoroethylene (PTFE) (Sigma Aldrich) in a weight ratio of 8:1:1, with ethanol as a solvent. The mixture was kneaded into a dough and cold-rolled with a stainless steel rolling machine (MTI corp.) into 200 µm thick rectangular electrodes with 20 cm^2 area, weighing between 0.35 – 0.45 g. After the cold-rolling, the electrodes were dried at 60 °C under vacuum.

Prior to cell assembly, two identical NiHCF electrodes were pre-treated in a three-electrode cell, with a platinum-coated titanium mesh counter, an Ag/AgCl electrode reference, and a 1 M Na_2SO_4 solution as an electrolyte. One electrode was saturated with Na^+, while the other was depleted, by discharging and charging them at 0 and 1 V vs. Ag/AgCl, respectively, for 1 h. After the pre-treatment, the electrodes were assembled into a cell, separated by nylon spacer channels (160 µm thick) and a MCM. Two identical 100 mL reservoirs containing feed solutions, whose compositions are provided in **Table 5.1**, fed the cell at a constant flow rate of 10 mL/min. The feed residence time in the cell was 4.3 seconds. The ion-selectivity experiments were performed with two types of feed solutions: one containing a mixture of mono- and divalent anions (**F1** and **F2**) and another containing a mixture of only monovalent anions (**F3** and **F4**), to respectively, provide an insight into the two frequently reported mechanisms of MCM selectivity based on charge exclusion [36] and dehydration energy of anions [22].

The ion-selectivity experiments were performed in a continuous desalination mode[4] during which the CDI cell was operated under constant voltage of ± 1 V via a potentiostat (Ivium n-stat, IVIUM Technologies). One complete desalination cycle consisted

of two steps lasting 0.5 h each. During the first step, a voltage of 1 V was applied to the cell. After 0.5 h, 800 µL was taken from both the reservoirs. The anion concentration was analyzed via ion chromatography (Eco IC, Metrohm) while the cation concentration was analyzed via inductively coupled plasma optical emission spectroscopy (PerkinElmer Avio 500 ICP-OES). Next, the electrode polarities were reversed, and the diluate and the concentrate reservoirs were manually switched between the cell chambers, by switching the pipes connecting the reservoirs and the chambers. Following this, a voltage of –1 V was applied for 0.5 h after which, 800 µL was taken from both the reservoirs for concentration analysis. The end of this step concluded one full desalination cycle. The experimental workflow is illustrated in detail in **Figure S5.2**. A sample current-voltage profile of one desalination cycle is given in **Figure S5.3**. The anionic selectivity of the MCM was investigated by varying the number of layers coated onto it and the type of ions in the feed solution. Since the cationic selectivity in symmetric cell with NiHCF electrodes was recently reported,[4] the experiments here focus mainly on the anionic selectivity of the MCM. The experiments were duplicated for reproducibility and the average values of the concentrations were used for selectivity calculations.

Table 5.1: Composition of the feed solutions (10 mM each) in the two chambers of the CDI cell with NiHCF electrodes separated by a MCM for ion selectivity experiments.

Feed number	Na^+ (mM)	NO_3^- (mM)	Cl^- (mM)	SO_4^{2-} (mM)	$H_2PO_4^-$ (mM)	Mg^{2+} (mM)
F1	10	-	10	10	-	10
F2	20	-	10	10	-	-
F3	20	-	10	-	10	-
F4	20	10	10	-	-	-

5.3 Results and Discussions

The chemical composition of the PEM-coated gold substrates was analyzed with XPS. The nitrogen/sulfur (N/S) ratio of the samples, provided in **Figure 5.1b**, shows an alternating trend with the number of polyelectrolyte layers, because nitrogen and sulfur are exclusively present in PDADMAC and PSS, respectively. Therefore, the trend serves as a clear evidence of a successful multilayer build-up on the gold surface, and is in line with literature.[36] Following the XPS, the SWA study of the PEM, results of which are presented in **Figure 5.1c**, shows an odd-even effect, characteristic of an LbL-prepared PEM.[52] This trend can be attributed to the higher hydrophobicity of the PDADMAC-terminated layer than that of the PSS-terminated layer, and gives a clear indication of a successful multilayer deposition on the membrane surface, further verifying the XPS data.

The continuous mode of desalination paired the diluate reservoir with the intercalating electrode, producing deionized water throughout the desalination cycle. Thus, the ion concentration in the diluate decreased continuously with an increasing number of cycles. Due to the symmetric cell operation, the ion concentration increased by a similar amount in the concentrate reservoir. The concentration of both cations and anions as a function of desalination steps, during the treatment of feed **F1**, is shown in **Figure 5.2a** and **5.2b**. The diluate and the concentrate reservoirs are depicted by fading and increasing color gradients, respectively. The trends in the figure confirm the symmetrical operation with respect to cations as well as anions, while they also demonstrate that the proposed cell can successfully distinguish between both cations (Na^+ and Mg^{2+}) and both anions (Cl^- and SO_4^{2-}), simultaneously. The MCM blocks the divalent SO_4^{2-} and allows the monovalent Cl^- to selectively pass through it, while the NiHCF electrode selectively intercalates monovalent Na^+ over divalent Mg^{2+}. Furthermore, the selective removal of monovalent ions remained highly independent of their concentration over divalent ions in the feed, even after the monovalent ion concentration reduced by over 90 % in the feed. For example, from cycle 3 to 4 in **Figure 5.2a**, the concentration of Cl^- in the diluate went from 12% to 2% while that of SO_4^{2-} went from 93% to 92%. This indicates that even at the ratio of 7:1 SO_4^{2-}: Cl^-, the

monovalent Cl^- was preferentially allowed through the MCM. Similar observation was also made during the selective adsorption of Na^+ over Mg^{2+} in the NiHCF electrode, as seen in **Figure 5.2b**.

The effect of the number of layers on the anion selectivity of the membrane was investigated by treating **F2** with a symmetric cell containing a MCM that consisted of 5, 6, 9, 10, 14, 15, 23, or 31 polyelectrolyte layers. **F2** contained only Na^+ to avoid any synergistic effect on the anion selectivity, caused by the presence of two different cations in the feed. Early evidence of such an effect is shown in **Figure S5.4**, but further investigation is required to reach a conclusion. The resulting concentration of Cl^- and SO_4^{2-} in the diluate for selected 5, 15, and 31 layer PEMs is presented in **Figure 5.2c**. (The full data set for MCM with all other layers, the control experiment with a bare membrane, and with a commercial, monovalent anion-selective membrane is given in **Figure S5.5.**) It is evident from **Figure 5.2c** that the removal and rejection of Cl^- and SO_4^{2-}, respectively, increases with increasing number of layers from 5 to 15 (**Figure 5.2c** and **S5.3a**). For example, the MCM with 5 layers removed ≈15% SO_4^{2-} at 50% Cl^- removal, while the MCM with 15 layers removed only ≈7% SO_4^{2-} at 50% of Cl^- removal. For an odd number of layers on membrane surface, the increase in selectivity follows from an increase in the excess charge density of the MCM. The highest selectivity of the MCM, obtained with 15 layers, towards the monovalent Cl^- over the divalent SO_4^{2-} is attributed to the charge exclusion effect of the outermost, negatively charged PSS layer. The electrostatic repulsion of this outermost layer is larger towards the −2 charge of the SO_4^{2-} than the −1 charge of the Cl^- ion. This charge-based exclusion is driven by the charge of the outermost layer since the MCM preference switched towards SO_4^{2-} when the terminating layer is positively charged, as observed for the even number of PEMs, namely 6, 10, and 14, as shown in **Figure 5.1b**, **5.1c**, and **S5.5b**. This property of PEMs has also been reported before in ED literature [36,53]. Here, the treatment of feeds **F1** and **F2**, containing a mixture of Cl^- and SO_4^{2-}, provides an insight into the charge-exclusion based selectivity of the MCM.

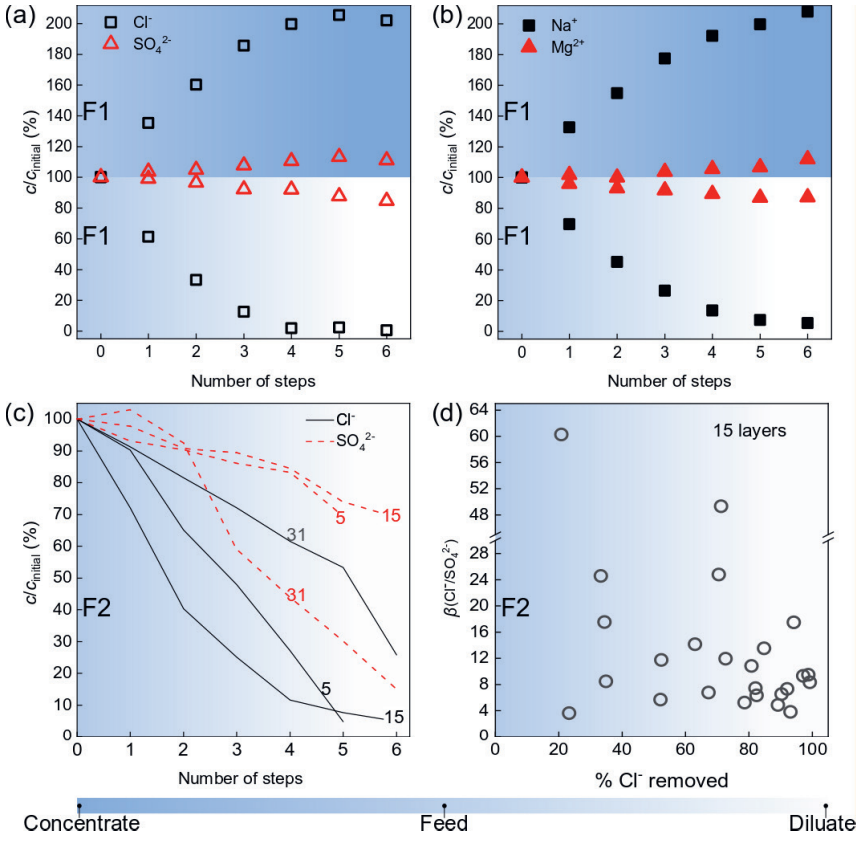

Figure 5.2: (a) Concentration of Cl^- (black hollow squares) and SO_4^{2-} (red hollow triangles) relative to the initial **F1** concentration, in the diluate and the concentrate chambers as a function of the number of steps, treated by the symmetric cell with identical NiHCF electrodes, separated by a MCM with 15 layers. **(b)** Concentration of Na^+ (black squares) and Mg^{2+} (red triangles) relative to the concentration of **F1**, in the diluate and the concentrate chamber as a function of the number of cycles, treated by a symmetric cell with identical NiHCF electrodes, separated by a MCM with 15 layers. **(c)** Concentration of anions in the diluate, during the treatment of **F2**, by MCM with 5, 15, and 31 layers. **(d)** Selectivity, β, of a MCM with 15 layers towards Cl^- over SO_4^{2-} from **F2**, as a function of Cl^- concentration in the diluate, obtained over multiple experiments.

A further increase in the number of layers to 23 (**Figure S5.5a**) and 31 switches the membrane selectivity towards SO_4^{2-}, resembling the selectivity properties of a bare membrane and MCMs with an even number of PEM, namely 6, 10, and 14, as shown in **Figures S5.5b** and **S5.5c**. The observed switch in preference of the MCM from monovalent towards divalent ions can be related to an overall positive bulk charge that develops on the MCM surface with an increasing number of layers.[54] This phenomenon has been attributed to the charge balance within the PEM which is reported to be a combination of an interlayer attraction between PDADMAC and PSS and extrinsic interactions between PDADMAC/PSS layers and the salt counterion.[54] In short, as the number of layers increase, the amount of newly adsorbed PSS reduces while the PDADMAC compensates its charge with external counter ions, other than PSS, giving the PEM an overall positive bulk charge. Thus, a switch in selectivity of the MCM, as obtained in this study between 15 and 23 layers, as shown in **Figure 5.2c** and **S3a,** is expected with increasing number of layers. Therefore, a PSS-terminated MCM with ≤ 15 layers prefers the monovalent ions, while divalent ions are preferred by an MCM with ≥ 23 layers, regardless the type of terminating layer. Interestingly, the MCM with ≤ 15 layers can also be made divalent ion-selective when the outermost layer is PDADMAC instead of PSS, as shown in **Figure S5.5b**.

The preference of MCM towards one anion over the other is quantified as β,[4,6,16,55]

$$\beta = \left(\frac{c_{1,initial} - c_{1,final}}{c_{2,initial} - c_{2,final}}\right)\left(\frac{c_{2,initial}}{c_{1,initial}}\right),$$

where 1 and 2 represent the two competing ions and $c_{1,initial}$, $c_{2,initial}$, $c_{1,final}$, and $c_{2,final}$ are the ion concentrations in the beginning and at the end of the adsorption step, respectively. The β for Cl^- over SO_4^{2-}, obtained for 15 layers from multiple experiments is shown in **Figure 5.2d**. Even with the scatter in the data, it can be safely concluded that the selectivity towards Cl^- was maintained even after 90 % of it was removed. The majority of the β values were found to be in the range of $7 < \beta < 14$. The NiHCF electrodes simultaneously removed Na^+ selectively over Mg^{2+} with an average $\beta \approx 17$. The β for Cl^- over SO_4^{2-} fell typically between $3 < \beta < 6$ for 5 layers and $4 < \beta < 9$ for 9 layers, as shown in **Figures S5.6a** and **S5.6b**,

highlighting the correlation between the anion selectivity and the number of layers. In contrast, the bare membrane from the control experiment showed an affinity towards SO_4^{2-} with $\beta \approx 2$. For further comparison, a $\beta \approx 7$ was obtained towards Cl^- over SO_4^{2-} during the treatment of **F2** with the symmetric CDI cell containing a commercial, monovalent anion-selective membrane (**Figure S5.5d**). The β values, obtained here for MCM with 15 layers, are higher than the values reported in electrodialysis[36] and reverse electrodialysis,[51] with membranes coated with poly(allylamine hydrochloride)/PSS and polyethylenimine/PSS PEs, respectively, that resulted in a selectivity of ≈ 2.5. Additionally, the β values presented in **Figure 5.2d** are also comparable to the Cl^-/SO_4^{2-} selectivity of 27, obtained in nanofiltration with PDADMAC/PSS-coated membrane.[56]

To investigate the mechanism of the ion selectivity of the MCM based on dehydration energy of the anions, two additional solutions containing a mixture of only monovalent anions were treated with the symmetric cell containing a MCM with 15 layers. Feeds **F3** and **F4,** as described in **Table 5.1** contained monovalent phosphate, $H_2PO_4^-$ and nitrate, NO_3^-, respectively, with Cl^-. The concentration of these anions in the diluate, as obtained during the desalination experiment, is given in **Figure 5.3a** and **5.3b**. It is evident from the graph that the PEM does not differentiate much between Cl^- and NO_3^-, as both were removed with only a marginal preference for NO_3^- ions. However, the modified membrane preferred Cl^- over $H_2PO_4^-$, delivering a $\beta \approx 3$ towards Cl ions. This selectivity behavior of the MCM can be ascribed to the dehydration energy of the passing anion, all carrying the same charge. $H_2PO_4^-$ was the second most rejected anion, after SO_4^{2-} which carried a −2 charge. Even though the dehydration energy of SO_4^{2-} is the largest among all the anions here ($\Delta G_{hydration}$ = 1080 kJ/mol),[23] its rejection is better explained by charge-exclusion because, for a bare AEM, SO_4^{2-} was preferentially transported over Cl^-, as shown in **Figure 5.5c**. Once the membrane surface had a negative charge (*e.g.* for MCM with 15 layers), the transport of SO_4^{2-} through the MCM was hindered, hinting that the $\Delta G_{hydration}$ did not play as significant a role as its −2 charge. On the other hand, the reduced degree of rejection of $H_2PO_4^-$ may be attributed to two factors: (a) reduced electrostatic repulsion

from the terminating PSS layer because of its −1 charge; (b) smaller dehydration energy ($\Delta G_{hydration}$ = 465 kJ/mol), which can ease the removal of the water solvation shell around the anion, facilitating its passage through the membrane. Finally, NO_3^- was the most preferred anion of all. This high preference may be attributed to its lowest dehydration energy ($\Delta G_{hydration}$ = 300 kJ/mol), which is even smaller than that of Cl^- ($\Delta G_{hydration}$ = 340 kJ/mol). In addition, it retains the advantage of reduced electrostatic repulsion because of its monovalent nature, like Cl^- and $H_2PO_4^-$ ions. Thus, the anion preference of the MCM, based on the ease of dehydration, can be summarized as: $NO_3^- > Cl^- > H_2PO_4^- > SO_4^{2-}$. Unlike the size-based exclusion seen towards cations in NiHCF electrodes, the trend observed here does not depend on the hydrated anion size, as NO_3^- is bigger than both Cl^- [57] and $H_2PO_4^-$ [23], and yet it is the easiest to remove. Thus, the size of an anion on its own does not provide complete information about the MCM selectivity.

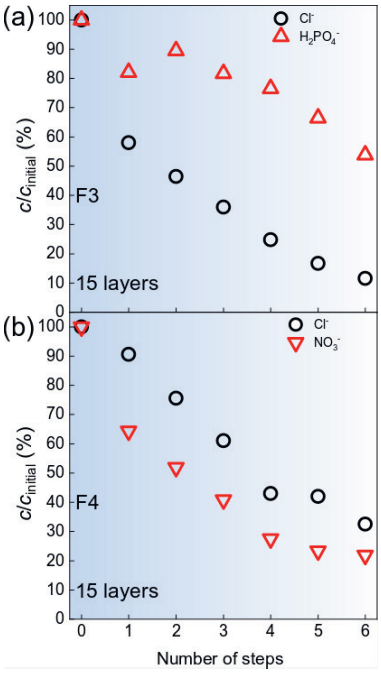

Figure 5.3: Change in concentration of **(a)** monovalent phosphate ($H_2PO_4^-$) and chloride (Cl^-) during treatment of feed **F3** and **(b)** nitrate (NO_3^-) and Cl^- during treatment of feed **F4** by symmetric NiHCF cell containing a MCM with 15 layers.

5.4 Conclusions

A unique combination of PEM-coated anion-exchange membranes with nickel hexacyanoferrate electrodes was successfully used for the first time, to simultaneously and selectively separate both mono- and divalent cations as well as anions. In addition, the selectivity values obtained here for each of them are on par with the current (M)CDI state-of-the-art. Furthermore, the obtained anionic selectivity could also be tuned by changing the number of layers coated onto the membrane, making the system highly adaptable. We also demonstrate the tunability of the membrane with multilayer thickness and the type of terminating layer, by which the ion selectivity can be controlled. Furthermore, the

dependence of the selectivity on the charge and the dehydration energy of the ions opens possibilities for enhanced selectivity or rejection towards anions that can change their valence depending on solution conditions like pH (*e.g.* $H_2PO_4^-$), providing a route to phosphate recovery. The synergistic effects of size-based cation intercalation was also presented in this study. Additional insights into this phenomenon and the effect of feed parameters, such as pH, on selectivity are expected to further optimize the proposed approach for simultaneous cation and anion separation.

References

(1) Singh, K.; Porada, S.; de Gier, H. D.; Biesheuvel, P. M.; de Smet, L. C. P. M. Timeline on the Application of Intercalation Materials in Capacitive Deionization. *Desalination* **2019**, *455*, 115–134. https://doi.org/10.1016/J.DESAL.2018.12.015.

(2) Suss, M. E.; Porada, S.; Sun, X.; Biesheuvel, P. M.; Yoon, J.; Presser, V. Water Desalination via Capacitive Deionization: What Is It and What Can We Expect from It? *Energy Environ. Sci.* **2015**, *8* (8), 2296–2319. https://doi.org/10.1039/c5ee00519a.

(3) Porada, S.; Zhao, R.; Van Der Wal, A.; Presser, V.; Biesheuvel, P. M. Review on the Science and Technology of Water Desalination by Capacitive Deionization. *Prog. Mater. Sci.* **2013**, *58* (8), 1388–1442. https://doi.org/10.1016/j.pmatsci.2013.03.005.

(4) Singh, K.; Qian, Z.; Biesheuvel, P. M.; Zuilhof, H.; Porada, S.; de Smet, L. C. P. M. Nickel Hexacyanoferrate Electrodes for High Mono/Divalent Ion-Selectivity in Capacitive Deionization. *Desalination* **2020**, *481*, 114346. https://doi.org/10.1016/j.desal.2020.114346.

(5) Wang, L.; Lin, S. Mechanism of Selective Ion Removal in Membrane Capacitive Deionization for Water Softening. *Environ. Sci. Technol.* **2019**, *53* (10), 5797–5804. https://doi.org/10.1021/acs.est.9b00655.

(6) Kim, T.; Gorski, C. A.; Logan, B. E. Ammonium Removal from Domestic Wastewater Using Selective Battery Electrodes. *Environ. Sci. Technol. Lett.* **2018**, *5* (9), 578–583. https://doi.org/10.1021/acs.estlett.8b00334.

(7) Cerón, M. R.; Aydin, F.; Hawks, S. A.; Oyarzun, D. I.; Loeb, C. K.; Deinhart, A.; Zhan, C.; Pham, T. A.; Stadermann, M.; Campbell, P. G. Cation Selectivity in Capacitive Deionization: Elucidating the Role of Pore Size, Electrode Potential, and Ion Dehydration. *ACS Appl. Mater. Interfaces* **2020**, *12* (38), 42644–42652. https://doi.org/10.1021/acsami.0c07903.

(8) Gamaethiralalage, J. G.; Singh, K.; Sahin, S.; Yoon, J.; Elimelech, M.; Suss, M. E.; Liang, P.; Biesheuvel, P. M.; Zornitta, R. L.; de Smet, L. C. P. M. Recent Advances in Ion Selectivity with Capacitive Deionization. *Energy Environ. Sci.* **2020**, *14*, 1095–1120. https://doi.org/10.1039/d0ee03145c.

(9) Seo, S. J.; Jeon, H.; Lee, J. K.; Kim, G. Y.; Park, D.; Nojima, H.; Lee, J.; Moon, S. H. Investigation on Removal of Hardness Ions by Capacitive Deionization (CDI) for Water Softening Applications. *Water Res.* **2010**, *44*, 2267–2275. https://doi.org/10.1016/j.watres.2009.10.020.

(10) Joo, H.; Kim, S.; Kim, S.; Choi, M.; Kim, S. H.; Yoon, J. Pilot-Scale Demonstration of an Electrochemical System for Lithium Recovery from the Desalination Concentrate. *Environ. Sci. Water Res. Technol.* **2020**, *6* (2), 290–295. https://doi.org/10.1039/c9ew00756c.

(11) Gabelich, C. J.; Tran, T. D.; Suffet, I. H. Electrosorption of Inorganic Salts from Aqueous Solution Using Carbon Aerogels. *Environ. Sci. Technol.* **2002**, *36*, 3010–3019. https://doi.org/10.1021/es0112745.

(12) Qian, Z.; Miedema, H.; de Smet, L. C. P. M.; Sudhὸlter, E. J. R. Modelling the Selective Removal of Sodium Ions from Greenhouse Irrigation Water Using Membrane Technology. *Chem. Eng. Res. Des.* **2018**, *134*, 154–161. https://doi.org/10.1016/j.cherd.2018.03.040.

(13) Suss, M. E. Size-Based Ion Selectivity of Micropore Electric Double Layers in Capacitive Deionization Electrodes. *J. Electrochem. Soc.* **2017**, *164* (9), E270--E275. https://doi.org/10.1149/2.1201709jes.

(14) Kim, J.; Jain, A.; Zuo, K.; Verduzco, R.; Walker, S.; Elimelech, M.; Zhang, Z.; Zhang, X.; Li, Q. Removal of Calcium Ions from Water by Selective Electrosorption Using Target-Ion Specific Nanocomposite Electrode. *Water Res.* **2019**, *160*, 445–453. https://doi.org/10.1016/j.watres.2019.05.016.

(15) Kim, Y.-J.; Choi, J.-H. Selective Removal of Nitrate Ion Using a Novel Composite Carbon Electrode in Capacitive Deionization. *Water Res.* **2012**, *46* (18), 6033–6039. https://doi.org/10.1016/J.WATRES.2012.08.031.

(16) Oyarzun, D. I.; Hemmatifar, A.; Palko, J. W.; Stadermann, M.; Santiago, J. G. Ion Selectivity in Capacitive Deionization with Functionalized Electrode: Theory and Experimental Validation. *Water Res. X* **2018**, *1*, 100008. https://doi.org/10.1016/j.wroa.2018.100008.

(17) Shi, W.; Liu, X.; Ye, C.; Cao, X.; Gao, C.; Shen, J. Efficient Lithium Extraction by Membrane Capacitive Deionization Incorporated with Monovalent Selective Cation Exchange Membrane. *Sep. Purif. Technol.* **2019**, *210*, 885–890. https://doi.org/10.1016/j.seppur.2018.09.006.

(18) Tang, W.; He, D.; Zhang, C.; Waite, T. D. Optimization of Sulfate Removal from Brackish Water by Membrane Capacitive Deionization (MCDI). *Water Res.* **2017**, *121*, 302–310. https://doi.org/10.1016/j.watres.2017.05.046.

(19) Sahin, S.; Dykstra, J. E.; Zuilhof, H.; Zornitta, R. L.; De Smet, L. C. P. M. Modification of Cation-Exchange Membranes with Polyelectrolyte Multilayers to Tune Ion Selectivity in Capacitive Deionization. *ACS Appl. Mater. Interfaces* **2020**, *12* (31), 34746–34754. https://doi.org/10.1021/acsami.0c05664.

(20) Choi, J.; Lee, H.; Hong, S. Capacitive Deionization (CDI) Integrated with Monovalent Cation Selective Membrane for Producing Divalent Cation-Rich Solution. *Desalination* **2016**, *400*, 38–46. https://doi.org/10.1016/j.desal.2016.09.016.

(21) Yeo, J. H.; Choi, J. H. Enhancement of Nitrate Removal from a Solution of Mixed Nitrate, Chloride and Sulfate Ions Using a Nitrate-Selective Carbon Electrode. *Desalination* **2013**, *320*, 10–16. https://doi.org/10.1016/j.desal.2013.04.013.

(22) Mubita, T.; Porada, S.; Aerts, P.; van der Wal, A. Heterogeneous Anion Exchange Membranes with Nitrate Selectivity and Low Electrical Resistance. *J. Memb. Sci.* **2020**, *607*, 118000. https://doi.org/10.1016/j.memsci.2020.118000.

(23) Cao, Z.; Gordiichuk, P. I.; Loos, K.; Sudhölter, E. J. R.; De Smet, L. C. P. M. The Effect of Guanidinium Functionalization on the Structural Properties and Anion Affinity of Polyelectrolyte Multilayers. *Soft Matter* **2016**, *12*, 1496–1505. https://doi.org/10.1039/c5sm01655j.

(24) Paltrinieri, L.; Remmen, K.; Müller, B.; Chu, L.; Köser, J.; Wintgens, T.; Wessling, M.; de Smet, L. C. P. M.; Sudhölter, E. J. R. Improved Phosphoric Acid Recovery from Sewage Sludge Ash Using Layer-by-Layer Modified Membranes. *J. Memb. Sci.* **2019**, *587*, 117162. https://doi.org/10.1016/j.memsci.2019.06.002.

(25) Cheng, C.; Yaroshchuk, A.; Bruening, M. L. Fundamentals of Selective Ion Transport through Multilayer Polyelectrolyte Membranes. *Langmuir* **2013**, *29* (6), 1885–1892. https://doi.org/10.1021/la304574e.

(26) Decher, G.; Hong, J. -D. Buildup of Ultrathin Multilayer Films by a Self-assembly Process, 1 Consecutive Adsorption of Anionic and Cationic Bipolar Amphiphiles on Charged Surfaces. *Makromol. Chemie. Macromol. Symp.* **1991**, *46*, 321–327. https://doi.org/10.1002/masy.19910460145.

(27) Decher, G. Fuzzy Nanoassemblies: Toward Layered Polymeric Multicomposites. *Science* **1997**, *277*, 1232–1237. https://doi.org/10.1126/science.277.5330.1232.

(28) Richardson, J. J.; Cui, J.; Björnmalm, M.; Braunger, J. A.; Ejima, H.; Caruso, F. Innovation in Layer-by-Layer Assembly. *Chem. Rev.* **2016**, *116* (23), 14828–14867. https://doi.org/10.1021/acs.chemrev.6b00627.

(29) Zhu, Y.; Ahmad, M.; Yang, L.; Misovich, M.; Yaroshchuk, A.; Bruening, M. L. Adsorption of Polyelectrolyte Multilayers Imparts High Monovalent/Divalent Cation Selectivity to Aliphatic Polyamide Cation-Exchange Membranes. *J. Memb. Sci.* **2017**, *537*, 177–185. https://doi.org/10.1016/j.memsci.2017.05.043.

(30) Said, Abdu, M.-C.; Manuel-César, Wong, J. E.; García-Gabaldón, M.; Wessling, M. Layer-by-Layer Modification of Cation Exchange Membranes Controls Ion Selectivity and Water Splitting. *ACS Appl. Mater. Interfaces* **2014**, *6*, 1843−1854.

(31) Rijnaarts, T.; Reurink, D. M.; Radmanesh, F.; de Vos, W. M.; Nijmeijer, K. Layer-by-Layer Coatings on Ion Exchange Membranes: Effect of Multilayer Charge and Hydration on Monovalent Ion Selectivities. *J. Memb. Sci.* **2019**, *570–571*, 513–521. https://doi.org/10.1016/j.memsci.2018.10.074.

(32) Stanton, B. W.; Harris, J. J.; Miller, M. D.; Bruening, M. L. Ultrathin, Multilayered Polyelectrolyte Films as Nanofiltration Membranes. *Langmuir* **2003**, *19* (17), 7038–7042. https://doi.org/10.1021/la034603a.

(33) Tansel, B. Significance of Thermodynamic and Physical Characteristics on Permeation of Ions during Membrane Separation: Hydrated Radius, Hydration Free Energy and Viscous Effects. *Sep. Purif. Technol.* **2012**, *86*, 119–126. https://doi.org/10.1016/j.seppur.2011.10.033.

(34) Cheng, W.; Liu, C.; Tong, T.; Epsztein, R.; Sun, M.; Verduzco, R.; Ma, J.; Elimelech, M. Selective Removal of Divalent Cations by Polyelectrolyte Multilayer Nanofiltration Membrane: Role of Polyelectrolyte Charge, Ion Size, and Ionic Strength. *J. Memb. Sci.* **2018**, *559*, 98–106. https://doi.org/10.1016/j.memsci.2018.04.052.

(35) Luo, T.; Abdu, S.; Wessling, M. Selectivity of Ion Exchange Membranes: A Review. *J. Memb. Sci.* **2018**, *555*, 429–454. https://doi.org/10.1016/j.memsci.2018.03.051.

(36) Mulyati, S.; Takagi, R.; Fujii, A.; Ohmukai, Y.; Matsuyama, H. Simultaneous Improvement of the Monovalent Anion Selectivity and Antifouling Properties of an Anion Exchange Membrane in an Electrodialysis Process, Using Polyelectrolyte Multilayer Deposition. *J. Memb. Sci.* **2013**, *431*, 113–120. https://doi.org/10.1016/j.memsci.2012.12.022.

(37) Cheng, C.; White, N.; Shi, H.; Robson, M.; Bruening, M. L. Cation Separations in Electrodialysis through Membranes Coated with Polyelectrolyte Multilayers. *Polymer* **2014**, *55* (6), 1397–1403. https://doi.org/10.1016/j.polymer.2013.12.002.

(38) Kim, S.; Yoon, H.; Shin, D.; Lee, J.; Yoon, J. Electrochemical Selective Ion Separation in Capacitive Deionization with Sodium Manganese Oxide. *J. Colloid Interface Sci.* **2017**, *506*, 644–648. https://doi.org/10.1016/j.jcis.2017.07.054.

(39) Porada, S.; Shrivastava, A.; Bukowska, P.; Biesheuvel, P. M.; Smith, K. C. Nickel Hexacyanoferrate Electrodes for Continuous Cation Intercalation Desalination of Brackish Water. *Electrochim. Acta* **2017**, *255*, 369–378. https://doi.org/10.1016/j.electacta.2017.09.137.

(40) Choi, S.; Chang, B.; Kim, S.; Lee, J.; Yoon, J.; Choi, J. W. Battery Electrode Materials with Omnivalent Cation Storage for Fast and Charge-Efficient Ion Removal of Asymmetric Capacitive Deionization. *Adv. Funct. Mater.* **2018**, *28* (35), 1–9. https://doi.org/10.1002/adfm.201802665.

(41) Pomerantseva, E.; Bonaccorso, F.; Feng, X.; Cui, Y.; Gogotsi, Y. Energy Storage: The Future Enabled by Nanomaterials. *Science* **2019**, *366* (6468). https://doi.org/10.1126/science.aan8285.

(42) Karyakin, A. A. Prussian Blue and Its Analogues: Electrochemistry and Analytical Applications. **2001**, 10, 813–819. https://doi.org/10.1002/1521-4109(200106)13:10<813::AID-ELAN813>3.0.CO;2-Z.

(43) Kim, T.; Gorski, C. A.; Logan, B. E. Low Energy Desalination Using Battery Electrode Deionization. *Environ. Sci. Technol. Lett.* **2017**, *4* (10), 444–449. https://doi.org/10.1021/acs.estlett.7b00392.

(44) Singh, K.; Zhang, L.; Zuilhof, H.; de Smet, L. C. P. M. Water Desalination with Nickel Hexacyanoferrate Electrodes in Capacitive Deionization: Experiment, Model and Comparison with Carbon. *Desalination* **2020**, *496*, 114647. https://doi.org/https://doi.org/10.1016/j.desal.2020.114647.

(45) Wang, R. Y.; Wessells, C. D.; Huggins, R. A.; Cui, Y. Highly Reversible Open Framework Nanoscale Electrodes for Divalent Ion Batteries. *Nano Lett.* **2013**, *13* (11), 5748–5752. https://doi.org/10.1021/nl403669a.

(46) Bocarsly, A. B.; Sinha, S. Effects of Surface Structure on Electrode Charge Transfer Properties. Induction of Ion Selectivity at the Chemically Derivatized Interface. *J. Electroanal. Chem.* **1982**, *140* (1), 167–172. https://doi.org/10.1016/0368-1874(82)85310-0.

(47) Lee, J.; Kim, S.; Yoon, J. Rocking Chair Desalination Battery Based on Prussian Blue Electrodes. *ACS Omega* **2017**, *2* (4), 1653–1659. https://doi.org/10.1021/acsomega.6b00526.

(48) Singh, K.; Bouwmeester, H. J. M.; de Smet, L.; Bazant, M. Z.; Biesheuvel, P. M. Theory of Water Desalination with Intercalation Materials. *Phys. Rev. Appl.* **2018**, *9* (6), 64036–64045. https://doi.org/10.1103/PhysRevApplied.9.064036.

(49) Durmaz, E. N.; Baig, M. I.; Willott, J. D.; de Vos, W. M. Polyelectrolyte Complex Membranes via Salinity Change Induced Aqueous Phase Separation. *ACS Appl. Polym. Mater.* **2020**. https://doi.org/10.1021/acsapm.0c00255.

(50) de Grooth, J.; Haakmeester, B.; Wever, C.; Potreck, J.; de Vos, W. M.; Nijmeijer, K. Long Term Physical and Chemical Stability of Polyelectrolyte Multilayer Membranes. *J. Memb. Sci.* **2015**, *489*, 153–159. https://doi.org/10.1016/j.memsci.2015.04.031.

(51) Gao, H.; Zhang, B.; Tong, X.; Chen, Y. Monovalent-Anion Selective and Antifouling Polyelectrolytes Multilayer Anion Exchange Membrane for Reverse Electrodialysis. *J. Memb. Sci.* **2018**, *567*, 68–75. https://doi.org/10.1016/j.memsci.2018.09.035.

(52) de Grooth, J.; Oborný, R.; Potreck, J.; Nijmeijer, K.; de Vos, W. M. The Role of Ionic Strength and Odd-Even Effects on the Properties of Polyelectrolyte Multilayer Nanofiltration Membranes. *J. Memb. Sci.* **2015**, *475*, 311–319. https://doi.org/10.1016/j.memsci.2014.10.044.

(53) White, N. Electrically Driven Ion Separations and Nanofiltration through Membranes Coated with Polyelectrolyte Multilayers. *ProQuest Diss. Theses Glob.* **2015**.

(54) Riegler, H.; Essler, F. Polyelectrolytes. 2: Intrinsic or Extrinsic Charge Compensation? Quantitative Charge Analysis of PAH/PSS Multilayers. *Langmuir* **2002**, *18* (17), 6694–6698. https://doi.org/10.1021/la020108n.

(55) Rassat, S. D.; Sukamto, J. H.; Orth, R. J.; Lilga, M. A.; Hallen, R. T. Development of an Electrically Switched Ion Exchange Process for Selective Ion Separations. *Sep. Purif. Technol.* **1999**, *15* (3), 207–222. https://doi.org/http://dx.doi.org/10.1016/S1383-5866(98)00102-6.

(56) Malaisamy, R.; Bruening, M. L. High-Flux Nanofiltration Membranes Prepared by Adsorption of Multilayer Polyelectrolyte Membranes on Polymeric Supports. *Langmuir* **2005**, *21* (23), 10587–10592. https://doi.org/10.1021/la051669s.

(57) Nightingale, E. R. Phenomenological Theory of Ion Solvation. Effective Radii of Hydrated Ions. *J. Phys. Chem.* **1959**, *63* (9), 1381–1387. https://doi.org/10.1021/j150579a011.

Supplementary Information to:

Simultaneous, Monovalent Ion Selectivity with Polyelectrolyte Multilayers and Intercalation Electrodes in Capacitive Deionization

Sample preparation for SWA and XPS. Gold substrates (1 cm × 1 cm purchased from ECsens) were sonicated for 5 min in MQ water, dried under argon flow and then plasma cleaned (Brand, model) for 5 min to remove any organic material. After cleaning, the gold substrates were coated by using the same approach for the Standard-grade (Neosepta ASE, Astom) ASE membrane and kept in a vacuum oven at 30 °C.

XPS spectra were obtained with a JPS-9200 photoelectron spectrometer (JEOL, Japan) under ultra-high vacuum conditions. It was obtained 20 scans per experiment by using a monochromatic Al Kα source at 12 kV and 20 mA. All spectra were processed with CASA XPS software (version 2.3.16) and fitted with Shirley background fitting.

SWA values were measured by using a Krüss drop shape analyzer (DSA 30). It was deposited 3 µL of Milli-Q water drops onto the samples. Contact angles were measured by using a sessile drop method. A charge-couple device camera was used for the analysis. The average values were calculated and reported based on three measurements at different locations on the samples.

Physical properties of PEM. The density of the PDADMAC/PSS multilayers, prepared by a similar procedure, has been reported to be 1.07 g/cm^3.[1] In addition, the dry thickness of 9, 13, and 17 layers of the PEM has been reported to be ≈ 32, 67, and 97 nm, respectively, demonstrating a linear growth in thickness upon the build-up.[2]

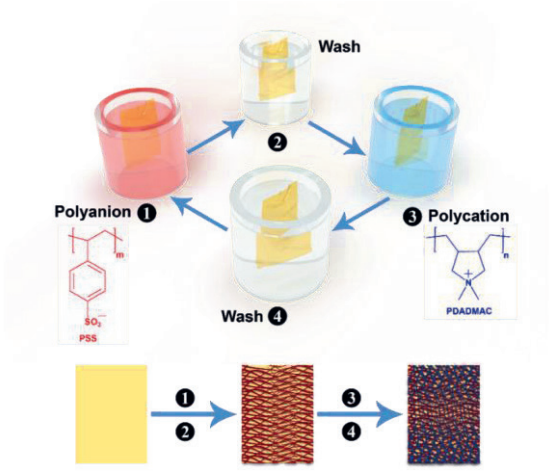

Figure S5.1: Schematic illustrating the procedure followed for the layer-by-layer deposition of PEM on an AEM surface. A washing step was introduced between the dip coating to get rid of the extra, loosely bound polyelectrolytes.

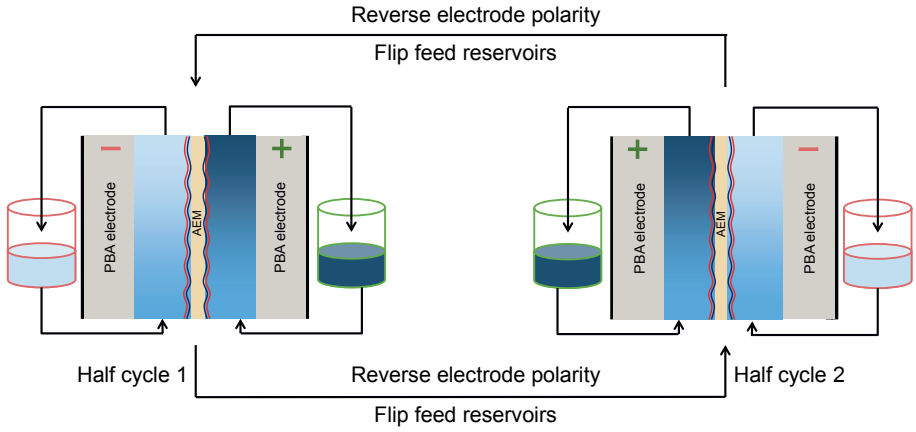

Figure S5.2: Schematic illustrating the procedure followed during the selectivity experiments. Left figure represents one half of the cycle during which, the left electrode selectively adsorbs cations, the membrane selectively allows anions to pass to the right chamber and the right electrode desorbs the intercalated ions. After 30 min, the electrode polarity and the feed reservoirs are reversed, and the second half of the cycle commences, depicted by the figure on the right, where the right electrode selectively adsorbs cations, the membrane selectively allows anions to pass to the left chamber and the left electrode desorbs the intercalated ions. Only one bilayer of PEs is shown over the membrane for simplicity.

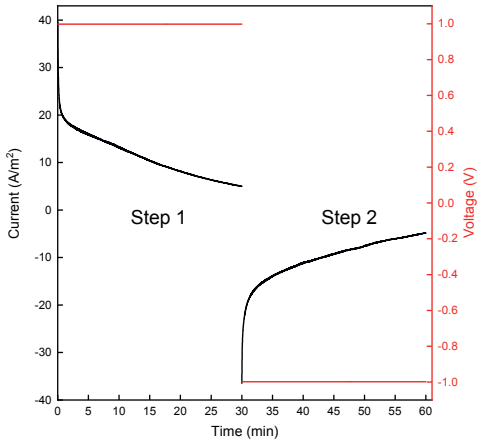

Figure S5.3: Sample current-voltage (IV) profile obtained during desalination of 10 mM NaCl + Na_2SO_4 feed in constant voltage mode, with symmetric CDI cell containing identical NiHCF electrodes, separated by PEM with 15 layers.

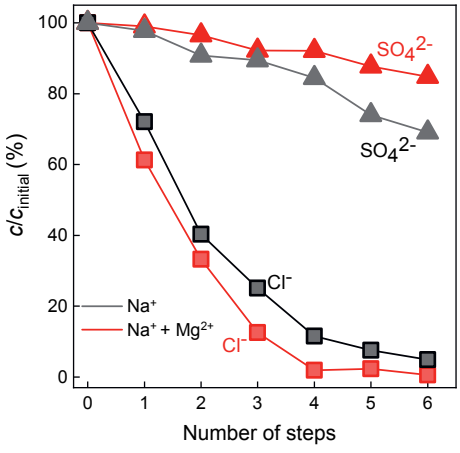

Figure S5.4: Concentration of anions in the diluate as a function of desalination steps, obtained from the treatment of feeds F1 and F2, containing two cations (Na^+ and Mg^{2+}) and only one cation (Na^+), respectively.

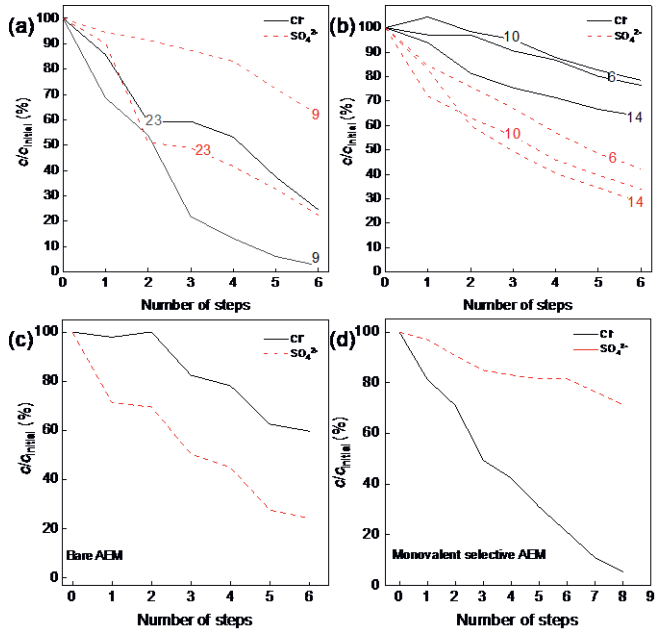

Figure S5.5: Concentration of anions in the diluate, during the treatment of F2, by MCM with 9 and 23 layers. **(b)** Concentration of anions in the diluate, during the treatment of F2, by MCM with 6, 10, and 14 layers. **(c)** Concentration of anions in the diluate, during the treatment of F2, by bare anion-exchange membrane. **(d)** Concentration of anions in the diluate, during the treatment of F2, by special-grade, monovalent selective anion-exchange membrane.

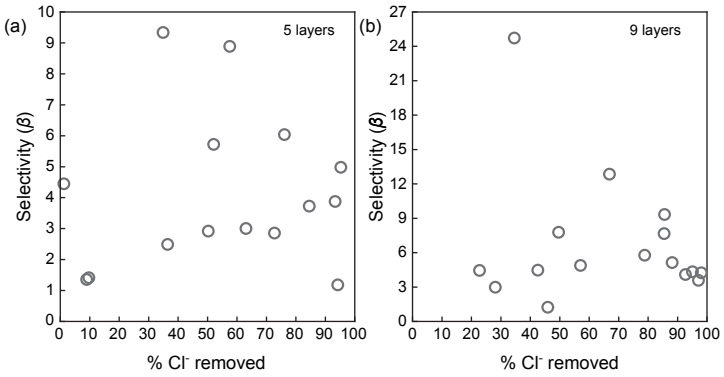

Figure S5.6: Selectivity, β, of MCM with 5 layers towards Cl^- over SO_4^{2-} from F2, as a function of Cl^- concentration in the diluate, obtained over multiple experiments. (b) Selectivity, β, of MCM with 9 layers towards Cl^- over SO_4^{2-} from F2, as a function of Cl^- concentration in the diluate, obtained over multiple experiments.

References

(1) Köhler, R.; Dönch, I.; Ott, P.; Laschewsky, A.; Fery, A.; Krastev, R. Neutron Reflectometry Study of Swelling of Polyelectrolyte Multilayers in Water Vapors: Influence of Charge Density of the Polycation. *Langmuir* **2009**, *25* (19), 11576–11585. https://doi.org/10.1021/la901508w.

(2) Reurink, D. M.; Haven, J. P.; Achterhuis, I.; Lindhoud, S.; Roesink, (Erik) H D W; de Vos, W. M. Annealing of Polyelectrolyte Multilayers for Control over Ion Permeation. *Adv. Mater. Interfaces* **2018**, *5* (20). https://doi.org/10.1002/admi.201800651.

Chapter 6

Enhanced Monovalent over Divalent Cation Selectivity with Polyelectrolyte Multilayers in Membrane Capacitive Deionization *via* Optimization of Operational Conditions

This chapter was adapted from:

Sahin, S.; Zuilhof, H.; Zornitta, R. L.; & de Smet; L. C. P. M. Enhanced Monovalent over Divalent Cation Selectivity with Polyelectrolyte Multilayers in Membrane Capacitive Deionization via Optimization of Operational Conditions. *Desalination*, **2022**, 522, 115391.

Abstract

In this work, we tuned the ion selectivity of a polyelectrolyte multilayer (PEM)-coated, cation-exchange membrane (CMX) in a membrane capacitive deionization (MCDI) process by carefully studying different operational modes, namely constant voltage (CV) and constant current (CC). The monovalent cation selectivity and its time-dependent behavior were monitored at different voltage and current values. Upon optimizing the current density (10 A/m^2) and the number of polyelectrolyte bilayers (5.5) on the CMX membranes, a time-independent and enhanced monovalent cation selectivity was obtained for various feed solutions, provided a polycation-terminated PEM was applied. Furthermore, the selectivity values of several commercially available cation-exchange membranes were tested under the optimized conditions and compared with CMX and PEM-CMX, yielding the best performance for PEM-CMX, regardless the composition of feed solution. Before this optimization, this MCDI system showed a time-dependent selectivity, which a maximum of $\rho \frac{Na}{Mg} \approx 3$. *The results were rationalized by applying an MCDI model based on the dynamic potential profile, describing the potential drops across the membrane and demonstrating a threshold for the current density.*

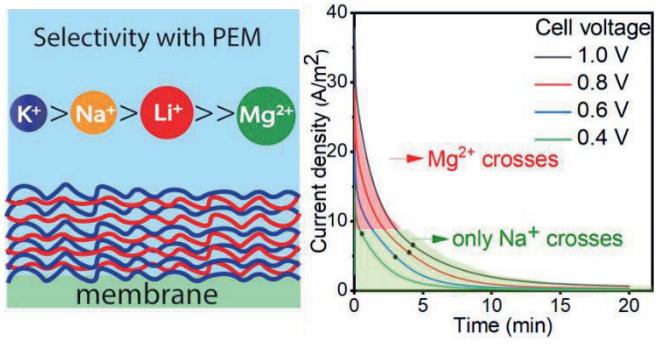

6.1 Introduction

Developing energy-efficient and affordable water treatment technologies is crucial to meet the increasing global demand for clean water.[1] In this context, capacitive deionization (CDI) has gained attention as an alternative desalination technique for the removal of ions from water at low salt concentrations.[2] CDI is typically based on the electrical double layer (EDL) formation in which ions are removed and stored on the surface of capacitive electrodes when a constant voltage (CV) or constant current (CC) is applied to the cell. In the last few years, CDI has become a promising technology for the selective removal – and even recovery – of specific ions from a mixture of ions.[3] Accordingly, CDI has been successfully employed in multiple applications such as softening water,[4] recovering nutrients (*e.g.*, phosphate, nitrate),[5,6] and harvesting lithium.[7] CDI can operate on relatively low voltage values (*i.e.*, 1 V) without need for high pressures or temperatures.[2] Therefore, it has been proven to be an interesting technology that can selectively remove and/or capture certain type of ions from multicomponent solutions at low salt concentration. Maximizing ion selectivity can lead to low-cost ion separation/recovery due the efficient use of energy with CDI technology.[8]

There are multiple parameters that can affect the ion selectivity in CDI. For instance, Li *et al.* investigated how the hydration ratio (the ratio of hydrated to ion radii) affects the ion selectivity in a mixture of ions. They hypothesized that the lower the hydration ratio of the ion the more efficient is their removal from the ionic solution, which agreed well with their experimental data.[9] Cèron *et al.* focused on size-based ion selectivity and optimized the average pore size of carbon aerogel monolith electrodes.[10] They switched from a Na^+-selective electrode to a Ca^{2+}-selective electrode by optimizing the synthetic procedure of the electrodes. Besides size-exclusion effect, the valence of ions also plays a major role on the selective removal of ions in CDI. Gao *et al*. demonstrated the preferential electrosorption of multivalent over monovalent cations by using carbon nanotubes and carbon nanofibers composite electrodes.[11] This preference was rationalized by higher Coulombic interactions between the ions in the solution with the polarized surface of the

electrode. For cations with the same valence, the authors observed a size-based trend where ions with smaller hydrated radius were electrosorbed in higher amounts.

Recently, multiple innovations were suggested to tailor ion selectivity in CDI, including modification of electrodes with ion-selective coatings, optimization of operational conditions of the electro-driven separation process, and implementation of ion-selective membranes.[3,4,12–17] Besides electrode modifications, membranes have also been employed in CDI (MCDI)[18] to achieve ion selectivity. Different types of membranes have been investigated to achieve cation selectivity in MCDI.[3,19,20] For instance, nanofiltration membranes were successfully used to introduce a size-based ion selectivity in MCDI.[19] In this case, the authors reported higher diffusion coefficients for NaCl through the nanofiltration membrane compared to $MgSO_4$, which explained the higher preference for the removal of monovalent species. Ion-exchange membranes (IEMs) are the most common type of membranes used to achieve ion selectivity in MCDI, and these typically have fixed charges that can reject the co-ions. For a standard CDI desalination process, the use of IEMs typically enhances the removal capacity and charge efficiency values compared to CDI.[2] Standard cation-exchange membranes (CEMs) have polyanions with negatively charged groups (*e.g.*, carboxylate and sulfonate) while anion-exchange membranes (AEMs) are made of polycations bearing positively charged functional groups such as quaternary ammonium.[21] Although standard-grade CEMs were not designed to separate cations from each other, negative charges of the membrane exhibited divalent cation selectivity due to charge-based interactions, and different transport mechanisms inside of the membrane.[4,22,23] Higher di-/monovalent ion selectivities of standard IEMs were attributed to the higher charge affinity between oppositely charged membrane surface and divalent ions compared to the monovalent ions. Besides standard-grade IEMs, special-grade membranes can function as a filter to specific ions allowing the rest to pass through. For instance, CMS (Neosepta) and CSO (Selemion) are special-grade CEMs that have been designed to be monovalent selective. The selectivity mechanism of CSO is based on divalent cation rejection caused by a thin layer of polyethylenimine coated on the membrane surface,[24] while the selectivity of CMS is based on size exclusion effects that result from the

crosslinked membrane surface. In MCDI, CMS has been investigated, and was reported to have a higher rejection of divalent than monovalent cations for a bicomponent solution.[20]

A simple alternative to produce special-grade membranes is by coating standard-grade IEMs with polyelectrolyte multilayers (PEMs). Such a multilayer can be built via a layer-by-layer (LbL) process on a substrate using oppositely charged polyelectrolytes.[25] PEMs are highly stable, and versatile coatings that are easy and affordable to prepare,[25,26] as we have also shown in our recent CDI work.[27] After the discovery of LbL-coated PEMs in 1990s by Decher,[28,29] rational combinations of polycations and polyanions have been extensively used in separation technologies such as gas separation, micropollutant removal, and resource recovery.[30] Furthermore, PEM coatings enable to control various physical and chemical characteristics such as layer thickness, morphology, and porosity as well as the type of charge and pK_a of the membrane surface. Additionally, tunability of pore size and surface charge of PEM-coated membranes introduces an ion-selective behavior for pressure-[31–34] and electro-driven desalination processes such as electrodialysis.[35–38] The main finding of these studies is that PEMs can regulate the mono-/divalent ion selectivity of the membranes by rejecting divalent and multivalent ions due to their higher valence and/or hydrated size. Recently, we reported – for the first time – a PEM-coated, standard-grade CEM (Neosepta, CMX) to tune Na^+/Mg^{2+} selectivity in under CDI operation conditions.[27] Moreover, in another study we showed that PEM coatings on an AEM can tailor monovalent anion selectivity in CDI.[39] In these studies PEM-coated IEMs achieved selectivity values up to ≈3 and ≈14 for monovalent cations and anions, respectively, values that were found to be time-dependent.

Although PEMs are proven to be a versatile way of tuning selectivity in CDI, there are various tunable parameters that allow one to achieve even higher monovalent ion selectivity values.[3] Especially, the effect of the CDI charging mode on ion selectivity has not been investigated yet. Constant current (CC) and constant voltage (CV) modes are the most common charging modes in (M)CDI.[40] In CC charging/discharging, the potential increases/decreases in time until it reaches a desired cut-off potential value. On the other hand, in a CV mode, a constant voltage is applied to the CDI cell during electrosorption and

the current starts at a maximum value right after the voltage is applied decreasing until the electrodes become saturated. For a solely EDL formation process, the ion-transfer kinetic rate in a CC mode is proportional to the charging current.[2,41,42] In other words, CC mode provides a constant cell effluent concentration during charging/discharge steps. CC *vs.* CV processes have already been thoroughly investigated for water desalination in CDI suggesting a higher energy efficiency for the CC operation.[43–45] For ion selectivity in MCDI, the different operational modes have not been properly studied. Ion selectivity using IEM may be dependent on the current applied as already reported in electrodialysis literature.[46]

We were wondering whether operational modes have a similar effect on ion selectivity in PEM-based MCDI, and if so, which conditions would be required to obtain the highest selectivity for a certain CDI system. Hence, in this work, we investigated the effect of different operational modes, namely CV and CC, on the monovalent cation selectivity using PEM-coated CMX (PEM-CMX) in MCDI. To the best of our knowledge, this is the first time a comprehensive investigation on the effect of the current and voltage on the ion selectivity in MCDI has been carried out. Different potentials were applied to the MCDI cell in order to find the threshold to which full sodium selectivity is achieved using the PEM-CMX. These selectivities were rationalized using an MCDI model based on the dynamic potential profile for the PEM-CMX. A CC experiment using a current below the threshold of the selectivity was employed to assess the cation selectivity based on the number of PEM deposited on the CMX. The number of polyelectrolyte layers on CMX was optimized, and then the selectivity performance of PEM-CMX with optimal number of layers was compared with commercial monovalent selective membranes. Finally, the selectivity values obtained from bare CMX, CSO, and PEM-CMX were tested in various feed solutions, including Na, K, Li, and Mg ions. We show that the PEM-CXM displays monovalent cation selectivity regardless the composition of the feed solution.

6.2 Materials and Methods

Materials. Hydrochloric acid (36.5−28.0% NF grade) was purchased from VWR International. Poly(allylamine hydrochloride) (PAH, Mw = 17 500 Da), poly(sodium 4-styrenesulfonate) (PSS, Mw = 70 000 Da), sodium chloride (NaCl, ≥99%), anhydrous magnesium chloride ($MgCl_2$, ≥98%), potassium chloride (≥99%), lithium chloride (≥99%) were purchased from Sigma-Aldrich. The gold (200 nm Au sputtered on glass) substrates (1 cm × 1 cm) were purchased from ECsens. The inorganic salts were kept in a vacuum oven overnight (60 °C, 0.01 mbar) prior to use. The porous carbon electrodes, which were deposited on a graphite foil substrate, were kindly supplied by Voltea B.V., Netherlands. Glass fiber prefilters (25 mm in diameter, 250 µm in thickness, 2.0 µm of pore size) were purchased from Merck Millipore and used as spacer in CDI experiments. Milli-Q water (18.2 MΩ·cm, Milli-Q Integral 3 system, Millipore) was used to prepare all aqueous solutions. Neosepta anion-exchange (AMX), and cation-exchange (CMX and CMS) membranes were purchased from Eurodia (France), and Selemion CSO membranes were purchased from Astom Corp. (Japan). All membranes were soaked in the stock solution of the relevant experiment at least 48 h before use.

Coating Polyelectrolyte Multilayers on Membrane. The coating procedure was adapted from our previous work.[39] Briefly, a robotic arm (Dobot Magician, Dobot) was employed to dip the standard-grade CMX membrane in PAH (polycation) and PSS (polyanion) solutions for 10 min each. After deposition of each layer, the membrane was dipped in three containers with Milli-Q water one by one, each for 3 min to get rid of the weakly attached/physisorbed polyelectrolytes. The procedure was repeated until the desired number of layers was reached, namely 2, 2.5, 5.5, and 20.5 bilayers, where a bilayer stands for the combination of one PAH and one PSS layer. The details of PEM characterization were explained in the SI.

ICP-OES analyses. Inductively coupled plasma optical emission spectroscopy (ICP-OES) (PerkinElmer Avio 500 ICP-OES) was used to measure the cation concentrations of the samples. For cation analysis a high-energy-based Avio 500 ICP-OES polychromator with two sulfur chemiluminescence detectors (SCD) was used. The SCD detectors had the spectral range of 163-782 nm and the measuring resolution of the ICP-OES was 0.006 nm at 200 nm. The samples were collected from minimum of three electrosorption cycles with minimum of five samples/cycle and then diluted 20 times with a 1% nitric acid solution prior to the ICP-OES analyses. Selectivity of Na^+ over Mg^{2+} (ρ_{Mg}^{Na}) was calculated as described in **Equation 6.1**,[4,15] where c_0 and c_f represent the initial and final ion concentrations in the solution, respectively:

$$\rho_{Mg}^{Na} = \frac{\frac{(c_{0,Na^+} - c_{f,Na^+})}{c_{0,Na^+}}}{\frac{(c_{0,Mg^{2+}} - c_{f,Mg^{2+}})}{c_{0,Mg^{2+}}}} \quad \textbf{(6.1)}$$

6.3 Results and Discussion

Characterization of the PEM Coating. The dry, optical thickness of 5, 11.5, and 20.5 bilayers on gold – a widely used model substrate, also in membrane studies – was measured with ellipsometry. The results showed a linear increase in thickness with increased number of layers (**Figure 6.S1**). The observed linear trend is in line with literature,[47–49] and indicate a successful PEM build-up. Moreover, the measured thickness were found to be comparable with literature.[24,27,50]

The electronic and ionic resistance of the PEM-containing CDI cell was first characterized under different current densities to study the effect of the PEM. Upon the build-up of a PEM, an increasing resistance of CMX was observed, indicating a successful deposition of the polyelectrolytes. According to literature, the CDI cell is composed of several elements that may act similar to resistors.[51,52] Therefore, when a constant current is applied to the cell, a large non-capacitive drop in potential is observed, typically called

ohmic or IR drop. The ohmic drop (**Figure 6.S2 A-D**) consists of resistive contributions of several elements inside the cell such as electrical junctions, current collector, electrode, membranes, and spacer. By keeping all elements unchanged except the CEM, it is possible to measure the contribution of the CEM and its surface modifications to the ohmic drop. **Figure 6.1** summarizes the results of the experiments conducted in 8 mM NaCl and $MgCl_2$ solutions.

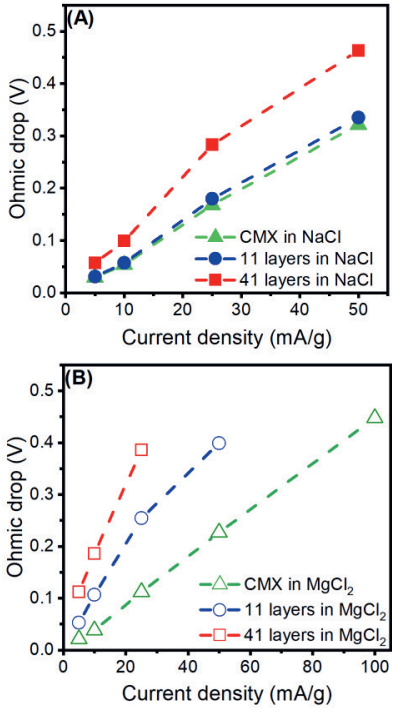

Figure 6.1. Ohmic drop values as function of current density for CMX, and PEM-CMX (11 and 41 layers) at 8 mM (A) NaCl and (B) $MgCl_2$.

The measured resistance is not completely ohmic over the full range of measured current densities as observed by a non-linear behavior of the curves. Nevertheless, it is still possible to approximate a linear resistance value for the points measured at low current densities, *i.e.* three smallest current densities. In **Figure 6.1A**, the resistance increases 7% and 71% when 5.5 and 20.5 bilayers of PEM are added to the CMX, respectively. In other words, an increase in layer thickness results in higher resistance values. This can be explained by the increase in the number of charged groups in the PEM due to which a higher energy is required for ions to pass through the PEM. Furthermore, the observed increase of only 7% suggests that sodium transport is not extensively affected by the presence of the PEM that consists of 5.5 bilayers. **Figure 6.1B** shows the ohmic drop in the $MgCl_2$ solution. Interestingly, the bare CMX membrane has a lower resistance compared to the NaCl solution (31% less resistive), which could be related to the higher ionic strength (*I*) of the solution of 8 mM of $MgCl_2$ (*I* = 24 mM) compared to 8 mM of NaCl (*I* = 8 mM). Furthermore, the CMX membrane has a higher affinity towards divalent cations due to the charge-based interactions between negatively charged membrane surface and divalent cations, as previously reported.[22,23] By increasing the number of bilayers to 5.5 and 20.5, the resistance increases by a factor of ≈1.3 and ≈2.7, respectively, compared to the bare CMX. The details of the calculation of IR drops were given in **Figure 6.S1D** in the SI. This suggests that Mg^{2+} experiences a much higher rejection by the PEM compared to the Na^+, which is in good agreement with our recently reported study on the ability of switching the selectivity of CMX from Mg^{2+} to Na^+ by the implementation of a PEM.[27] Furthermore, it is clear that higher number of layers within the PEM increases the resistance of the membrane, indicating a successful deposition of 20.5 bilayers on membrane.

Constant Voltage Mode. Electrosorption experiments were conducted in CV mode with cell potentials ranging from 0.4 V to 1.0 V. PEM-CMX with 5.5 bilayers of PEM was used to study the effect of voltage on Na^+/Mg^{2+} selectivity. **Figure 6.2A** shows the normalized removal of Na^+ and Mg^{2+} during electrosorption cycles at 0.4 V and 1.0 V.

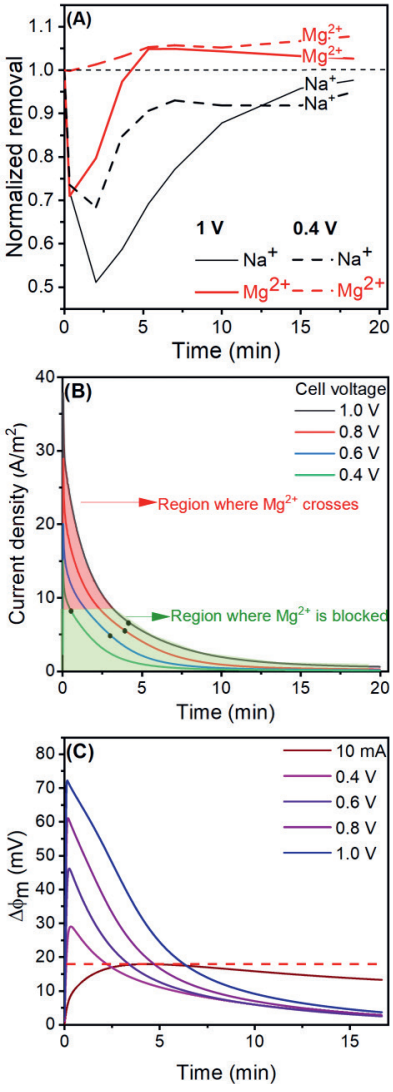

Figure 6.2. (A) Normalized removal of Na^+ and Mg^{2+} during electrosorption cycles at 0.4 and 1.0 V, and (B) the variation in current density as a function of time for the constant voltage experiments with PEM-CMX. (C) Variation of the potential across the membrane based on the MCDI dynamic model. It is noted that the feed solution was recycled during the experiments.

The effluent concentration of Na^+ and Mg^{2+} decreases during adsorption cycles. Since the feed solution is recycled during the experiment, the effluent concentrations eventually go back to the feed concentration values. However, the Mg^{2+} concentration increases to values above up to ≈7 % the feed concentration after Mg^{2+} initially was adsorbed and its origin may be due to experimental errors. For all experiments, the effluent concentration of Na^+ and Mg^{2+} decreases faster in the beginning of the cycle due the higher electrosorption rate. Subsequently, the electrodes start to reach saturation and the effluent concentration eventually returns to its initial value. Therefore, the amounts of electrosorbed Na^+ and Mg^{2+} changed as a function of time, and a time-dependent selectivity behavior was observed. At 1.0 V, the point with the highest Na^+/Mg^{2+} selectivity, defined here as t_s, was ≈ 250 s. The reduction of the potentials to 0.8 V and to 0.6 V reduces the t_s, and full sodium selectivity is achieved after 238 s and 178 s, respectively (**Figure 6.S3**). Finally, by applying 0.4 V, t_s achieves a minimum value close to 0 s, reaching an almost full Na^+-selective behavior during the entire electrosorption half cycle. On the one hand, using low potentials seems to maximize the Na^+ selectivity, being also beneficial for the reduction of energy consumption. On the other hand, low potentials largely limit the total removal capacity of the CDI electrodes. Therefore, it is important to understand what causes this improvement in Na^+ selectivity by reducing the cell potential, and how to maximize the ion removal.

In order to understand the dependence of the selectivity on the potential applied, an MCDI model[53] was employed to rationalize our experimental data (details in S2 and "MCDI Model" section of SI). **Figure 6.2B** shows the change in current density as a function of time for the constant voltage experiments, and the region where the transport of Mg^{2+} through the membrane is completely blocked. These regions were calculated based on the t_s values from **Figures 6.2A** and **6.S2**, and suggest that high current densities assist the transport of Mg^{2+} across the membrane. This is in good agreement with ED literature that reported mono- over divalent cation selectivity for PEM-modified membranes.[24,36] In more detail, it was suggested that at high current values in ED, water splitting may cause an increase in the local pH near the PEM/membrane interface. Therefore, either the film

permeability changes or there is an increase in the passage of $Mg(OH)_x$ species. Since the permeability of $Mg(OH)_x$ is much higher than the one of Mg^{2+} higher current values decrease the monovalent cation selectivity of the ED operations.[46] However, there is no easy way to check the validity of this hypothesis, as that would require measuring the pH directly at the PEM-membrane interface. Also, since in (M)CDI systems, strong pH variations are rarely observed due to the low applied voltages,[54] a pH-dependent change in monovalent cation selectivity is more unlikely in our case.

Aiming to understand the effect of the applied current density/potential on the monovalent cation selectivity of the PEM-modified membranes, we used a simplified dynamic MCDI model for a mono-component solution. The model permits to calculate the potential drop across the membrane for different voltages applied to the cell, as depicted in **Figure 6.2C**. Moreover, the potential drop profile across the membrane resembles the current density profile (**Figure 6.2B**), reaching values much lower than obtained for ED systems.[36,46] For such systems, it was reported that water splitting on the PEM-membrane interface affected the monovalent cation selectivity. However, the electric field caused by the potential drop across the membrane could increase the electromigration of ions with higher valence, which agrees with the Boltzmann theory typically used to describe EDL profiles.[53] Based on this reasoning, we suggest that a current density lower than the threshold for Mg^{2+} rejection would only allow the transport of Na^+. Indeed, the potential across the membrane calculated for a constant current experiment with a current density of 5.6 mA/g was smaller than the potential drop for the application of 0.4 V, as depicted in **Figure 6.2C**.

Constant Current Mode. Based on the results obtained from the aforementioned model, a CC experiment was carried out using a current density of 5.6 mA/g, which is the region of **Figure 6.2B** where Mg^{2+} expected to be completely rejected. All other experimental parameters were kept the same as the ones used for the CV experiment. The potential and conductivity profiles of the electrosorption of the experiment are reported in **Figure 6.S4**. **Figure 6.3** shows the change in Na^+ concentration during the electrosorption cycle, while a

negligible variation in Mg^{2+} concentration was observed. This is also in good agreement with our hypothesis stating that there is a maximum current density that should be used in order to avoid transport of Mg^{2+} in the PEM-CMX. **Figure 6.3** also reveals that the outlet ion concentration remained constant after ca. 400 s, suggesting a time-independent selectivity behavior for PEM-CMX in CC mode. The change in Na^+ adsorption was calculated to be 16 ± 3% based on three cycles of the experiment with five samples per cycle. This monovalent cation selectivity agrees well with our previous studies,[27,39] which reported monovalent selectivity for cations and anions using PEM-modified CEMs and AEM, respectively, due to the charge (Donnan) exclusion effect.[31] When using current densities of 8.4 mA/g instead of 5.6 mA/g (*i.e.*, 15 mA instead of 10 mA), ρ_{Mg}^{Na} decreased drastically compared to the monovalent cation selectivity that was found with the lower current densities. The change in Na^+ and Mg^{2+} adsorption values were calculated as 10 ± 2 % and 8 ± 1 %, respectively, based on three cycles and four samples per cycle, indicating a ρ_{Mg}^{Na} of ≈ 1.3.

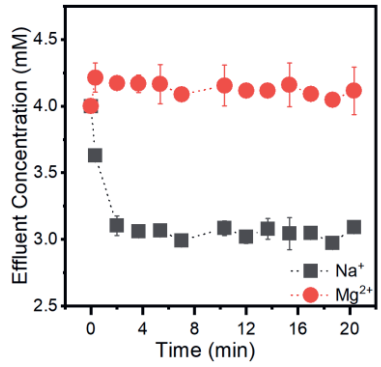

Figure 6.3. Change in sodium and magnesium ion concentrations in time during electrosorption cycles of a CC experiment with a PEM-CMX (current density: 5.6 mA/g, flow rate: 7.5 mL/min, feed solution: 4 mM of NaCl and 4 mM of $MgCl_2$). All data points are obtained by averaging the results of three different cycles.

PEM Thickness and Membrane Comparison. From **Figure 6.1** it becomes clear that the resistance – and therefore the energy demand – increases with PEM thickness. In our search for a proper balance between a low resistance and a high monovalent cation selectivity, we investigated the optimal amount of polyelectrolyte layers. As observed in **Figure 6.4A**, the amount of electrosorbed Na^+ increases by increasing the number of bilayers until 5.5 bilayers while the amount of electrosorbed Mg^{2+} decreases. It is noteworthy that PSS-terminating PEM (2 bilayers) shows no significant selectivity while PAH-terminating PEM (2.5 bilayers) already displays some selectivity towards monovalent cation. This can be explained by the negatively charged surface of the PSS-terminated PEM. In order to reject the divalent cations via charge (Donnan) rejection, the outermost layer should be positively charged. This phenomenon was investigated earlier by Mulyati *et al.* where a PEM-coated AEM was used to tune Cl^-/SO_4^{2-} selectivity in an electrodialysis process.[55] Recently, we also observed a similar trend in the mono/divalent anion selectivity of a CDI process, where a positively charged terminating layer did not reject the divalent anions as much as the negatively charged terminating layer.[39] At the same time, we checked whether the selectivity is different when the thickness is significantly high (20.5 bilayers) to see any possible advantage of higher number of layers. It is observed that going beyond 5.5 bilayers did not improve the Na^+-selectivity further.

In order to better understand the effect of the PEM on cation selectivity, the PEM-CMX with 5.5 bilayers was also compared with monovalent selective commercially available membranes under the same experimental conditions. **Figure 6.4B** indicates that the bare CMX has affinity towards Mg^{2+} since the amount of % ion electrosorption is 5.4 ± 2.0 and 15.6 ± 2.3 for Na^+ and Mg^{2+}, respectively. Similarly, in the case of CMS, the amounts of ion electrosorption were 5.2 ± 1.5 and 7.5 ± 2.4 for Na^+ and Mg^{2+}, respectively. Based on **Equation 6.1**, $\rho\,^{\mathrm{Na}}_{\mathrm{Mg}}$ values were calculated to be 0.3 for CMX and 0.7 for CMS. On the other hand, for CSO, this value was much higher reaching $\rho\,^{\mathrm{Na}}_{\mathrm{Mg}} \approx 3$. Although CSO displays a fair selectivity towards monovalent ions, it is clear that the commercial membranes (CSO and CMS) did not improve the monovalent cation selectivity as much as the PEM coating. Thus,

the selectivity mechanism based on the charge-exclusion effect of the PEM seems to be more effective than the possible size-exclusion effect of a crosslinked membrane.

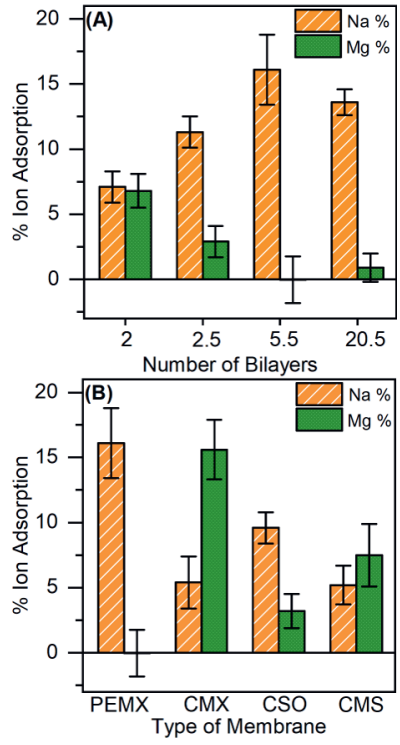

Figure 6.4. (A) Comparison of the amount of ion electrosorbed with increased number of bilayers for the PEM-CMX, and (B) the comparison of PEM-CMX with 5.5 bilayers with commercial cation-exchange membranes. The reported data are based on three experiments with three cycles each. A minimum of five samples was used per reported experiment.

Mixture of Monovalent Ions. Given the high selectivity of PEM-CMX, a set of experiments were conducted to test the effect of ion composition on cation selectivity. For these experiments, we have used solution compositions 2, 4, and 5 presented in **Table 6.S1**. Regardless the composition of the feed solution, the PEM-CXM displays monovalent cation

selectivity as illustrated in **Figure 6.5A**, while the bare CMX still displays Mg^{2+} selectivity for the same feed solution. For the commercial monovalent selective membrane CSO, the total electrosorption was fairly similar for the mono- and divalent cations. Interestingly, for all membranes, the total removal of K^+ was found to be higher compared to the other cations. In order to elucidate the effect of the PEM on the monovalent selectivity, the PEM-CMX was tested for different combinations of Na, K, and Li ions. **Figure 6.5B** reveals that hydrated size of the cations plays the most important role on monovalent selectivity for the PEM-CMX.

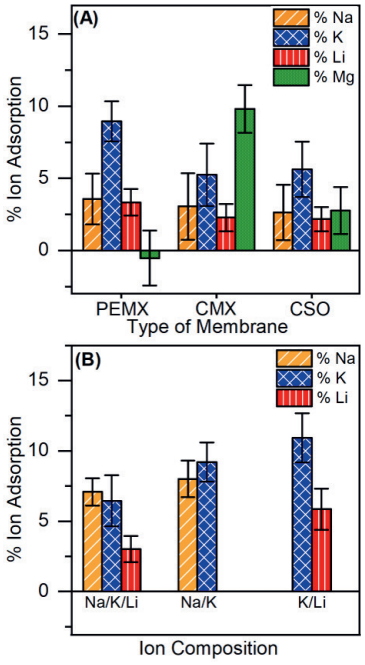

Figure 6.5. (A) Comparison of the amount of ion electrosorption values for a mixture of mono- and divalent cations using PEMX, CMX, and CSO. (B) Comparison of amount of ion electrosorption values for a mixture of monovalent ions using PEM-CMX with 5.5 bilayers. The reported data are based on three experiments with three cycles each. A minimum of five samples was used per reported experiment.

In other words, the order of hydrated size of the monovalent cations is K (3.31 Å) < Na (3.58 Å) < Li (3.82 Å),[56] and adsorption values of these cations followed the order of K^+ > Na^+ > Li^+, showing that the transport of larger cations is hampered.[23] Such a trend was also found for anions in CDI with PEM-coated AEMs, where the selectivity followed the order of hydration energy of monovalent anions (NO_3^- > Cl^- > $H_2PO_4^-$).[39]

6.4 Conclusions

The key finding of this study is that the monovalent selectivity of a polyelectrolyte multilayer (PEM)-coated cation-exchange membrane (CMX) in an MCDI operation can be boosted tremendously by tuning operational parameters such as the potential and current density as well as the PEM thickness. Potential drops across the membrane – described by modelling dynamic potential profiles – result in an electrical field and should be kept at minimum to reduce the electromigration of ions with higher valence. Current densities as low as 10 A/m^2 result in monovalent ion selectivity as they cause lower potential drops across the membrane. Unlike the divalent cation-selective behavior of CMX, PEM-CMX rejects Mg^{2+} as divalent cations experience a higher resistance from the positively charged outermost layer compared to the monovalent cations. In terms of multilayer thickness, the trade-off between selectivity and resistance was found to be 5.5 bilayers for the PEM-CMX system. Furthermore, the nature of the terminal polyelectrolyte of the PEM affects the selectivity: a PAH-terminated PEM was found to have a higher Na^+ selectivity compared to a PSS-terminated PEM. Finally, the selectivity values obtained from bare CMX, CSO, and PEM-CMX were tested in various feed solutions including Na, K, Li, and Mg ions. The PEM-CXM displays monovalent cation selectivity for all tested compositions of the feed solution. The high selectivity of PEM-CMX towards monovalent cations is promising for ion recovery applications using MCDI. This is further highlighted by the limited selectivity displayed by commercial membranes such as CMX, CSO, and CMS. Overall, this work demonstrates a novel way to achieve a time-independent, enhanced monovalent cation selectivity via a

simple PEM coating in MCDI in combination with tuning of the operational conditions. Considering the possible combinations of commercial and/or functionalized polyelectrolytes, PEM coatings are a promising way of introducing ion selectivity for future CDI applications, particularly when combined with fine-tuned operational parameters. It is anticipated that the outcome of our investigation is a large step towards a low-cost and energy efficient technology for ion recovery, as a high ion separation factor is a requirement for the techno-economic feasibility of MCDI.[8] Further explorations in such a direction, eventually up to pilot scale, would require studies on the effects of up-scaling, prolonged operation times and natural water samples on the PEM stability and mapping the system-dependency of the operational parameters that are required for high selectivities. This also includes the compatibility of advanced, automated water flow systems to swiftly control the diluate and the concentrate streams to enable ion separation.

References

(1) Mekonnen, M. M.; Hoekstra, A. Y. Sustainability: Four Billion People Facing Severe Water Scarcity. *Sci. Adv.* **2016**, *2* (2), 1–7. https://doi.org/10.1126/sciadv.1500323.

(2) Suss, M. E.; Porada, S.; Sun, X.; Biesheuvel, P. M.; Yoon, J.; Presser, V. Water Desalination via Capacitive Deionization: What Is It and What Can We Expect from It? *Energy Environ. Sci.* **2015**, *8*, 2296–2319. https://doi.org/10.1039/c5ee00519a.

(3) Gamaethiralalage, J. G.; Singh, K.; Sahin, S.; Yoon, J.; Elimelech, M.; Suss, M. E.; Liang, P.; Biesheuvel, P. M.; Zornitta, R. L.; de Smet, L. C. P. M. Recent Advances in Ion Selectivity with Capacitive Deionization. *Energy Environ. Sci.* **2020**, *14*, 1095–1120. https://doi.org/10.1039/d0ee03145c.

(4) Wang, L.; Lin, S. Mechanism of Selective Ion Removal in Membrane Capacitive Deionization for Water Softening. *Environ. Sci. Technol.* **2019**, *53* (10), 5797–5804. https://doi.org/10.1021/acs.est.9b00655.

(5) Zhu, E.; Hong, X.; Ye, Z.; Hui, K. S.; Hui, K. N. Influence of Various Experimental Parameters on the Capacitive Removal of Phosphate from Aqueous Solutions Using LDHs/AC Composite Electrodes. *Sep. Purif. Technol.* **2019**, *215*, 454–462. https://doi.org/10.1016/j.seppur.2019.01.004.

(6) Mubita, T. M.; Dykstra, J. E.; Biesheuvel, P. M.; van der Wal, A.; Porada, S. Selective Adsorption of Nitrate over Chloride in Microporous Carbons. *Water Res.* **2019**, *164*, 114885. https://doi.org/10.1016/j.watres.2019.114885.

(7) Shi, W.; Liu, X.; Ye, C.; Cao, X.; Gao, C.; Shen, J. Efficient Lithium Extraction by Membrane Capacitive Deionization Incorporated with Monovalent Selective Cation Exchange Membrane. *Sep. Purif. Technol.* **2019**, *210*, 885–890. https://doi.org/10.1016/j.seppur.2018.09.006.

(8) Hand, S.; Cusick, R. D. Emerging Investigator Series: Capacitive Deionization for Selective Removal of Nitrate and Perchlorate: Impacts of Ion Selectivity and Operating Constraints on Treatment Costs. *Environ. Sci. Water Res. Technol.* **2020**, *6* (4), 925–934. https://doi.org/10.1039/c9ew01105f.

(9) Li, Y.; Zhang, C.; Jiang, Y.; Wang, T. J.; Wang, H. Effects of the Hydration Ratio on the Electrosorption Selectivity of Ions during Capacitive Deionization. *Desalination* **2016**, *399*, 171–177. https://doi.org/10.1016/j.desal.2016.09.011.

(10) Ceron, M. R.; Aydin, F.; Hawks, S. A.; Oyarzun, D. I.; Loeb, C. K.; Deinhart, A.; Zhan, C.; Pham, T. A.; Stadermann, M.; Campbell, P. G. Cation Selectivity in Capacitive Deionization: Elucidating the Role of Pore Size, Electrode Potential, and Ion Dehydration. *ACS Appl. Mater. Interfaces* **2020**, *12*, 42644–42652. https://doi.org/10.1021/acsami.0c07903.

(11) Gao, Y.; Pan, L.; Li, H. B.; Zhang, Y.; Zhang, Z.; Chen, Y.; Sun, Z. Electrosorption Behavior of Cations with Carbon Nanotubes and Carbon Nanofibres Composite Film Electrodes. *Thin Solid Films* **2009**, *517*, 1616–1619. https://doi.org/10.1016/j.tsf.2008.09.065.

(12) Srimuk, P.; Su, X.; Yoon, J.; Aurbach, D.; Presser, V. Charge-Transfer Materials for Electrochemical Water Desalination, Ion Separation and the Recovery of Elements. *Nat. Rev. Mater.* **2020**, 5, 517–538. https://doi.org/10.1038/s41578-020-0193-1.

(13) Chen, R.; Feng, J.; Jeon, J.; Sheehan, T.; Rüttiger, C.; Gallei, M.; Shukla, D.; Su, X. Structure and Potential-Dependent Selectivity in Redox-Metallopolymers: Electrochemically Mediated Multicomponent Metal Separations. *Adv. Funct. Mater.* **2021**, *31* (15), 1–11. https://doi.org/10.1002/adfm.202009307.

(14) Vapnik, H.; Elbert, J.; Su, X. Redox-Copolymers for the Recovery of Rare Earth Elements by Electrochemically Regenerated Ion-Exchange. *J. Mater. Chem. A* **2021**, *9* (35), 20068–20077. https://doi.org/10.1039/d1ta03334d.

(15) He, C.; Ma, J.; Zhang, C.; Song, J.; Waite, T. D. Short-Circuited Closed-Cycle Operation of Flow-Electrode CDI for Brackish Water Softening. *Environ. Sci. Technol.* **2018**, *52* (16), 9350–9360. https://doi.org/10.1021/acs.est.8b02807.

(16) Yoon, H.; Lee, J.; Kim, S. R.; Kang, J.; Kim, S.; Kim, C.; Yoon, J. Capacitive Deionization with Ca-Alginate Coated-Carbon Electrode for Hardness Control. *Desalination* **2016**, *392*, 46–53. https://doi.org/10.1016/j.desal.2016.03.019.

(17) Zhi Yi Leong, H. Y. Y. Capacitive Deionization of Divalent Cations for Water Softening Using Functionalized Carbon Electrodes. *ACS Omega* **2020**, *5*, 2097–2106.

(18) Lee, J. B.; Park, K. K.; Eum, H. M.; Lee, C. W. Desalination of a Thermal Power Plant Wastewater by Membrane Capacitive Deionization. *Desalination* **2006**, *196* (1–3), 125–134. https://doi.org/10.1016/j.desal.2006.01.011.

(19) Mao, S.; Chen, L.; Zhang, Y.; Li, Z.; Ni, Z.; Sun, Z.; Zhao, R. Fractionation of Mono- and Divalent Ions by Capacitive Deionization with Nanofiltration Membrane. *J. Colloid Interface Sci.* **2019**, *544*, 321–328. https://doi.org/10.1016/j.jcis.2019.02.093.

(20) Choi, J.; Lee, H.; Hong, S. Capacitive Deionization (CDI) Integrated with Monovalent Cation Selective Membrane for Producing Divalent Cation-Rich Solution. *Desalination* **2016**, *400*, 38–46. https://doi.org/10.1016/j.desal.2016.09.016.

(21) Hassanvand, A.; Wei, K.; Talebi, S.; Chen, G. Q.; Kentish, S. E. The Role of Ion Exchange Membranes in Membrane Capacitive Deionisation. *Membranes.* **2017**, *7*, 1–23. https://doi.org/10.3390/membranes7030054.

(22) Hassanvand, A.; Chen, G. Q.; Webley, P. A.; Kentish, S. E. A Comparison of Multicomponent Electrosorption in Capacitive Deionization and Membrane Capacitive Deionization. *Water Res.* **2018**, *131*, 100–109. https://doi.org/10.1016/j.watres.2017.12.015.

(23) Epsztein, R.; DuChanois, R. M.; Ritt, C. L.; Noy, A.; Elimelech, M. Towards Single-Species Selectivity of Membranes with Subnanometre Pores. *Nat. Nanotechnol.* **2020**, *15* (6), 426–436. https://doi.org/10.1038/s41565-020-0713-6.

(24) Rijnaarts, T.; Reurink, D. M.; Radmanesh, F.; de Vos, W. M.; Nijmeijer, K. Layer-by-Layer Coatings on Ion Exchange Membranes: Effect of Multilayer Charge and Hydration on Monovalent Ion Selectivities. *J. Memb. Sci.* **2019**, *570–571*, 513–521. https://doi.org/10.1016/j.memsci.2018.10.074.

(25) Richardson, J. J.; Cui, J.; Björnmalm, M.; Braunger, J. A.; Ejima, H.; Caruso, F. Innovation in Layer-by-Layer Assembly. *Chem. Rev.* **2016**, *116* (23), 14828–14867. https://doi.org/10.1021/acs.chemrev.6b00627.

(26) Richardson, J. J.; Björnmalm, M.; Caruso, F. Technology-Driven Layer-by-Layer Assembly of Nanofilms. *Science.* **2015**, *348* (6233). https://doi.org/10.1126/science.aaa2491.

(27) Sahin, S.; Dykstra, J. E.; Zuilhof, H.; Zornitta, R. L.; de Smet, L. C. P. M. Modification of Cation-Exchange Membranes with Polyelectrolyte Multilayers to Tune Ion Selectivity in Capacitive Deionization. *ACS Appl. Mater. Interfaces* **2020**, *12* (31), 34746–34754. https://doi.org/10.1021/acsami.0c05664.

(28) Decher, G.; Hong, J. D.; Schmitt, J. Buildup of Ultrathin Multilayer Films by a Self-Assembly Process: III. Consecutively Alternating Adsorption of Anionic and Cationic Polyelectrolytes on Charged Surfaces. *Thin Solid Films* **1992**, *210–211*, 831–835. https://doi.org/10.1016/0040-6090(92)90417-A.

(29) Decher, G. Fuzzy Nanoassemblies: Toward Layered Polymeric Multicomposites. *Science.* **1997**, *277*, 1232–1237. https://doi.org/10.1126/science.277.5330.1232.

(30) Li, X.; Liu, C.; Van Der Bruggen, B. Polyelectrolytes Self-Assembly: Versatile Membrane Fabrication Strategy. *J. Mater. Chem. A* **2020**, *8* (40), 20870–20896. https://doi.org/10.1039/d0ta07154d.

(31) Cheng, W.; Liu, C.; Tong, T.; Epsztein, R.; Sun, M.; Verduzco, R.; Ma, J.; Elimelech, M. Selective Removal of Divalent Cations by Polyelectrolyte Multilayer Nanofiltration Membrane: Role of Polyelectrolyte Charge, Ion Size, and Ionic Strength. *J. Memb. Sci.* **2018**, *559*, 98–106. https://doi.org/10.1016/j.memsci.2018.04.052.

(32) Kazemabad, M.; Verliefde, A.; Cornelissen, E. R.; D'Haese, A. Crown Ether Containing Polyelectrolyte Multilayer Membranes for Lithium Recovery. *J. Memb. Sci.* **2020**, *595*, 117432. https://doi.org/10.1016/j.memsci.2019.117432.

(33) Cheng, C.; Yaroshchuk, A.; Bruening, M. L. Fundamentals of Selective Ion Transport through Multilayer Polyelectrolyte Membranes. *Langmuir* **2013**, *29*, 1885–1892. https://doi.org/10.1021/la304574e.

(34) Armstrong, J. A.; Bernal, E. E. L.; Yaroshchuk, A.; Bruening, M. L. Separation of Ions Using Polyelectrolyte-Modified Nanoporous Track-Etched Membranes. *Langmuir* **2013**, *29*, 10287–10296. https://doi.org/10.1021/la401934v.

(35) Ahmad, M.; Yaroshchuk, A.; Bruening, M. L. Moderate pH Changes Alter the Fluxes, Selectivities and Limiting Currents in Ion Transport through Polyelectrolyte Multilayers Deposited on Membranes. *J. Memb. Sci.* **2020**, *616*, 118570. https://doi.org/10.1016/j.memsci.2020.118570.

(36) White, N.; Misovich, M.; Alemayehu, E.; Yaroshchuk, A.; Bruening, M. L. Highly Selective Separations of Multivalent and Monovalent Cations in Electrodialysis through Nafion Membranes Coated with Polyelectrolyte Multilayers. *Polymer.* **2016**, *103*, 478–485. https://doi.org/10.1016/j.polymer.2015.12.019.

(37) Zhu, Y.; Ahmad, M.; Yang, L.; Misovich, M.; Yaroshchuk, A.; Bruening, M. L. Adsorption of Polyelectrolyte Multilayers Imparts High Monovalent/Divalent Cation Selectivity to Aliphatic Polyamide Cation-Exchange Membranes. *J. Memb. Sci.* **2017**, *537*, 177–185. https://doi.org/10.1016/j.memsci.2017.05.043.

(38) Ahmad, M.; Tang, C.; Yang, L.; Yaroshchuk, A.; Bruening, M. L. Layer-by-Layer Modification of Aliphatic Polyamide Anion-Exchange Membranes to Increase Cl^-/SO_4^{2-} Selectivity. *J. Memb. Sci.* **2019**, *578*, 209–219. https://doi.org/10.1016/j.memsci.2019.02.018.

(39) Singh, K.; Sahin, S.; Gamaethiralalage, J. G.; Zornitta, R. L.; de Smet, L. C. P. M. Simultaneous, Monovalent Ion Selectivity with Polyelectrolyte Multilayers and Intercalation Electrodes in Capacitive Deionization. *Chem. Eng. J.* **2021**, 128329. https://doi.org/10.1016/j.cej.2020.128329.

(40) Porada, S.; Zhao, R.; van der Wal, A.; Presser, V.; Biesheuvel, P. M. Review on the Science and Technology of Water Desalination by Capacitive Deionization. *Prog. Mater. Sci.* **2013**, *58* (8), 1388–1442. https://doi.org/10.1016/j.pmatsci.2013.03.005.

(41) Wang, L.; Lin, S. Membrane Capacitive Deionization with Constant Current vs Constant Voltage Charging: Which Is Better? *Environ. Sci. Technol.* **2018**, *52* (7). https://doi.org/10.1021/acs.est.7b06064.

(42) Zhao, R.; Biesheuvel, P. M.; van der Wal, A. Energy Consumption and Constant Current Operation in Membrane Capacitive Deionization. *Energy Environ. Sci.* **2012**, *5* (11), 9520–9527. https://doi.org/10.1039/c2ee21737f.

(43) Kang, J.; Kim, T.; Jo, K.; Yoon, J. Comparison of Salt Adsorption Capacity and Energy Consumption between Constant Current and Constant Voltage Operation in Capacitive Deionization. *Desalination* **2014**, *352*, 52–57. https://doi.org/10.1016/j.desal.2014.08.009.

(44) Han, L.; Karthikeyan, K. G.; Gregory, K. B. Energy Consumption and Recovery in Capacitive Deionization Using Nanoporous Activated Carbon Electrodes. *J. Electrochem. Soc.* **2015**, *162* (12), E282–E288. https://doi.org/10.1149/2.0431512jes.

(45) Qu, Y.; Campbell, P. G.; Gu, L.; Knipe, J. M.; Dzenitis, E.; Santiago, J. G.; Stadermann, M. Energy Consumption Analysis of Constant Voltage and Constant Current Operations in Capacitive Deionization. *Desalination* **2016**, *400*. https://doi.org/10.1016/j.desal.2016.09.014.

(46) White, N.; Misovich, M.; Yaroshchuk, A.; Bruening, M. L. Coating of Nafion Membranes with Polyelectrolyte Multilayers to Achieve High Monovalent/Divalent Cation Electrodialysis Selectivities. *ACS Appl. Mater. Interfaces* **2015**, *7*, 6620−6628. https://doi.org/10.1021/am508945p.

(47) Lavalle, P.; Gergely, C.; Cuisinier, F. J. G.; Decher, G.; Schaaf, P.; Voegel, J. C.; Picart, C. Comparison of the Structure of Polyelectrolyte Multilayer Films Exhibiting a Linear and an Exponential Growth Regime: An in Situ Atomic Force Microscopy Study. *Macromolecules* **2002**, *35* (11), 4458–4465. https://doi.org/10.1021/ma0119833.

(48) Schönhoff, M.; Bieker, P. Linear and Exponential Growth Regimes of Multilayers of Weak Polyelectrolytes in Dependence on PH. *Macromolecules* **2010**, *43* (11), 5052–5059. https://doi.org/10.1021/ma1007489.

(49) Elzbieciak-Wodka, M.; Kolasińska-Sojka, M.; Nowak, P.; Warszyński, P. Comparison of Permeability of Poly(Allylamine Hydrochloride)/and Poly(Diallyldimethylammonium Chloride)/Poly(4-Styrenesulfonate) Multilayer Films: Linear vs. Exponential Growth. *J. Electroanal. Chem.* **2015**, *738*, 195–202. https://doi.org/10.1016/j.jelechem.2014.11.035.

(50) Cao, Z.; Gordiichuk, P. I.; Loos, K.; Sudhölter, E. J. R.; de Smet, L. C. P. M. The Effect of Guanidinium Functionalization on the Structural Properties and Anion Affinity of Polyelectrolyte Multilayers. *Soft Matter* **2016**, *12*, 1496–1505. https://doi.org/10.1039/c5sm01655j.

(51) Choi, J. H. Determination of the Electrode Potential Causing Faradaic Reactions in Membrane Capacitive Deionization. *Desalination* **2014**, *347*, 224–229. https://doi.org/10.1016/j.desal.2014.06.004.

(52) Dykstra, J. E.; Zhao, R.; Biesheuvel, P. M.; Van der Wal, A. Resistance Identification and Rational Process Design in Capacitive Deionization. *Water Res.* **2016**, *88*, 358–370. https://doi.org/10.1016/j.watres.2015.10.006.

(53) Biesheuvel, P. M.; Zhao, R.; Porada, S.; van der Wal, A. Theory of Membrane Capacitive Deionization Including the Effect of the Electrode Pore Space. *J. Colloid Interface Sci.* **2011**, *360* (1), 239–248. https://doi.org/10.1016/j.jcis.2011.04.049.

(54) Dykstra, J. E.; Keesman, K. J.; Biesheuvel, P. M.; van der Wal, A. Theory of PH Changes in Water Desalination by Capacitive Deionization. *Water Res.* **2017**, *119*. https://doi.org/10.1016/j.watres.2017.04.039.

(55) Mulyati, S.; Takagi, R.; Fujii, A.; Ohmukai, Y.; Matsuyama, H. Simultaneous Improvement of the Monovalent Anion Selectivity and Antifouling Properties of an Anion Exchange Membrane in an Electrodialysis Process, Using Polyelectrolyte Multilayer Deposition. *J. Memb. Sci.* **2013**, *431*, 113–120. https://doi.org/10.1016/j.memsci.2012.12.022.

(56) Nightingale, E. R. Phenomenological Theory of Ion Solvation. Effective Radii of Hydrated Ions. *J. Phys. Chem.* **1959**, *63* (9), 1381–1387. https://doi.org/10.1021/j150579a011.

Supplementary Information to:

Enhanced Monovalent over Divalent Cation Selectivity with Polyelectrolyte Multilayers in Membrane Capacitive Deionization *via* Optimization of Operational Conditions

Spectroscopic Ellipsometry Analyses. The gold substrates were sonicated for 5 min in Milli-Q water, and dried in a gentle stream of argon. Then, the substrates were subsequently cleaned with air-based plasma by a plasma cleaner (Diener electronic GmbH, Germany) for 5 minutes. After cleaning, the gold substrates were coated with 2.5, 9, and 20.5 bilayers of PEM by using the procedure that was used for membrane coating. The PEM-coated gold substrates were analyzed by spectroscopic ellipsometry to determine their optical (dry) thicknesses. The data were obtained in air at room temperature by using an Accurion Nanofilm_ep4 imaging ellipsometry. The wavelength range of the light was λ = 400.6−761.3 nm at an angle of incidence of 50°. The data were fitted with EP4 software using a multilayer model by using a refractive index of 1.397 for gold.

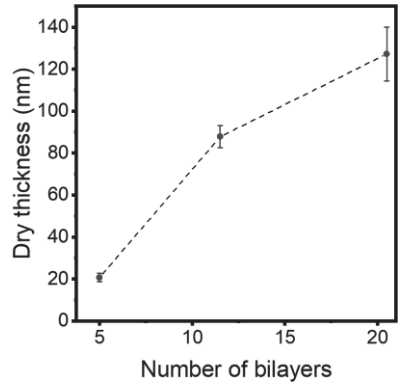

Figure S6.1: Dry (optical) PEM thickness as function of the number of bilayers.

Resistance Analyses of PEM-Coated Membranes. CC experiments were carried out for PEM-CMX with 5.5 and 20.5 bilayers as well as the pristine CMX. Each experiment consists of three cycles with current densities of 5, 10, 25, 50, and 100 mA/g. The experiments were conducted in 8 mM of NaCl, followed by 8 mM of $MgCl_2$ for each membrane. The potential drop measured when switching from charging to discharging is defined as half of the IR (ohmic) drop. Based on the IR drop values, the resistance of different membranes for

different salt solutions could be estimated. A higher ohmic drop means a higher resistance of the membrane. The magnitude of ohmic drops was calculated by using the 3rd cycle of the aforementioned current density values for all experiments.

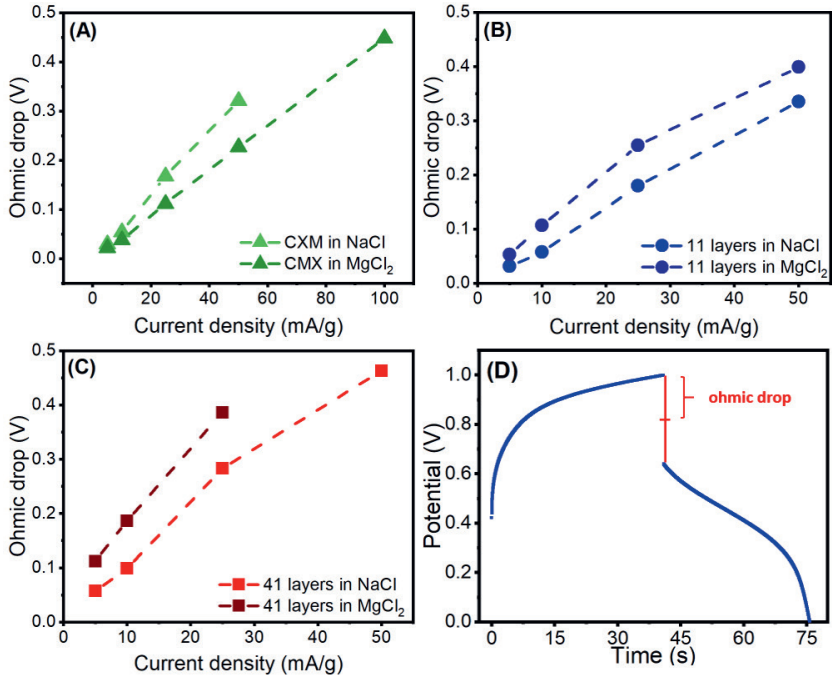

Figure S6.2. Ohmic drop (V) values of (A) CMX (B) PEM-CMX with 11 layers and (C) PEM-CMX with 41 layers in 8 mM NaCl and $MgCl_2$ solutions. (D) Typical potential profile for a constant current at ±25 mA/g in 8 mM NaCl charging and discharging illustrating the presence of the ohmic drop for the PEM-CMX with 11 layers. The potential drop measured when switching from charging to discharging (shown as a red line) is defined as half of the ohmic drop (shown as half of the red line).

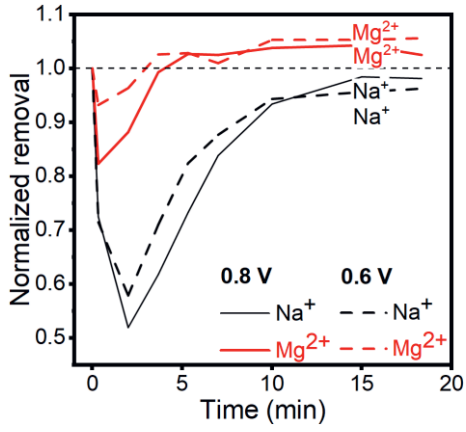

Figure S6.3. Transient normalized removal of Na^+ and Mg^{2+} during electrosorption cycles at 0.6 and 0.8 V.

Electrosorption Experiments. The experiments were performed using a home-built, lab-scale MCDI system.[1] The dimensions of the MCDI cell are 6 cm × 10.5 cm × 18.5 cm with total volume of 70 mL. The cell was assembled with two carbon-based electrodes (5.6 cm × 6.0 cm), each with a square opening inside (1.5 cm × 1.5 cm), separated with CMX, AMX, and a spacer. The de-aerated feed solution (5 L of 4 mM of each relevant salt) was pumped using a peristaltic pump (Masterflex) through the system at a constant flow rate of 7.5 mL/min. Due to the large volume of the feed solution and the small size of the electrodes, the experiments behaved like a single-pass experiment, as described previously in literature.[2] Firstly, the effect of operational modes (CV and CC) on monovalent cation selectivity was investigated. In CV mode, a potentiostat (Autolab PGSTAT302N, Metrohm) provided a charging voltage (ranging from 0.4 to 1.0 V) and a discharge voltage of 0 V (short circuit) during the electrosorption and desorption, respectively. The experiments in CV mode were carried out for 10 cycles (electrosorption + desorption) of 40 min each. The threshold current value was optimized and guided by a MCDI model (details in Section 3) to

maximize the sodium selective removal. Therefore, a constant current value (*i.e.* ±10 mA) below the threshold for magnesium electrosorption was chosen. The cut-off potentials were 1.0 V for electrosorption and 0 V for desorption cycles. For all MCDI experiments, the conductivity was monitored online at the exit of the MCDI cell (conductivity module 856, Metrohm). The electrosorption/desorption experiments were carried out for minimum 2 cycles per each voltage value in CV mode and 10 cycles per experiment in CC mode. The selectivity values in the CC mode were calculated based on a minimum of three cycles per experiment and a minimum of two separate experiments. Experiments were conducted by using different feed solutions containing different cations as displayed in **Table S6.1**. The counter anion was chloride for all experiments. Feed concentration number 1 was used to determine the optimum current and the number of polyelectrolyte layers, as well as comparing different type of membranes. Depending on the experiment, a CMX, CMX-PEM, CMS, or CSO membrane was used as a cation-exchange membrane. All CDI experiments were performed at least two times for each membrane. After the optimized conditions to obtain the highest Na^+/Mg^{2+} selectivity with PEM-CMX were obtained, the selectivity values were calculated for bare CMX, CSO, and PEM-CMX in various experiments with feed compositions 2–5 (**Table S6.1**).

Table S6. 1. Compositions of the feed solutions used in the electrosorption experiments.

Feed number	Na^+ (mM)	K^+ (mM)	Li^+ (mM)	Mg^{2+} (mM)
1	4 mM	-	-	4 mM
2	4 mM	4 mM	4 mM	-
3	4 mM	4 mM	4 mM	4 mM
4	4 mM	4 mM	-	-
5	-	4 mM	4 mM	-

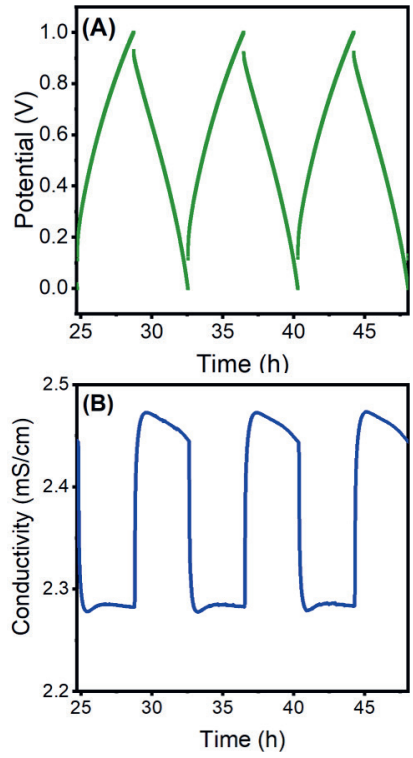

Figure S6.4. (A) Potential and (B) conductivity profile of the CC experiment with PEM-CMX (5.5 bilayers) by using a current density of 5.6 mA/g.

Membrane Capacitive Deionization (MCDI) Model . The dynamic model used to describe the membrane capacitive deionization (MCDI) process has been proposed elsewhere.[3,4] Here, the model was adapted and simplified for our cell setup considering the presence of a thin layer between the membrane and electrode for a 1:1 salt solution, as depicted in **Figure S6.5**.

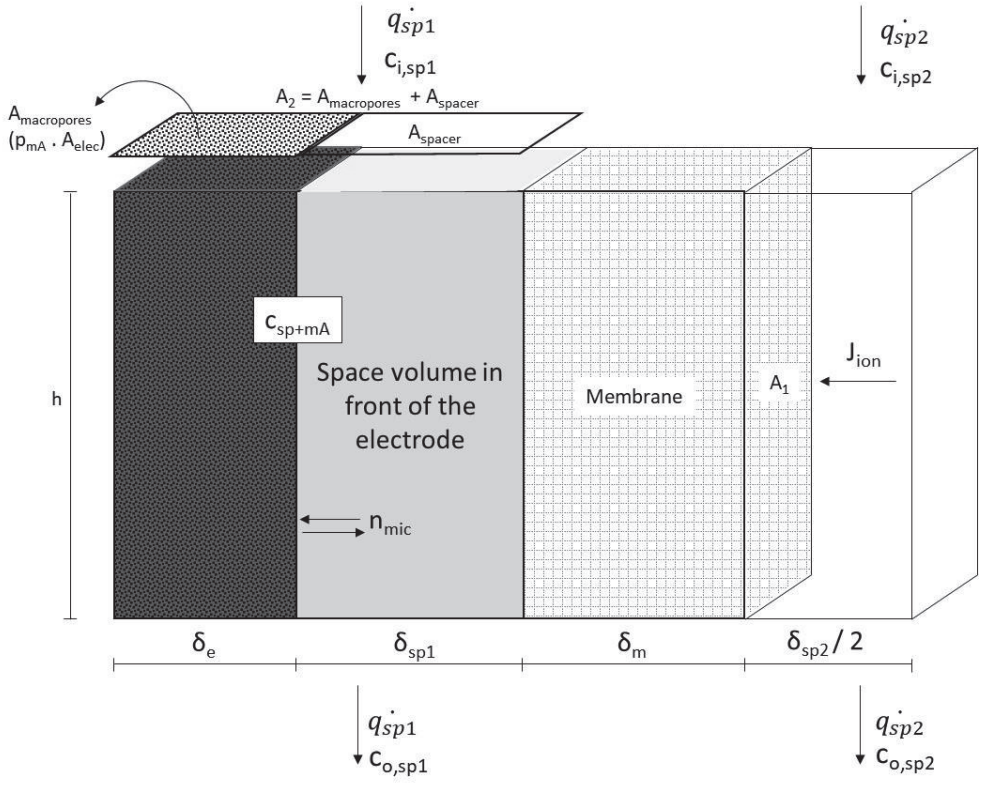

Figure S6.5. Schematic representation of the mass balance used in the half-cell of the PEM-CMX.

6

The mass balance for this system is:

$$\frac{d}{dt}\left[2.\, c_{sp+mA} + \frac{1}{\frac{p_{mA}}{p_{mi}} + \frac{V_{sp,ele}}{V_e \cdot p_{mi}}} c_{mi}\right] = \frac{J_{ion}}{\delta_T} - \frac{v}{h}(c_{o,sp1} - c_{i,sp1}) \qquad \textbf{(S6.1)}$$

where c_{sp+mA} is the concentration in the macropores and space in front of the electrode, p_{mA} and p_{mi} are the macro and micropore porosity of the electrode, respectively, $V_{sp,ele}$ is the

space volume in front of the electrode, V_e is the volume of the electrode, c_{mi} is the concentration in the micropores, J_{ion} is the ion flux, δ_T is the total thickness of electrode and space in front of the electrode, v is the velocity of the flux through and in front of the electrode, $c_{o,sp1}$ and $c_{i,sp1}$ are the outlet and inlet concentration in and in front of the electrode. The flow in the space of the electrode was considered to be 2% of the total flow in the cell.

The concentration in the micropores, c_{mi}, was calculated based on the modified Donnan model:

$$c_{mi} = 2.c_{sp+mA}.\exp(\mu_{att}).\cosh(\Delta\varphi_{mD}) \quad \textbf{(S6.2)}$$

Where μ_{att} is the attractive term for the electrode surface, and $\Delta\varphi_{mD}$ is the Donnan potential inside of the micropores. The **Equation S6.3** is then used to calculate the equilibrium between $\Delta\varphi_{mD}$ and the other potentials inside of the cell.

$$\frac{V_{cell}}{2.V_T} = \Delta\phi_e + \Delta\phi_m + \Delta\phi_{sp1} + \Delta\phi_{sp2} + \Delta\phi_{Stern} + \Delta\phi_{mD} + \Delta\phi_{donnan,sp2} - \Delta\phi_{donnan,sp1} \quad \textbf{(S6.3)}$$

For simplicity, it was considered that the voltage in the half-cell was half of the total cell voltage applied. In **Equation S6.3**, $\Delta\phi_e$ is the electrode potential drop, $\Delta\phi_m$ is the potential drop across the membrane caused by ionic resistance, $\Delta\phi_{donnan,sp2}$ and $\Delta\phi_{donnan,sp1}$ are the Donnan potential from the solution to the membrane interfaces, $\Delta\phi_{sp1}$ is the potential drop in the volume space in front of the electrode, $\Delta\phi_{sp2}$ is the potential drop across the spacer for the solution being treated, and $\Delta\phi_{Stern}$ is the Stern potential of the electrode. These potential values can be calculated using the following correlations:

$$\Delta\phi_e = -\frac{I.F.R_{ele}}{V_T.c_{sp+mA}} \quad \textbf{(S6.4)}$$

$$\Delta\phi_m = -\frac{I.\delta_m}{D_m.\langle c_{T,m}\rangle} \quad \textbf{(S6.5)}$$

$$\Delta\phi_{sp} = -\frac{I.\delta_{sp}}{2.D_i.c_{sp}} \quad \textbf{(S6.6)}$$

$$\Delta\phi_{Stern} = -\frac{\sigma_{mi}.F}{V_T.C_{St,vol}} \quad \textbf{(S6.7)}$$

$$C_{St,vol} = C_{St,vol0} + \alpha.\sigma_{mi}^2 \quad \textbf{(S6.8)}$$

$$\Delta\phi_{donnan} = \sinh^{-1}\left(\frac{\omega.X}{2.c_{salt}}\right) \quad \textbf{(S6.9)}$$

In these equations, I is the ionic current, F is the Faraday's constant, R_{ele} is the electrode resistance, V_T is the thermal voltage, δ_m is the membrane thickness, D_m is the diffusion coefficient of ions across the membrane, $\langle c_{T,m} \rangle$ is the average concentration of ions inside of the membrane, δ_{sp} is the spacer thickness in the front of the membrane and electrode, D_i is the diffusion of ions in the spacer, c_{sp} is the concentration of ions in the spacer, σ_{mi} is the ionic charge, $C_{St,vol0}$ are the standard volumetric Stern capacity, α is parameter to describe the non-linear Stern capacity, ω is the charge of the membrane (ω = -1 for CEM), X is the volumetric concentration of the membrane, and c_{salt} is the salt concentration in the interface in both sides of the membrane.

The charge in the micropores can be calculated using:

$$\sigma_{mi} = -2.c_{sp\_mA}.\exp(\mu_{att}).\sinh(\Delta\phi_{mD}) \quad \textbf{(S6.10)}$$

and

$$\frac{d\sigma_{mi}}{dt} = -\frac{\mathrm{I}}{\mathrm{p_{mi}}.\delta_e} \quad \textbf{(S6.11)}$$

The concentration variation in the spacer in front of the membrane is calculated using the following mass balance, solved for *M* sub-cells simultaneously:

$$\frac{dc_{sp2}}{dt} = \frac{J_{ion}}{\delta_{sp2}} + \frac{M}{\tau_{sp2}}(c_{sp2,i} - c_{sp2,i-1}) \quad \textbf{(S6.12)}$$

The ion flux crossing the membrane is calculated based on the linearization of the Nernst-Plank equation:

$$J_m = -\frac{D_m}{\delta_m}(\Delta c + \omega . X . \Delta\phi_m) \quad \textbf{(S6.13)}$$

The values used in the model are provided in **Table S6.2**. Some of the parameters, such as diffusion coefficients, were based on typical values presented in literature,[5] while other parameters, such as thickness of components, were based on our experimental setup. The actual values of the parameters in **Table S6.2** were not measured since this model was used for a single−salt solution, instead of a mixture used in our experiments. Nevertheless, the main outcomes from the model, such as the profile of the potential drop across the membrane by only changing cell voltage and current density, are barely affected by these parameters, and do not influence the conclusions from this work.

Table S6.2. Parameters used for the MCDI transport model.

Parameter	Value
F	96485 C/mol
R_{ele}	0.12 Ω mol/m
V_T	25.6 mV
$\boldsymbol{\delta_e}$	150 µm
$\boldsymbol{\delta_m}$	150 µm
$\boldsymbol{\delta_{sp1}}$	150 µm
$\boldsymbol{\delta_{sp2}}$	250 µm
$\boldsymbol{D_m}$	0.17 . 10^{-9} m²/g
$\boldsymbol{D_i}$	1.70 . 10^{-9} m²/g
$\boldsymbol{C_{St,vol0}}$	200 MF/m³
$\boldsymbol{\alpha}$	20 F/m³ mol²
X	3000
$\boldsymbol{\mu_{att}}$	2 kT
$\boldsymbol{p_{mi}}$	0.35
$\boldsymbol{p_{mA}}$	0.30

References

(1) Sahin, S.; Dykstra, J. E.; Zuilhof, H.; Zornitta, R. L.; De Smet, L. C. P. M. Modification of Cation-Exchange Membranes with Polyelectrolyte Multilayers to Tune Ion Selectivity in Capacitive Deionization. *ACS Appl. Mater. Interfaces* **2020**, *12* (31), 34746–34754. https://doi.org/10.1021/acsami.0c05664.

(2) Lee, J.; Srimuk, P.; Zwingelstein, R.; Zornitta, R. L.; Choi, J.; Kim, C.; Presser, V. Sodium Ion Removal by Hydrated Vanadyl Phosphate for Electrochemical Water Desalination. *J. Mater. Chem. A* **2019**, *7* (8), 4175–4184. https://doi.org/10.1039/c8ta10087j.

(3) Biesheuvel, P. M.; Zhao, R.; Porada, S.; van der Wal, A. Theory of Membrane Capacitive Deionization Including the Effect of the Electrode Pore Space. *J. Colloid Interface Sci.* **2011**, *360* (1), 239–248. https://doi.org/10.1016/j.jcis.2011.04.049.

(4) Porada, S.; Bryjak, M.; van der Wal, A.; Biesheuvel, P. M. Effect of Electrode Thickness Variation on Operation of Capacitive Deionization. *Electrochim. Acta* **2012**, *75*, 148–156. https://doi.org/10.1016/j.electacta.2012.04.083.

(5) Biesheuvel, P. M.; Zhao, R.; Porada, S.; van der Wal, A. Theory of Membrane Capacitive Deionization Including the Effect of the Electrode Pore Space. *J. Colloid Interface Sci.* **2011**, *360* (1), 239–248. https://doi.org/10.1016/j.jcis.2011.04.049.

Chapter 7

Crown Ether-Modified Polyelectrolytes and their Interactions with Cations – a QCM Study

This chapter was adapted from:

Sahin, S.; van Weeren, E.; Zuilhof, H.; de Smet, L.C.P.M. Crown Ether-Modified Polyelectrolytes and their Interactions with Cations – a QCM Study (accepted for a publication in *Applied Surface Science Advances*)

Abstract

In this study, the build-up of polyelectrolyte multilayers (PEMs) containing 15-crown-5 (CE) groups and their interactions with various cations were studied by using quartz crystal microbalance with dissipation monitoring (QCM-D). First, poly(allylamine hydrochloride) (PAH) was modified with 4'-carboxybenzo-CE via carbodiimide chemistry. CE was chosen as its complexes with Na^+ and K^+ are reported to be more stable compared to those with other cations. The resulting functionalized polyelectrolyte (PAHCE) and poly(4-styrene sulfonic acid) (PSS) were used in the layer-by-layer build-up of a multilayer onto gold-coated quartz resonators, enabling their characterization with QCM-D. Compared to $(PAH/PSS)_4$, $(PAHCE/PSS)_4$ resulted in slightly thicker layers based on Voigt (65 ± 5 vs. 57 ± 3 nm) and Sauerbrey (45 ± 2 vs. 38 ± 3 nm) modelling of the QCM-D data. The same trend was found for the optical, dry thickness, as obtained with ellipsometry (15 ± 0.3 vs. 13 ± 1 nm). Next, the QCM-D characteristics of these PEMs were monitored in situ when exposed to various aqueous salt solutions (LiCl, NaCl, KCl, CsCl, RbCl, and $MgCl_2$). Starting from Cs^+, the frequency change of the $(PAHCE/PSS)_4$ system upon changing to K^+ and Na^+ solutions was found to be ≈ 3 times larger than for $(PAH/PSS)_4$. With a polycation (PAHCE) as the outermost PEM layer, the salt-exchange behavior was less visible due to increased charge rejection of cations. Therefore, we also modified a bio-based polyanion, pectin with 4'-aminobenzo-CE and built $(PAH/pectinCE)_4$. Also, in this case the addition of CE increased the PEM layer thickness compared to $(PAH/pectin)_4$, both in a wet state (Sauerbrey modelling, 447 ± 19 vs. 314 ± 17 nm) and when dry (115 ± 4 vs. 66 ± 3 nm). Again, we observed the largest QCM-D responses for K^+ and Na^+ solutions (≈ 6 and 12 times larger, respectively) compared to the $(PAH/pectin)_4$. The effect of CE is more prominent in pectin-based PEMs due their relatively higher thickness. Given the large toolbox of available polyelectrolytes and ionophores, we anticipate that functionalized PEMs can facilitate the further development of ion separation applications.

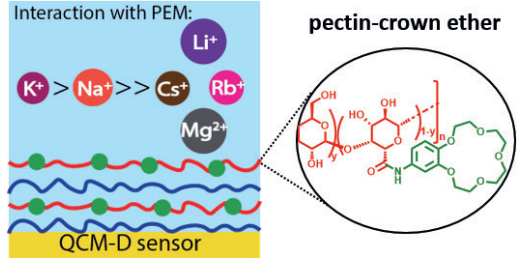

7.1 Introduction

Selectivity is crucial for applications that involve the detection and separation of ions, including in clinical chemistry,[1] environmental monitoring,[2] and water treatment.[3–6] For instance, K^+ and Na^+ selectivity is important for a rapid and reliable detection of these ions, which both play a regulating role in the cellular electrolyte metabolism,[7] while K^+ over Na^+ selectivity is important for greenhouse applications, as it assists the recycling of irrigation water.[4] Other examples from the field of water treatment include the reduction of water hardness (divalent over monovalent selectivity),[3,5] and the recovery of nutrients, such as phosphate,[5,6,8,9] and valuable metals such as lithium.[10,11] Similarly, levels of arsenic, lead, and mercury are monitored to check heavy metal contamination in the environment and blood samples.[12]

One interesting and attractive way to tune ion selectivity is to introduce polyelectrolyte multilayers (PEMs).[3,5,6,8,10,11,13–15] PEMs are composed of alternating layers of oppositely charged polymers and can control the physicochemical properties of various surfaces, including those of membranes and electrodes.[16–20] As such, PEMs provide a versatile and facile way to tune separation processes of various species like gases, solvents and ions.[21,22] Moreover, the selectivity of PEMs strongly depends on structural features like the molecular weight and/or charge density of the constituting polyelectrolytes,[18,23–25] the number of layers in the PEM, as well as experimental conditions, including the ionic strength,[26–28] the type of supporting electrolyte[29–32] and the pH[33–36] of the solution in which the PEM is prepared or in contact with.

The ion-separation properties of PEMs mostly rely on their charge- and size-dependent rejection mechanisms towards certain (type of) ions.[3,21,22,37] Interestingly, the ion-selective behavior of PEMs can be further tuned via the incorporation of ionophores. Typically one of the polyelectrolytes is replaced by an ionophore during layer build-up, or the ionophore is trapped within the PEM.[38–40] For example, Toutianoush *et al.* combined various negatively charged calixarene derivatives with poly(vinyl amine) to build calixarene-functionalized PEMs which demonstrated ion-selective properties towards monovalent, divalent, or trivalent cations based on the ring size of the calixarene ring.[38] However, the

lack of covalent bonds between the macromolecular polyelectrolytes and low-molecular-weight ionophores makes such systems limited in stability due to the problem of leaching of the ionophore to the environment. Alternatively, ionophores are covalently attached to the polyelectrolyte backbone.[9,10] For instance, Cao *et al.* chemically attached guanidinium moieties to a polycation, to yield a functional macromolecule that was found to be useful in building PEMs that showed increased interactions with phosphate ions.[8,9,41]

Given the importance of PEMs in alkali metal ion recognition processes, including those relevant for ion sensors[1,4,39,40,42–45] and pressure-driven ion separations,[38,46,47] we now covalently attached a crown ether to polyelectrolytes and incorporated these in PEMs for ion selectivity.

In order to study the structure of (functionalized) PEMs and their interaction with different ions, quartz crystal microbalance with dissipation monitoring (QCM-D) is a widely used technique.[9,48–51] In short, QCM-D makes use of a resonating gold-coated, piezo-active sensor onto which PEM layers can be built.[52,53] The resonance frequency is monitored online and frequency changes are proportional to the changes in mass, as shown by Equation 1: [54]

$$\Delta m = \frac{-C \times \Delta f_{\mathrm{n}}}{n} \qquad \textbf{(7.1)}$$

where Δm (ng · cm^{-2}) is the areal mass density of the adsorbed film, C (1.77 ng · cm^{-2} · Hz^{-1}) is the mass-sensitivity constant, Δf_{n} (Hz) is the frequency shift and n is the harmonic number (3, 5, 7, 9, 11). The thickness of the films is determined either using the Sauerbrey model, which is suitable for rigid layers, or using a viscoelastic model that is mainly used for soft PEM coatings.[48,49,55] Furthermore, the dissipation mode of QCM-D enables one to obtain information on the viscoelastic properties of the layers.

In this study, we aim to extend the scope of ion-selective PEM coatings by attaching crown ether units as ionophore to two polyelectrolytes, and to better understand the interactions between the functionalized PEMs – as well as their non-functionalized equivalents – and various cations. Although the effects of different anions on the PEM structure have been studied previously via QCM-D,[27,32,56–59] a comparable comprehensive study with alkali (earth) metal cations has not been reported yet. Also, the cation preference

of an ionophore-containing PEM has not been studied yet with QCM-D. In addition, apart from an interesting series of adsorption selectivity studies on crown ether-functionalized chitosan,[60–66] the number of studies on crown ether-functionalized, bio-based polyelectrolytes for ion studies is limited.[60] Moreover, in those studies atomic adsorption spectrophotometry was exclusively used to analyze the metal concentrations in supernatant solutions of centrifuged polyelectrolyte-salt solutions. While this was useful in terms of adsorption selectivity at the single polyelectrolyte level, the use of PEMs also enables the use of surface-related analytical techniques. In this study, we covalently attached 15-crown-5 (CE) to both poly(allylamine hydrochloride) (PAH) and pectin, to obtain different PEMs that are decorated with ionophore groups. Pectin was the natural polyelectrolyte of choice since it can be obtained from citrus peel, making it an affordable and biodegradable polyanion, while PAH is widely used polycation to build PEMs. CE was chosen as its complexes with Na^+ and K^+ are reported to be more stable compared to those with other cations.[67–70] The interactions between various cations and CE-containing PEMs and their non-functionalized equivalents as well as the effect of CE modification on PEM properties were studied by a real-time gravimetric method, QCM-D.

7.2 Materials and Methods

Materials. Poly(allylamine hydrochloride) (PAH, M_w ≈ 450,000 Da), poly(sodium 4-styrenesulfonic acid) solution (PSS, M_w ≈ 75,000, 18 wt. % in H_2O), pectin (from citrus peel, galacturonic acid ≥74.0% (dried basis)), 4'-carboxybenzo-15-crown-5 (>98%), 4'-aminobenzo-15-crown-5 (97%), *N*-hydroxysuccinimide (NHS, 98%), *N*-(3-dimethylaminopropyl)-*N*'-ethylcarbodiimide hydrochloride (EDC, >98%), lithium chloride (BioXtra, ≥99.0%), sodium chloride (NaCl, ≥ 99%), potassium chloride (BioXtra, ≥99.0%), rubidium chloride (ReagentPlus®, ≥99.0% (metals basis)), cesium chloride (ReagentPlus®, 99.9%), anhydrous magnesium chloride ($MgCl_2$, ≥ 98%), sodium dodecyl sulfate (ACS reagent, ≥99.0%), 3-(trimethylsilyl)propionic-2,2,3,3-d_4 acid sodium salt (TSP-D4), and Hellmanex™ III (cleaning concentrate) were purchased from Sigma Aldrich. Hydrochloric acid (36.5 - 28.0% NF grade) was purchased from VWR International. All chemicals were

used as received without further purification. The inorganic salts were kept in a vacuum oven overnight prior to use. Dialysis membrane cellulose tubing (with a cut-off ≈ 14 kDa) was bought from Sigma Aldrich. Milli-Q water (18.2 MΩ·cm, Milli-Q Integral 3 system, Millipore) was used to prepare salt and polyelectrolyte solutions. Gold-coated quartz resonators (AT-cut, QSense 301, < 1 nm RMS, 100 nm Au) with a fundamental frequency (f_0) of 5 MHz were purchased from Biolin Scientific, Sweden.

Synthesis and Purification of the Crown-Ether Functionalized Polyelectrolytes. EDC-NHS carbodiimide-assisted coupling reactions were used to synthesize crown-ether containing polyelectrolytes. The protocol was adapted from the work of Zheng *et al.*[9]

A series of PAH derivatives with different degrees of substitution were synthesized by changing the molar feed ratio of the monomeric allylamine hydrochloride and 4'-carboxybenzo-15-crown-5 (carboxy-CE). The synthesized products were abbreviated as PAHCE #1, PAHCE #2, and PAHCE #3 for the feed ratios of 10:1, 10:2, and 10:3, respectively. Amino groups of the PAH reacted with the carboxylic acid groups of the carboxy-CE to yield a conjugate of the two molecules joined by a stable amide bond (Scheme 1A). Briefly, for the 10:2 ratio case, PAH (0.2 g, 2.140 mmol, 1 equiv.) and carboxy-CE (0.134 g, 0.428 mmol, 0.2 equiv.) were dissolved 30 mL of Milli-Q water. Followed by the addition of 1-ethyl-3-(3-dimethylaminopropyl)carbodiimide (0.984 g, 5.136 mmol, 2.4 equiv.) and *N*-hydroxysuccinimide (0.492 g, 4.28 mmol, 2 equiv.). The reaction mixture was stirred for 72 h at room temperature. The mixture was afterwards transferred to a dialysis tube (cut-off 14 kDa), which was then kept in ample Milli-Q water for 48 h. The water was refreshed every 12 h, and at the end of the dialysis the retained mixture was freeze dried. In the rest of the study, PAHCE #2 derivative was used unless otherwise stated.

Similarly, pectin was functionalized with 15-crown-5 (Scheme 1B). The carboxylic acids group (of which the pK_A is generally believed to be in the range from pH 3.5 to 4.5) of pectin do not only make it a polyanion, but can also be used to covalently attach an amino-CE. In more detail, pectin was functionalized with 4'-aminobenzo-15-crown-5 (amino-CE) by using a 10:2 feed ratio. Pectin (0.1 g, 0.497 mmol, 1 equiv.) and amino-CE (0.028 g, 0.099

mmol, 0.2 equiv.) were dissolved in 20 mL of Milli-Q water, to which was subsequently added 1-ethyl-3-(3-dimethylaminopropyl)carbodiimide (0.229 g, 1.193 mmol, 2.4 equiv.) and *N*-hydroxysuccinimide (0.114 g, 0.994 mmol, 2 equiv.). The reaction mixture was stirred for 72 h at room temperature. The mixture was afterwards transferred to a dialysis tube (cut-off 14 kDa) and kept in ample Milli-Q water for 48 h. The water was refreshed every 12 h, and at the end of the dialysis the mixture was freeze dried.

Since the molecular weight of the functionalized polyelectrolytes was not exactly known, yields were calculated by dividing the mass of the product obtained after the purification by the sum of the masses of the reactants (either PAH and carboxy-CE or pectin and amino-CE,) as described in the literature.[9]

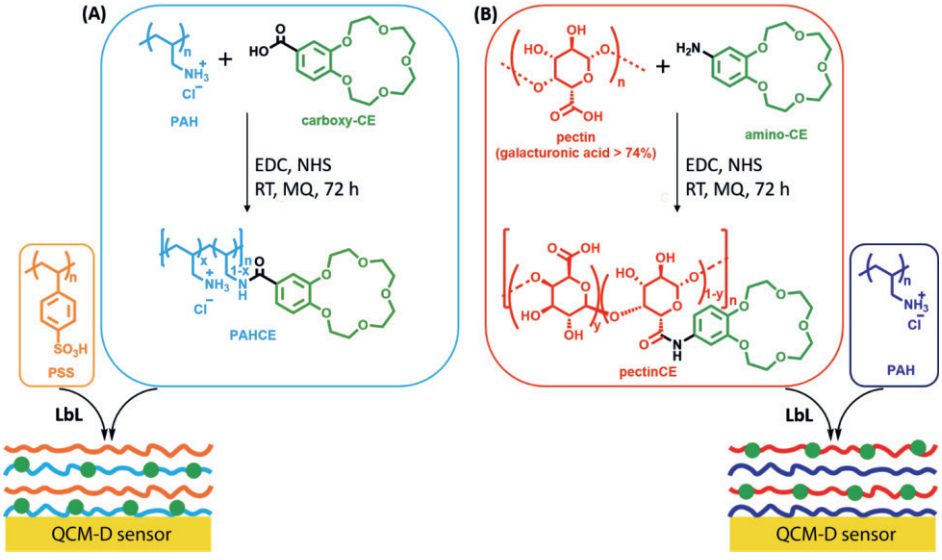

Scheme 7.1. Reaction schemes for the synthesis of (A) PAHCE and (B) pectinCE and schematic representations of the PEM-coated QCM sensors.

Characterization of PAHCE and pectinCE. The structures of the products were characterized by nuclear magnetic resonance (NMR) spectroscopy (Bruker AVANCE, 400 MHz for ^{1}H and 101 MHz for ^{13}C with deuterated water (D_2O) as solvent). In addition to one-dimensional NMR experiments, two-dimensional NMR experiments, correlation spectroscopy (COSY), heteronuclear single quantum coherence (HSQC), and heteronuclear multiple bond correlation (HMBC), were conducted for PAHCE. Additionally, diffusion-ordered spectroscopy (DOSY) was used to confirm the covalent bounds between the CE moieties and PAH backbone. TSP-d_4 was used as an internal standard when acquiring the ^{1}H-NMR spectrum of pectinCE by dissolving 14.1 mg of pectinCE and 0.65 mg of TSP-d_4 in 1 mL of D_2O. The spectra were processed with MasterNova 14.1.0.

Fourier-transform infrared (FT-IR) spectra were recorded with a Bruker Tensor 27 spectrometer equipped with a platinum attenuated total reflection (ATR) accessory. The samples were placed on the crystal of the ATR accessory as powder. Each spectrum was acquired with 64 scans with a resolution of 4 cm^{-1}.

Preparation of Polyelectrolyte and Salt Solutions. Salt solutions (0.15 M) were prepared by dissolving the appropriate amount of salt in Milli-Q water. The pH of these solutions was adjusted to 5.0 (using a pH meter, Innolab, WTW series) by adding drops of a diluted HCl solution. Polyelectrolyte solutions were prepared by dissolving 25 mg of the polyelectrolyte in 50 mL of CsCl solution (0.15 M, at pH 5.0).

Multilayer Build-up. The experiments were performed by using gold-coated quartz sensors in a QCM-D set-up (Q-Sense E4, Biolin Scientific, Sweden) at 18 ^{o}C. Prior to the experiments, the sensors were dipped in 2% sodium dodecyl sulfate solution for 30 min, and rinsed excessively with Milli-Q water. After rinsing, they were dried with a flow of nitrogen and treated with UV-ozone cleaner (Procleaner UV.PC.220, Bioforce Nanosciences) for 20 min.

All polyelectrolyte and salt solutions were bubbled with nitrogen for 15 min in order to reduce the concentration of dissolved oxygen that may cause unstable baseline. The flow rate of solutions was 50 µL/min in all experiments.

Before each experiment, a CsCl solution (0.15 M, at pH 5.0) was pumped through the QCM-D cells via a peristaltic pump (Ismatec, high precision multichannel dispenser) for 30 min to have a stabile baseline. Afterwards, the resonance frequency and dissipation values obtained with CsCl were recorded as baseline and the deposition of polyelectrolytes started by switching to the appropriate solution. The real-time build-up of PEMs started with a polycation for each experiment. The PEMs abbreviated as $(PAH/PSS)_n$, $(PAHCE/PSS)_n$, $(PAH/pectin)_n$, and $(PAH/pectinCE)_n$, where *n* indicates the number of bilayers. Alternating layers of polycation and polyanion were deposited on the gold sensors by alternate pumping of each solution for a minimum of 10 min to build the PEMs. After the build-up, a CsCl solution was pumped to the PEM to remove any weakly attached polyelectrolytes. Then, salt-exchange experiments were performed by using the PEM-coated sensors. Note that the term salt- or ion-exchange,[9,56] or alternatively specific ion effect,[59] is regularly used in studies where coatings are exposed to different salt conditions.

Frequency (Δf) and dissipation shifts (ΔD) were acquired at the 3rd (15 MHz), 5th (25 MHz), 7th (35 MHz), 9th (45 MHz), and 11th (55 MHz) harmonic overtones. The 3rd overtone was chosen for the comparison of various experiments as it is one of the most suitable harmonics to reflect the surface character of the film.[9,33,34] The data was recorded with QSoft (version 2.8.0.913, Analyzer) and analyzed with DFind (version 1.2.7) software. The mass of the assembled PEMs was calculated by using the Sauerbrey equation (Equation 1), and the (wet) PEM thicknesses were calculated based on Sauerbrey modelling in DFind. Equation 1 shows that decrease of frequency is associated with increase in mass, therefore a higher thickness value. As Sauerbrey modelling is for rigid films, the wet thicknesses of the films were also estimated via Voigt modelling in DFind. In Voigt modelling, the density of the default bulk liquid water (20 °C) was chosen as 998 g/L and the densities for the default layer materials were chosen as 1020 g/L (PAH), 1050 g/L (PSS), and 1300 g/L (pectin).

Spectroscopic Ellipsometry Analyses. The optical (dry) thickness of the PEM coatings was measured after freshly-coated sensors were rinsed with Milli-Q water and dried with a gentle flow of nitrogen. The data were obtained by using an Accurion Nanofilm_ep4 imaging

ellipsometer in air at room temperature. The wavelength range of the light was λ = 400.6−761.3 nm at an angle of incidence of 50°. The data were fitted with EP4 software using a multilayer model and a refractive index of 1.397 for gold.

Salt-Exchange Experiments with QCM-D. After the aforementioned PEMs were built, a CsCl solution (0.15 M, pH 5.0) was flushed through the QCM-D cell for at least 30 min to get a stable baseline. Once achieved, various salt solutions (*e.g.* LiCl, NaCl, KCl, RbCl, $MgCl_2$, etc.) were pumped to the QCM-D cells one by one. Each salt solution was pumped through the QCM-D cell for at least 30 min. Finally, the salt solutions were replaced by a CsCl (0.15 M, pH 5.0) solution to reach the baseline.

After the experiments, 50 mL of 1% (v/v) Hellmanex III solution was run through the QCM-D cell at 40 °C. Then, the system was rinsed with at least 50 mL of Milli-Q water, before drying it upon air. All PEM build-up and salt-exchange experiments were repeated at least three times, and the reported values result from averaging the resulting data.

7.3 Results and Discussions

Synthesis and characterization of PAHCE and PectinCE. Crown ether-functionalized PAH derivatives (PAHCE #1, PAHCE #2, and PAHCE #3) were synthesized via a carbodiimide-assisted coupling reaction as shown in **Scheme 7.1A** by using different molar feed ratios of the polymer and CE. The combination of bands in the aromatic and aliphatic region of the ^{1}H-NMR spectrum of PAHCE #2 (**Figure 7.1A**) does not only show that the attachment was successful; it can also be used for a quantitative analysis. In more detail, the bands in the 3.53-0.25 ppm region are attributed to the protons in the PAH backbone (−C<u>H</u>$_2$−C<u>H</u>−) and the methylene protons in the side chain (−C<u>H</u>$_2$−NH$_2$ / C<u>H</u>$_2$−NHR). The chemical shift of these aliphatic signals was confirmed by ^{1}H-NMR and HSQC spectra of the unmodified PAH (**Figures S7.1** and **S7.2**). The signals at 7.69 – 6.69 ppm and 4.50 – 3.56 ppm can be attributed to three protons of the aromatic moiety in the CE and the aliphatic CH_2O signals of the crown ether, respectively. The degree of modification was calculated by comparing

the integration of the aromatic protons of the crown ether and the aliphatic protons of PAH. Based on this calculation, the degree of substitution for PAHCE #2, for which the feed ratio was 20%, was found to be 9±1%, which is comparable to those of other functionalized polyelectrolytes.[9,19] Additionally, also ^{13}C NMR, DOSY, and COSY spectra confirmed the attachment of CE units to the polymer backbone (**Figures S7.8-10**). After the purification step, PAHCE was obtained as a yellow solid with a yield of 91% ± 4. Similarly, the degree of modification for PAHCE #1 and PAHCE #3 was found to be 5% and 14% **(Figures S7.5** and **S7.6**).

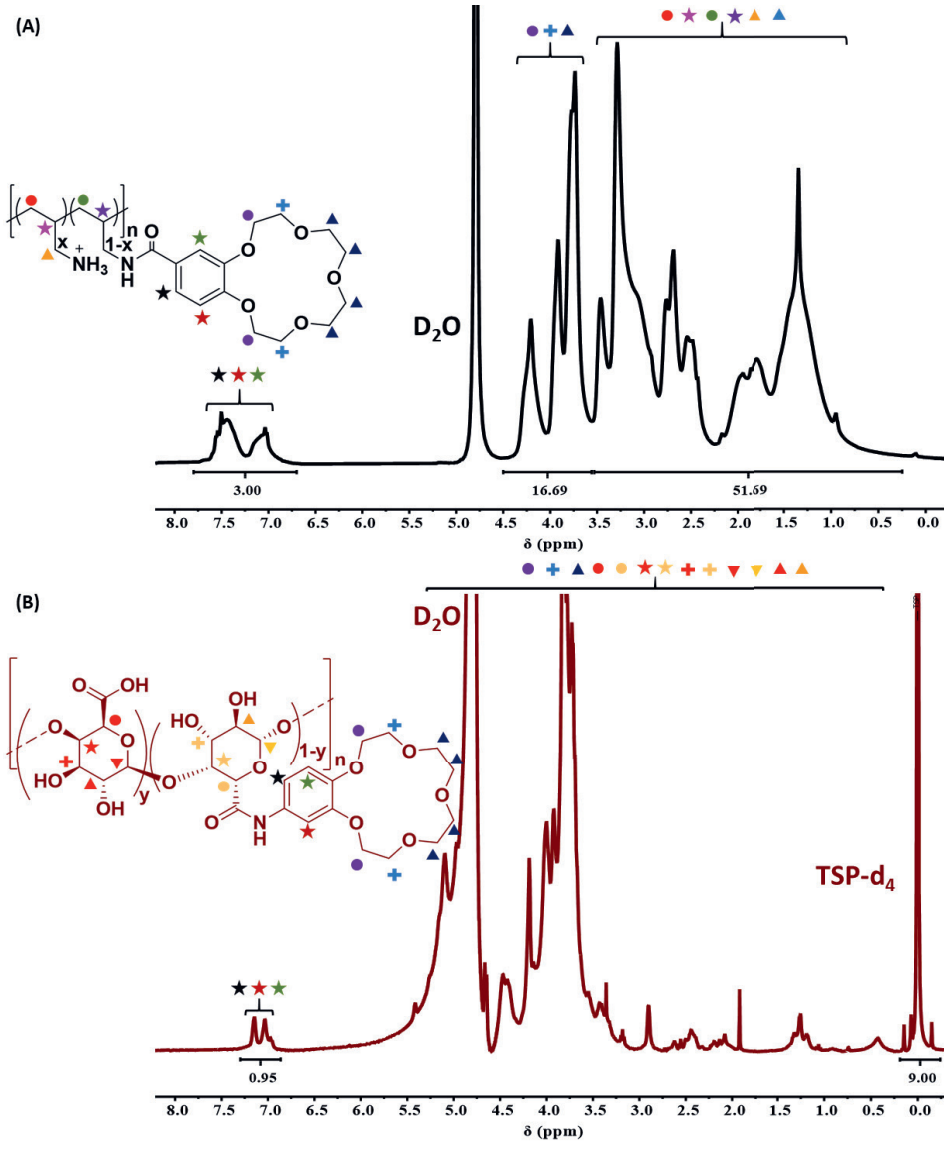

Figure 7.1. ^{1}H-NMR spectra of (A) PAHCE #2 (400 MHz, D_2O) δ 7.69 – 6.69 (m, 3H), 4.50 – 3.56 (m, 17H), 3.53 – 0.25 (m, 52H), and (B) pectinCE with TSP-d_4 as an internal standard.

Pectin was also successfully functionalized with CE as confirmed with ^{1}H-NMR (**Figure 7.1B**). After purification, pectinCE was obtained as white solid with a yield of 75% ± 9. The degree of modification was calculated based on the known concentration of pectinCE and TSP-d_4 dissolved in D_2O and the observed integral values of the aromatic protons and TSP- d_4 signal. This showed that w/w% of CE units in the pectinCE is 2.3 ± 0.3, meaning ≈1.7 mol% CE in pectinCE. Although, the degree of functionalization is relatively lower than the one of PAHCE (9 ± 1%), this can partly be explained by the nature of pectin. It is noted that this percentage is with respect to all monomer units, *i.e.*, those with free carboxylic acid moieties (>74%) and those with the non-reactive methyl esters (<26%). Therefore not all monomers of pectin is available for functionalization, unlike PAH.

All four polymers, *i.e.* PAH, PAHCE, pectin, and pectinCE, were also analyzed by FT-IR (**Figure 7.2**) and here we describe the main differences upon functionalization. In case of PAHCE (**Figure 7.2A**) the characteristic amide C=O stretching peak at 1632 cm^{-1} and in-plane N–H bending peak at 1527 cm^{-1} confirm the presence of the C=O amide bond between PAH and CE moieties.[9] Also, C–H stretching bands of unsaturated (sp^2) carbon bonds (3100-3000 cm^{-1}) correspond the aromatic ring of the crown ether moieties. Lastly, although difficult to assign with certainty as it is in the middle of the fingerprint region, the strong signal at 1127 cm^{-1} can likely be attributed to C-O stretching vibrations, and thus also point to the presence of crown ether moieties.[71]

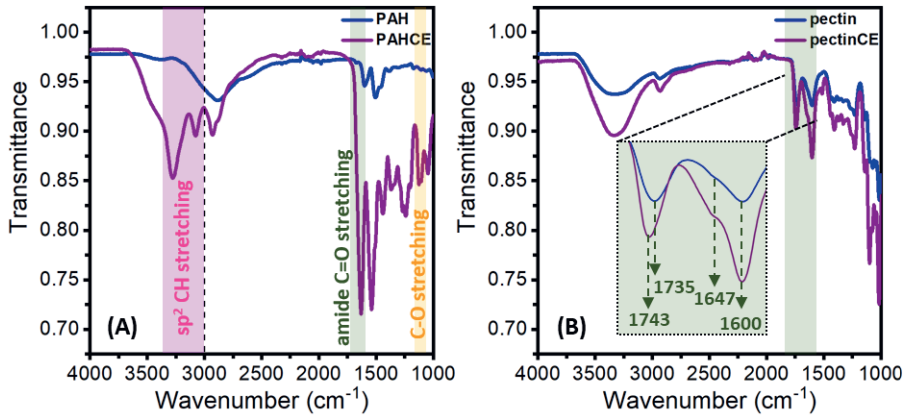

Figure 7.2. FT-IR spectra of (A) PAH (blue) and PAHCE (purple) (B) pectin (blue) and pectinCE (purple). The bands that appear upon the functionalization are designated by the boxes and related text labels.

The differences between the FT-IR spectra of pectin and pectinCE are less prominent. In case of pectin, the signals at 1600 cm^{-1} and 1735 cm^{-1} correspond to the vibrations of the acid and ester carbonyls, respectively.[72] Although in case of pectinCE an additional amide-based carbonyl signal would be expected, it is difficult to observe such a signal due to the overlapping signals in the carbonyl region. Instead, in this region, while the other two carbonyl-related signals in the IR spectra of pectin and pectinCE appear at the same position, one of the bands shifts from 1735 cm^{-1} to 1743 cm^{-1} upon the functionalization, suggesting a change in the structure after additional of CE groups.

To further analyze the structure of pectinCE, X-ray photoelectron spectroscopy was used in addition to ^{1}H-NMR and FTIR. **Figure S7.14** shows the % change in elemental compositions of the pectin- and pectinCE-modified gold surfaces. The increase in the relative amount of N from 0 to nearly 3% upon the functionalization of pectin indicates the presence of crown ether units linked via amide bonds. This percentage actually suggests a higher degree of functionalization compared to the one based on ^{1}H-NMR (≈3 *vs.* ≈1.7%),

but it is noted that the peak integration accuracy is low for small peaks. Qualitatively XPS shows that that the synthesis was successful, just like ^{1}H-NMR.

In conclusion, both PAHCE and pectinCE were synthesized successfully and their structures were characterized with various spectroscopic techniques. After characterization of PAHCE and pectinCE, the build-up of PEMs on gold-coated QCM sensors was studied with QCM-D.

PEM Build-Up of (PAHCE/PSS)$_4$. First, a well-studied PAH/PSS PEM[18,49,73] was chosen to see the effect of CE moieties in the layer build-up. In order to compare the layer properties, an equal number of layers (four bilayers) was coated for all types of PEMs. **Figure 7.3** shows a representative real-time change in frequency and dissipation response for the 3rd, 5th, and 7th harmonics of (PAHCE/PSS)$_4$ and (PAH/PSS)$_4$. CsCl was chosen as the supporting electrolyte for the PE solutions as the relatively large Cs^+ ions have less interaction with CE derivatives compared due to the smaller alkali metal ions.[67,74] Therefore, each build-up (and intermediate washing step) was started by flushing a 0.15 M CsCl solution over a bare QCM sensors until a stable base line was observed. Each time that a polyelectrolyte solution was flushed through the QCM-D cell in an alternating fashion in terms of polycation and polyanion, the frequency decreased with a concomitant increase in the dissipation, resulting in cumulative plots that are typical for the build-up of PEMs.[9,59,75,76] **Table 7.1** provides an overview of the averaged QCM data for the various samples. The overall averaged frequency shift for (PAHCE/PSS)$_4$ was found to be higher than the one of (PAH/PSS)$_4$ (257 ± 10 Hz *vs.* 218 ± 14 Hz), while the average change in the dissipation was comparable (41 ± 4 ppm and 43 ± 5 ppm, respectively). These results indicate the CE units contribute to the adsorbed mass, but that this has no effect on the viscoelastic properties of the PEM.

Next, based on the frequency and dissipation shifts the thickness of the PEMs was calculated by using the Sauerbrey and Voigt models (**Table 7.1**, top entries). For the PAH/PSS system the use of PAHCE results in a larger (wet) thickness. Although the Sauerbrey

model gives an approximate thickness based on frequency change,[77] the Voigt model gives a more realistic thickness value for viscous and hydrated layers.[48,53,55] For such systems, harmonics are well separated from each other and spread as shown in **Figure 7.3**. After the QCM-D experiments, the QCM sensors were rinsed with MQ water and dried with a flow of nitrogen to measure their optical thickness values via ellipsometry. As expected, given their air-dried state, the optical thickness of $(PAHCE/PSS)_4$ and $(PAH/PSS)_4$ PEMs are smaller than the modelled wet thickness values. Although less pronounced, the CE does result in a larger optical thickness. The obtained wet and dry thickness values for $(PAH/PSS)_4$ were found to be in line with values reported in literature.[9,76,78]

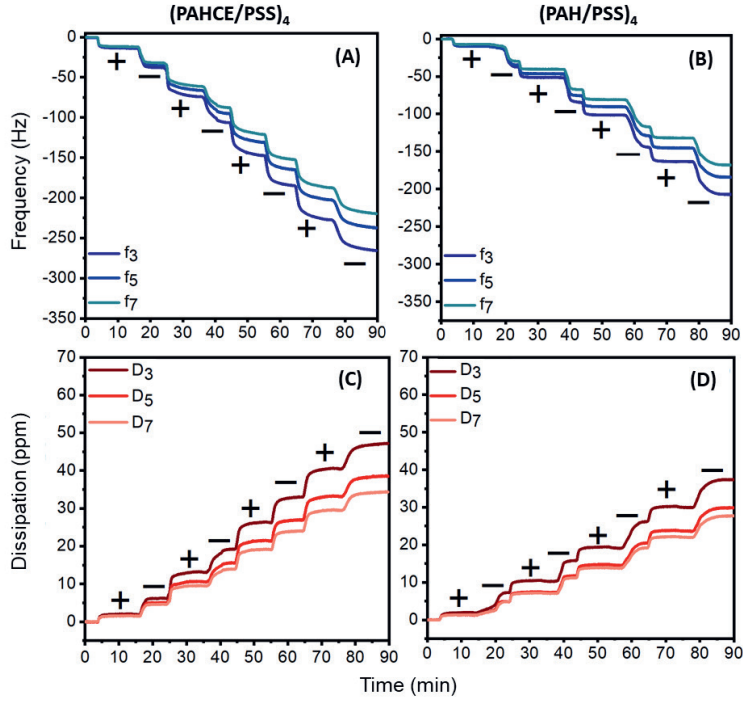

Figure 7.3. Real-time QCM-D data showing representative changes in the frequency (A and B) and dissipation (C and D) for the 3rd, 5th, and 7th overtones of the build-up of $(PAHCE/PSS)_4$ (A and C) and $PAH/PSS)_4$ (B and D) in 0.15 M CsCl. The plus and minus signs represent the polycation and polyanion in the PEMs, respectively.

Table 7.1. The total change in frequency and dissipation for $(PAH(CE)/PSS)_4$, $(PAHCE/PSS)_{3.5}$, and $(PAH/pectin(CE))_4$ multilayers and the modelled (Sauerbrey and Voigt) and the optical thickness values of the PEMs. Each value is the average of three independent experiments.

Type of PEM	Δf_3 (Hz)	ΔD_3 (ppm)	Sauerbrey thickness (nm)	Voigt thickness (nm)	Optical thickness (nm)
$(PAH/PSS)_4$	–218 ± 14	41 ± 4	38 ± 3	57 ± 3	13 ± 1
$(PAHCE/PSS)_4$	–257 ± 10	43 ± 5	45 ± 2	65 ± 5	15 ± 0.3
$(PAHCE/PSS)_{3.5}$	–235 ± 8	37 ± 1	41 ± 1	60 ± 4	15 ± 2
$(PAH/pectin)_4$	–1757 ± 93	303 ± 44	314 ± 17	-*	66 ± 3
$(PAH/pectinCE)_4$	–2497 ± 105	455 ± 56	447 ± 19	-*	115 ± 4

*Data did not fit the Voigt modelling. Please see section 3.3 for further explanation and discussion.

PEM Build-Up of $(PAH/pectin(CE))_4$ with QCM-D. Next, as an alternative to PAH/PSS PEM, which is fully of fossil-based origin, we studied the use of a natural polyanion, pectin. PAH/pectin and PAH/pectinCE PEMs were built on the QCM sensors in a similar fashion as the PAH(CE)/PSS PEMs. **Figure 7.4** shows the real-time change in the frequency and dissipation responses of the 3rd, 5th, and 7th harmonics, confirming the successful the build-up of $(PAH/pectinCE)_4$ and $(PAH/pectin)_4$ PEMs. Compared to PAH(CE)/PSS PEMs, PAH/pectin(CE) PEMs have higher frequency and dissipation shifts. From these data it becomes clear that the differences in frequency and dissipation are mainly originating from the polyanion (pectin or pectinCE) layers, which is in line with the few reported QCM studies using pectin.[79,80]

Using pectin instead of PSS resulted not only in higher overall shifts, but also affected the PEM build-up in at least the following two ways. First, coating steps that involve pectin(CE) show longer stabilization times compared to PSS (30 *vs*. 10 min per layer). Second, while the PAH(CE)/PSS system shows an almost linear frequency change during the PEM build-up, the PAH/pectin(CE) system shows a non-uniform growth pattern, where

changes in *f* and *D* increase during the PEM build-up. In more detail, the overtones overlap more in the beginning of the process and the PEM eventually becomes more viscoelastic. It becomes clear from the growth patterns that pectin-containing PEMs are larger in size and more heterogeneous compared to the ones with PSS (with or without CE units). The heterogeneity (*e.g.* more voids) in the structure of the PAH/pectin(CE) could explain the aforementioned non-linear growth pattern, as in such a system more PAH can move in the PEM and lead to further interpenetration of polyelectrolytes. This would cause a less neatly stacked PEM and therefore would increase the possibility of adsorption of larger amounts of pectin(CE).

Furthermore, the use of pectinCE instead of pectin resulted in a higher total frequency. This trend was also observed for PAH(CE)/PSS PEMs, but for pectin(CE) the increase is more pronounced (≈40 *vs*. ≈18%). Also, the dissipation value increases ≈50% when using pectinCE, while we observed hardly any dissipation effect of CE in the PAH(CE)/PSS system, as CE units possibly cause more voids in the PAH/pectin system.

Based on the above-described QCM-D data the thickness values of the $(PAH/pectin(CE))_4$ were modelled in a similar fashion with the $(PAH(CE)/PSS)_4$ via the Sauerbrey equation (**Table 7.1**, bottom entries). As expected based on its higher frequency shift, $(PAH/pectinCE)_4$ resulted in a thickness that is ≈40% higher than the one of $(PAH/pectin)_4$. Due to limitations of the modelling software (DFind), Voigt thicknesses could not be obtained for PAH/pectin(CE) as the data did not fit the modelling after a certain number of layers (≈6^{th} layer).

Finally, the optical thickness of air-dried PEMs were measured and found to be smaller than the wet thickness values, as expected. $(PAH/pectinCE)_4$ was found to be ≈1.7 times thicker than $(PAH/pectin)_4$. Moreover, when compared to PAH(CE)/PSS PEMs, PAH/pectin(CE) PEMs were found to be thicker (**Table 7.1**, bottom entries). For instance, the Sauerbrey thickness of $(PAH/pectin)_4$ is ≈8 times thicker than $(PAH/PSS)_4$, indicating the effect of different polyanion on PEM thickness. Also, the Sauerbrey thickness of $(PAH/pectinCE)_4$ is ≈10 times thicker than the one of $(PAHCE/PSS)_4$.

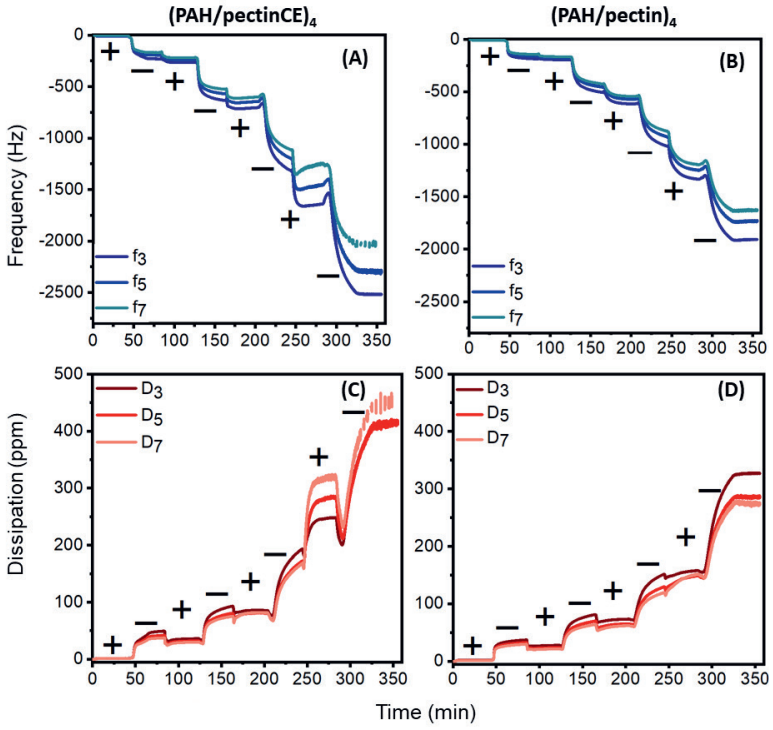

Figure 7.4. Real-time QCD-D data showing representative changes in the frequency (A and B) and dissipation (C and D) for the 3rd, 5th, and 7th overtones of the build-up of $(PAH/pectinCE)_4$ and $PAH/pectin)_4$ in 0.15 M CsCl. The plus and minus signs represent the polycation and polyanion in the PEMs, respectively.

7

Salt-Exchange Experiments with QCM-D. Since PEM properties are determined by the type of counterion and the ion concentration, PEMs are sensitive to post-assembly conditions.[29,48] Therefore, interactions between PEMs and various ions can be studied via salt-exchange experiments. This approach has been pursued for PEMs (without ionophore units) to study the post-assembly changes in PEMs by exposing them to solutions with

different anions.[56,57] When a PEM is rinsed successively with solutions that each contain a different salt, ionic interactions can be understood based on the changes in frequency and dissipation. For this purpose, we performed a series of experiments and tested the effect of various parameters on cationic interactions of CE-containing and PEMs and their non-functionalized equivalents. In order to study whether PEMs with a crown ether show a preference towards a certain type of cation, CsCl was chosen as a supporting electrolyte in during the build-up of all PEM coatings and also as the background electrolyte during all washing and stabilization steps.

Effect of Crown Ether Units in $(PAH/PSS)_4$ PEMs. Figure 7.5 presents the frequency shifts as a function of time recorded for both $(PAH/PSS)_4$ and $(PAHCE/PSS)_4$ before and after exposure to solutions containing 0.15 M of LiCl, NaCl, KCl, or RbCl. When switching from CsCl to another salt solution, a certain amount of Cs^+ can be replaced by the other cation due to the concentration gradient (diffusion), as previously described for various QCM-D experiments where anion-exchange behavior of the PEMs was investigated.[9,29,56] Each salt was studied in a separate experiment and for all experiments the PEMs were rinsed with CsCl solution before and after being exposed to the specified salt (indicated with dashed lines in **Figure 7.5**).

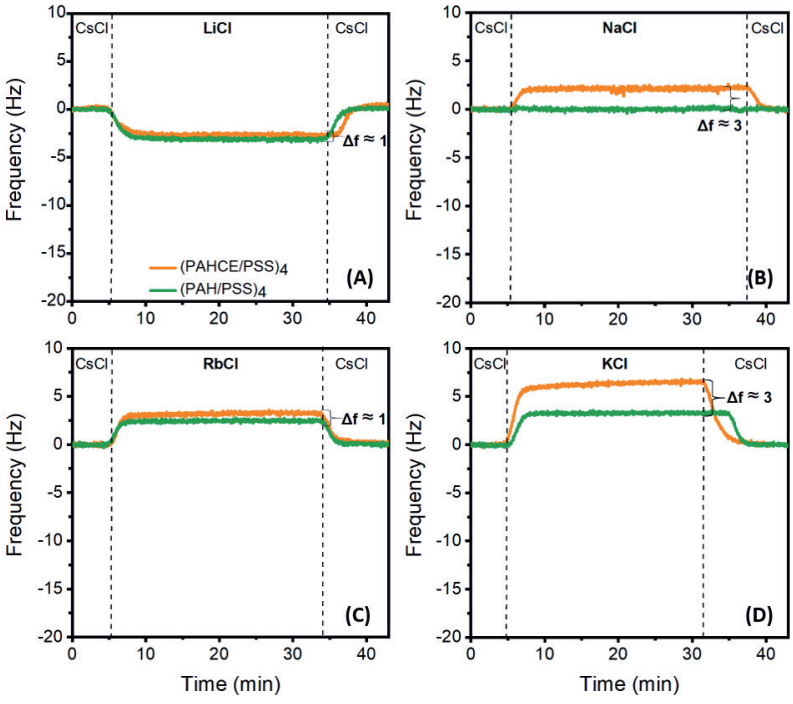

Figure 7.5. Frequency change (3rd harmonic) as a function of time, recorded for the QCM-D sensors coated with $(PAHCE/PSS)_4$ (orange), $(PAH/PSS)_4$ (green) exposed to cycle of changing the 0.15 salt solution: from CsCl to XCl (where X is Li, Na, Rb or Cs), followed by a final rinsing step using CsCl. The dashed lines indicate the moment in time at which the salt solutions were switched.

Before investigating the effect of CE on the PEM-cation interactions, the interactions of $(PAH/PSS)_4$ with different salts were studied (indicated as green lines in **Figure 7.5**). The shifts in frequency and dissipation were observed to be salt-dependent. A change in frequency can be explained by a combined effect of the *i)* difference in amount and weight of any cation exchange, and *ii)* difference in the amount of water that is associated to the PEM and/or counterion present in the PEM. Upon changing from Cs^+ to

Li^+ the frequency decreased (**Figure 7.5A**), indicated an increase in adsorbed mass. Considering the much smaller atomic mass of Li compared to Cs (6.94 amu *vs*. 132.91 amu), this difference can be attributed to the higher degree of hydration of Li^+ (3.82 Å *vs*. 3.29 Å for Li^+ and Cs^+, respectively)[81] and/or the uptake of more Li^+. On the other hand, when switching from Cs^+ to K^+ or Rb^+ (**Figures 7.5C** and **7.5D**) an increase in frequency is observed, suggesting a decrease in mass. Considering that the hydrated sizes of Rb^+ and Cs^+ are comparable (~3.29 Å)[81] and the difference in atomic mass (132.91 amu *vs*. 85.47 amu for Cs and Rb, respectively), the difference in *f* can be rationalized by the difference in atomic mass of the cation itself. Similarly, K^+ has a smaller atomic mass (39.10 amu) than Cs^+ , but their hydrated sizes are comparable (3.31 Å *vs*. 3.29 Å, for K^+ and Cs^+, respectively),[81] indicating that the increase in frequency (*i.e.* lower mass) can be explained by the smaller atomic mass of K^+ compared to Cs^+. Lastly, when switching to Na^+ (3.58 Å,[81] 22.99 amu) the difference in atomic weight and hydrated size of Na^+ and Cs^+ balance each other and no significant change in frequency was observed. Trend-wise our observations are in line with studies where anion-exchange properties of PEMs were studied.[27,32,59] In these studies, increased changes in frequency were observed when PEMs were exposed to solutions with anions with higher atomic mass and/or hydrated size.

Next we discuss the changes in QCM-D data for the $(PAHCE/PSS)_4$ system. The orange-colored graphs in **Figure 7.5** represent the frequency changes for $(PAHCE/PSS)_4$ for different salt solutions. While the changes in frequency for Li^+ and Rb^+ are within ≈1 Hz, the difference for K^+ and Na^+ due to the presence of CE units is larger (3 Hz). Qualitatively, these results are in line with literature reporting on the use of 15-crown-5 in membrane-based electrodialysis[4] and nanofiltration[10] processes. Furthermore, the selectivity of CE units for both Na^+ and K^+ has also been studied theoretically.[82]

After comparing $(PAHCE/PSS)_4$ with $(PAH/PSS)_4$ for monovalent cations, 0.15 M CsCl solution was replaced with 0.15 M $MgCl_2$ solution to study the effect of a divalent cation. **Figure 7.6** shows a change in frequency of ≈15 Hz when changing the salt solutions from CsCl to $MgCl_2$ to CsCl, indicating an increased mass. As the atomic mass of Mg is smaller than the one of Cs (24.31 amu *vs*. 132.91 amu), the difference originated from differences

in the amount of hydration. The hydrated size of Mg^{2+} is larger than the one of Cs (4.28 Å *vs*. 3.29 Å).[81] A comparable effect was also observed in literature where a monovalent anion, Cl^-, was replaced by divalent anions, SO_4^{2-} and HPO_4^{2-}.[58] As the difference between the two PEM systems for Mg^{2+} was found to be ≈1 Hz, similar to the results of Li^+ and Rb^+, the QCM data indicates that the presence of CE units does not affect the affinity to Mg^{2+}. It is noted that the overall frequency change, *i.e.*, after switching back to CsCl, is about -2 Hz, but at the same time the frequency signal seemed to have drifted with a comparable value during the exposure of the PEM to $MgCl_2$.

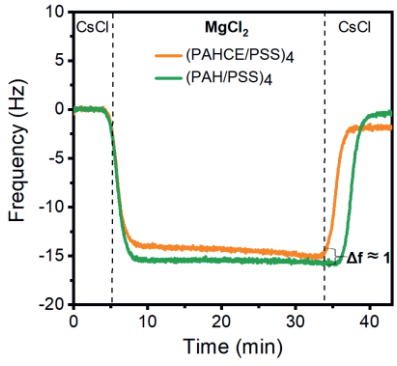

Figure 7.6. Frequency change (3rd harmonic) as a function of time, recorded for the QCM-D sensors coated with $(PAHCE/PSS)_4$ (orange), $(PAH/PSS)_4$ (green) exposed to cycle of changing the 0.15 salt solution: from CsCl to $MgCl_2$, followed by a final rinsing step using CsCl. The dashed lines indicate the moment in time at which the salt solutions were switched.

All frequency and dissipation data for the aforementioned experiments were combined in **Figures S7.15** and **S7.16** in SI. The dissipation data supports the trends observed in frequency trends. In other words, when there is decrease in frequency, an increase in dissipation is observed. Also, cations with a relatively larger hydrated size cause a larger increase in dissipation.

Effect of Type of Terminating Layer. In addition to the effect of CE units, we studied the effect of the type of terminating layer on the salt-exchange behavior of the PEMs. For this purpose, $(PAHCE/PSS)_{3.5}$ was coated on gold QCM sensors. **Figure S7.17** demonstrates the change in frequency and dissipation shifts for the build-up of $(PAHCE/PSS)_{3.5}$ where the outermost layer is PAHCE. The trends in frequency and dissipation are in line with our observations for $(PAHCE/PSS)_4$, just like those of the modelled data and optical thickness (**Table 7.1**).

After the $(PAHCE/PSS)_{3.5}$ PEM was built-up in a 0.15 M CsCl solution, salt-exchange experiments with LiCl, NaCl, and KCl were conducted. **Figure 7.7** shows the change in frequency in time for $(PAHCE/PSS)_{3.5}$ before and after exposure to different salt solutions. Unlike the trends observed for PAHCE-terminated PEM, obtaining a stable signal takes longer or it is not obtained at all. Also, the overall changes are clearly smaller than the ones for PSS-terminated PEM (**Table S7.1**, SI), further confirming that the PSS-terminated PEM provides a better stability and increased salt-exchange. These differences can be explained by the rejection between the positively-charged terminating layer and the cations, a phenomenon that also has been described in, *e.g.*, PEM-assisted electrodialysis processes.[15,83]

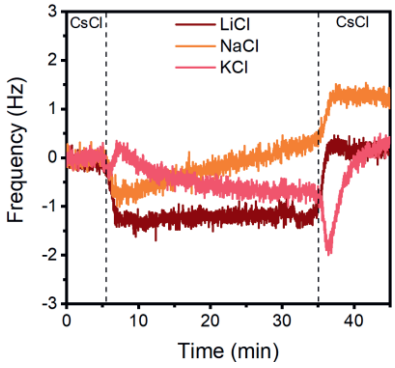

Figure 7.7. Frequency change (3rd harmonic) as a function of time, recorded for the QCM-D sensors coated with $(PAHCE/PSS)_4$ (orange), $(PAH/PSS)_4$ (green) exposed to cycle of changing the 0.15 M salt solution: from CsCl to XCl (where X is Li, Na, or K), followed by a final rinsing step using CsCl. The dashed lines indicate the moment in time at which the salt solutions were switched.

Effect of PEM Structure on Salt-Exchange. Next, the salt-exchange experiments were performed for the two different PEM structures. For this purpose, $(PAH/pectin)_4$ and $(PAH/pectinCE)_4$ were exposed to LiCl, NaCl, and KCl solutions and the resulting QCM transients are shown in **Figure 7.8**. The green lines represent $(PAH/pectin)_4$ and when the CsCl solution is replaced by solutions containing other salts, the frequency values increase, *i.e.* 12.8 ± 1.8, 10.5 ± 1.0, and 14.0 ± 1.6 Hz for Li^+, Na^+, and K^+, respectively. The absolute values of these changes are larger than those of the $(PAH/PSS)_4$ (-0.3 ± 0.7 -0.4 ± 0.7, and 3.3 ± 0.5 Hz for Li^+, Na^+, and K^+, respectively), due to the bigger size of the $(PAH/pectin)_4$ multilayer. It should be realized that they are roughly the same for all three cations (12 ± 3 Hz).

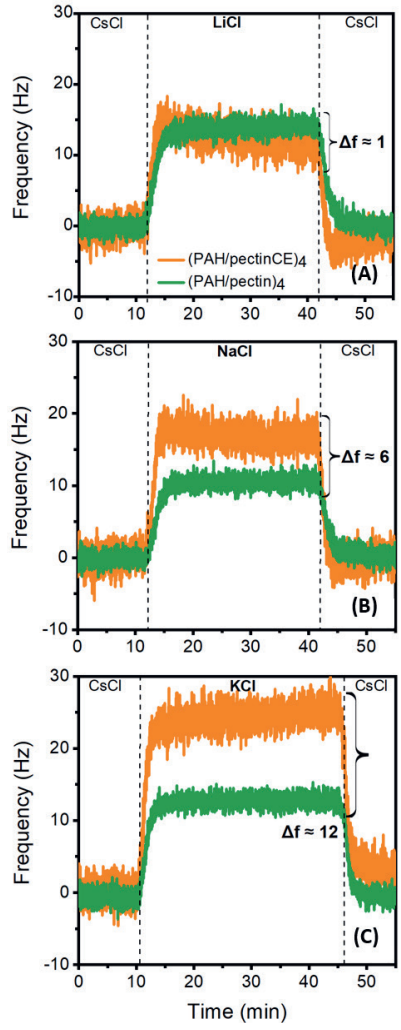

Figure 7.8. Frequency change (3rd harmonic) as a function of time, recorded for the QCM-D sensors coated with (PAH/pectinCE)$_4$ (orange), (PAH/pectin)$_4$ (green) exposed to cycle of changing the 0.15 salt solution: from CsCl to XCl (where X is Li, Na, or K), followed by a final rinsing step using CsCl. The dashed lines indicate the moment in time at which the salt solutions were switched.

When CE units are introduced to (PAH/pectin)$_4$, the difference in frequency shifts was found to be ≈1 Hz for after switching to a LiCl solution, a result that is similar to what was observed for the (PAH(CE)/PSS)$_4$ PEMs. Just like in the case of (PAHCE/PSS)$_4$, both Na^+ and K^+ result in a larger frequency, 6 and 12 Hz, respectively), which can again be related to the preferred interaction with the CE. These values are a factor of 2 to 4 higher than the ones observed for (PAHCE/PSS)$_4$, *i.e.*, 3 Hz for both Na^+ and K^+. This may be related to the position of the CE units as for the (PAH/pectinCE)$_4$ system these are attached to the terminating layers, making them in direct contact with the solution. Additionally, the larger heterogeneity of the layers in PAH/pectinCE, and therefore the increase in pectinCE adsorption, can contribute to a higher number of CE units in the PEM, resulting in higher frequency values during the salt-exchange experiments.

7.4. Conclusions

The cation exchange behavior of PEMs can be modified via covalently attached crown ethers. This works both for the fossil-based PAH/PSS and for the more bio-based PAH/pectin PEM systems. The differences, as observed in detail by QCM-D, point to a significant effect of the inner PEM structure and which layer 'lies on top' in the PEM, and vary substantially for different monovalent metal cations and between mono- and divalent metal cations. Considering the large amount of possible combinations of bio-based and/or synthetic polyelectrolytes with various ionophores, tailor-made, stable, ion-selective PEM coatings can likely be made for different desalination and medical applications, where ion selectivity is the crucial part of the separation or detection process. Such work is currently ongoing in our laboratories.

References

(1) Zhang, Z.; Dou, Q.; Gao, H.; Bai, B.; Zhang, Y.; Hu, D.; Yetisen, A. K.; Butt, H.; Yang, X.; Li, C.; et al. 30 s Response Time of K^+ Ion-Selective Hydrogels Functionalized with 18-Crown-6 Ether Based on QCM Sensor. *Adv. Healthc. Mater.* **2018**, *7* (5) 1700873. https://doi.org/10.1002/adhm.201700873.

(2) Cao, Z.; Guo, J.; Fan, X.; Xu, J.; Fan, Z.; Du, B. Detection of Heavy Metal Ions in Aqueous Solution by P(MBTVBC-Co-VIM)- Coated QCM Sensor. *Sensors Actuators, B Chem.* **2011**, *157* (1), 34–41. https://doi.org/10.1016/j.snb.2011.03.023.

(3) Sahin, S.; Dykstra, J. E.; Zuilhof, H.; Zornitta, R. L.; de Smet, L. C. P. M. Modification of Cation-Exchange Membranes with Polyelectrolyte Multilayers to Tune Ion Selectivity in Capacitive Deionization. *ACS Appl. Mater. Interfaces* **2020**, *12* (31), 34746–34754. https://doi.org/10.1021/acsami.0c05664.

(4) Qian, Z.; Miedema, H.; Sahin, S.; de Smet, L. C. P. M.; Sudhölter, E. J. R. Separation of Alkali Metal Cations by a Supported Liquid Membrane (SLM) Operating under Electro Dialysis (ED) Conditions. *Desalination* **2020**, *495*, 114631. https://doi.org/10.1016/j.desal.2020.114631.

(5) Singh, K.; Sahin, S.; Gamaethiralalage, J. G.; Zornitta, R. L.; de Smet, L. C. P. M. Simultaneous, Monovalent Ion Selectivity with Polyelectrolyte Multilayers and Intercalation Electrodes in Capacitive Deionization. *Chem. Eng. J.* **2021**, 128329. https://doi.org/10.1016/j.cej.2020.128329.

(6) Paltrinieri, L.; Wang, M.; Sachdeva, S.; Besseling, N. A. M.; Sudhölter, E. J. R.; de Smet, L. C. P. M. Fe_3O_4 Nanoparticles Coated with a Guanidinium-Functionalized Polyelectrolyte Extend the pH Range for Phosphate Binding. *J. Mater. Chem. A* **2017**, *5*, 18476–18485. https://doi.org/10.1039/c7ta04054g.

(7) Birukov, A.; Rakova, N.; Lerchl, K.; Olde Engberink, R. H. G.; Johannes, B.; Wabel, P.; Moissl, U.; Rauh, M.; Luft, F. C.; Titze, J. Ultra-Long-Term Human Salt Balance Studies Reveal Interrelations between Sodium, Potassium, and Chloride Intake and Excretion. *Am. J. Clin. Nutr.* **2016**, *104* (1), 49–57. https://doi.org/10.3945/ajcn.116.132951.

(8) Paltrinieri, L.; Remmen, K.; Müller, B.; Chu, L.; Köser, J.; Wintgens, T.; Wessling, M.; de Smet, L. C. P. M.; Sudhölter, E. J. R. Improved Phosphoric Acid Recovery from Sewage Sludge Ash Using Layer-by-Layer Modified Membranes. *J. Memb. Sci.* **2019**, *587*, 117162. https://doi.org/10.1016/j.memsci.2019.06.002.

(9) Cao, Z.; Gordiichuk, P. I.; Loos, K.; Sudhölter, E. J. R.; De Smet, L. C. P. M. The Effect of Guanidinium Functionalization on the Structural Properties and Anion Affinity of Polyelectrolyte Multilayers. *Soft Matter* **2016**, *12* (5), 1496–1505. https://doi.org/10.1039/c5sm01655j.

(10) Kazemabad, M.; Verliefde, A.; Cornelissen, E. R.; D'Haese, A. Crown Ether Containing Polyelectrolyte Multilayer Membranes for Lithium Recovery. *J. Memb. Sci.* **2020**, *595*, 117432. https://doi.org/10.1016/j.memsci.2019.117432.

(11) Gamaethiralalage, J. G.; Singh, K.; Sahin, S.; Yoon, J.; Elimelech, M.; Suss, M. E.; Liang, P.; Biesheuvel, P. M.; Zornitta, R. L.; de Smet, L. C. P. M. Recent Advances in Ion Selectivity with Capacitive Deionization. *Energy Environ. Sci.* **2020**, *14*, 1095–1120. https://doi.org/10.1039/d0ee03145c.

(12) Jose, A.; Ray, J. G. Toxic Heavy Metals in Human Blood in Relation to Certain Food and Environmental Samples in Kerala, South India. *Environ. Sci. Pollut. Res.* **2018**, *25* (8), 7946–7953. https://doi.org/10.1007/s11356-017-1112-x.

(13) White, N.; Misovich, M.; Yaroshchuk, A.; Bruening, M. L. Coating of Nafion Membranes with Polyelectrolyte Multilayers to Achieve High Monovalent/Divalent Cation Electrodialysis Selectivities. *ACS Appl. Mater. Interfaces* **2015**, *7*, 6620−6628. https://doi.org/10.1021/am508945p.

(14) Ahmad, M.; Tang, C.; Yang, L.; Yaroshchuk, A.; Bruening, M. L. Layer-by-Layer Modification of Aliphatic Polyamide Anion-Exchange Membranes to Increase Cl^-/SO_4^{2-} Selectivity. *J. Memb. Sci.* **2019**, *578*, 209–219. https://doi.org/10.1016/j.memsci.2019.02.018.

(15) Mulyati, S.; Takagi, R.; Fujii, A.; Ohmukai, Y.; Matsuyama, H. Simultaneous Improvement of the Monovalent Anion Selectivity and Antifouling Properties of an Anion Exchange Membrane in an Electrodialysis Process, Using Polyelectrolyte Multilayer Deposition. *J. Memb. Sci.* **2013**, *431*, 113–120. https://doi.org/10.1016/j.memsci.2012.12.022.

(16) Richardson, J. J.; Björnmalm, M.; Caruso, F. Technology-Driven Layer-by-Layer Assembly of Nanofilms. *Science* **2015**, *348* (6233). https://doi.org/10.1126/science.aaa2491.

(17) Richardson, J. J.; Cui, J.; Björnmalm, M.; Braunger, J. A.; Ejima, H.; Caruso, F. Innovation in Layer-by-Layer Assembly. *Chem. Rev.* **2016**, *116* (23), 14828–14867. https://doi.org/10.1021/acs.chemrev.6b00627.

(18) Caruso, F.; Niikura, K.; Furlong, D. N.; Okahata, Y. 1. Ultrathin Multilayer Polyelectrolyte Films on Gold: Construction and Thickness Determination. *Langmuir* **1997**, *13* (13), 3422–3426. https://doi.org/10.1021/la960821a.

(19) Movilli, J.; Huskens, J. Functionalized Polyelectrolytes for Bioengineered Interfaces and Biosensing Applications. *Org. Mater.* **2020**, *02* (02), 078–107. https://doi.org/10.1055/s-0040-1708494.

(20) Zahn, R.; Voros, J.; Zambelli, T. Tuning the Electrochemical Swelling of Polyelectrolyte Multilayers toward Nanoactuation. *Langmuir* **2014**, *30*, 12057–12066. https://doi.org/10.1021/la503051n.

(21) Joseph, N.; Ahmadiannamini, P.; Hoogenboom, R.; Vankelecom, I. F. J. Layer-by-Layer Preparation of Polyelectrolyte Multilayer Membranes for Separation. *Polym. Chem.* **2014**, *5* (6), 1817–1831. https://doi.org/10.1039/c3py01262j.

(22) Li, X.; Liu, C.; Van Der Bruggen, B. Polyelectrolytes Self-Assembly: Versatile Membrane Fabrication Strategy. *J. Mater. Chem. A* **2020**, *8* (40), 20870–20896. https://doi.org/10.1039/d0ta07154d.

(23) Bütergerds, D.; Kateloe, C.; Cramer, C.; Schönhoff, M. Influence of the Degree of Ionization on the Growth Mechanism of Poly(Diallyldimethylammonium)/Poly(Acrylic Acid) Multilayers. *J. Polym. Sci. Part B Polym. Phys.* **2017**, *55* (5), 425–434. https://doi.org/10.1002/polb.24283.

(24) Riegler, H.; Essler, F. Polyelectrolytes. 2: Intrinsic or Extrinsic Charge Compensation? Quantitative Charge Analysis of PAH/PSS Multilayers. *Langmuir* **2002**, *18* (17), 6694–6698. https://doi.org/10.1021/la020108n.

(25) Fares, H. M.; Schlenoff, J. B. Equilibrium Overcompensation in Polyelectrolyte Complexes. *Macromolecules* **2017**, *50* (10), 3968–3978. https://doi.org/10.1021/acs.macromol.7b00665.

(26) Tang, K.; Besseling, N. A. M. Formation of Polyelectrolyte Multilayers: Ionic Strengths and Growth Regimes. *Soft Matter* **2016**, *12* (4), 1032–1040. https://doi.org/10.1039/c5sm02118a.

(27) Dubas, S. T.; Schlenoff, J. B. Factors Controlling the Growth of Polyelectrolyte Multilayers. *Macromolecules* **1999**, *32* (24), 8153–8160. https://doi.org/10.1021/ma981927a.

(28) Lösche, M.; Schmitt, J.; Decher, G.; Bouwman, W. G.; Kjaer, K. Detailed Structure of Molecularly Thin Polyelectrolyte Multilayer Films on Solid Substrates as Revealed by Neutron Reflectometry. *Macromolecules* **1998**, *31* (25), 8893–8906. https://doi.org/10.1021/ma980910p.

(29) Salomäki, M.; Laiho, T.; Kankare, J. Counteranion-Controlled Properties of Polyelectrolyte Multilayers. *Macromolecules* **2004**, *37* (25), 9585–9590. https://doi.org/10.1021/ma048701u.

(30) Salomäki, M.; Kankare, J. Specific Anion Effect in Swelling of Polyelectrolyte Multilayers. *Macromolecules* **2008**, *41* (12), 4423–4428. https://doi.org/10.1021/ma800315j.

(31) El Haitami, A. E.; Martel, D.; Ball, V.; Nguyen, H. C.; Gonthier, E.; Labbe, P.; Voegel, J. C.; Schaaf, P.; Senger, B.; Boulmedais, F. Effect of the Supporting Electrolyte Anion on the Thickness of PSS/PAH Multilayer Films and on Their Permeability to an Electroactive Probe. *Langmuir* **2009**, *25* (4), 2282–2289. https://doi.org/10.1021/la803534y.

(32) Salomäki, M.; Tervasmäki, P.; Areva, S.; Kankare, J. The Hofmeister Anion Effect and the Growth of Polyelectrolyte Multilayers. *Langmuir* **2004**, *20* (9), 3679–3683. https://doi.org/10.1021/la036328y.

(33) Schönhoff, M.; Bieker, P. Linear and Exponential Growth Regimes of Multilayers of Weak Polyelectrolytes in Dependence on PH. *Macromolecules* **2010**, *43* (11), 5052–5059. https://doi.org/10.1021/ma1007489.

(34) Vidyasagar. A.; Sung, C.; Losensky, K, Lutkenshaus, J. L. pH-Dependent Thermal Transitions in Hydrated Layer-by-Layer Assemblies Containing Weak Polyelectrolytes. *Macromol. Res.* **2012**, *45*, 9169–9176. https://doi.org/10.1021/ma3020454.

(35) Ahmad, M.; Yaroshchuk, A.; Bruening, M. L. Moderate pH Changes Alter the Fluxes, Selectivities and Limiting Currents in Ion Transport through Polyelectrolyte Multilayers Deposited on Membranes. *J. Memb. Sci.* **2020**, *616*, 118570. https://doi.org/10.1016/j.memsci.2020.118570.

(36) Yoo, D.; Shiratori, S. S.; Rubner, M. F. Controlling Bilayer Composition and Surface Wettability of Sequentially Adsorbed Multilayers of Weak Polyelectrolytes. *Macromolecules* **1998**, *31* (13), 4309–4318. https://doi.org/10.1021/ma9800360.

(37) Rijnaarts, T.; Reurink, D. M.; Radmanesh, F.; de Vos, W. M.; Nijmeijer, K. Layer-by-Layer Coatings on Ion Exchange Membranes: Effect of Multilayer Charge and Hydration on Monovalent Ion Selectivities. *J. Memb. Sci.* **2019**, *570–571*, 513–521. https://doi.org/10.1016/j.memsci.2018.10.074.

(38) Toutianoush, A.; Schnepf, J.; Hashani, A. El; Tieke, B. Selective Ion Transport and Complexation in Layer-by-Layer Assemblies of p-Sulfonato-Calix[n] Arenes and Cationic Polyelectrolytes. *Adv. Funct. Mater.* **2005**, *15* (4), 700–708. https://doi.org/10.1002/adfm.200400223.

(39) Gu, H.; Dai, R.; Wei, Y.; Ji, H. F. Functional Layer-by-Layer Multilayer Films for Ion Recognition. *Anal. Methods* **2013**, *5* (14), 3454–3457. https://doi.org/10.1039/c3ay40372f.

(40) Stekolshchikova, A. A.; Radaev, A. V.; Orlova, O. Y.; Nikolaev, K. G.; Skorb, E. V. Thin and Flexible Ion Sensors Based on Polyelectrolyte Multilayers Assembled onto the Carbon Adhesive Tape. *ACS Omega* **2019**, *4*, 15421–15427. https://doi.org/10.1021/acsomega.9b01464.

(41) Petrov, K. V; Paltrinieri, L.; Poltorak, L.; de Smet, L. C. P. M.; Sudhölter, E. J. R. Modified Cation-Exchange Membrane for Phosphate Recovery in an Electrochemically Assisted Adsorption – Desorption Process. *Chem. Commun.,* **2020**, 56, 5046-5049. https://doi.org/10.1039/C9CC09563B.

(42) Awual, M. R.; Yaita, T.; Taguchi, T.; Shiwaku, H.; Suzuki, S.; Okamoto, Y. Selective Cesium Removal from Radioactive Liquid Waste by Crown Ether Immobilized New Class Conjugate Adsorbent. *J. Hazard. Mater.* **2014**, *278*, 227–235. https://doi.org/10.1016/j.jhazmat.2014.06.011.

(43) Guo, J.; Lee, J.; Contescu, C. I.; Gallego, N. C.; Pantelides, S. T.; Pennycook, S. J.; Moyer, B. A.; Chisholm, M. F. Crown Ethers in Graphene. *Nat. Commun.* **2014**, *5*, 1–6. https://doi.org/10.1038/ncomms6389.

(44) Özbek, O.; Isildak, Ö.; Gürdere, M. B.; Cetin, A. The Use of Crown Ethers as Sensor Material in Potentiometry Technique. *Org. Commun.* **2021**, No. 3, 228–239. https://doi.org/10.25135/acg.oc.110.2106.2114.

(45) Klitzing, R.; Tieke, B. Polyelectrolyte Membranes. *Adv. Polym. Sci.* **2004**, No. 165, 177–210. https://doi.org/10.1007/b11270.

(46) Krasemann, L.; Tieke, B. Selective Ion Transport across Self-Assembled Alternating Multilayers of Cationic and Anionic Polyelectrolytes. *Langmuir* **2000**, *16*, 287–290. https://doi.org/10.1021/la991240z.

(47) Huang, T.; Alyami, M.; Kashab, N. M.; Nunes, S. P. Engineering Membranes with Macrocycles for Precise Molecular Separations. *J. Mater. Chem. A* **2021**, *9* (34), 18102–18128. https://doi.org/10.1039/d1ta02982g.

(48) O'Neal, J. T., Dai, E. Y.; Zhang, Y., Clark, K. B.; Wilcox, K. G.; George, I. M.; Ramasamy, N. E.; Enriquez, D.; Batys, P.; Sammalkorpi, M. QCM-D Investigation of Swelling Behavior of Layer-by-Layer Thin Films upon Exposure to Monovalent Ions. *Langmuir* **2018**, *34*, 999–1009. https://doi.org/10.1021/acs.langmuir.7b02836.

(49) Feldötö, Z.; Varga, I.; Blomberg, E. Influence of Salt and Rinsing Protocol on the Structure of PAH/PSS Polyelectrolyte Multilayers. *Langmuir* **2010**, *26* (22), 17048–17057. https://doi.org/10.1021/la102351f.

(50) Wei, J.; Hoagland, D. A.; Zhang, G.; Su, Z. Effect of Divalent Counterions on Polyelectrolyte Multilayer Properties. *Macromolecules* **2016**, *49* (5), 1790–1797. https://doi.org/10.1021/acs.macromol.5b02151.

(51) Cao, Z.; Zhang, Y.; Luo, Z.; Li, W.; Fu, T.; Qiu, W.; Lai, Z.; Cheng, J.; Yang, H.; Ma, W.; et al. Construction of a Self-Assembled Polyelectrolyte/Graphene Oxide Multilayer Film and Its Interaction with Metal Ions. **2021**. https://doi.org/10.1021/acs.langmuir.1c02058.

(52) Qiao, X.; Zhang, X.; Tian, Y.; Meng, Y. Progresses on the Theory and Application of Quartz Crystal Microbalance. *Appl. Phys. Rev.* **2016**, *3* (3). https://doi.org/10.1063/1.4963312.

(53) Dixon, M. C. Quartz Crystal Microbalance with Dissipation Monitoring: Enabling Real-Time Characterization of Biological Materials and Their Interactions. *J. Biomol. Tech.* **2008**, *19* (3), 151–158.

(54) Sauerbrey, G. Verwendung von Schwingquarzen Zur Wägung Dünner Schichten Und Zur Mikrowägung. *Zeitschrift für Phys.* **1959**, *155* (2), 206–222. https://doi.org/10.1007/BF01337937.

(55) Parveen, N.; Jana, P. K.; Schönhoff, M. Viscoelastic Properties of Polyelectrolyte Multilayers Swollen with Ionic Liquid Solutions. *Polymers* **2019**, *11* (8). https://doi.org/10.3390/polym11081285.

(56) Zahn, R.; Boulmedais, F.; Vörös, J.; Schaaf, P.; Zambelli, T. Ion and Solvent Exchange Processes in PGA/PAH Polyelectrolyte Multilayers Containing Ferrocyanide. *J. Phys. Chem. B* **2010**, *114* (11), 3759–3768. https://doi.org/10.1021/jp9106074.

(57) Wang, L.; Lin, Y.; Su, Z. Counterion Exchange at the Surface of Polyelectrolyte Multilayer Film for Wettability Modulation. *Soft Matter* **2009**, *5* (10), 2072–2078. https://doi.org/10.1039/b900638a.

(58) Dressick, W. J.; Wahl, K. J.; Bassim, N. D.; Stroud, R. M.; Petrovykh, D. Y. Divalent-Anion Salt Effects in Polyelectrolyte Multilayer Depositions. *Langmuir* **2012**, *28* (45), 15831–15843. https://doi.org/10.1021/la3033176.

(59) Liu, G.; Hou, Y.; Xiao, X.; Zhang, G. Specific Anion Effects on the Growth of a Polyelectrolyte Multilayer in Single and Mixed Electrolyte Solutions Investigated with Quartz Crystal Microbalance. *J. Phys. Chem. B* **2010**, *114* (31), 9987–9993. https://doi.org/10.1021/jp1018263.

(60) Chopin, N.; Guillory, X.; Weiss, P.; Bideau, J.; Colliec-Jouault, S. Design Polysaccharides of Marine Origin: Chemical Modifications to Reach Advanced Versatile Compounds. *Curr. Org. Chem.* **2014**, *18* (7), 867–895. https://doi.org/10.2174/1385272818071405151523334.

(61) Ding, S.; Zhang, X.; Feng, X.; Wang, Y.; Ma, S.; Peng, Q.; Zhang, W. Synthesis of N,N'-Diallyl Dibenzo 18-Crown-6 Crown Ether Crosslinked Chitosan and Their Adsorption Properties for Metal Ions. *React. Funct. Polym.* **2006**, *66* (3), 357–363. https://doi.org/10.1016/j.reactfunctpolym.2005.08.008.

(62) Radwan, A. A.; Alanazi, F. K.; Alsarra, I. A. Microwave Irradiation-Assisted Synthesis of a Novel Crown Ether Crosslinked Chitosan as a Chelating Agent for Heavy Metal Ions (M^{+n}). *Molecules* **2010**, *15* (9), 6257–6268. https://doi.org/10.3390/molecules15096257.

(63) Zhang, X.; Ding, S.; Wang, Y.; Feng, X.; Peng, Q.; Ma, S. Synthesis and Adsorption Properties of Metal Ions of Novel Azacrown Ether Crosslinked Chitosan. **2006**, 2–6. https://doi.org/10.1002/app.22941.

(64) Peng, C.; Wang, Y.; Tang, Y. Synthesis of Crosslinked Chitosan-Crown Ethers and Evaluation of These Products as Adsorbents for Metal Ions. **1998**, 70 501–506. https://doi.org/10.1002/(SICI)1097-4628(19981017)70:3<501::AID-APP11>3.0.CO;2-3.

(65) Tang, X.; Tan, S.; Wang, Y. Study of the Synthesis of Chitosan Derivatives Containing Benzo-21-Crown-7 and Their Adsorption Properties for Metal Ions. **2002**, 1886–1891. https://doi.org/10.1002/app.2316.

(66) Wan, L.; Wang, Y.; Qian, S. Study on the Adsorption Properties of Novel Crown Ether Crosslinked Chitosan for Metal Ions. **2002**, No. September 2000, 29–34. https://doi.org/10.1002/app.10180.

(67) Pedersen, C. J. Salts, Cyclic Polyethers and Their Complexes with Metal Salts. *J. Am. Chem. Soc.* **1967**, 157, 7017–7036. https://doi.org/10.1021/ja00986a052.

(68) Helgeson, R. C.; Koga, K., Timko, J. M.; Cram, D. J. Structural Requirements for Cyclic Ethers to Complex and Lipophilize Metal Cations or A-Amino Acids. *J. Am. Chem. Soc.* **1973**, *95* (9), 3023–3025.

(69) Izatt, R. M.; Bradshaw, J. S.; Nielsen, S. A.; Lamb, J. D.; Christensen, J. J.; Sen, D. Thermodynamic and Kinetic Data for Cation-Macrocycle Interaction. *Chem. Rev.* **1985**, *85* (4), 271–339. https://doi.org/10.1021/cr00068a003.

(70) Lin, S. Y.; Liu, S. W.; Lin, C. M.; Chen, C. H. Recognition of Potassium Ion in Water by 15-Crown-5 Functionalized Gold Nanoparticles. *Anal. Chem.* **2002**, *74* (2), 330–335. https://doi.org/10.1021/ac0156316.

(71) Zhai, H.; Qu, R.; Li, X.; Liu, Y.; Wei, Y.; Feng, L. Crown Ether Modified Membranes for Na^+-Responsive Controllable Emulsion Separation Suitable for Hypersaline Environments. *J. Mater. Chem. A* **2020**, *8* (5), 2684–2690. https://doi.org/10.1039/c9ta12418g.

(72) Moffat, J.; Noel, T. R.; Parker, R.; Wellner, N.; Ring, S. G. The Environmental Response and Stability of Pectin and Poly-l-Lysine Multilayers. *Carbohydr. Polym.* **2007**, *70* (4), 422–429. https://doi.org/10.1016/j.carbpol.2007.05.001.

(73) Ball, V.; Voegel, J. C.; Schaaf, P. Effect of Thiocyanate Counterion Condensation on Poly(Allylamine Hydrochloride) Chains on the Buildup and Permeability of Polystyrenesulfonate/ Polyallylamine Polyelectrolyte Multilayers. *Langmuir* **2005**, *21* (9), 4129–4137. https://doi.org/10.1021/la047610n.

(74) Gokel, G. W.; Leevy, W. M.; Weber, M. E. Crown Ethers: Sensors for Ions and Molecular Scaffolds for Materials and Biological Models. *Chem. Rev.* **2004**, *104*, 2723–2750. https://doi.org/10.1021/cr020080k.

(75) Notley, S. M.; Eriksson, M.; Wågberg, L. Visco-Elastic and Adhesive Properties of Adsorbed Polyelectrolyte Multilayers Determined in Situ with QCM-D and AFM Measurements. *J. Colloid Interface Sci.* **2005**, *292* (1), 29–37. https://doi.org/10.1016/j.jcis.2005.05.057.

(76) Iturri Ramos, J. J.; Stahl, S.; Richter, R. P.; Moya, S. E. Water Content and Buildup of Poly(Diallyldimethylammonium Chloride)/Poly(Sodium 4-Styrenesulfonate) and Poly(Allylamine Hydrochloride)/Poly(Sodium 4-Styrenesulfonate) Polyelectrolyte Multilayers Studied by an in Situ Combination of a Quartz Crystal Microb. *Macromolecules* **2010**, *43* (21), 9063–9070. https://doi.org/10.1021/ma1015984.

(77) Reviakine, I.; Johannsmann, D.; Richter, R. P. Hearing What You Cannot See and Visualizing What You Hear: Interpreting Quartz Crystal Microbalance Data from Solvated Interfaces. *Anal. Chem.* **2011**, *83* (23), 8838–8848. https://doi.org/10.1021/ac201778h.

(78) Kittle, J.; Levin, J.; Levin, N. Water Content of Polyelectrolyte Multilayer Films Measured by Quartz Crystal Microbalance and Deuterium Oxide Exchange. *Sensors* **2021**, *21* (3), 1–12. https://doi.org/10.3390/s21030771.

(79) Pastorino, L.; Erokhina, S.; Ruggiero, C.; Erokhin, V.; Petrini, P. Fabrication and Characterization of Chitosan and Pectin Nanostructured Multilayers. *Macromol. Chem. Phys.* **2015**, *216* (10), 1067–1075. https://doi.org/10.1002/macp.201400576.

(80) Lin, D.; Lopez-Sanchez, P.; Selway, N.; Gidley, M. J. Viscoelastic Properties of Pectin/Cellulose Composites Studied by QCM-D and Oscillatory Shear Rheology. *Food Hydrocoll.* **2018**, *79*, 13–19. https://doi.org/10.1016/j.foodhyd.2017.12.019.

(81) Nightingale, E. R. Phenomenological Theory of Ion Solvation. Effective Radii of Hydrated Ions. *J. Phys. Chem.* **1959**, *63* (9), 1381–1387. https://doi.org/10.1021/j150579a011.

(82) Hill, S. E.; Feller, D. Theoretical Study of Cation/Ether Complexes: 15-Crown-5 and Its Alkali Metal Complexes. *Int. J. Mass Spectrom.* **2000**, *201* (1–3), 41–58. https://doi.org/10.1016/S1387-3806(00)00214-1.

(83) Cheng, W.; Liu, C.; Tong, T.; Epsztein, R.; Sun, M.; Verduzco, R.; Ma, J.; Elimelech, M. Selective Removal of Divalent Cations by Polyelectrolyte Multilayer Nanofiltration Membrane: Role of Polyelectrolyte Charge, Ion Size, and Ionic Strength. *J. Memb. Sci.* **2018**, *559*, 98–106. https://doi.org/10.1016/j.memsci.2018.04.052.

Supplementary Information to:

Crown Ether-Modified Polyelectrolytes and their Interactions with Cations – a QCM Study

Additional NMR Spectra of Reactants and CE-Containing Polyelectrolytes.

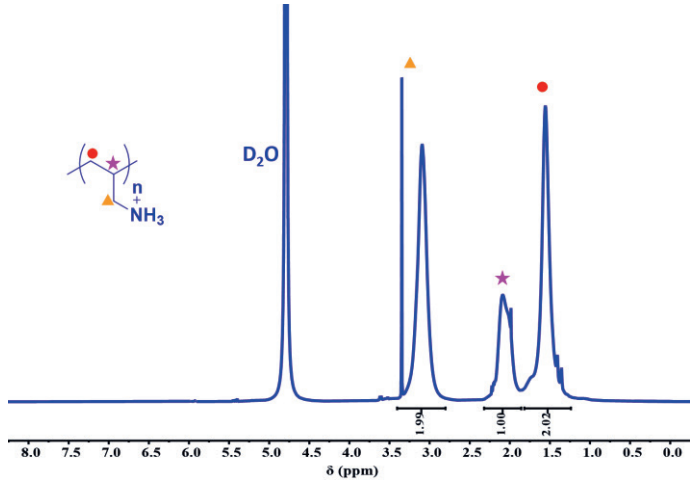

Figure S7.1. ^{1}H NMR of PAH (400 MHz, D_2O) δ 3.22 (d, J = 102.1 Hz, 2H), 2.04 (d, J = 40.2 Hz, 1H), 1.56 (s, 2H).

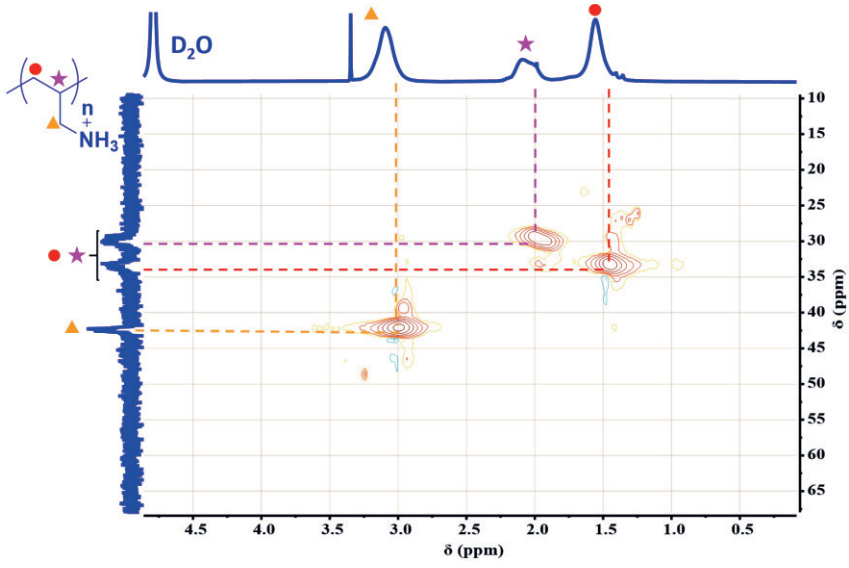

Figure S7.2. Heteronuclear single quantum coherence (HSQC) spectrum of PAH in D_2O.

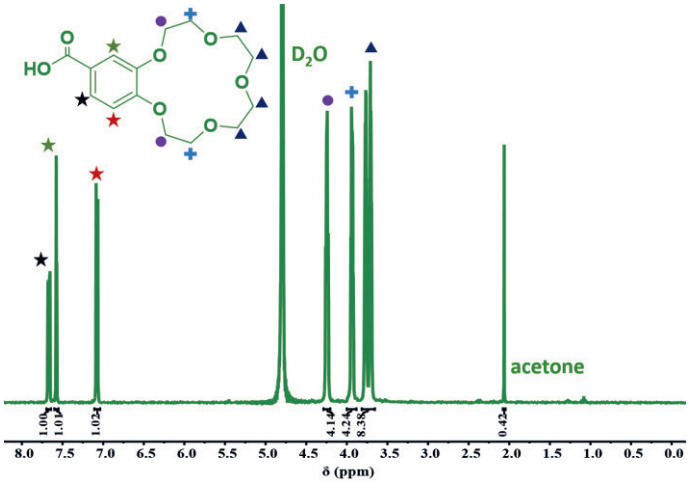

Figure S7.3. ^{1}H NMR of carboxy-crown ether (400 MHz, D_2O) δ 7.67 (dd, J = 8.4, 2.0 Hz, 1H), 7.57 (d, J = 2.0 Hz, 1H), 7.08 (d, J = 8.5 Hz, 1H), 4.24 (td, J = 5.1, 2.1 Hz, 4H), 3.93 (dt, J = 7.1, 2.6 Hz, 4H), 3.82 – 3.65 (m, 8H).

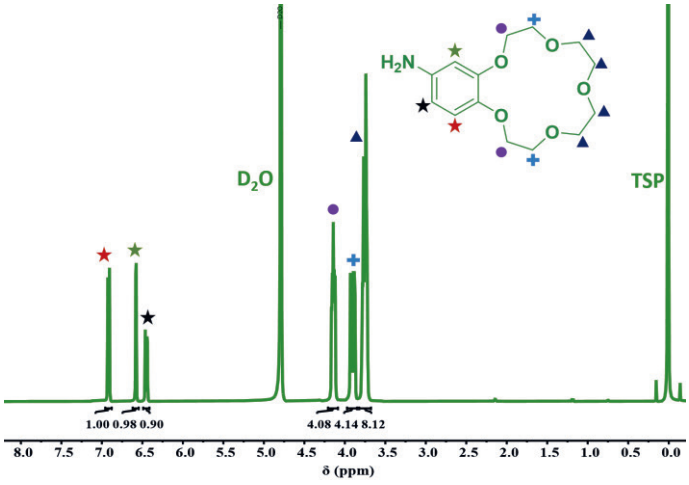

Figure S7.4. ^{1}H NMR of amino-crown ether (400 MHz, D_2O) δ 6.92 (d, J = 8.5 Hz, 1H), 6.58 (d, J = 2.5 Hz, 1H), 6.45 (dd, J = 8.5, 2.5 Hz, 1H), 4.21 – 4.08 (m, 4H), 3.97 – 3.85 (m, 4H), 3.82 – 3.68 (m, 8H) with trimethylsilylpropanoic acid (TSP-d_4) as an internal standard.

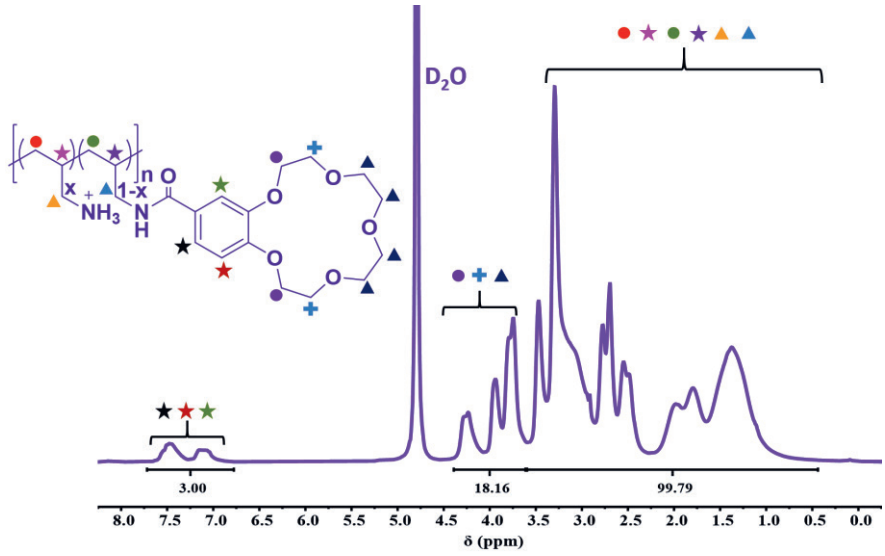

Figure S7.5. ^{1}H NMR of PAHCE #1 (400 MHz, D_2O) δ 7.71-6.77 (m, 3H), 4.39 – 3.61 (m, 18H), 3.59 – 0.44 (m, 100H).

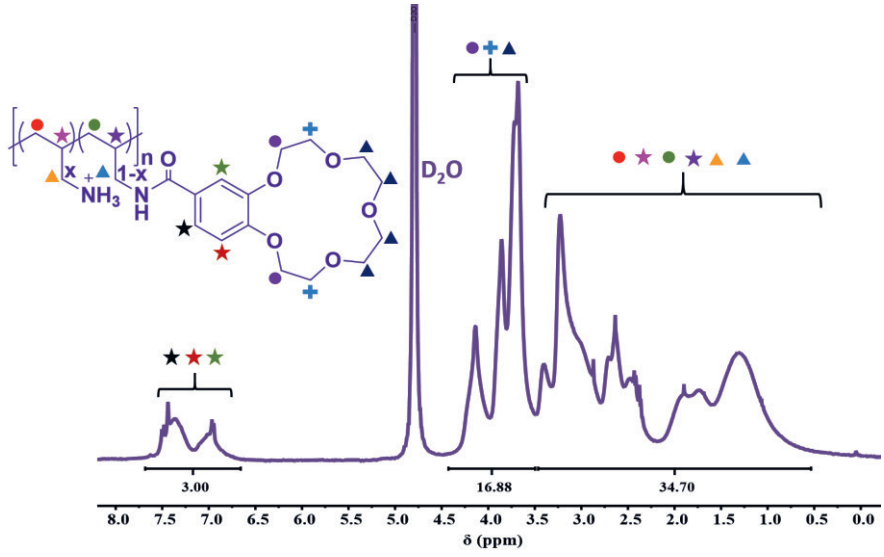

Figure S7.6. ^{1}H NMR of PAHCE # 3 (400 MHz, D_2O) δ 7.69-6.64 (m, 3H), 4.43 – 3.50 (m, 17H), 3.46 – 0.53 (m, 35H).

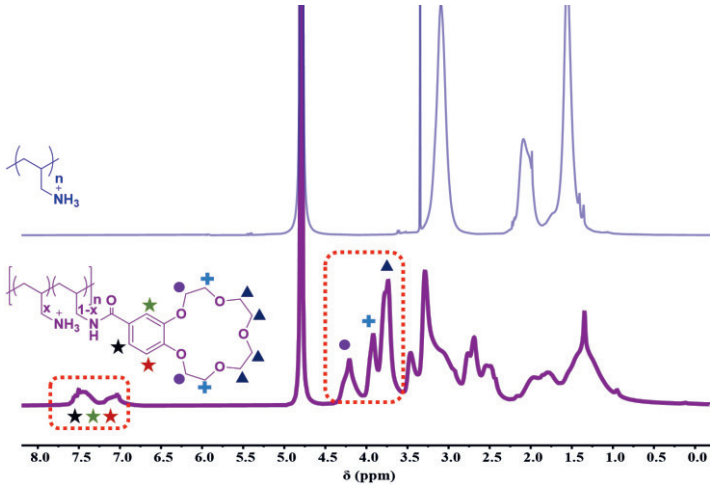

Figure S7.7. Comparison of the ^{1}H NMR spectra of PAH and PAHCE # 2 in D_2O. The area circled with red line indicates the additional signals of the crown ether units in ^{1}H NMR spectrum of PAHCE # 2.

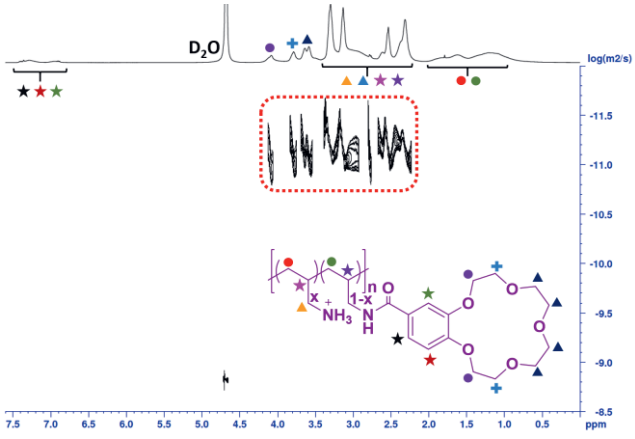

Figure S7.8. Diffusion-ordered (DOSY) spectrum of PAHCE # 2 in D_2O. The area circled with red line indicates that the signals from both crown ether and the PAH backbone have comparable values that indicate that the CE units are covalently attached to the polymer backbone.

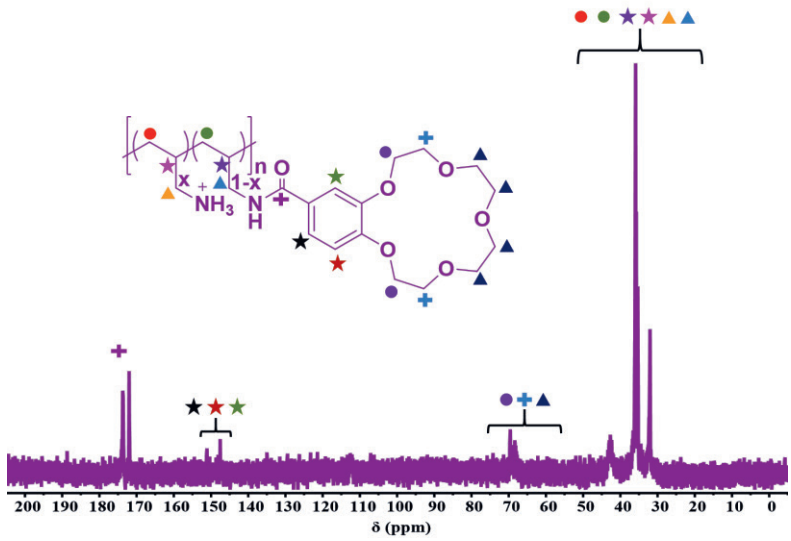

Figure S7.9. ^{13}C NMR spectrum of PAHCE # 2 (101 MHz, D_2O) δ 173.70, 172.01, 147.54, 69.60, 42.73, 35.91, 35.75, 32.04.

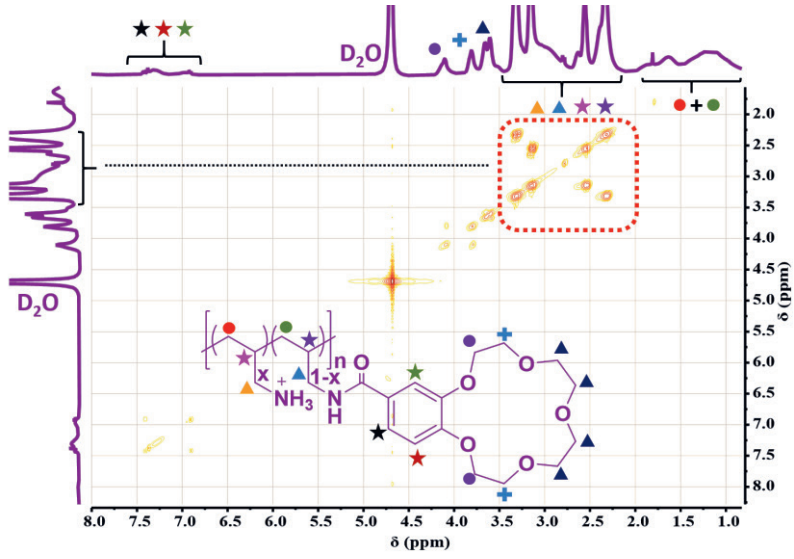

Figure S7.10. Correlated (COSY) spectrum of PAHCE # 2 in D_2O.

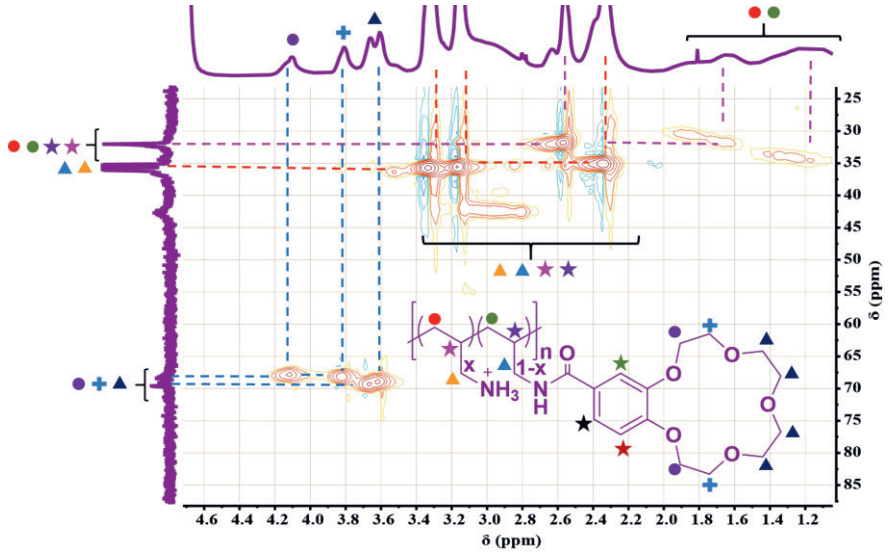

Figure S11. Heteronuclear single quantum coherence (HSQC) spectrum of PAHCE # 2 in D_2O.

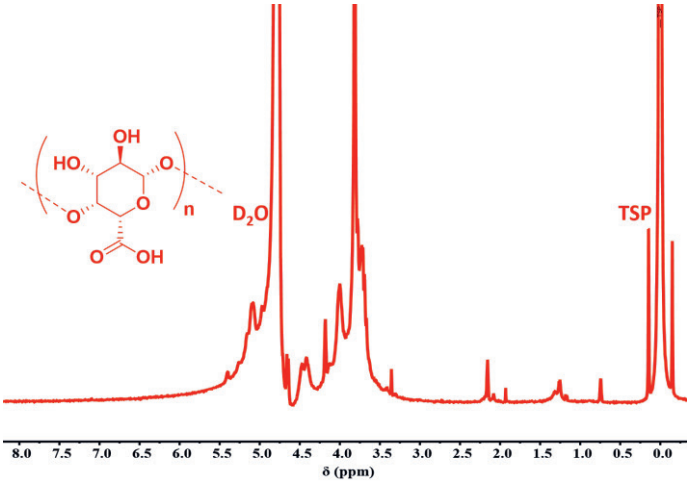

Figure S7.12. ^1H NMR (400 MHz, D_2O) spectrum of pectin with trimethylsilylpropanoic acid (TSP-d_4) as an internal standard.

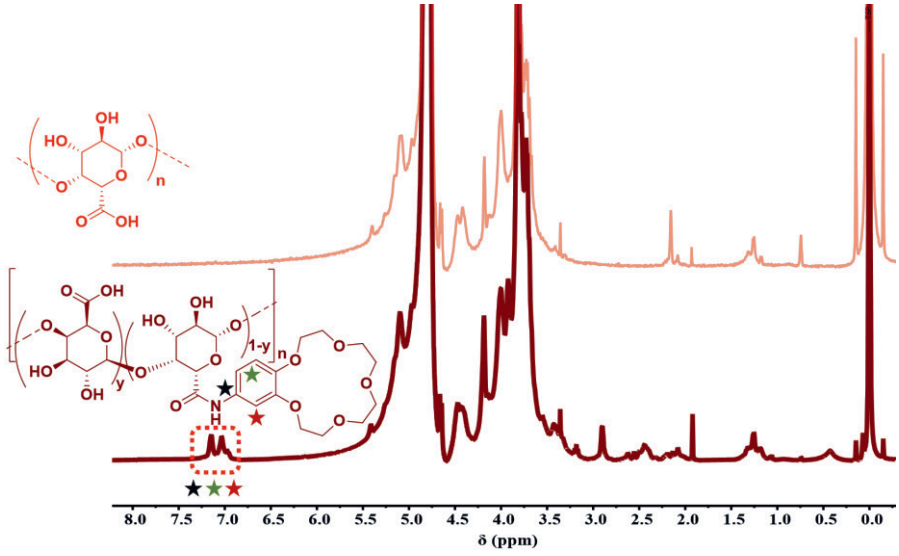

Figure S7.13. Comparison of the ^{1}H NMR spectra of pectin and pectinCE in D_2O. The area circled with red line indicates the aromatic signals of the benzo-crown ether units.

XPS Characterization of PectinCE-coated Gold Substrates. Prior to coating the gold substrates with pectinCE, the bare substrates were sonicated for 5 min in Milli-Q water, and dried in a stream of nitrogen. Sonication was repeated with acetone, and ethanol, then the gold substrates were cleaned from organic material by 5 min of air-based plasma by a plasma cleaner (Diener electronic GmbH, Germany).

After the cleaning procedure, a pectinCE solution was prepared as described in Materials and Methods section and the gold substrates were dip coated in the pectinCE solution for 20 min. Afterwards, the coated surfaces were rinsed with MQ water and dried in a stream of nitrogen.

The wide-scan XPS spectra of pectin and pectinCE coated gold substrates were obtained by a JPS-9200 photoelectron spectrometer (JEOL, Japan) with a monochromatic Al Kα source at 12 kV and 20 mA. Under ultrahigh vacuum conditions, a total of 20 scans was made for each measurement. Shirley background fitting was performed to correct the spectra and they were processed with CASA XPS software (version 2.3.16).

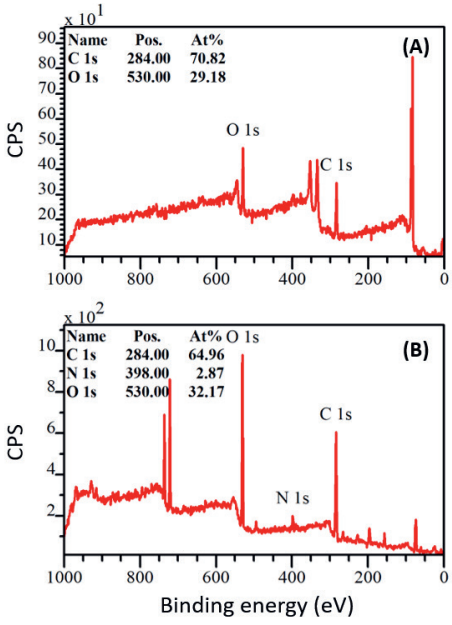

Figure S7.14. Wide-scan XPS spectra of the (A) bare and (B) pectinCE-coated gold substrates.

Additional Data for PEM Build-up and Salt Exchange Experiments with QCM-D

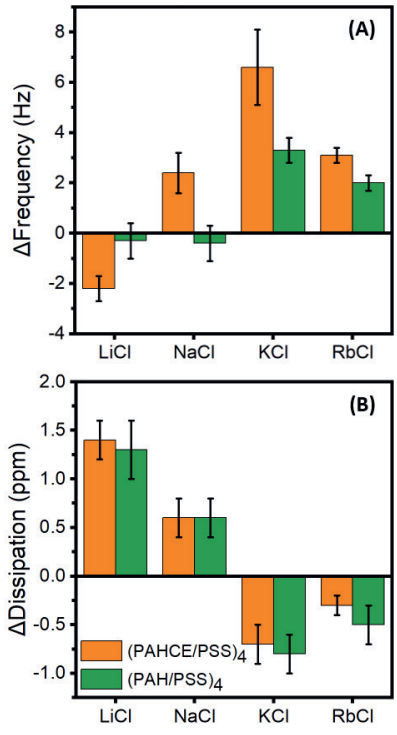

Figure S7.15. Comparison of the frequency (A) and dissipation (B) shifts at the third harmonic for $(PAHCE/PSS)_4$ (orange) and $(PAH/PSS)_4$ (green)-coated sensors after exposed to different solutions containing 0.15 M of LiCl, NaCl, KCl, and RbCl. Data is obtained from min. three experiments.

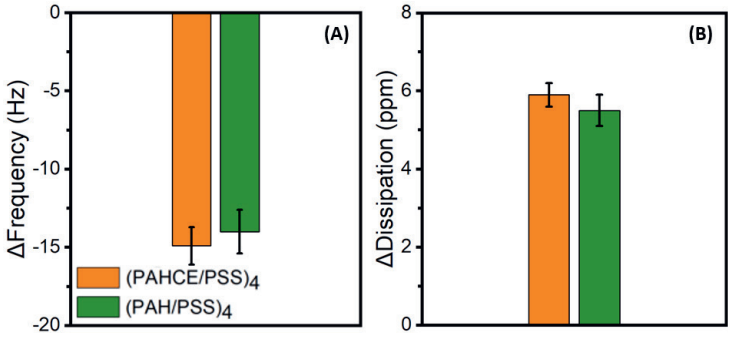

Figure S7.16. Comparison of the frequency (A) and dissipation (B) shifts at the third harmonic for $(PAHCE/PSS)_4$ (orange) and $(PAH/PSS)_4$ (green)-coated sensors after exposed to 0.15 M of $MgCl_2$ solution. Data is obtained from min. three experiments.

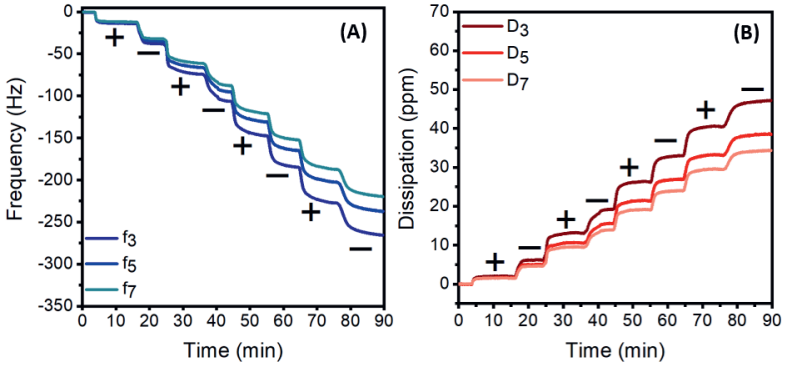

Figure S7.17. Real-time change in the (A) frequency and (B) dissipation shifts for the build-up of $(PAHCE/PSS)_{3.5}$ in 0.15 M CsCl.

Table S7.1. Overview of the frequency and dissipation shifts during the salt exchange experiments with $(PAHCE/PSS)_{3.5}$.

	LiCl	NaCl	KCl
Δf_3 (Hz)	–1.6 ± 0.3	0.3 ± 0.1	-0.5 ± 0.1
ΔD_3 (ppm)	0.5 ± 0.1	0 ± 0.03	-0.6 ± 0.02

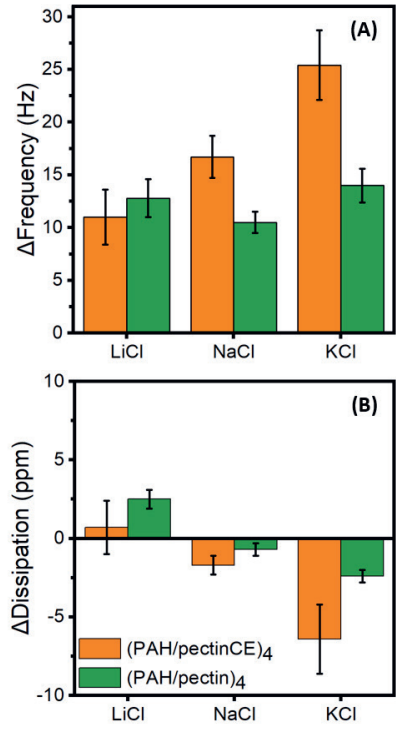

Figure S7.18. The comparison of the frequency (A) and dissipation (B) shifts at the third harmonic for $(PAH/pectinCE)_4$ (orange) and $(PAH/pectin)_4$ (green)-coated sensors after exposed to different solutions containing 0.15 M of LiCl, NaCl, KCl, and RbCl.

Table S7.2. Overview of the change in frequency and dissipation during the salt exchange experiments for $(PAH/pectinCE)_4$ and $(PAH/pectin)_4$.

	LiCl	**NaCl**	**KCl**
Δf_3: $(PAH/pectinCE)_4$ (Hz)	11.0 ± 2.6	16.7 ± 2.0	25.4 ± 3.3
Δf_3: $(PAH/pectin)_4$ (Hz)	12.8 ± 1.8	10.5 ± 1.0	14.0 ± 1.6
ΔD_3: $(PAH/pectinCE)_4$ (ppm)	0.7 ± 1.7	-1.7 ± 0.6	-6.4 ± 2.2
ΔD_3: $(PAH/pectin)_4$ (ppm)	2.5 ± 0.6	-0.7 ± 0.4	-2.4 ± 0.4

Chapter 8

General Discussion and Outlook

“The truth is out there.”

(X Files)

8.1 General Discussion

The main goal of the work described in this thesis was to investigate the use of polyelectrolyte multilayer (PEM) coatings for tuning ion selectivity of capacitive deionization (CDI). Although CDI is an established and well-known technique for desalination brackish water, it is not designed to differentiate among the ions with the same type of charge. Therefore, in order to introduce and also tune ion selectivity in CDI, implementation of an ion-selective layer (*e.g.* ion-selective membranes), tuning pore size of the electrode material, and/or optimizing the operational parameters (*e.g.* current density, applied voltage, pH, and feed concentration) of the process are required. In the strive towards ion-selective CDI operations for resource recovery, heavy metal removal, water softening, and other separation processes, various attempts have been carried out, as outlined in **Chapter 1** and **Chapter 2**. Based on the ever-growing amount of literature on ion-selective CDI, it is evident that implementing an ion-selective layer that can allow the ion(s) of interest to pass through, concurrently rejecting other ions present in the solution is one of most efficient approaches to tune ion selectivity in CDI. However, this layer should be easy to implement, stable, and environment-friendly. Layer-by-layer (LbL)-coated PEMs can meet these criteria, making them suitable candidates for such ion-selective layers. Also, due to the wide variety in polyelectrolyte structures, tunability of the physical and chemical characteristics of PEMs, and their possible combinations with ionophores, (functional) PEM coatings are highly versatile and they can expand the window of control of ion-selective properties (**Chapter 3**).

In this thesis, we first showed the proof-of-concept of a PEM-coated cation-exchange membrane (PEM-CMX) as a new approach to improve mono-/divalent cation selectivity in a CDI operation (**Chapter 4**). The key finding of this study was that by implementing a thin PEM on a cation-exchange membrane (CEM), it is possible to switch a Mg^{2+}-selective membrane into a Na^{+}-selective membrane. The Na^{+}/Mg^{2+} selectivity values ($\beta_{Mg^{2+}}^{Na^{+}}$) of the PEM-CMX and CMX membranes were found as 2.8 ± 0.2 and 0.5 ± 0.04, respectively. Besides, a detailed analysis of CDI metrics (salt adsorption capacity, charge

efficiency, specific energy consumption, Coulombic efficiency, and desalination capacity) of the experiments with PEM-CMX as well as the long-term stability test (>40 cycles) of the PEM-CMX further indicated the feasibility of this approach.

After demonstrating the tunability of mono-/divalent cation selectivity of CDI *via* a PEM-CMX in CDI, a similar method was employed to achieve monovalent anion selectivity (**Chapter 5**). In this case, a standard-grade anion-exchange membrane (AEM) was coated with a PEM that resulted in an increase in mono-/divalent anion selectivity. In more detail, while the $\beta_{SO_4^{2-}}^{Cl^-}$ of a bare AEM was found to be ≈ 0.5, it reached values up to 14 upon adding a PEM coating. Another highlight of this work is the combination of a PEM-coated AEM with nickel hexacyanoferrate (NiHCF) electrodes to achieve a tandem monovalent cation and anion selectivities. NiHCF acts as an intercalation electrode that shows an inherent size-based selectivity towards monovalent cations. In our experiments, the values of $\beta_{Mg^{2+}}^{Na^+}$ was found to be as high as ≈ 17. It can be concluded that this combination enables a tandem separation for both monovalent cations and anions. Additionally, the selectivity values were preserved at relatively lower concentrations of monovalent ions as well, indicating that this approach is feasible for a wide range of concentrations.

Although, the obtained selectivity values in **Chapter 4** and **Chapter 5** are on par with the current (M)CDI literature, we have investigated the parameters that affect the ion selectivity to further maximize the selectivity coefficient. In **Chapter 6**, the effect of operational parameters of CDI (*e.g.* mode of operation, voltage, concentration and composition of the feed solution) as well as the number of PE layers within PEM on the overall monovalent cation selectivity were investigated. After the optimization of the number of polyelectrolyte bilayers (5.5) on the CMX membrane and the current density (10 A/m^2), a time-independent and virtually 100 % monovalent cation selectivity was achieved. Before this optimization, a time-dependent selectivity, which a maximum of $\beta_{Mg^{2+}}^{Na^+}$ ≈ 3 was obtained.

Overall, PEM functions as a filter to reject some (types of) ions based on charge- and size-exclusion principles. In order to obtain the highest possible selectivity, there are a

number of parameters that should be considered while designing a (PEM-based) CDI experiment.

8.1.1 Number of PE Layers within PEM

The number of PE layers in a PEM has a significant effect on mono-/divalent ion selectivity, as charge-exclusion towards divalent ions increases upon increasing the number of layers. As the total amount of charged groups increases with the PEM thickness, ions require a higher energy to pass through the PEM. Since divalent and other multivalent ions experience a higher amount of rejection by the PEM compared to monovalent ions, the overall mono-/divalent ion selectivity increases with higher number of layers. By using a constant current (CC) mode CDI operation the use of a $(PAH/PSS)_{2.5}$ PEM yielded a $\beta_{Mg^{2+}}^{Na^{+}}$ value of ≈ 4, while a $(PAH/PSS)_{5.5}$ PEM resulted in a virtually 100 % Na^{+} selectivity, showing how the increase in number of layers can boost the monovalent cation selectivity (**Chapter 6)**. Similarly, in **Chapter 5**, where the PEM was coated on an AEM to achieve mono-/divalent anion selectivity, the selectivity fell between $3 < \beta_{SO_4^{2-}}^{Cl^{-}} < 6$ for $(PSS/PDADMAC)_{2.5}$ and $4 < \beta_{SO_4^{2-}}^{Cl^{-}} < 9$ for $(PSS/PDADMAC)_{4.5}$. Furthermore, in case of $(PSS/PDADMAC)_{7.5}$, $7 < \beta_{SO_4^{2-}}^{Cl^{-}} < 14$ was obtained, further indicating that the rejection of divalent ions increases with higher number of layers. However, this does not imply that the highest possible number of layers should be used in any type of experiment. After all, the electrical resistance increases upon increasing the PEM thickness and, in certain cases, the selectivity can level of. For instance, in **Chapter 6**, coating $(PAH/PSS)_{20.5}$ instead of $(PAH/PSS)_{5.5}$ caused an extra 64 % increase in resistance, even though the selectivity was practically the same. Moreover, in **Chapter 5**, $(PSS/PDADMAC)_{11.5}$ and $(PSS/PDADMAC)_{15.5}$ both resulted in ≈ 2 times more SO_4^{2-} selectivity, resembling the properties of a bare AEM membrane, even though the outermost layer was the polyanion. It is known that for the PSS/PDADMAC system the overall charge of the PEMs is positive for more that ~15 PE layers, irrespective of the outermost layer.[1] Consequently, the monovalent selectivity of such a system is lost

for PEMS with more than ~15 PE layers as the PEM interacts more with divalent and multivalent anions compared to the monovalent ones due to the higher Coulombic interactions, similar to behavior of a bare AEM membrane.[2,3] As demonstrated in various studies,[1,4–6] the overcompensation of charge by the polycation (*e.g.* PAH and PDADMAC) causes an excess positive charge in the PEM after certain number of layers. Although this is a desired effect for monovalent cation selectivity, an excess positive charge would only decrease the rejection of divalent anions and therefore result in a lower monovalent anion selectivity.

8.1.2 Terminating Layer in PEM

Next to the total number of PE layers, the type of the terminating layer is also very important while tuning the ion selectivity. The outermost PE layer should have the same type of fixed charges as the one of the ion(s) that is/are desired to be rejected, facilitating the rejection of divalent and multivalent ions. For instance, in **Chapter 6**, when a polyanion-terminating PEM was used, there was no significant selectivity towards monovalent cations. The PEM displayed Na^+ over Mg^{2+} selectivity, only when a polycation-terminating PEM was used. Basically, a negatively charged terminating multilayer would attract cations with a higher valence due to coulombic interactions, and therefore diminish the charge-exclusion effect towards divalent and multivalent cations. A similar trend was observed for anions in **Chapter 5**, where all the polycation-terminating PEMs resulted in divalent anion selectivity like a bare AEM, instead of monovalent anion selectivity, regardless the number of layers in the PEM. Therefore, changing the number of layers and the type of outermost layer in a PEM enables one to switch and tune ion selectivity in a CDI process, making the ion separation process highly controllable.

8.1.3 Type of Ion-Exchange Membrane

In this thesis, various standard- and special-grade ion-exchange membranes (IEMs) have been used to compare the ion-selective behavior of the bare IEMs with the one of the PEM-coated IEMs. As described in **Chapter 1** and **Chapter 2**, standard-grade IEMs have fixed charges that reject the co-ions and improve the salt removal and energy consumption values in MCDI operations.[7–9] Typically, CEMs are composed of negatively-charged polymers, while AEMs are made of positively-charged polymers.[8] Although a standard IEM can reject the co-ions based on charge rejection, they are not designed to differentiate between the ions that have the same type of charge. For this purpose, there are special-grade IEMs that have additional features improving monovalent ion selectivity. For instance, monovalent cation-selective CEMs (*e.g.* Neosepta CMS and Selemion CSO) have a crosslinked outermost layer to reject cations that have a relatively larger size or have a thin positively charged surface to reject cations with a higher valence. Furthermore, monovalent anion-selective AEMs (*e.g.* Neosepta ACS and Selemion ASV) have crosslinked surfaces to reduce the transport of divalent and multivalent anions through the membrane. Although some of these special-grade IEMs have been implemented in MCDI in previous studies,[10–12] we aimed to compare their ion-selective behavior with the PEM-coated IEMs by using the same experimental conditions.

When a bare standard CEM or AEM is used, a divalent ion selectivity was measured in all cases, which can be explained by the higher interaction between the divalent ions in the solution and the charged membrane surface. For example, the surface of Neosepta CMX (a standard CEM) is negatively charged to be able to reject anions. Therefore, it interacts more with cations that have a higher valency (*e.g.* Mg^{2+}) than with monovalent cations (*e.g.* Na^{+}), yielding a $\beta_{Mg^{2+}}^{Na^{+}}$ of 0.5 ± 0.04 (**Chapter 4**). Similarly, in **Chapter 5**, Neosepta ASE (a standard AEM) resulted in a $\beta_{SO_4^{2-}}^{Cl^{-}}$ of ≈ 0.5. Moreover, special-grade CEMs (Selemion CSO and Neosepta CMS) (**Chapter 4** and **Chapter 6**) and AEM (Neosepta ACS) (**Chapter 5**) have been investigated by using binary and multicomponent feed solutions. In **Chapter 4**, the

$\beta^{Na^+}_{Mg^{2+}}$ value of CMS was 0.4 ± 0.1 by using a CV operational mode. Furthermore, in **Chapter 6**, where a CC mode was used instead of a CV mode, CMX and CMS had $\beta^{Na^+}_{Mg^{2+}}$ values of ≈ 0.3 and ≈ 0.7, respectively. Therefore, regardless the mode of operation, CMX and CMS resulted in similar $\beta^{Na^+}_{Mg^{2+}}$ values. Although the $\beta^{Na^+}_{Mg^{2+}}$ values of CMS are slightly higher than the ones of CMX, the selectivity values are smaller than 1 in all cases, indicating their divalent cation-selective behavior. On the other hand, CSO had a $\beta^{Na^+}_{Mg^{2+}}$ of ≈ 3, displaying a fair selectivity towards monovalent cations, resembling the monovalent cation-selective behavior of the PEM-CMX. Thus, it is clear that CSO had a higher selectivity number compared to the one of CMS. This difference in the selectivity number can be explained by higher rejection of divalent cations by the positively charged CSO compared to the crosslinked outermost layer of CMS, suggesting that the contribution of charge exclusion is higher than the one of size exclusion on the overall cation selectivity. However, even CSO could not improve the monovalent cation-selectivity as much as a PEM coating that is sufficiently thick (*i.e.* 5.5 bilayers). Similarly, in **Chapter 5**, the maximum $\beta^{Cl^-}_{SO_4^{2-}}$ of Neosepta ACS was ≈ 7, while PEM-coated AEM reached a $\beta^{Cl^-}_{SO_4^{2-}}$ of 14.

8.1.4 Feed Solution

As mentioned in **Chapter 1** and **Chapter 3**, PEM characteristics can depend on various parameters, including the composition,[13–16] and ionic strength[17–19] and pH of the media. The electrostatic interactions between the polyelectrolyte layers, PEM morphology, amount of swelling and thickness of the PEM are determined by the conditions of the environment, in our case the feed solution.[2,20] For example, exposing the PEM to a solution with a very high ionic strength would change the amount of intrinsic charge compensation within the PEM and cause more coiled structure. When the ionic strength is higher than 0.5 M,[5] the PEM morphology changes drastically and eventually PE layers desorb from the surface as the electrostatic interactions are very weak at such conditions. Moreover, when

a pH-dependent (weak) polyelectrolyte is used in PEM build-up, the stability and function (*e.g.* ion-selective behavior) of the PEM would alter depending on the pH of the feed solution. However, PEMs that are composed of strong polyelectrolytes can be built and remain intact at pH values ranging from 2.3 to 9.3.[21] Therefore, while designing PEM-based CDI experiments, one should consider the boundary conditions to obtain a stable and selective PEM, especially when the speciation of the anion depends on the pH of the media. For instance, in **Chapter 5**, a strong polyelectrolyte couple – $(PSS/PDADMAC)_n$ – was used in the PEM formation. Since the relative concentrations of the monobasic and dibasic phosphate and sulphate anions depend on the pH of the media, the pH of the solution should be adjusted accordingly. Therefore, building a pH-independent PEM with strong polyelectrolytes would allow some pH flexibility for such experiments.

The composition and properties of the feed solution can also affects the CDI process and the ion selectivity values. Various studies have been reported where the feed ratio of ions and the ionic strength of the solution were carefully controlled and their effect on ion selectivity was studied, as discussed in **Chapter 2**. For instance, Zhao *et al.* demonstrated that higher concentrations of one type of ion results in higher diffusion values of the ion to the pores of the electrode, causing an increase in selectivity towards this ion.[22] Hou and Huang drew a similar conclusion by reporting that a higher concentration of a certain ion in the feed solution would result in a preferential adsorption of this ion.[23]

Not only the feed concentration and the ratio, but also the type of ions in the feed solution affects the ion selectivity in (M)CDI. Especially, the valence and the dehydration energy of ions are key factors to consider. The dependence of the selectivity on the charge and dehydration energy of the anions is studied in **Chapter 5**. The anion selectivity followed the order of $NO_3^- > Cl^- > H_2PO_4^- > SO_4^{2-}$, indicating that the smaller the dehydration energy and valence, the easier it is for an to pass through a PEM-coated AEM. PEM-induced rejection of target ions with higher valence and/or larger dehydration energy values can be of interest for providing a feasible way to, *e.g.*, recover phosphate from multicomponent solutions efficiently. Moreover, in **Chapter 6**, when a PEM-CMX was used, the cation

selectivity followed the order of $K^+ > Na^+ > Li^+ > Mg^{2+}$, which is in good agreement with our observations in **Chapter 5**.

8.1.5 Mode of Operation in CDI

The most common charging modes in CDI are constant current (CC) and constant voltage (CV) modes.[24] So far, the characteristics of these modes and their effect on the desalination characteristics (*e.g.* charge efficiency, salt adsorption capacity, salt adsorption rate, and energy consumption) of CDI operations have been extensively studied.[25–29] In **Chapters 4** and **6**, we further compared these two modes to understand their effect on the monovalent cation selectivity in PEM-based CDI operations. One of the most important conclusions is that the increased selectivity after implementation of an ion-selective layer (*e.g.* PEM coating) can be further improved by optimizing the characteristics of the CDI operation, including the applied voltage/current. For instance, in **Chapter 4**, a $\beta^{Na^+}_{Mg^{2+}}$ of ≈ 3 was reached in a CV operation where 1 V and 0 V was applied during adsorption and desorption cycles, respectively. Typically in CV operations, the electrosorption rate and the amount of ion adsorption change during the adsorption cycle, as the electrodes become more saturated near the end of the adsorption cycle compared to the beginning of the cycle. Therefore the $\beta^{Na^+}_{Mg^{2+}}$ values varied in time during the adsorption cycle. The highest selectivity was observed at ~220 s of the adsorption cycle. Unlike the CV mode, the CC mode allows one to control the electrosorption rate and change in effluent concentration during the adsorption (**Chapter 6**). Therefore, a stable transport of ions to the electrodes, resulting in time-independent selectivity, was obtained by using a constant current. Another key finding of **Chapter 6** is that the amount of current density and voltage applied to the CDI cell has a major effect on $\beta^{Na^+}_{Mg^{2+}}$. While low current densities (*e.g.* 10 A/m^2) resulted in nearly 0 % Mg^{2+} electromigration across the membrane and only allow the transport of Na^+ through the PEM-CMX to the electrode, higher current density values (up to 15 A/m^2, the highest value tested) caused smaller $\beta^{Na^+}_{Mg^{2+}}$ values. The relationship between the applied

voltage/current values and the selectivity numbers can be explained by the change in potential drop across the membrane. We rationalized the selectivity based on the dynamic potential profile described by a standard MCDI model, which indicates that the applied current should be kept below a certain threshold to reject divalent cations. In more detail, the rejection of divalent cations by the PEM is mainly based on the charge rejection. When a strong electrical field is applied to the cell, a higher drop in potential across the membrane would occur, and therefore the rejection of divalent cations by the PEM decreases. If the electrical field is kept under a threshold, electromigration of ions with higher valence can be prevented.

8.1.6 PEMs with Ionophore Units

Although PEM coatings demonstrated high mono-/divalent ion selectivities based on size- and charge-based rejections of divalent ions (**Chapters 4-6**), it is possible to tune their selectivity further to increase their affinity towards target ions by modifying polyelectrolyte layers with ion-selective receptors (ionophores). **Chapter 7** demonstrates such an alternative way to achieve Na^+ and K^+ selectivity by using a PEM decorated with 15-crown-5 (crown ether, CE) units. A real-time gravimetric method, quartz crystal microbalance with dissipation monitoring (QCM-D), was used to study the effect of CE units on the affinity towards different cations without the use of an electrical field. The presence of CE groups resulted in ≈ 1.2 – 1.4 times larger thickness and a higher degree of swelling in PEMs, and increased their selectivity towards Na^+ and K^+ ≈ 3-6 times more, compared to other cations in the solution (*i.e.* Li^+, Rb^+, Cs^+, and Mg^{2+}). This chapter is a proof-of-concept to achieve affinity-based PEM systems that are now ready to be explored for the separating ions that have the same valence in CDI processes. Although it is possible to reach modest selectivity values based on different dehydration of ions by using PEMs without ionophore units, tailor-made PEM-ionophore combinations have the potential to provide a more controlled way to tune ion selectivity in CDI.

8.2 Outlook

8.2.1 Perspectives on Future PEM-Based CDI Operations

As outlined in **Chapter 1** and **Section 8.1**, the main focus of this thesis is to utilize PEM coatings (with and without ionophore units) to achieve improved – and even tune – ion selectivity values in CDI. While PEM-based CDI processes can have high mono- over divalent ion selectivities, it is not possible *yet* to selectively capture one specific ion from a multi-component solution in one-step with current membrane technologies.[30] As explained in more detail in **Chapter 1**, selectively removing one type of ion from brackish water would be beneficial for various water treatment processes, including harvesting nutrients (*e.g.* phosphate, nitrate) and valuable metals (*e.g.* lithium). In order to increase the affinity of an electrode and/or a membrane towards a certain type of ion, tailor-made coatings can be used. For example, calcium alginate coatings on carbon electrodes increases the affinity of the electrodes towards Ca^{2+} in CDI.[31] However, while such a layer would increase the electrosorption of the ion of interest, it does not guarantee that the competing ions will be fully rejected by the electrode. In the search for approaches to tackle this challenge and strive for a high ion selectivity for a particular target ion, several (physico) chemical aspects and technical/operational need to be considered.

Next to interesting recent developments on alternative electrode materials,[12] a key step in achieving ion selectivity would be the development of a library of tailor-made coatings. Considering the tunable nature of PEMs, and their PE building blocks, and the wide range of ionophores that can be incorporated into PEMs *via* a simple one-step reaction in water (as described in **Chapter 1** and **Chapter 7**), PEM coatings are promising candidates for such tailor-made coatings for CDI applications. Depending on the ion of interest and the composition of the feed solution, the characteristics of the PEM and the type of ionophore can be adjusted. For instance, when the target ion is Li^+, a dense PEM with a positively charged surface would already eliminate the majority of multivalent cations while an ionophore (*e.g.* 12-crown-4) can enhance the affinity towards Li^+. However, also the type of

membrane and the electrode material, *i.e.*, not only alternatives to carbon, but also various types of porous carbon, as well as the operational conditions of CDI can alter the ion preference of the system. For example, coulombic interactions between porous carbon electrodes and divalent cations can increase divalent cation selectivity or the electrode can already have a preference towards a certain ion based on the size and mobility of the ion.[12] Therefore, a careful design of the CDI cell and a better understanding of selectivity mechanisms are crucial. Since the selectivity is mostly a combination of several factors in CDI, exploring the contribution of each element (*e.g.* size-based selectivity of electrode and affinity-based selectivity of membrane) on selectivity would help to understand the separation process, all set to obtain a high overall ion selectivity. Moreover, apart from the ion selectivity, also the cost, efficiency, and environmental impact of the process should be evaluated. For example, aiming for a higher energy efficiency and low cost, while using bio-based polyelectrolytes instead of the synthetic ones, like some of the building blocks used in **Chapter 7** would make such systems more environmentally friendly.

8.2.2 Tandem Cation and Anion Selectivities

Another interesting research topic would be to combine a PEM-coated AEM and PEM-coated CEM in the same CDI cell to achieve a tandem selectivity for the desired cations and anions as illustrated in **Figure 8.1**. For example, improving Cl^-/SO_4^{2-} and Na^+/Mg^{2+} selectivities simultaneously could lead to a synergistic effect. A preliminary result exemplifying such a synergistic effect was observed in **Chapter 5**. In more detail, the $\beta_{SO_4^{2-}}^{Cl^-}$ value of an experiment containing two types of cations (Na^+ and Mg^{2+}) was found to be higher than a control experiment containing only one type of cation (Na^+). However, further investigation is required to understand the mechanism behind this result.

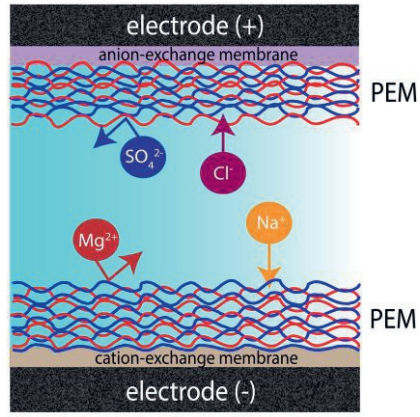

Figure 8.1. Schematic representation of a system where simultaneous monovalent anion and cation selectivities are achieved by combining a PEM-coated CEM and a PEM-coated AEM.

8.2.3 Coating Carbon Electrodes with PEMs

Although coating PEMs on IEMs is a promising way to tune ion selectivity, IEMs are amongst the most dominant components that determine the cost of a CDI operation. That is to say: IEMs are generally more expensive than other components in a CDI cell (*e.g.* porous carbon electrode, glass-fiber spacer, graphite sheet current collector). In a typical MCDI operation, the cost of IEMs is approximately 81% of the overall cost, making the IEMs the dominating cost of the operation compared to the other module components.[32] In more detail, the price of IEMs varies depending on the characteristics. For instance, currently a standard CEM membrane costs around 300 €/m^2, while a special-grade CMS membrane can be as expensive as 600 €/m^2. However, in both cases shipping and handling fees will further increase the costs. Selemion IEMs can be given as example here, as they are only produced in Japan. Furthermore, IEMs have a limited life-time as they degrade and face fouling problems over time, requiring them to be replaced. Interestingly, a special class of PEs, the

one of zwitterionic materials, has attractive anti-fouling properties, and the use thereof as membrane-modifying materials may thus be of interest.[33]

An alternative and relatively less costly way to introduce PEMs to CDI would be to coat them directly on electrodes. To explore the potential of this approach, we coated porous carbon electrodes LbL with $(PAH/PSS)_{10}$ by using the same methodology as the one described in **Chapter 6**. First, we characterized the elemental composition of the samples for each number of layer *via* X-ray photoelectron spectroscopy (XPS) to check if the layer formation is successful. **Table 8.1** shows the percentage of carbon (C), oxygen (O), nitrogen (N), sulfur (S), and fluorine (F) of the PEM-coated carbon samples. Since the bare carbon includes polytetrafluoroethylene (PTFE) as a binder and it is the only source of fluorine in the samples, so the % F can be used as a marker to evaluate the success of coating process. From the data in **Table 8.1** it becomes clear that, upon increasing the number of PE layers, the % F in the sample decreases and eventually reaches to 0 % when 10 layers of polyelectrolytes were coated. Considering the penetration depth of X-rays that are used in XPS, the dry thickness of the PEM coating can be roughly estimated as 10 nm for that later system. Although this is a rough calculation and the thickness of a PEM highly depends on the coating method and deposition conditions (*e.g.* pH, salt, PE concentration),[34] the obtained value is within the expectations for $(PAH/PSS)_n$ PEM system.[35,36] Furthermore, when a freshly-made sample is compared with a sample that was used in a CDI experiment, it is evident that the PEM coating was still present since the % F remains to be 0.

Table 8.1 The percentual abundances of carbon, oxygen, nitrogen, sulfur, and fluorine in various PEM-coated carbon electrodes for each number of PE layers based on wide-scan XPS spectra. The initial sample is the bare carbon electrode. Standard deviations – based on the measurements of two different spots on each sample – were found to be ≤ 2% and in most cases even ≤ 1%.

No. Layers	% Carbon	% Oxygen	% Nitrogen	% Sulfur	% Fluorine
0	85	4	0	0	11
PAH	85	3	3	0	9
PAH-PSS	74	11	4	5	6
$(PAH\text{-}PSS)_{1.5}$	73	11	6	4	6
$(PAH\text{-}PSS)_{2}$	71	14	6	6	4
$(PAH\text{-}PSS)_{2.5}$	73	12	6	5	5
$(PAH\text{-}PSS)_{3}$	70	15	7	7	2
$(PAH\text{-}PSS)_{3.5}$	70	14	8	6	2
$(PAH\text{-}PSS)_{4}$	70	14	7	7	2
$(PAH\text{-}PSS)_{4.5}$	70	14	8	7	2
$(PAH\text{-}PSS)_{5}$	70	8	7	7	0
$(PAH\text{-}PSS)_{5}$ after CDI experiment	71	15	8	6	0

Apart from the decrease in the % F upon increasing number of layers (**Figure 8.2A**), the % N and % S can also evaluated during the layer build-up. Since N and S only present in PAH and PSS, respectively, the ratio of % N to % S would show an odd-even effect depending on the number of layers, fully along the lines of **Figure 4.2**. In other words, for odd number of layers (when the terminating layer is PAH) N/S ratio increases and for even number of layers (when the terminating layer is PSS) N/S ratio decreases (**Figure 8.2B**), showing that the PEM build-up directly on the electrode was successful.

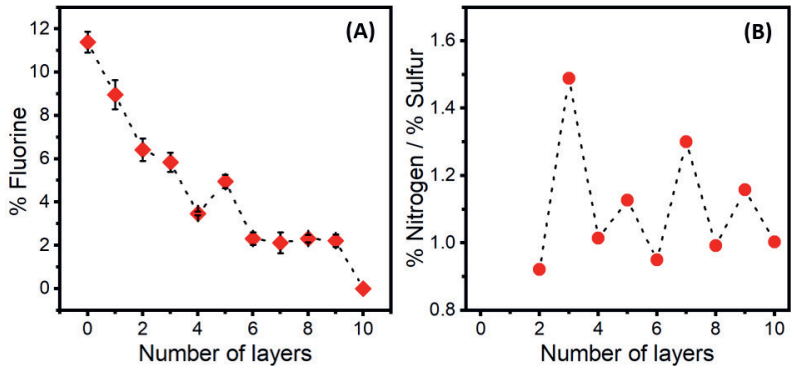

Figure 8.2. (A) The % F and (B) nitrogen/sulfur atomic ratios that are obtained from wide-scan X-ray photoelectron spectra for each number of layers. (Reported data are based on the measurements of two different spots on the samples. Dotted lines are a guide to eye).

Next, CC experiments were performed with the PEM-coated electrodes at current densities in the range of 10 to 50 mA/g to compare the ohmic drop of pristine and PEM-coated electrodes. The experimental conditions are the same as those of the ohmic drop experiments described in **Chapter 6**. In a CC mode operation, the ohmic drop can be evaluated to understand the resistive contributions of several elements in the CDI cell. When all the cell components are the same except the coating on the electrode, the difference in ohmic drop can be used to understand the effect of this coating on overall resistance. **Figure 8.3** illustrates the change in ohmic drop values as function of current density for pristine and PEM-coated carbon electrodes in (A) 4 mM of NaCl and (B) 4 mM of $MgCl_2$ solutions. When the ohmic drop values of the pristine and coated electrodes are compared in a NaCl solution, there is no significant change. However, when $MgCl_2$ solution is used, there is an increase in ohmic drop of PEM-coated electrode. Although this preliminary data does not directly indicate that the PEM coating improved Na^+/Mg^{2+} selectivity of the carbon electrode, the observed higher ohmic drop values could be the result of a higher Mg^{2+} rejection.

Further experiments are required to understand whether a PEM coating can improve the ion selectivity of a carbon electrode. In order to study the ion selectivity of such a system, the concentration of ions should be measured with ion chromatography (IC) and/or inductive coupled plasma- optical emission spectrometry (ICP-OES) during adsorption cycles of the experiments. Additionally, a combination of surface characterization techniques (*e.g.* XPS, water contact angle measurement, AFM, QCM-D) are required to fully understand how the hydrophilicity, pore size, charge, and morphology of the electrode surface change depending on the number of layers and the type of polyelectrolyte layer. Overall, this approach can open up an interesting avenue for designing future ion-separation technologies.

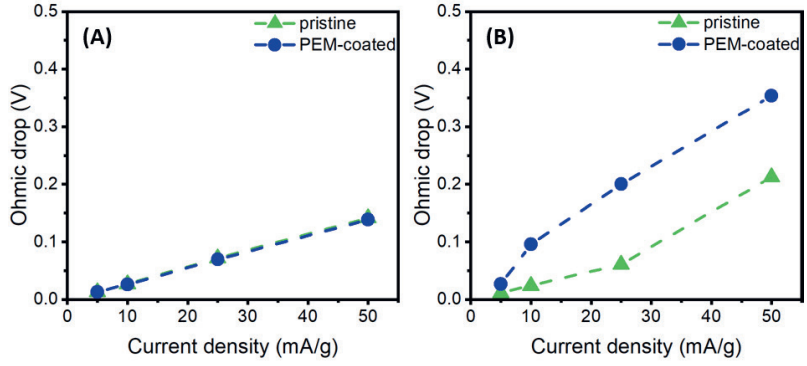

Figure 8.3. Ohmic drop values as function of current density for pristine and PEM-coated carbon electrodes in (A) 4 mM of NaCl and (B) 4 mM of $MgCl_2$ solutions.

8.2.4 Zwitterionic Polymer Brush-Coated Electrodes

Zwitterionic polymer brushes are known for their antifouling properties[37,38] and they were recently combined with carbon electrodes to improve the antifouling properties of a CDI process.[39] In more detail, porous carbon electrodes were modified with

poly(sulfobetaine methacrylate) (SBMA) brushes *via* surface-initiated atom transfer radical polymerization (SI-ATRP). These brush-coated electrode improved antifouling properties towards a model protein, bovine serum albumin. In another study, various zwitterionic polymer brushes demonstrated different affinities towards Na^+ and Mg^{2+} in QCM-D experiments.[40] Based on these results, we hypothesize that they could be an alternative coating for carbon electrodes in CDI and several functionalities of the zwitterionic polymers (*e.g.* increasing the number of ions adsorption sites and the surface area,[41] tuning affinities towards certain ions,[40] and enhancing antifouling properties[37]) can be combined for CDI operations.

To test this, we covalently attached poly(carboxybetaine methacrylate) (CBMA) to porous carbon electrodes (YP-80F). First, we polymerized dopamine on the electrode. Then, the initiator (2-bromo-2-methylpropanonyl bromide) was attached to the polydopamine coating by acylation of surface hydroxyl and amino groups. Then, CBMA monomer was added and the brush was grown *via* SI-ATRP. During the preparation of the brush-coated electrodes, XPS analysis was performed to check the success of each reaction step. The detailed description of the production of the brush-coated electrodes as well as the XPS data for each reaction step can be found in **Appendix 1**.

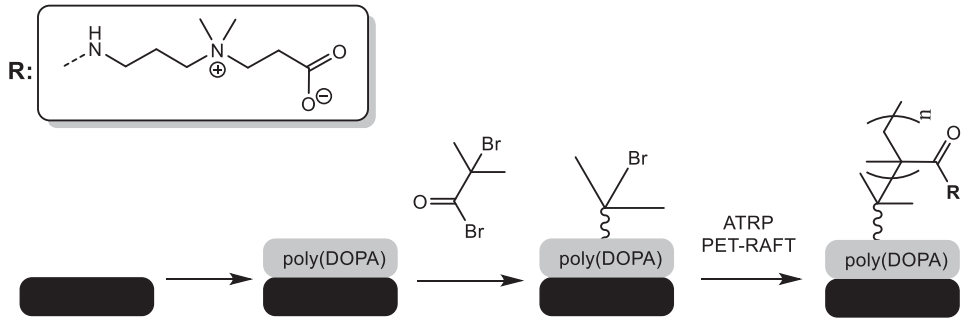

Figure 8.4. Multi-step reaction scheme of the CBMA-coated porous carbon electrodes.

After their preparation, the brush-coated electrodes were investigated in CDI experiments by applying a CC of 10 mA in a solution of 4 mM NaCl and 4 mM KCl. While the maximum conductivity values are slightly lower upon the addition of the brush, the reversibility of the CDI cycles is maintained (**Figure 8.5**). Typically, in a CC process where an IEM is used, the effluent salinity – and hence also the conductivity – remains stable throughout the adsorption step, meaning that the salt adsorption rate is constant.[24] As shown in Figure **8.5a** the brush-coated electrode also shows a similar conductivity profile. In contrast, for a pristine electrode an asymmetrical conductivity profile is observed (**Figure 8.5b**). Such an asymmetry usually is attributed to the co-ion repulsion, suggesting that not all current is used for ion removal during the adsorption.[24] While these preliminary data are promising, the CDI metrics as well as the ion-selective properties of brush-coated electrodes should be compared with those of the pristine electrodes in a systematic way.

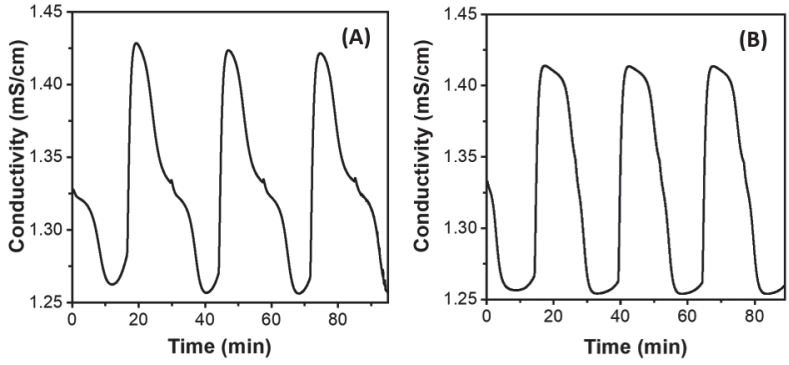

Figure 8.5. Conductivity trends of the (A) pristine and (B) brush-coated carbon electrodes in a CC experiment with a current of 10 mA by using a solution of 4 mM NaCl and 4 mM KCl.

8.2.5 Intercalation Electrodes with Ionophore Units

Carbon electrodes have been the most popular electrode material for CDI conventionally. The high abundance, low cost, electronic conductivity, and high surface area of the carbon make it a suitable electrode material.[42–44] However, carbon electrodes

demonstrates only modest ion selectivities.[45–47] The obtained selectivities with bare carbon electrodes are generally based on difference in size/hydration energy, electronegativity, and the diffusion of ions.[12]

Only recently, a different class of electrode materials, the one of intercalation electrodes has been introduced in CDI as an alternative to carbon electrodes.[48] Intercalation electrodes store cations in their interstitial lattice sites, a process that goes along with changes in the oxidation state of transition metals present in the intercalation material.[49–51] Several studies with intercalation electrodes have focused on the selective adsorption of alkali metal ions[49,50,52–54] and reported a preference towards smaller alkali metal ions, demonstrating a size-based selectivity. Although the high selectivity numbers, $\beta^{Na^+}_{Mg^{2+}}$ up to ≈ 25 [49] and $\beta^{NH4^+}_{Na^+}$ up to ≈ 3 [54], were achieved *via* intercalation electrodes, we envision that it could be possible to tune the selectivity even further by decorating the electrodes with ion-selective receptors or certain functional groups that could increase the local ion concentration and/or affinity towards the target ion(s). The implementation of ionophores could be done by coating the electrodes with a polyelectrolyte layer that is conjugated with ionophore units.

8.2.6 Future Separation Technologies with Polyelectrolytes

Besides the ion-selective separations, PEMs have also been used in a wide range of separation processes including the separation of gases, organic solvents, polysaccharides, and colloidal nanoparticles.[55] However, despite the efforts that have been made already, there are still areas to explore. For instance, recently polyelectrolyte-coated carbon electrodes have been used in CDI to electrosorb proteins from the solution.[56] Polydiallyldimethylammonium chloride (PDMAC) and polystyrene sulfonate (PSS) were incorporated onto the carbon electrodes and the amount of exchanged protein enhanced compared to the one of bare electrodes. This new approach can pave the way for protein separations with PEMs that are decorated with specific tags for each type of protein. Therefore, protein-specific, electro-driven separations could be possible in different areas

such as food and drug industries. Similarly, PEMs with covalently-bound functionalities and incorporated/intercalated additives (*e.g.* biotin, ionophore, enzymes) have been used as (bio)engineered interfaces for sensing and drug delivery applications.[55,57] Although based on the early examples, functionalized PEMs are proven to be very promising for various sensing and separation applications, future research is needed to make the processes more solute-specific. Finally, PEMs have a great potential to be used as "free-standing membranes" without being coated on a substrate.[55] Free-standing PEMs, like hot-pressed polyelectrolyte complexes,[58] could eventually replace the traditional membranes, considering that multiple functionalities (*e.g.* self-healing ability, low fouling, stimuli-responsiveness and high stability) can be combined in one type of PEM.[55]

References

(1) Mulyati, S.; Takagi, R.; Fujii, A.; Ohmukai, Y.; Matsuyama, H. Simultaneous Improvement of the Monovalent Anion Selectivity and Antifouling Properties of an Anion Exchange Membrane in an Electrodialysis Process, Using Polyelectrolyte Multilayer Deposition. *J. Memb. Sci.* **2013**, *431*, 113–120. https://doi.org/10.1016/j.memsci.2012.12.022.

(2) Joseph, N.; Ahmadiannamini, P.; Hoogenboom, R.; Vankelecom, I. F. J. Layer-by-Layer Preparation of Polyelectrolyte Multilayer Membranes for Separation. *Polym. Chem.* **2014**, *5* (6), 1817–1831. https://doi.org/10.1039/c3py01262j.

(3) Riegler, H.; Essler, F. Polyelectrolytes. 2: Intrinsic or Extrinsic Charge Compensation? Quantitative Charge Analysis of PAH/PSS Multilayers. *Langmuir* **2002**, *18* (17), 6694–6698. https://doi.org/10.1021/la020108n.

(4) Sahin, S.; Dykstra, J. E.; Zuilhof, H.; Zornitta, R. L.; de Smet, L. C. P. M. Modification of Cation-Exchange Membranes with Polyelectrolyte Multilayers to Tune Ion Selectivity in Capacitive Deionization. *ACS Appl. Mater. Interfaces* **2020**, *12* (31), 34746–34754. https://doi.org/10.1021/acsami.0c05664.

(5) Rijnaarts, T.; Reurink, D. M.; Radmanesh, F.; de Vos, W. M.; Nijmeijer, K. Layer-by-Layer Coatings on Ion Exchange Membranes: Effect of Multilayer Charge and Hydration on Monovalent Ion Selectivities. *J. Memb. Sci.* **2019**, *570–571*, 513–521. https://doi.org/10.1016/j.memsci.2018.10.074.

(6) Singh, K.; Sahin, S.; Gamaethiralalage, J. G.; Zornitta, R. L.; de Smet, L. C. P. M. Simultaneous, Monovalent Ion Selectivity with Polyelectrolyte Multilayers and Intercalation Electrodes in Capacitive Deionization. *Chem. Eng. J.* **2021**, 128329. https://doi.org/10.1016/j.cej.2020.128329.

(7) Kim, J. S.; Kim, C. S.; Shin, H. S.; Rhim, J. W. Application of Synthesized Anion and Cation Exchange Polymers to Membrane Capacitive Deionization (MCDI). *Macromol. Res.* **2015**, *23*, 360–366. https://doi.org/10.1007/s13233-015-3049-6.

(8) Hassanvand, A.; Wei, K.; Talebi, S.; Chen, G. Q.; Kentish, S. E. The Role of Ion Exchange Membranes in Membrane Capacitive Deionisation. *Membranes* **2017**, *7*, 1–23. https://doi.org/10.3390/membranes7030054.

(9) Li, H.; Zou, L. Ion-Exchange Membrane Capacitive Deionization: A New Strategy for Brackish Water Desalination. *Desalination* **2011**, *275*, 62–66. https://doi.org/10.1016/j.desal.2011.02.027.

(10) Shi, W.; Liu, X.; Ye, C.; Cao, X.; Gao, C.; Shen, J. Efficient Lithium Extraction by Membrane Capacitive Deionization Incorporated with Monovalent Selective Cation Exchange Membrane. *Sep. Purif. Technol.* **2019**, *210*, 885–890. https://doi.org/10.1016/j.seppur.2018.09.006.

(11) Choi, J.; Lee, H.; Hong, S. Capacitive Deionization (CDI) Integrated with Monovalent Cation Selective Membrane for Producing Divalent Cation-Rich Solution. *Desalination* **2016**, *400*, 38–46. https://doi.org/10.1016/j.desal.2016.09.016.

(12) Gamaethiralalage, J. G.; Singh, K.; Sahin, S.; Yoon, J.; Elimelech, M.; Suss, M. E.; Liang, P.; Biesheuvel, P. M.; Zornitta, R. L.; de Smet, L. C. P. M. Recent Advances in Ion Selectivity with Capacitive Deionization. *Energy Environ. Sci.* **2020**, *14*, 1095–1120. https://doi.org/10.1039/d0ee03145c.

(13) Salomäki, M.; Laiho, T.; Kankare, J. Counteranion-Controlled Properties of Polyelectrolyte Multilayers. *Macromolecules* **2004**, *37* (25), 9585–9590. https://doi.org/10.1021/ma048701u.

(14) Salomäki, M.; Kankare, J. Specific Anion Effect in Swelling of Polyelectrolyte Multilayers. *Macromolecules* **2008**, *41* (12), 4423–4428. https://doi.org/10.1021/ma800315j.

(15) El Haitami, A. E.; Martel, D.; Ball, V.; Nguyen, H. C.; Gonthier, E.; Labbe, P.; Voegel, J. C.; Schaaf, P.; Senger, B.; Boulmedais, F. Effect of the Supporting Electrolyte Anion on the Thickness of PSS/PAH Multilayer Films and on Their Permeability to an Electroactive Probe. *Langmuir* **2009**, *25* (4), 2282–2289. https://doi.org/10.1021/la803534y.

(16) Salomäki, M.; Tervasmäki, P.; Areva, S.; Kankare, J. The Hofmeister Anion Effect and the Growth of Polyelectrolyte Multilayers. *Langmuir* **2004**, *20* (9), 3679–3683. https://doi.org/10.1021/la036328y.

(17) Tang, K.; Besseling, N. A. M. Formation of Polyelectrolyte Multilayers: Ionic Strengths and Growth Regimes. *Soft Matter* **2016**, *12* (4), 1032–1040. https://doi.org/10.1039/c5sm02118a.

(18) Dubas, S. T.; Schlenoff, J. B. Factors Controlling the Growth of Polyelectrolyte Multilayers. *Macromolecules* **1999**, *32* (24), 8153–8160. https://doi.org/10.1021/ma981927a.

(19) Lösche, M.; Schmitt, J.; Decher, G.; Bouwman, W. G.; Kjaer, K. Detailed Structure of Molecularly Thin Polyelectrolyte Multilayer Films on Solid Substrates as Revealed by Neutron Reflectometry. *Macromolecules* **1998**, *31* (25), 8893–8906. https://doi.org/10.1021/ma980910p.

(20) Visakh, P. M.; Bayraktar, O.; Pico, G. A. *Polyelectrolytes: Thermodynamics and Rheology*; **2014**. https://doi.org/10.1007/978-3-319-01680-1.

(21) Yang, L.; Tang, C.; Ahmad, M., Yaroshcuk, A.; Bruening, M. L. High Selectivities among Monovalent Cations in Dialysis through Cation-Exchange Membranes Coated with Polyelectrolyte Multilayers. *ACS Appl. Mater. Interfaces* **2018**, *10*, 44134–44143. https://doi.org/10.1021/acsami.8b16434.

(22) Zhao, R.; van Soestbergen, M.; Rijnaarts, H. H. M.; van der Wal, A.; Bazant, M. Z.; Biesheuvel, P. M. Time-Dependent Ion Selectivity in Capacitive Charging of Porous Electrodes. *J. Colloid Interface Sci.* **2012**, *384*, 38–44. https://doi.org/10.1016/j.jcis.2012.06.022.

(23) Hou, C. H.; Huang, C. Y. A Comparative Study of Electrosorption Selectivity of Ions by Activated Carbon Electrodes in Capacitive Deionization. *Desalination* **2013**, *314*, 124–129. https://doi.org/10.1016/j.desal.2012.12.029.

(24) Porada, S.; Zhao, R.; Van Der Wal, A.; Presser, V.; Biesheuvel, P. M. Review on the Science and Technology of Water Desalination by Capacitive Deionization. *Prog. Mater. Sci.* **2013**, *58* (8), 1388–1442. https://doi.org/10.1016/j.pmatsci.2013.03.005.

(25) Zhao, R.; Satpradit, O.; Rijnaarts, H. H. M.; Biesheuvel, P. M.; van der Wal, A. Optimization of Salt Adsorption Rate in Membrane Capacitive Deionization. *Water Res.* **2013**, *47* (5), 1941–1952. https://doi.org/10.1016/j.watres.2013.01.025.

(26) Choi, J. H. Comparison of Constant Voltage (CV) and Constant Current (CC) Operation in the Membrane Capacitive Deionisation Process. *Desalin. Water Treat.* **2015**, *56* (4), 921–928. https://doi.org/10.1080/19443994.2014.942379.

(27) Wang, L.; Lin, S. Membrane Capacitive Deionization with Constant Current vs Constant Voltage Charging: Which Is Better? *Environ. Sci. Technol.* **2018**, *52* (7). https://doi.org/10.1021/acs.est.7b06064.

(28) Kang, J.; Kim, T.; Jo, K.; Yoon, J. Comparison of Salt Adsorption Capacity and Energy Consumption between Constant Current and Constant Voltage Operation in Capacitive Deionization. *Desalination* **2014**, *352*, 52–57. https://doi.org/10.1016/j.desal.2014.08.009.

(29) Qu, Y.; Campbell, P. G.; Gu, L.; Knipe, J. M.; Dzenitis, E.; Santiago, J. G.; Stadermann, M. Energy Consumption Analysis of Constant Voltage and Constant Current Operations in Capacitive Deionization. *Desalination* **2016**, *400*, 18–24. https://doi.org/10.1016/j.desal.2016.09.014.

(30) Epsztein, R.; DuChanois, R. M.; Ritt, C. L.; Noy, A.; Elimelech, M. Towards Single-Species Selectivity of Membranes with Subnanometre Pores. *Nat. Nanotechnol.* **2020**, *15* (6), 426–436. https://doi.org/10.1038/s41565-020-0713-6.

(31) Yoon, H.; Lee, J.; Kim, S. R.; Kang, J.; Kim, S.; Kim, C.; Yoon, J. Capacitive Deionization with Ca-Alginate Coated-Carbon Electrode for Hardness Control. *Desalination* **2016**, *392*, 46–53. https://doi.org/10.1016/j.desal.2016.03.019.

(32) Metzger, M.; Kuppan, S.; Hellstrom, S.; Kim, S.; Sebti, E.; Subban, C. V; Christensen, J. Techno-Economic Analysis of Capacitive and Intercalative Water Deionization. **2020**, *13*, 1544–1560. https://doi.org/10.1039/d0ee00725k.

(33) Baggerman, J.; Smulders, M. M. J.; Zuilhof, H. Romantic Surfaces: A Systematic Overview of Stable, Biospecific, and Antifouling Zwitterionic Surfaces. *Langmuir* **2019**, *35* (5), 1072–1084. https://doi.org/10.1021/acs.langmuir.8b03360.

(34) Guzmán, E.; Rubio, R. G.; Ortega, F. A Closer Physico-Chemical Look to the Layer-by-Layer Electrostatic Self-Assembly of Polyelectrolyte Multilayers. *Adv. Colloid Interface Sci.* **2020**, *282*. https://doi.org/10.1016/j.cis.2020.102197.

(35) Elzbieciak-Wodka, M.; Kolasińska-Sojka, M.; Nowak, P.; Warszyński, P. Comparison of Permeability of Poly(Allylamine Hydrochloride)/and Poly(Diallyldimethylammonium Chloride)/Poly(4-Styrenesulfonate) Multilayer Films: Linear vs. Exponential Growth. *J. Electroanal. Chem.* **2015**, *738*, 195–202. https://doi.org/10.1016/j.jelechem.2014.11.035.

(36) Cao, Z.; Gordiichuk, P. I.; Loos, K.; Sudhölter, E. J. R.; de Smet, L. C. P. M. The Effect of Guanidinium Functionalization on the Structural Properties and Anion Affinity of Polyelectrolyte Multilayers. *Soft Matter* **2016**, *12* (5), 1496–1505. https://doi.org/10.1039/c5sm01655j.

(37) Kuzmyn, A. R.; De Los Santos Pereira, A.; Pop-Georgievski, O.; Bruns, M.; Brynda, E.; Rodriguez-Emmenegger, C. Exploiting End Group Functionalization for the Design of Antifouling Bioactive Brushes. *Polym. Chem.* **2014**, *5*, 4124–4131. https://doi.org/10.1039/c4py00281d.

(38) Kuzmyn, A. R.; Nguyen, A. T.; Teunissen, L. W.; Zuilhof, H.; Baggerman, J. Antifouling Polymer Brushes via Oxygen-Tolerant Surface-Initiated PET-RAFT. *Langmuir* **2020**, *36* (16), 4439–4446. https://doi.org/10.1021/acs.langmuir.9b03536.

(39) Zhang, P.; Fritz, P. A.; Schroën, K.; Duan, H.; Boom, R. M.; Chan-Park, M. B. Zwitterionic Polymer Modified Porous Carbon for High-Performance and Antifouling Capacitive Desalination. *ACS Appl. Mater. Interfaces* **2018**, *10* (39), 33564–33573. https://doi.org/10.1021/acsami.8b11708.

(40) Víšová, I.; Vrabcová, M.; Forinová, M.; Zhigunová, Y.; Mironov, V.; Houska, M.; Bittrich, E.; Eichhorn, K. J.; Hashim, H.; Schovánek, P.; et al. Surface Preconditioning Influences the Antifouling Capabilities of Zwitterionic and Nonionic Polymer Brushes. *Langmuir* **2020**, *36* (29), 8485–8493. https://doi.org/10.1021/acs.langmuir.0c00996.

(41) Jung, Y.; Yang, Y.; Kim, T.; Shin, H. S.; Hong, S.; Cha, S.; Kwon, S. Enhanced Electrochemical Stability of a Zwitterionic-Polymer-Functionalized Electrode for Capacitive Deionization. *ACS Appl. Mater. Interfaces* **2018**, *10* (7), 6207–6217. https://doi.org/10.1021/acsami.7b14609.

(42) Huang, Z. H.; Yang, Z.; Kang, F.; Inagaki, M. Carbon Electrodes for Capacitive Deionization. *J. Mater. Chem. A* **2017**, *5* (2), 470–496. https://doi.org/10.1039/c6ta06733f.

(43) Porada, S.; Weinstein, L.; Dash, R.; Van Der Wal, A.; Bryjak, M.; Gogotsi, Y.; Biesheuvel, P. M. Water Desalination Using Capacitive Deionization with Microporous Carbon Electrodes. *ACS Appl. Mater. Interfaces* **2012**. https://doi.org/10.1021/am201683j.

(44) Zornitta, R. L.; Barcelos, K. M.; Nogueira, F. G. E.; Ruotolo, L. A. M. Understanding the Mechanism of Carbonization and KOH Activation of Polyaniline Leading to Enhanced Electrosorption Performance. *Carbon N. Y.* **2020**, *156*, 346–358. https://doi.org/10.1016/j.carbon.2019.09.058.

(45) Suss, M. E. Size-Based Ion Selectivity of Micropore Electric Double Layers in Capacitive Deionization Electrodes. *J. Electrochem. Soc.* **2017**, *164* (9), E270--E275. https://doi.org/10.1149/2.1201709jes.

(46) Jeon, S. Il; Park, H. R.; Yeo, J. G.; Yang, S.; Cho, C. H.; Han, M. H.; Kim, D. K. Desalination via a New Membrane Capacitive Deionization Process Utilizing Flow-Electrodes. *Energy Environ. Sci.* **2013**, *6* (5), 1471–1475. https://doi.org/10.1039/c3ee24443a.

(47) Mubita, T. M.; Dykstra, J. E.; Biesheuvel, P. M.; van der Wal, A.; Porada, S. Selective Adsorption of Nitrate over Chloride in Microporous Carbons. *Water Res.* **2019**, *164*, 114885. https://doi.org/10.1016/j.watres.2019.114885.

(48) Singh, K.; Porada, S.; de Gier, H. D.; Biesheuvel, P. M.; de Smet, L. C. P. M. Timeline on the Application of Intercalation Materials in Capacitive Deionization. *Desalination* **2019**, *455*, 115–134. https://doi.org/10.1016/J.DESAL.2018.12.015.

(49) Singh, K.; Qian, Z.; Biesheuvel, P. M.; Zuilhof, H.; Porada, S.; de Smet, L. C. P. M. Nickel Hexacyanoferrate Electrodes for High Mono/Divalent Ion-Selectivity in Capacitive Deionization. *Desalination* **2020**, *481*, 114346. https://doi.org/10.1016/j.desal.2020.114346.

(50) Porada, S.; Shrivastava, A.; Bukowska, P.; Biesheuvel, P. M.; Smith, K. C. Nickel Hexacyanoferrate Electrodes for Continuous Cation Intercalation Desalination of Brackish Water. *Electrochim. Acta* **2017**, *255*, 369–378. https://doi.org/10.1016/j.electacta.2017.09.137.

(51) Choi, S.; Chang, B.; Kim, S.; Lee, J.; Yoon, J.; Choi, J. W. Battery Electrode Materials with Omnivalent Cation Storage for Fast and Charge-Efficient Ion Removal of Asymmetric Capacitive Deionization. *Adv. Funct. Mater.* **2018**, *28* (35), 1–9. https://doi.org/10.1002/adfm.201802665.

(52) Ikeshoji, T. Separation of Alkali Metal Ions by Intercalation into a Prussian Blue Electrode. *J. Electrochem. Soc.* **1986**, *133* (10), 2108–2109. https://doi.org/10.1149/1.2108350.

(53) Lilga, M. A.; Orth, R. J.; Sukamto, J. P. H.; Haight, S. M.; Schwartz, D. T. Metal Ion Separations Using Electrically Switched Ion Exchange. *Sep. Purif. Technol.* **1997**, *11* (3), 147–158. https://doi.org/10.1016/S1383-5866(97)00017-8.

(54) Kim, T.; Gorski, C. A.; Logan, B. E. Ammonium Removal from Domestic Wastewater Using Selective Battery Electrodes. *Environ. Sci. Technol. Lett.* **2018**, *5* (9), 578–583. https://doi.org/10.1021/acs.estlett.8b00334.

(55) Durmaz, E. N.; Sahin, S.; Virga, E.; Beer, S. De; Smet, L. C. P. M. De; Vos, W. M. De. Polyelectrolytes as Building Blocks for Next-Generation Membranes with Advanced Functionalities. **2021**. https://doi.org/10.1021/acsapm.1c00654.

(56) Fritz, P. A.; Zhang, P.; Bruschinski, T.; Sahin, S.; de Smet, L. C. P. M.; Chan-Park, M. B.; Boom, R. M.; Schroën, C. G. P. H. Steering Protein and Salt Ad- and Desorption by an Electrical Switch Applied to Polymer-Coated Electrodes. *Sep. Purif. Technol.* **2020**, *250*. https://doi.org/10.1016/j.seppur.2020.117195.

(57) Movilli, J.; Huskens, J. Functionalized Polyelectrolytes for Bioengineered Interfaces and Biosensing Applications. *Org. Mater.* **2020**, *02* (02), 078–107. https://doi.org/10.1055/s-0040-1708494.

(58) B, A. K.; Lindhoud, S.; Vos, W. M. De. Hot-Pressed Polyelectrolyte Complexes as Novel Alkaline Stable Monovalent-Ion Selective Anion Exchange Membranes. *J. Colloid Interface Sci.* **2021**, *593*, 11–20. https://doi.org/10.1016/j.jcis.2021.02.077.

Summary

Water desalination processes typically focus on the production of fresh water by reducing the overall salt concentration. The removal of one type of salt – a compound consisting of ions, *i.e.*, charged species – specifically, e.*g.*, toxic or high-value ions, require selective water desalination processes. This research topic has attracted considerable attention in recent years within the context of various sustainability development goals. Given the ability of polyelectrolyte multilayers (PEMs) to add and tune ion selectivity in pressure-driven water treatment processes, it is aimed in this thesis, to explore the use of PEMs in capacitive deionization (CDI), a process that is driven by an electrical potential difference. This aim is outlined in more detail in **Chapter 1** after introducing the relevance and potential of ion-selective desalination. In addition, this chapter provides a general introduction on the techniques (*e.g.*, CDI, quartz crystal microbalance with dissipation monitoring, QCM-D) and materials (*e.g.*, PEMs, ion-selective receptors, membranes) used in the thesis.

Chapter 2 reviews recent approaches for tuning cation selectivity in CDI with a focus on mono-/divalent cation selectivity. The selectivity towards a certain (group of) cation(s) can be enhanced *via* optimizing the pore size of the electrodes, tuning the operational parameters of the CDI process, implementation of ion-selective coatings on the electrodes or a combination of these approaches. This chapter also covers the frequently used ion-selectivity definitions and the main factors affecting the selectivity of a CDI operation. **Chapter 3** provides an overview of recent advances of applying PEM-coated dense membranes in separation processes and discusses how PEMs are used as antifouling and/or (ion/solvent) selective layers in various membrane applications. Furthermore, this chapter discusses the mechanisms of ion selectivity of PEM-coated membranes and the main factors that vary the ion-selective properties of PEMs by comparing the selectivity numbers of various studies in a systematic way.

From the aforementioned chapters it becomes clear that PEMs have interesting properties that enable one to control the permeability and rejection of ions, and with that, to control ion selectivity, but also that their implementation with the CDI is yet to be

explored. **Chapter 4** shows a proof-of-concept to achieve selectivity among monovalent and divalent cations *via* a PEM-coated membrane in CDI. A standard-grade cation-exchange membrane (CMX) was coated with a PEM to obtain PEM-CMX *via* a layer-by-layer deposition scheme using poly(allylamine hydrochloride) (PAH) and poly(styrene sulfonate) (PSS). Next, the Na^+/Mg^{2+} selectivity numbers as well as various CDI metrics (salt adsorption capacity, charge efficiency, specific energy consumption, Coulombic efficiency, and desalination capacity) of the bare CMX and the PEM-CMX were compared. Upon the addition of a PEM, the Na^+/Mg^{2+} selectivity value increased from 0.5 ± 0.04 to 2.8 ± 0.2, showing that it is possible to switch the divalent cation-selective CMX into a monovalent cation-selective membrane *via* the addition of a ≈16 nm thick PEM coating. Besides, the long-term stability test (>40 cycles) of the PEM-CMX confirmed the feasibility of the approach.

Next, a similar method was employed to achieve monovalent anion selectivity (**Chapter 5**). In this chapter, a standard-grade anion-exchange membrane (AEM) was coated with a PEM built from poly(diallyldimethylammonium chloride) and PSS and the mono-/divalent anion selectivity values of the bare and PEM-coated AEM were compared. Similar to the results obtained in the previous chapter, the addition of a PEM affected the selectivity as in resulted in a change of the Cl^-/SO_4^{2-} selectivity from ≈0.5 times up 14. Moreover, in this work, the PEM-coated AEM was combined with intercalating nickel hexacyanoferrate (NiHCF) electrodes, which have an inherent size-based selectivity towards monovalent cations, to achieve monovalent cation and anion selectivities simultaneously. In our experiments, the Na^+/Mg^{2+} selectivity value was found to be as high as ≈17. Moreover, the selectivity of the PEM-AEM towards NO_3^-, Cl^-, SO_4^{2-}, and $H_2PO_4^-$ was investigated and it was concluded that apart from the valence also the hydration energy of the anion affects the selectivity. Finally, this chapter also demonstrates that the selectivity number varies with the type of charge of the polyelectrolyte that is on top as well as with the no. polyelectrolyte layers.

After successfully tuning the monovalent cation and anion selectivities in **Chapters 4** and **5** and obtaining high selectivity numbers that are on par with state-of-the-art CDI

literature, the operational parameters of CDI and the no. polyelectrolyte layers in the PEM were tuned to maximize the monovalent cation selectivity (**Chapter 6**). By scanning through different voltage/current density values and varying the composition of the feed solution systematically, the optimized conditions were found. After optimizing the no. polyelectrolyte bilayers (5.5, *i.e.*, 11 polyelectrolyte layers) on the CMX membrane and the current density (10 A/m^2), a time-independent and virtually 100 % monovalent cation selectivity was achieved. Before this optimization, a time-dependent selectivity with a maximum of $Na^+/Mg^{2+} \approx 3$ was obtained. Next, the obtained selectivity numbers were rationalized by using an MCDI model based on the dynamic potential profile.

Although PEM coatings demonstrated high mono-/divalent ion selectivities in the previous CDI-based chapters, it was aimed in **Chapter 7** to further tune the selectivity of cations that have the same valence by functionalizing PEMs with ion-selective receptors (*i.e.*, 15-crown-5 derivatives, CE). Apart from using PAH and PSS, this study also includes the covalent attachment of CE to pectin, a bio-based polyanion. A real-time, surface-sensitive technique (QCM-D) was used to follow the effect of the presence of these CE units on the build-up of PEMs onto gold, here used as a model surface, and to study the interactions between these coatings and various monovalent cations. The presence of CE units resulted in an increased layer thickness and as the uptake of Na^+ and K^+ was found to be ≈3-6 times higher compared to those of other cations present in the solution (Li^+, Rb^+, Cs^+, and Mg^{2+}), these PEM systems are now ready to be further explored in ion separation.

Chapter 8 provides a general discussion on the results obtained in **Chapters 3-7** which is presented in a broader context and also include several suggestions for future research, partly supported with preliminary data.

Samenvatting

Ontziltingsprocessen richten zich voornamelijk op de productie van vers water door het verminderen van de algehele zoutconcentratie. Het specifiek verwijderen van één type zout – een stof bestaande uit ionen, *i.e.* geladen deeltjes –, bijvoorbeeld giftige of waardevolle ionen, vereist selectieve ontziltingsprocessen. Dit onderzoeksonderwerp heeft de afgelopen jaren aanzienlijke aandacht gekregen in de context van verscheidende duurzame ontwikkelingsdoelen. Gezien de eigenschap van polyelektroliet multilagen (PEMs) om ionselectiviteit toe te voegen en te controleren in drukgedreven waterbehandelingsprocessen, richt dit proefschrift zich op het verkennen van het gebruik van PEMs in capacitieve deïonisatie (CDI); een ontziltingsproces dat gedreven wordt door een elektrisch potentiaalverschil. Dit doel wordt in **Hoofdstuk 1** in meer detail beschreven, na het introduceren van de relevantie en het potentieel van ion-selectieve ontzilting. Daarnaast verschaft dit hoofdstuk een algemene introductie van de technieken (bijv. CDI, een kwartskristallen microbalans waarmee ook de dissipatie bestudeerd kan worden, QCM-D) en de materialen (bijv. PEMs, ion-selectieve receptoren, membranen) die gebruikt worden in deze thesis.

Hoofdstuk 2 geeft een overzicht van recente methodes om de kationselectiviteit in CDI te tunen, met een nadruk op mono-/divalente (een-/tweewaardige) kationselectiviteit. De selectiviteit voor een bepaalde (groep) kationen kan worden verhoogd door het optimaliseren van de poriegrootte in de elektrodes, het afstemmen van de operationele parameters van het CDI proces, het gebruik van ionselectieve *coatings* op de elektrodes, of een combinatie van deze methodes. Dit hoofdstuk behandelt ook de veelgebruikte definities van ionselectiviteit en de belangrijkste factoren die de selectiviteit van een CDI-operatie beïnvloeden. **Hoofdstuk 3** verschaft een overzicht van recente ontwikkelingen in het toepassen van PEM-gecoate, dichte membranen in scheidingsprocessen, en bespreekt hoe PEMs gebruikt worden als antifouling- en/of (ion/oplosmiddel)selectieve lagen in verschillende membraanapplicaties. Daarnaast behandelt dit hoofdstuk de mechanismes van de ionselectiviteit van PEM-gecoate membranen, en – door het systematisch vergelijken van de selectiviteitswaardes van

verschillende studies – de belangrijkste factoren die de ionselectiviteit van PEMs beïnvloeden.

Uit de eerdergenoemde hoofdstukken wordt duidelijk dat PEMs interessante eigenschappen hebben die men de mogelijkheid geeft om de doorlaatbaarheid en afstoting van ionen te controleren, en daardoor de ionselectiviteit te tunen, maar ook dat hun implementatie met CDI nog onderzocht moet worden. **Hoofdstuk 4** demonstreert een *proof-of-concept* om selectiviteit tussen mono- en divalente ionen te bereiken via een PEM-gecoat membraan in CDI. Een standaard kation uitwisselingsmembraan (CMX) werd gecoat met een PEM om een PEM-CMX te krijgen door middel van *layer-by-layer* (laagje-voor-laagje) depositie met poly(allylamine hydrochloride) (PAH) en poly(styreen sulfonaat) (PSS). Daarna werden de Na^+/Mg^{2+} selectiviteitswaardes, alsmede verschillende CDI statistieken (zoutabsorptiecapaciteit, charge efficiency, specifieke energieconsumptie, Coulombische efficiëntie en ontziltingscapaciteit) van de onbehandelde CMX en de PEM-CMX vergeleken. Na toevoeging van een PEM nam de Na^+/Mg^{2+} selectiviteit toe van 0.5 ± 0.04 tot 2.8 ± 0.2, wat aangeeft dat het mogelijk is om de selectieviteit van CMX te veranderen van di- naar monovalente ionen door het toevoegen van een ≈16 nm dikke PEM coating. Daarnaast bevestigde de lange-termijn stabiliteitstest (>40 cycli) van de PEM-CMX de uitvoerbaarheid van deze methode.

Vervolgens is een vergelijkbare methode gebruikt om monovalente anionselectiviteit te bereiken (**Hoofdstuk 5**). In dit hoofdstuk werd een standaard anion uitwisselingsmembraan (AEM) gecoat met een PEM gemaakt van poly(diallyldimethylammonium chloride) en PSS, en werden de mono-/divalente anion selectiviteitwaardes van de onbehandelde en PEM-gecoate AEM vergeleken. In lijn met de resultaten uit het vorige hoofdstuk had de toevoeging van een PEM invloed op de selectiviteit, met als resultaat een verandering van de Cl^-/SO_4^{2-} selectiviteit van ≈0.5 naar 14. Verder werd in dit werk de PEM-gecoate AEM gecombineerd met intercalerende nikkel hexacyanoferraat (NiHCF) elektrodes – die een op grootte gebaseerde selectiviteit voor monovalente kationen hebben – om tegelijkertijd selectiviteit voor monovalente kationen

en anionen te verkrijgen. In onze experimenten werd een Na^+/Mg^{2+} selectiviteitswaarde van maar liefst ≈17 gevonden. Daarnaast werd de selectiviteit van de PEM-AEM voor NO_3^-, Cl^-, SO_4^{2-}, en $H_2PO_4^-$ onderzocht en werd geconcludeerd dat naast de valentie ook de hydratie-energie van het anion effect had op de selectiviteit. Als laatste demonstreert dit hoofdstuk dat de selectiviteitswaarde verandert met zowel het type lading van de bovenste polyelektroliet als het aantal polyelectrolietlagen.

Nadat in **Hoofdstuk 4** en **5** de kation- en anionselectiviteit succesvol zijn geoptimaliseerd, en nadat hoge selectiviteitswaardes zijn behaald die in lijn liggen met vooraanstaande CDI literatuur, worden nu de operationele parameters van CDI en het aantal polyelectrolietlagen in de PEM gevarieerd om de monovalente kationselectiviteit te maximaliseren (**Hoofdstuk 6**). De optimale condities werden gevonden door systematisch door verschillende waardes voor het voltage / de stroomdichtheid te scannen, en door de samenstelling van de voedingsoplossing aan te passen. Na het optimaliseren van de stroomdichtheid (10 A/m^2) en het aantal dubbellagen aan polyelektroliet (5.5, *i.e.,* 11 polyelektrolietlagen) op het CMX membraan werd een tijdsonafhankelijke en vrijwel 100% monovalente kationselectiviteit behaald. Vóór deze optimalisatie werd een tijdsafhankelijke selectiviteit van maximaal Na^+/Mg^{2+} ≈ 3 behaald. Vervolgens zijn de behaalde selectiviteitswaardes verklaard door het gebruik van een MCDI model gebaseerd op het dynamische potentiaalprofiel.

Ondanks dat PEM coatings een hoge mono-/divalente ionselectiviteit hebben laten zien in de vorige CDI-gebaseerde hoofdstukken, was het doel van **Hoofdstuk 7** om de selectiviteit tussen kationen met eenzelfde valentie verder te tunen door PEMs te functionaliseren met ion-selectieve receptoren (*i.e.*, 15-crown-5 derivaten, CE). Naast het gebruik van PAH en PSS omvat deze studie ook het covalent verbinden van CE aan pectine, een *bio-based* polyanion. Een *real time*, oppervlakte-gevoelige techniek (QCM-D) werd gebruikt om het effect van de aanwezigheid van deze CE units op de opbouw van de PEMs op goud – hier gebruikt als een modeloppervlak – te volgen, en om de interacties tussen deze coatings en verschillende monovalente kationen te bestuderen. De aanwezigheid van

CE units leidde tot een grotere laagdikte, en aangezien de opname van Na^+ en K^+ ≈3-6 keer hoger was vergeleken met die van andere kationen in de oplossing (Li^+, Rb^+, Cs^+, en Mg^{2+}), zijn deze PEM systemen nu beschikbaar om verder te worden onderzocht voor het scheiden van ionen.

Hoofdstuk 8 verschaft een algemene discussie van de resultaten behaald in **Hoofdstukken 3-7**, waarin de resultaten in een bredere context worden geplaatst. Ook geeft **Hoofdstuk 8** meerdere suggesties voor toekomstig onderzoek, gedeeltelijk ondersteund met voorlopige data.

Appendix I

Supplementary Information to Outlook

"I am, and always will be, the optimist. The hoper of far-flung hopes, and the dreamer of improbable dreams."

(The 11th Doctor, Doctor Who)

Preparation of Polydopamine-Coated Electrodes. 5 g of porous carbon (YP80) in 2 L of 1:1 water/ethanol mixture was sonicated for 30 min. 2 g of dopamine and 2 mM of trisbuffer were added to the mixture. Then, the reaction was mixed at 37 ◦C overnight. Afterwards, the slurry was filtrated via vacuum filtration and washed with ethanol. The electrodes were dried at 65 ◦C overnight in a vacuum oven. After the electrodes were dried, 5 g of the polydopamine-modified electrode was mixed with 0.43 g of PTFE (binder) and a non-sticky dough was made by adding ethanol to this mixture. After small portions of the dough was cut and the electrode thickness was adjusted to 300 µm via a rolling machine, the electrodes were dried at 120 ◦C overnight under vacuum.

Immobilization of ATRP Initiator. The initiator, 2-bromo-2-methylpropanoyl bromide, was covalently attached to the polydopamine in the carbon electrode by acylation with surface hydroxyl and amino groups. The substrate was immersed in a 250 mL solution of 0.24 M triethylamine and 0.24 M 2-bromo-2-methylpropanoyl bromide at 0 ◦C. The reaction proceeds for 1 h, and then the substrates were washed with ethanol, water, and dried under reduced pressure at 65 ◦C.

SI-ATRP of poly(CBMA) Brushes on Carbon Electrodes. The ethanol (20 mL) was degassed using three freeze–pump–thaw cycles and transferred to a Schlenk tube containing degassed CuBr (38.2 mg, 266 mmol), $CuBr_2$ (11.8 mg, 53 mmol), and Me_4Cyclam (82.1 mg, 320 mmol). The solution of the catalyst was added to the degassed monomer CBMAA (3243 mg, 13.4 mmol). The polymerization solution was transferred to the reactor containing the prior degassed substrate coated with a carbon electrode with an immobilized initiator, and the reaction was allowed to proceed for 2h at 30 ◦C. The substrates coated with poly(CBAA) brushes were washed water. The resulting brush-coated electrodes were used in the CDI experiments as described in **Chapter 8**.

XPS Data of the Brush-Coated Carbon Electrodes.

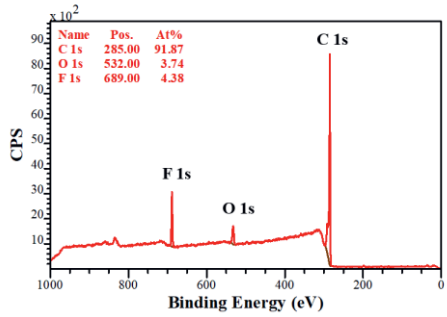

Figure I.1. Wide-scan XPS spectrum of the bare carbon electrode with PTFE binder.

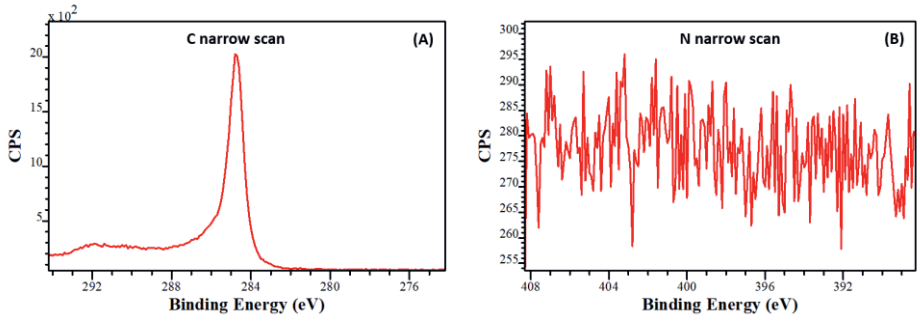

Figure I.2. Narrow-scan (A) C1s region and (B) N1s region XPS spectra of the bare carbon electrode with PTFE binder.

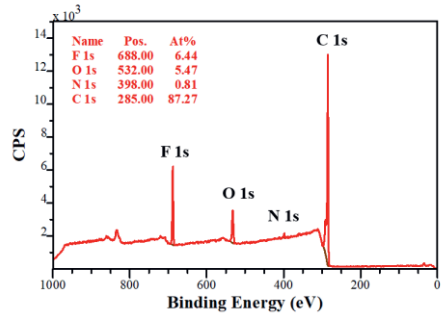

Figure I.3. Wide-scan XPS spectrum of the electrode after polymerization of the dopamine.

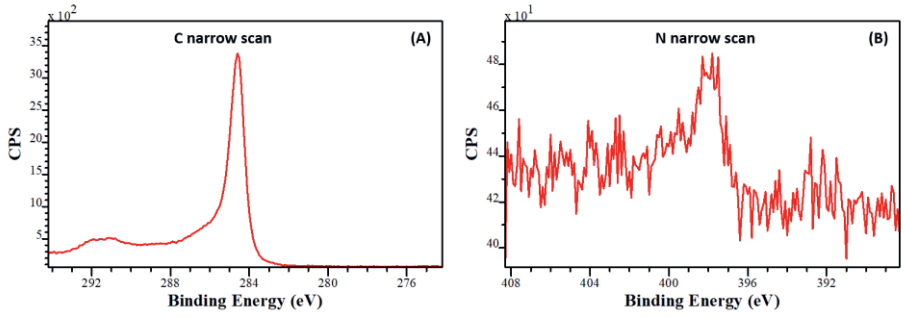

Figure I.4. Narrow-scan XPS spectra of (A) C1s region and (B) N1s region of the electrode after polymerization of the dopamine.

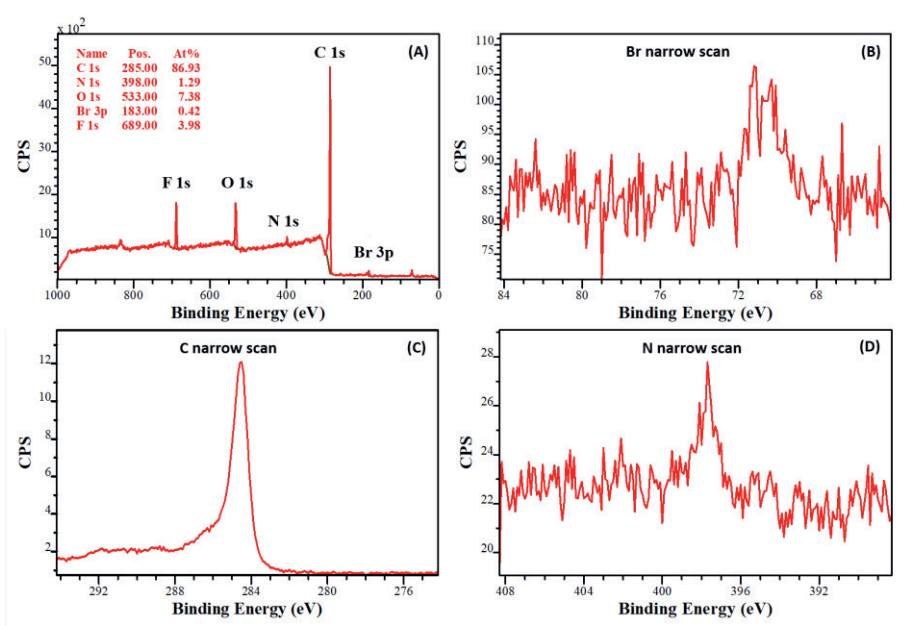

Figure I.5. (A) Wide-scan, (B) Br3d, (C) C1s, (D) N1s regions narrow scan XPS spectra of the carbon electrode after immobilization of the ATRP initiator.

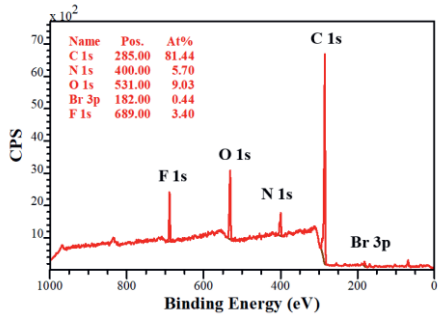

Figure I.6. Wide-scan XPS spectra of the carbon electrode of the CBMA-coated electrodes.

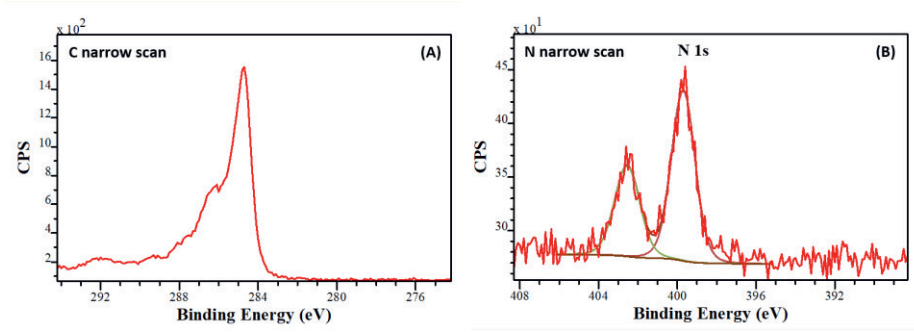

Figure I.7. Narrow scan (A) C1s and (B) N1s regions XPS spectra of the CBMA-coated electrodes.

About the Author

Curriculum Vitae

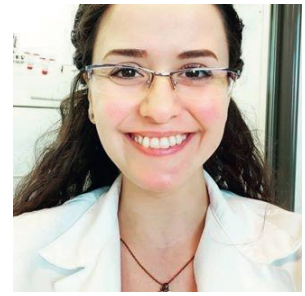

Sevil Sahin received her BSc degree from the Department of Chemistry at Istanbul Technical University, and her MSc degree from the Department of Pharmaceutical Chemistry at Istanbul University, Turkey. During her MSc research, she synthesized porphyrin derivatives for photodynamic therapy. In 2017, she started to do a PhD in the Laboratory of Organic Chemistry at Wageningen University, The Netherlands. Her doctoral research includes, among others, the use of polyelectrolyte multilayers for tuning ion selectivity in capacitive deionization. As of October 2021, Sevil has been working as a post-doctoral researcher at the Department of Molecular Nanofabrication at University of Twente.

List of Publications

Sahin, S.; van Weeren, E.; Zuilhof, H.; de Smet, L. C. P. M. Crown Ether-Modified Polyelectrolytes and their Interactions with Cations – a QCM Study *(manuscript accepted, Applied Surface Science Advances,* **2022***)*

Sahin, S.; Zuilhof, H.; Zornitta, R. L.; de Smet; L. C. P. M. Enhanced Monovalent over Divalent Cation Selectivity with Polyelectrolyte Multilayers in Membrane Capacitive Deionization *via* Optimization of Operational Conditions. *Desalination*, **2022**, 522, 115391.

Durmaz, E. N.*; Sahin, S.*; Virga, E.*; de Beer, S.; de Smet, L. C. P. M.; de Vos W. M. Polyelectrolytes as Building Blocks for Next-Generation Membranes with Advanced Functionalities, *ACS Appl. Polym. Mater.*, **2021**, 3 (9), 4347-4374.

Singh, K.*****; Sahin, S.*****; Gamaethiralalage, J. G.; Zornitta, R. L.; de Smet, L. C. P. M. Simultaneous, Monovalent Ion Selectivity with Polyelectrolyte Multilayers and Intercalation Electrodes in Capacitive Deionization. *Chem. Eng. J.* **2021**, 128329.

Gamaethiralalage, J. G.; Singh, K.; Sahin, S.; Yoon, J.; Elimelech, M.; Suss, M. E.; Liang, P.; Biesheuvel, P. M.; Zornitta, R. L.; de Smet, L. C. P. M. Recent Advances in Ion Selectivity with Capacitive Deionization. *Energy Environ. Sci.* **2021**, 14, 1095-1120 (*featured on the cover*).

Sahin, S.; Dykstra, J. E.; Zuilhof, H.; Zornitta, R. L.; de Smet, L. C. P. M. Modification of Cation-Exchange Membranes with Polyelectrolyte Multilayers to Tune Ion Selectivity in Capacitive Deionization. *ACS Appl. Mater. Interfaces* **2020**, 12, 31, 34746–34754 (*featured on the cover*).

Qian, Z., Miedema, H., Sahin, S., de Smet, L. C. P. M., Sudhölter, E. J. R. Separation of Alkali Metal Cations by a Supported Liquid Membrane (SLM) Operating Under Electrodialysis (ED) Conditions. *Desalination* **2020**, 495, 114631.

Fritz, P. A.; Zhang, P.; Bruschinski, T.; Sahin, S.; de Smet, L. C. P. M.; Chan-Park, M. B.; Boom, R. M.; Schroën, C. G. P. H. Steering Protein and Salt Ad- and Desorption by an Electrical Switch Applied to Polymer-Coated Electrodes. *Sep. Purif. Technol.* **2020**, 250, 117195.

van Dam-Engelbert, A., Pujari, S., Sahin, S., de Smet, L. C. P. M. Bio-organic Chemistry at Surfaces: Tuning the Outermost Nanometer: Laboratory Manual. Laboratory of Organic Chemistry, Wageningen University, **2020**.

Pujari, S., Sahin, S., de Smet, L. C. P. M. Bio-organic Chemistry at Surfaces: Tuning the Outermost Nanometer: Laboratory Manual. Laboratory of Organic Chemistry, Wageningen University, **2019**.

Cimir, S. Some Synthetic Modifications Employing 6,9-dihydroxy-7a,14a dihydronaphthofuranofuro [2,1-b]naphthofuran. *J. Turkish Chem. Soc.* **2014**, 1 (1), 6.

**authors contributed equally.*

Selected Conference Abstracts

Sahin, S.; van Weeren, E.; Zuilhof, H.; de Smet, L.C.P.M. QCM-D Study of Interactions between Cations with Crown Ether-Modified, Bio-based Polyelectrolytes. International Symposium of Polyelectrolytes, online/Shanghai, China, 21-25 June **2021** *(oral presentation)*.

Sahin, S., de Smet, L. C. P. M. High Monovalent over Divalent Ion Selectivities with Polyelectrolyte Multilayers in Membrane Capacitive Deionization. 5th International Conference on Capacitive Deionization and Electrosorption, online/Atlanta, USA, 11-14 May **2021** *(oral presentation).*

Sahin, S., Zuilhof, H., de Smet L. C. P. M. Physicochemical Properties of Layer-by-Layer Assembled Polyelectrolyte Multilayers. Workshop: Chemistry on Surfaces and Applied Materials, Ben Gurion, Israel, 7 February **2019** *(poster presentation)*.

Sahin, S.; Dykstra, J. E.; Zuilhof, H.; Zornitta, R. L.; De Smet, L. C. P. M. Polyelectrolyte Multilayers for Capacitive Deionization: Tuning Ion Selectivity in Desalination. CHAINS, Eindhoven, Netherlands, 10-11 December **2019** *(poster presentation)*.

Cimir S.; Turkyilmaz S. Synthetic Studies Towards Zn(II)-Bisdipicolylamine (Zn_2BDPA) Complex Bearing Porphyrin Derivatives as Targeted Antibacterial Photodynamic Therapy (PDT) Agents. Abstract #917, 6th EuCheMS Chemistry Congress, Seville, Spain, 11-15 September **2016** (*oral presentation*).

Cimir S.; Turkyilmaz S. Studies Towards Bacterial Cell Targeting Porphyrin Derivatives. Book of Abstracts, p.S29. 3rd National Organic Chemistry Congress, Trabzon, Turkey, 5-8 September **2016** (*oral presentation*).

Turkyilmaz, S.; Rice, D. R.; Cimir, S.; Palumbo, R.; Smith, B. Studies Towards Multivalent Zn(II)-Bisdipicolylamine Systems for Theranostic Applications, Trans Mediterranean Colloquium on Heterocyclic Chemistry-TRAMECH VIII, Antalya, Turkey, 11-15 November **2015** (*oral presentation*).

Overview of Completed Training Activities

Discipline-specific activities	Organizing institute (s)	Year
Wageningen Molecular Life Sciences Seminars	ORC	2017-2020
Advanced Organic Chemistry Course	ORC	2018-2020
12th International Symposium of Polyelectrolytes (ISP)	VLAG/PCC	2018
WETSUS: Water Tech Week	WETSUS	2018
Chemistry As INovating Science (CHAINS)	NWO	2019
Workshop: Chemistry on Surfaces and Applied Materials*	Ben Gurion University, Israel/ORC PhD Trip Committee	2019
Chemistry As INovating Science (CHAINS)*	NWO	2020
Q-Sense User Week	Biolin Scientific, Sweden	2020
Workshop: Real-time Insight into Polymer Adsorption and Conformation	Biolin Scientific, Sweden	2020
Workshop: Surface and Interface Chemistry	4 TU, Netherlands	2020
5th International Conference on Capacitive Deionization and Electrosorption (CDI-E) **	Georgia Tech, Atlanta, GA, USA	2021
12th European Symposium on Electrochemical Engineering (ESEE)	WETSUS	2021
13th International Symposium of Polyelectrolytes (ISP)**	East China University of Science and Technology, China	2021

**poster presentation **oral presentation*

General Courses	Organizing institute (s)	Year
VLAG PhD week	VLAG	2018
The Essentials of Scientific Writing & Presenting	WGS	2018
Project and Time Management	WGS	2018
Supervising Thesis Students	Education Support WUR	2018
Scientific Artwork	Library WUR	2019
Presenting with Impact	WGS	2019
Scientific Writing	WGS	2019

Other Activities	Year
Preparation of PhD research proposal	2017
Group meetings	2017-2021
Colloquia	2017-2022
PhD Study Tour to Israel (and member of organization committee)	2019

Teaching Activities	Year
Supervision BSc and MSc Thesis Students	2017-2021
Bio-Organic Chemistry for Life Sciences	2017-2020
Bio-Organic Chemistry	2017-2020
OCAM ORC-11806 (Spectroscopy)	2017-2019
Organic Chemistry I & Organic Chemistry II	2017-2018
Bio-organic Chemistry at Surfaces: Tuning the Outermost Nanometer	2018-2020

Acknowledgments

"So long, and thanks for all the fish."

(Hitchhiker's Guide to Galaxy)

Acknowledgments! Traditionally, this is the place where we start reading a PhD thesis from. After a five-year-long PhD journey, now it is my turn to express my gratitude to the people who have supported, helped, inspired, and encouraged me along the way. I consider myself a very lucky person as I have been surrounded by amazing colleagues, friends, and family. Therefore, the acknowledgments will be a bit long :)

First of all, my thesis committee, **Prof. Ernst Sudhölter**, **Prof. Marleen Kamperman**, **Assoc. Prof. Renko de Vries**, and **Dr. Armin Michel**, thank you for your time, evaluation, and critical remarks.

Next, I would like to thank my daily supervisor and promoter **Louis** for giving me the chance to pursue my childhood dream. One of the happiest moments of my life is the moment that I was accepted as a PhD student in your group. Since then, this journey has been like a roller-coaster for me, challenging but rewarding and exciting in many ways. I have grown not only professionally but also personally, thanks to your honesty, constructive criticism, and constant support. Thank you for being there for me not only when things worked well, but also when the experiments failed. Thank you for the motivation, believing in me, genuinely caring about my wellbeing (especially for reminding me to take more holidays :D), and providing me the tools I needed to become an independent researcher. I have learned a lot from you during our meetings: critical and creative thinking, analyzing the data in detail, writing manuscripts meticulously... Well, as a side effect, now I see all the typos *etc.* in a publication and noticing the different shades of a color in a figure immediately. What has been seen cannot be unseen :D I highly appreciate that you included me in collaborations, projects, teaching activities (*e.g.* writing a manual for lab practicals), or any other opportunity whenever possible so that I could gain experience and grow. Last but not least, you have always listened and respected me as a colleague, valued my ideas, and gave me the freedom to choose which direction to go.

Of course, none of these would be possible if I haven't met **Han**, now my promoter, in EuChemS 2016 conference in Sevilla. Back then, I was an excited MSc student who presents her master thesis in the conference. It was something remarkable for me that you took me seriously, listened to my presentation, and asked me genuine questions about my research. Thank you for being approachable and always ready to discuss science! Afterwards, you recommended me to Louis for his PhD position and welcomed me to ORC. Thank you for encouraging me when I needed by saying "laat je niet gek maken" (do not let anything distract you from your focus). Your comments and suggestions during our surface group meetings (*aka.* pizza-cat meetings) helped me. I should also thank you for keeping the labs open during the Covid-19 pandemic.

Rafael, I cannot imagine my thesis without your contributions. You are a real teammate, an enthusiastic teacher, and a very talented *yet* humble researcher. Even after your post-doc, you kept helping us (the CDI team) and answering our questions. Special thanks for opening the mysterious world of "modelling" to me! I will miss the 80s rock songs at the lab and our chats on random topics (*e.g.* food, travel, academia, politics...) while I was taking samples from the CDI cell for hours :D

The CDI team, **Jay** and **Kaustub** – I am happy that you joined the team especially because you were the only PhDs that actually understand my research (lol). Our best ideas came to life during the discussions at the coffee corner and ended up in nice publications. Although, sometimes you needed to listen way too many voice records about typos or to change the same figure 857985th time, it was totally worth it. Kaustub, I am glad that we combined our approaches in a unique way. Jay, thanks for being the "analytical chemist" of the team, helping with the robot and IC, and being the plant daddy of the office. P.S. you are a great cook but I can't eat hot peppers.

My students, **Robbert** and **Emma** – Robbert, you started your thesis in the very beginning of my PhD as my first student and we have learned many things together. I will miss our looong brainstorming meetings in front of the white board. Emma, you came to our group almost at the end of my PhD and we shared the passion for QCM and polyelectrolytes with you. Luckily, the long QCM experiments paid off and these data became a part of my thesis. I am glad to see you both sparkling in your new journeys.

The collaborations I had during my PhD was not limited to ORC members, of course. **Elif**, **Ettore**, **Wiebe**, and **Sissi** – I really appreciate your invitation for the review. It was a pleasure to work with you. During our Teams meetings, I realized how much I like polyelectrolytes and I should be working with them in the future. Best activity of covid times! **Pina** and **Karin**, thanks for our mini CDI chats with big impacts. Pina, you were the first one that mentioned me about time-dependent selectivity trends, thanks! You are always kind, positive, and easy to work with. I am glad that one of our chats resulted in a publication. **Zexin**, you spent the most "synthetic" part of your thesis with me at ORC. Multiple visits from Leeuwarden to Wageningen...At first, it was orange, chaotic, and frustrating but then we did it, yey! All the best, with your future career.

Teris, **Michiel**, **Maurice**, **Maarten**, **Gert**, **Floris**, and **Fedor** – thanks for your questions/comments during my Monday morning seminars and group meetings. Also, thanks for arranging AOC lectures/teaching schedules/office spaces, replying my random questions...It was a privilege to meet you and work with you.

ORC technical staff and researchers – **Barend**, I really appreciate your help in building the CDI system, arrangements with the workshop, NMR analyses, IRRAS and XPS characterizations (together with Sidhu), keeping the stock room full, en Nederlandse praktijken tijdens koffiepauzes (dank je wel!)....and many other things. You are an inseparable part of ORC. **Sidhu**, thanks for helping me with XPS and Auger as well as the discussions on surface chemistry. You are always so kind and trying to help anyone who needs you. **Henny**, most of the time, when I came to your office to ask something about an order, we ended up chatting about different countries, cultures, weather, history, and even sports :D We can chat for hours and hours without noticing the time. Well, I am glad we did so and I will always cherish these moments! Also, thank you for ordering chemicals and consumables for us. I admire your communication skills and the number of languages you can speak! You fixed sooo many ordering issues for me on the phone. **Judith**, **Hendra**, **Frank**, **Elbert**, **Tjerk**, **Hans**, **Dieuwertje**, **Anne-Marie**, and **Carel**, it was fun to teach together with you. A special mention goes to Judith for being the problem-solver of our teaching lab and to Tjerk for making sure that I have a working PC and software all the time!

Somewhere in the middle of my thesis, ICP-OES became my second favorite instrument and this resulted in too many visits to the Environmental Technology (ETE) Department. Thanks to **Pieter** and **Jill**, everything worked smoothly. Thank you for the quick solutions, trouble-shootings, and making exceptions for me, a non-ETE person, so that I can access the lab during corona times.

Elly, **Aleida**, **Meta**, **Esther**, and **Meike** – thank you for your support in a very wide range of topics: finding the available slot in Han's agenda, helping in financial stuff during the preparations of PhD trip, organizing events and gifts together...and many other things.

My paranymphs and dear friends **Alyssa** and **Ellen** – it would take many pages to express my appreciation for you. Thank you for supporting and encouraging me along the way. Together, we have been the non-alcohol corner of the office and the extra clean corner of the lab :D You two are my go-to people whenever I have an issue regardless the topic. Mounting an Ikea furniture? No problem. Listening to my presentations, checking typos in posters? Sure. Organizing events together? Of course! Alyssa, thanks for being my dance buddy, I will miss the salsa and belly dance classes with you. I am also grateful for your help in translation of the thesis summary. Ellen, our cooking sessions and hiking tours should continue!

Arne, thanks for the emergency 3D printing and the trip in Germany!

Fun fact: I have changed 2 labs, 4 fumehoods, and at least 3 desks during my 4-year-long ORC time. **Fred**, you became my "ORC buddy" and the first friend in the Netherlands. You showed me around, helped me in the lab, replied my questions...It took a while to get used to your office pranks and jokes, though :P **Pepijn** (*aka.* Pepiciin and many more wrong pronunciations), my old and new colleague! We were officemates back then and now we are working together on the same project. We have grown a lot together! You truly master "Sevil language" and appreciate a "good sarma". I love your sense of humor & dancing and karaoke skills :D **Alice**, my Italian sister, your presence made ORC a much better and more cheerful place. You are a shining star and it is not possible to feel down around you. Thanks for the good Italian food, countless AH coffees, plants, chats, and hugs. Special thanks for your help in the last stretch of my thesis writing. **Satesh** and **Alexandre** thank you for the time together and being a part of the karaoke crew together with **Carolina**, Fred, **Pepijn**, **Alice**, **Jorick**, **Alyssa**, and **Ellen**. **Andrada**, it was a pleasure to share the office with you. You are always so calm and thoughtful. I will see you in the next game night in Enschede!

Andriy, our little polymer brush project is now a part of the outlook section of this thesis. You were also a great help when it comes to XPS analyses and booking way too many slots in XPS for my PEMs. I wish you all the best in your future career and may the Force be with you. Together with **Lucas** and **Esther R.** you were my fellow QCM people :D **Esther R.**, I enjoyed the coffee breaks and scientific & not-so-scientific discussions with you.

Jorick, **Jordi**, **Sjoerd** (vier! ze viel!), **Esther R.**, **Esther vA.**, **Andriy**, **Annemieke**, **Milou**, **Ian** I met you at the beginning of my PhD time and you guys made me feel welcomed here. Later on, we got more crowded at ORC. **Canan**, **Ariadni**, **Daniele**, **Julian**, **Si**, **Wei**, **Sybren**, **Natassa**, **Irene**, **Anouk**...and the rest of ORC PhDs & postdocs – thank you for the game nights, drinks, Christmas and Sinterklaas celebrations, PhD and lab trips, lunches at the pond, round table chats at the coffee corner, teaching together, and all the fun. I hope to keep in touch with many of you!

Canan, **Ariadni**, **Alyssa**, and **Fatma** – We had Mediterranean dinners (which included too much olive oil and yoghurt), dance classes, endless WhatsApp chats, and lots of laughs together! I treasure our friendship.

Wageningen became "my city" immediately after I start living here and it will always stay like that. Since I needed to move four times (without counting the Airbnb stays *etc*.), I had the chance to meet with many incredible people here. Although I can't list all names here, I would like to thank to **Elveda** and **Uğur** for the "first dinner in Wageningen", being the "muhtar" of Wageningen, helping me and Adem in countless things, and your

friendship. **Goshia**, you were our first neighbor in Wageningen. Thank you for the time together. Have fun in Germany! **Açalya** and **Jens**, many thanks for the mini trips, breakfasts, and chats. Ik wil **mijn buren van Mörfelden-Walldorfplein** bedanken voor de bloemen, vers fruit uit eigen tuin, zelfgemaakte jam en de praatjes ondanks mijn niet-bestaande Nederlands. Thank you **Drink & Draw Wageningen** and **ISOW belly dancing** people for coloring my days. **Oscar**, bedankt dat je een geweldige leraar Nederlands bent.

Burak, thanks for the trips together and your kindness & friendship.

My Twente colleagues and friends – **Hazal** & **Aytaç**, **Nergiz**, **Ege**, **Jacopo**, **Krishnendu**, **my office** (*aka.* chicken coop), **Dilu**, **Pepijn**, **Nienke**, **Asst. Prof. Albert Wong**, **Prof. Dr. Loes Segerink** and **Prof. Jurriaan Huskens**, thank you for the smooth start I had in Twente and the welcoming atmosphere. You definitely made the last stretch of this thesis much easier for me!

My ITUKIM family, **Malhun**, **Dilek A.**, **Dilek K.**, **Simge**, **İpek**, **Ece**, **Zeynep**, **Eren**, **Çağkan**, **Recep** – Since our bachelor years we are together and I always feel your support regardless which city/country we are in. Hep yanımda olduğunuz için teşekkür ederim!

I would like to express my deepest appreciation to my MSc thesis supervisor, **Assoc. Prof. Serhan Türkyılmaz**, for providing me the knowledge and tools I needed as a student. I wouldn't be here today without your invaluable advice, patience, and continuous support.

My warm and heartfelt thanks go to my family for allowing me to follow my dreams, cheering for me, and the tremendous support, strength, and hope they had given to me. **Mom**, you always say "kendi ayakların üzerinde durmalısın" to me. Literal translation would be "stand on your own feet". I think, I do so now.

Adem, my love, we are together for 13 years now. You have seen me growing, becoming an adult, graduating from BSc and MSc degrees...You were exposed to so much chemistry that you almost have been studying with me all those years :P You always stand by me wherever I go: from Istanbul to Wageningen, then to Twente...You share my dreams and understand me better than anyone else. My life wouldn't be the same without your infinite love and support.

Sevil

The research described in this thesis has received funding from the European Research Council (ERC) under the European Union's Horizon 2020 research and innovation program (ERC Consolidator Grant to Dr. Louis C.P.M. de Smet, Grant agreement No. 682444).

Financial support from Wageningen University for printing this thesis is gratefully acknowledged.

Cover design by Sevil Şahin and Bregje Jaspers

Printed by ProefschriftMaken